REPORT DOCUMENTATION PAGE

Form Approved
OMB No. 0704-0188

The public reporting burden for this collection of information is estimated to average 1 hour per response, including the time for reviewing instructions, searching existing data sources, gathering and maintaining the data needed, and completing and reviewing the collection of information. Send comments regarding this burden estimate or any other aspect of this collection of information, including suggestions for reducing the burden, to Department of Defense, Washington Headquarters Services, Directorate for Information Operations and Reports (0704-0188), 1215 Jefferson Davis Highway, Suite 1204, Arlington, VA 22202-4302. Respondents should be aware that notwithstanding any other provision of law, no person shall be subject to any penalty for failing to comply with a collection of information if it does not display a currently valid OMB control number.
PLEASE DO NOT RETURN YOUR FORM TO THE ABOVE ADDRESS.

1. REPORT DATE *(DD-MM-YYYY)*	2. REPORT TYPE	3. DATES COVERED *(From - To)*
07/14/2014	Final	8-15-2011 - 8-14-2014

4. TITLE AND SUBTITLE
Renewavle Bio-Solar Hyrdrogen Production From Robust Oxygenic Phototrophs: The Second Generation (Part D)

5a. CONTRACT NUMBER

5b. GRANT NUMBER
FA9550-11-1-0218

5c. PROGRAM ELEMENT NUMBER
61102

6. AUTHOR(S)
John Peters

5d. PROJECT NUMBER

5e. TASK NUMBER

5f. WORK UNIT NUMBER

7. PERFORMING ORGANIZATION NAME(S) AND ADDRESS(ES)
Montana State University

8. PERFORMING ORGANIZATION REPORT NUMBER

9. SPONSORING/MONITORING AGENCY NAME(S) AND ADDRESS(ES)
AFOSR
875 North Randolph Street
Arlington VA 22203

10. SPONSOR/MONITOR'S ACRONYM(S)

11. SPONSOR/MONITOR'S REPORT NUMBER(S)

12. DISTRIBUTION/AVAILABILITY STATEMENT
Unlimited

13. SUPPLEMENTARY NOTES

14. ABSTRACT
Key advances during the 2011-2014 funding period include: (a) We have established a battery of hydrogenase specific activity assays and H cluster spectroscopic probes to assess oxygen tolerance in a quantitative manner. (b) We have characterized the changes in microbial community structure and hydrogenase diversity as a function of the vertical transect of the water column in the Great Salt Lake. (c) We have tested the hypothesis that sequence variations observed through the GSL water column include structural determinants for

15. SUBJECT TERMS

16. SECURITY CLASSIFICATION OF:			17. LIMITATION OF ABSTRACT	18. NUMBER OF PAGES	19a. NAME OF RESPONSIBLE PERSON
a. REPORT	b. ABSTRACT	c. THIS PAGE			John Peters
			Unclass	3	19b. TELEPHONE NUMBER *(Include area code)* 406-994-7212

Period Covered: 8/15/2011 to 7/14/2014

Title of Proposal: Renewable Bio-Solar H_2 Production from Robust Oxygenic Phototrophs: The Second Generation.

Grant Number: FA9550-11-1-0218.

Institutions: Montana State University

List of Reporting Period Manuscripts Published, In Press, or Submitted:

1. J.W. Peters and J.B. Broderick, "The Maturation of [FeFe]-Hydrogenases: A Paradigm for Complex Iron-Sulfur Cofactor Assembly and Insertion" *Annu. Rev. Biochem.* **2012**, 81:32.1 – 32.22.

2. J.W. Peters, E.S. Boyd, S. D'Adamo, D.W. Mulder, J. Therien, and M.C. Posewitz, "Hydrogenases, Nitrogenases, Anoxia, and H_2 Production in water-oxidizing phototrophs. In: Algae for Biofuels and Energy" Michael Borowitzka (Ed.), Springer, **2012**

3. B.R. Duffus, T.L. Hamilton, E.M. Shepard, E.S. Boyd, J.W. Peters, and J.B. Broderick, "Radical AdoMet enzymes in complex inorganic metallocluster biosynthesis" *BBA – Proteins and Proteomics*, **2012**, 1824:1254-1256

4. J.E. Meuser, B.K. Baxter, J.R. Spear, J.W. Peters, M.C. Posewitz, and E.S. Boyd. "Contrasting patterns of community assembly in the stratified water column of Great Salt Lake, Utah" *Microb Ecol.* **2013** 66:268-280

5. E.M. Shepard, A.S. Byer, K.D. Swanson, E.S. Boyd, J.W. Peters, and J.B. Broderick, "[FeFe]-Hydrogenase H-Cluster Assembly" in *Metals in Cells, Encyclopedia of Inorganic and Bioinorganic Chemistry.* **2013** *1–15.*

6. S. D'Adamo , R.E. Jinkerson, E.S. Boyd, S.L. Brown, B.K. Baxter, J.W. Peters, M.C. Posewitz **"**Evolutionary and Biotechnological Implications of Robust Hydrogenase Activity in Halophilic Strains of Tetraselmis" *PLOS One* 9(1):1-13 (2014)

7. K.D. Swanson, M.W. Ratzloff, D.W. Mulder, J.H. Artz, S. Ghose, A. Hoffman, S. White, O. A. Zadvornyy, J.B. Broderick, B. Bothner, P.W. King, .J.W. Peters, "[FeFe]-hydrogenase oxygen inactivation is initiated by the modification and degradation of the H cluster 2Fe subcluster" *Submitted to J. Am. Chem Soc.*

8. D.W. Mulder, M.W. Ratzloff, M. Bruschi, C. Greco, E. Koonce, J.W. Peters, a.P.W. King "Investigations on the role of proton-coupled electron transfer in hydrogen activation by [FeFe]-hydrogenase" *Submitted to J. Am. Chem Soc.*

9. J.W. Peters, G.J. Schut, E.S. Boyd, D.W. Mulder, E.M. Shepard, J.B. Broderick, P.W. King, M.W.W. Adams "[FeFe]- and [NiFe]-Hydrogenase Diversity, Mechanism, and Maturation" *Submitted to Biochim. Biophys. Acta*

10. E.S. Boyd, T.L. Hamilton, K. Swanson, A. Howells, B.K. Baxter, M.C. Posewitz, J.W. Peters "Distribution, Abundance, and Diversity of Multimeric Bifurcating [FeFe]-Hydrogenases Along a Vertical Redox Gradient in Great Salt Lake, USA" *Draft In preparation*

11. J.B. Therien, T.L. Hamilton, Z. Liu, S.M. Noone, P.W. King, D.A. Bryant, J.W. Peters "Draft genome and targeted transcriptional analysis of *Clostridium pasteurianum* (strain W5) provides insights into possible determinants of H_2 oxidation and reduction" *Draft In preparation*

Presentations:

1. "Hydrogen as component of a future balanced global energy portfolio" First Annual Montana Green Conference for Students and Educators, Belgrade, MT 3/10/2011

2. "Hydrogen and the Environment - The Quest for Alternative Fuels" Energy and Telecommunications Interim Committee of the Montana Legislature, Helena MT 1/13/2012

3. "Rationalizing the structural determinants for oxygen tolerant [FeFe]-hydrogenases" 2012 Air Force Office of Sponsored Research Bioenergy Program Review, Arlington, VA, 8/6/2012-8/10/2012

4. "Overcoming Key Barriers Toward Engineering Superior Biosholar H2 Solutions" 2011 Air Force Office of Sponsored Research Bioenergy Program Review, Arlington, VA, 6/6/2011-6/9/2011

5. "Hydrogenase Structure, Function, and Evolution" NSF sponsored workshop on Catalytic mechanisms and the emergence of metabolic networks Arlington, VA, 5/23/2012-5/25/2012

6. "Rationalizing the structural determinants for oxygen tolerant [FeFe]-hydrogenases" 2012 Air Force Office of Sponsored Research Bioenergy Program Review, Arlington, VA, 8/6/2012-8/10/2012

7. "Biological Hydrogen Metabolism: The Origin and Future of Life on Earth" Bioenegry Systems Research Institute, University of Georgia, Oct. 11, 2012

8. "An alternative path for the evolution of biological nitrogen fixation" Department of Biochemistry & Molecular Biology, University of Georgia, March 6, 2013

9. "An alternative path for the evolution of biological nitrogen fixation" National Renewable Energy Laboratory, March 29, 2013

10. "Biogenesis of the H cluster of the [FeFe]-hydrogenase" 7th International Conference on Iron-Sulfur Cluster Biogenesis and Regulation, University of South Carolina, May 20-24, 2013

Key Finding/Results/Accomplishments:

Enzymes are biochemically classified as hydrogenases if they carry out either 1). the oxidation of hydrogen to feed energy in the form of reduced electrons into metabolism or 2). the reduction of protons to recycle reduced electron carriers during fermentative metabolism. These enzymes also have a structural classification based of their transition metal cofactor into one of three classes – [Fe]-hydrogenases, [NiFe]-hydrogenases, and [FeFe]-hydrogenases. The first of these produces hydrogen gas through dehydrogenation of methylene-tetrahydromethanopterin, while the latter two both catalyze the oxidation of diatomic hydrogen or the reduction of protons to hydrogen gas. Of these three classes, [FeFe]-hydrogenase has been shown to be the most effective in the production of hydrogen gas.

However, [FeFe]-hydrogenases are very oxygen sensitive and become inactive when exposed. This would require strictly anaerobic reactor conditions, which adds a layer of complexity due to oxygen's natural prevalence in air. Furthermore, oxygenic photosynthesis, the most effective photosynthesis, is inherently incompatible with such a hydrogen-producing metabolism as it introduces oxygen internally to the microorganism. Therefore, oxygen tolerance in an [FeFe]-hydrogenase is highly desirable.

Oxygen attacks the H-cluster, the active site inorganic core of [FeFe]-hydrogenases. The H-cluster is composed of a [4Fe-4S] subcluster connected by a cysteine thiol to a unique [2Fe-2S] subcluster with CO and CN^- ligands. Environments that support microbial growth and feature an oxygen gradient, such as bodies of water with a sharp halocline, may provide a selection pressure to produce an aerotolerant [FeFe]-hydrogenases. The Guerrero Negro hyper-saline ponds and the Great Salt Lake have such characteristics and were sampled for [FeFe]-hydrogenase sequences for this application. Variations may be studied either by inserting a consensus sequences into a well characterized [FeFe]-hydrogenase, such as that of *Clostridium pasteurianum* (CpI), or by a shotgun approach of making and screening insertions into CpI with a mixed sample of many degenerately primed [FeFe]-hydrogenase sequences from a hyper-saline environment. Using nature as a guide may allow us to overcome some of the limitations of previous studies, using rational/computational protein design and random mutagenesis. These studies have been limited in part due to the enzymes inherent properties associated with maturation.

In conjunction with bioprospecting and construction of [FeFe]-hydrogenase variants, various supporting analytical and spectroscopic tests are used to characterize the [FeFe]-hydrogenase and variants. Assays have been developed to measure the effect of oxygen on [FeFe]-hydrogenase activity to determine the half-lives. In addition, UV-Visible spectroscopy has been used to provide direct characterization of H-cluster degradation. This technique can be utilized to characterize interesting [FeFe]-hydrogenase mutations and natural variations. The [FeFe]-hydrogenase produced by *Chlamydomonas reinhardtii* (CrHydA) is particularly useful with this method because it lacks the iron-sulfur cluster containing ferredoxin-like domains that are present in CpI. Therefore, any visible absorption by iron-sulfur clusters in this protein or any modification of it is due to one or both of the active site subclusters.

Key advances during the 2011-2014 funding period include: (a) We have established a battery of hydrogenase specific activity assays and H cluster spectroscopic probes to assess oxygen

tolerance in a quantitative manner. Hydrogen oxidation and hydrogen production assays conducted at specific time points during oxygen exposure allow for the determination of a half-life as an indicator of relative oxygen tolerance. Comparative examination of the [FeFe]-hydrogenases from *Chlamydomonas reinhardtii* and *Clostridium pasteurianum* indicate significantly different levels of oxygen tolerance with the half life of the *C. pasteurianum* having a significant longer half life and higher oxygen tolerance that *C. reinhardtii* in line with the results of previous studies. (b) We have characterized the changes in microbial community structure and hydrogenase diversity as a function of the vertical transect of the water column in the Great Salt Lake. The findings reveal significant changes in community structure as a function of changing salinity and large hydrogenase diversity in the transition zone between the oxic and anoxic layers as well as the anaerobic water and benthic layers. (c) We have tested the hypothesis that sequence variations observed through the GSL water column include structural determinants for oxygen tolerance. Using both single amino acid substitution and cassette mutagenesis to probe the effect of observed natural sequence variations on oxygen tolerance and through single amino acid substitutions experiments have been able to single sites for which sequence variations result in clear differences in oxygen tolerance. (d) In collaboration with the Posewitz group we have identified and characterized a strain of Tetraselmis, *Tetraselmis GSL1*, that has robust hydrogen producing growth characteristics that the model organism *Chlamydomonas reinhardtii* including growth under halophilic conditions. (e) We have analyzed data on the distribution of 16S ribosomal RNA genes and HydA, [FeFe]-hydrogenase structural, genes in the water column of the Great Salt Lake in collaboration with the Posewitz group and have some interesting insights into the distribution of HydA in the water column and the influence of light intensity and oxygen concentration. (f) We have been examining specific sequence variations in the region of the active site H cluster and putative gas channels that correlate with differences in oxygen concentration in the water column and by site-specific amino acid substitution testing potential structural determinants for greater oxygen tolerance. (g) We have in collaboration with Paul King and David Mulder at the National Renewable Energy Laboratory (NREL) where we have been examining the mechanism of oxygen inactivation of [FeFe]-hydrogenases. We are interested in the mechanism of oxygen inactivation to provide additional insights into mechanisms to prevent it. We have concentrated our efforts on characterizing the spectroscopic properties and structural features of [FeFe]-hydrogenases exposed to controlled amounts of oxygen. The results of UV/Vis, EPR, and IR spectroscopic characterization indicate the initial site of oxygen attack is the 2Fe subcluster that becomes modified and then becomes depleted relative to the 2[4Fe-4S] subcluster. We have shown that oxygen inactivated hydrogenase can be reactivated in vitro through addition of new 2Fe subcluster by the activity of HydF produced in a genetic background having both HydE and HydG in the presence of a strong reducing agent. Structural characterization of inactive hydrogenase and intermediates supports that oxygen inactivation occurs through modification and depletion of the 2Fe subcluster and shows that the free cysteine thiol implicated in proton transfer has been oxidized. Presumably this explains in part the requirement for strong reducing conditions for activation. These observations provide significant new insights into activation and challenge the established paradigms. (h) We have sequenced the genome of the model hydrogen producing fermentative organism *Clostridium pastuerianum* and conducted preliminary transcriptional analysis. This organism expresses multiple [FeFe]-hydrogenases presumed to function in hydrogen production and hydrogen oxidation in response to different physiological conditions. The hypothesis based on mainly biochemical data was that one [FeFe]-hydrogenase

functioned in proton reduction during sugar fermentation to recycle reduced electron carriers. Also a model diazotroph, *C. pasteurianum*, is relieved of the burden of recycling electron carriers when fixing nitrogen and actually would benefit from capturing the reducing equivalents produced as hydrogen during the nitrogenase reaction. Presumably a proton reducing [FeFe]-hydrogenase is produced under non nitrogen fixing conditions and under nitrogen fixing conditions, this hydrogenase is down regulated in lieu of a second [FeFe]-hydrogenase that is unregulated and functions in hydrogen oxidation. Through sequence analysis and subsequent transcriptional analysis, we aimed to identify the hydrogenase involved in hydrogen oxidation during nitrogen fixation and through sequence comparison identify potential structural determinants (sequence motifs) that define superior proton reduction or hydrogen oxidation activity (or in others words the motifs that control the reaction equilibrium by effecting the proton donation and/or electron transfer reactions). We have completed this study and have identified the hydrogen oxidizing hydrogenase and have provided new insights into both hydrogen metabolism and nitrogen fixation in *C. pasteurianum* and have identified several features of sequence variation that could potentially fine tune enzymes toward proton reduction and hydrogen oxidation activities.

The results of studies from the three year funding period are detailed either in published works, submitted manuscripts, or draft manuscripts. Submitted manuscripts and draft manuscripts not yet published are attached in an appendix.

Appendix – Attached Manuscripts – AFOSR 2014 Final Report (John W. Peters)

Sarah D'Adamo , Robert E. Jinkerson, Eric S. Boyd, Susan L. Brown, Bonnie K. Baxter, John W. Peters, Matthew C. Posewitz **"**Evolutionary and Biotechnological Implications of Robust Hydrogenase Activity in Halophilic Strains of Tetraselmis" *PLOS One* 9(1):1-13 (2014)

Kevin D. Swanson, Michael W. Ratzloff, David W. Mulder, Jacob H. Artz, Shourjo Ghose, Andrew Hoffman, Spencer White, Oleg A. Zadvornyy, Joan B. Broderick, Brian Bothner, Paul W. King, and John W. Peters, "[FeFe]-hydrogenase oxygen inactivation is initiated by the modification and degradation of the H cluster 2Fe subcluster" *Submitted to J. Am. Chem Soc.*

David W. Mulder, Michael W. Ratzloff, Maurizio Bruschi, Claudio Greco, Evangeline Koonce, John W. Peters, and Paul W. King "Investigations on the role of proton-coupled electron transfer in hydrogen activation by [FeFe]-hydrogenase" *Submitted to J. Am. Chem Soc.*

John W. Peters, Gerrit J. Schut, Eric S. Boyd, David W. Mulder, Eric S. Shepard, Joan B. Broderick, Paul W. King, and Michael W. W. Adams "[FeFe]- and [NiFe]-Hydrogenase Diversity, Mechanism, and Maturation" *Submitted to Biochim. Biophys. Acta*

Eric S. Boyd, Trinity L. Hamilton, Kevin Swanson, Alta Howells, Bonnie K. Baxter, Matthew C. Posewitz, and John W. Peters "Distribution, Abundance, and Diversity of Multimeric Bifurcating [FeFe]-Hydrogenases Along a Vertical Redox Gradient in Great Salt Lake, USA" *Draft In preparation*

Jesse B. Therien, Trinity L. Hamilton, Zhenfeng Liu, Seth M. Noone, Paul W. King, Donald A. Bryant, John W. Peters "Draft genome and targeted transcriptional analysis of *Clostridium pasteurianum* (strain W5) provides insights into possible determinants of H_2 oxidation and reduction" *Draft In preparation*

OPEN ACCESS Freely available online

PLOS ONE

Evolutionary and Biotechnological Implications of Robust Hydrogenase Activity in Halophilic Strains of Tetraselmis

Sarah D'Adamo[1], Robert E. Jinkerson[1], Eric S. Boyd[2], Susan L. Brown[3], Bonnie K. Baxter[4], John W. Peters[2,5], Matthew C. Posewitz[1]*

1 Department of Chemistry and Geochemistry, Colorado School of Mines, Golden, Colorado, United States of America, **2** Department of Microbiology and the Thermal Biology Institute, Montana State University, Bozeman, Montana, United States of America, **3** Center for Marine Microbial Ecology and Diversity, University of Hawaii, Honolulu, Hawaii, United States of America, **4** Department of Biology and the Great Salt Lake Institute, Westminster College, Salt Lake City, Utah, United States of America, **5** Department of Chemistry and Biochemistry, Montana State University, Bozeman, Montana, United States of America

Abstract

Although significant advances in H_2 photoproduction have recently been realized in fresh water algae (e.g. Chlamydomonas reinhardtii), relatively few studies have focused on H_2 production and hydrogenase adaptations in marine or halophilic algae. Salt water organisms likely offer several advantages for biotechnological H_2 production due to the global abundance of salt water, decreased H_2 and O_2 solubility in saline and hypersaline systems, and the ability of extracellular NaCl levels to influence metabolism. We screened unialgal isolates obtained from hypersaline ecosystems in the southwest United States and identified two distinct halophilic strains of the genus Tetraselmis (GSL1 and QNM1) that exhibit both robust fermentative and photo H_2-production activities. The influence of salinity (3.5%, 5.5% and 7.0% w/v NaCl) on H_2 production was examined during anoxic acclimation, with the greatest in vivo H_2-production rates observed at 7.0% NaCl. These Tetraselmis strains maintain robust hydrogenase activity even after 24 h of anoxic acclimation and show increased hydrogenase activity relative to C. reinhardtii after extended anoxia. Transcriptional analysis of Tetraselmis GSL1 enabled sequencing of the cDNA encoding the FeFe-hydrogenase structural enzyme (HYDA) and its maturation proteins (HYDE, HYDEF and HYDG). In contrast to freshwater Chlorophyceae, the halophilic Tetraselmis GSL1 strain likely encodes a single HYDA and two copies of HYDE, one of which is fused to HYDF. Phylogenetic analyses of HYDA and concatenated HYDA, HYDE, HYDF and HYDG in Tetraselmis GSL1 fill existing knowledge gaps in the evolution of algal hydrogenases and indicate that the algal hydrogenases sequenced to date are derived from a common ancestor. This is consistent with recent hypotheses that suggest fermentative metabolism in the majority of eukaryotes is derived from a common base set of enzymes that emerged early in eukaryotic evolution with subsequent losses in some organisms.

Citation: D'Adamo S, Jinkerson RE, Boyd ES, Brown SL, Baxter BK, et al. (2014) Evolutionary and Biotechnological Implications of Robust Hydrogenase Activity in Halophilic Strains of Tetraselmis. PLoS ONE 9(1): e85812. doi:10.1371/journal.pone.0085812

Editor: Wagner L. Araujo, Universidade Federal de Vicosa, Brazil

Received June 7, 2013; **Accepted** December 2, 2013; **Published** January 21, 2014

Copyright: © 2014 D'Adamo et al. This is an open-access article distributed under the terms of the Creative Commons Attribution License, which permits unrestricted use, distribution, and reproduction in any medium, provided the original author and source are credited.

Funding: This research is part of the United States Air Force Office of Scientific Research under Grant FA9550-11-1-0211 and FA9550-11-1-0218. For the transcriptome part this research was funded in part by the Gordon and Betty Moore Foundation through Grant #2637 to the National Center for Genome Resources. The funders had no role in study design, data collection and analysis, decision to publish, or preparation of the manuscript.

Competing Interests: The authors have declared that no competing interests exist.

* E-mail: mposewit@mines.edu

Introduction

The phylogenetically unrelated NiFe- and FeFe-hydrogenases have convergently evolved to catalyze the reversible reduction of protons to H_2 ($2H^+ + 2e^- <=> H_2$) [1]. Several recent studies have documented the diversity of hydrogenase-encoding genes in environments that span a broad range of geochemistry [2–8]. In some systems, e.g., terrestrial or marine hydrothermal communities, H_2 oxidation has been suggested to represent the primary mechanism of energy conservation [9], [10]. Yet, in other systems, e.g., terrestrial or intertidal phototrophic communities, H_2 evolution appears to be of critical importance to the functioning of the assemblage, in particular at night when the systems become net sources of H_2 [11–13].

Biological H_2 production requires low-potential reducing equivalents derived from either fermentative pathways that oxidize fixed carbon (typically carbohydrates), or from photosynthetic pathways [14–19]. Several eukaryotic algae generate fermentative H_2 during dark, anoxic acclimation as part of a suite of fermentative pathways that catabolize carbohydrates to alcohols, organic acids and H_2, which are secreted. These metabolites likely provide a rich source of carbon building blocks and reducing equivalents to organisms inhabiting ecological niches adjacent to the algae, which are responsible for the majority of primary productivity during the day. Algae are also able to use reducing equivalents from the photosynthetic electron transport chain under some conditions to directly reduce hydrogenases at the level of ferredoxin without the input of ATP, a pathway that is theoretically regarded as the most efficient biological means to transform the energy in sunlight to H_2 for biotechnological applications [19–23]. To date, only FeFe-hydrogenases have been unambiguously identified in algae, with organisms such as Chlamydomonas reinhardtii encoding truncated enzymes with only the catalytic H-cluster; a 4Fe4S cluster linked via a bridging

cysteine to a two Fe center coordinated by CN^-/CO ligands and a bridging dithiolate. In contrast, Chlorella variabilis NC64A encodes two hydrogenase enzymes with both the H-cluster catalytic domain and an F-cluster domain that coordinates additional FeS clusters that putatively function in electron transfer [18], [19], [24–26].

Despite widespread interest in algal H_2 production, contemporary research is focused almost exclusively on freshwater species of Chlamydomonas, Scenedesmus, and Chlorella, with C. reinhardtii being the model system for the vast majority of algal hydrogenase research [27], [28]. Significant advances in H_2 photoproduction from C. reinhardtii have recently been reported [29–33]; whereas relatively few studies have examined H_2 production from marine or halophilic algae [34–36].

Halophilic algae offer several advantages for large-scale algal H_2 production. First, the use of halophilic algae will enable H_2 production in readily available salt water, thereby minimizing the potential use of limited fresh water resources. Secondly, gas solubility is reduced in aquatic saline systems [37], which is potentially advantageous because the levels of soluble O_2, a potent inhibitor of most FeFe-hydrogenases [38], are diminished in salt water relative to fresh water. Hydrogen is also less soluble in saline systems and therefore more easily removed. Lastly, ATP hydrolysis is increased in saline media to maintain proper cellular ion gradients. Hydrogenase activity is an ATP neutral process, and photosynthetic electron transport has been shown to decline as photosynthetic ATP levels rise during H_2 photoproduction in some freshwater algae [39], [23]. Salt stress represents a potential mechanism to alleviate ATP accumulation, which can inhibit the metabolic pathways supplying reductant to hydrogenase.

To further expand our understanding of H_2 metabolism in extreme environments, and to potentially discover novel organisms with enzymes that have superior biotechnological attributes, we initiated an effort to isolate hydrogen-producing organisms from hypersaline ecosystems. Although salt water systems are ubiquitous around the world, relatively little is known regarding H_2 metabolism in saline systems, or whether unique enzyme features are necessary for activity in halophiles [40], [41].

Methods

Algal strains and growth conditions

Halophilic algae from the genus Tetraselmis (Chlorophyceae) were isolated from water samples collected at (a) a roadside pool bordering the Great Salt Lake (GSL), Utah, USA, with a salinity of 6.0% w/v (Tetraselmis GSL1) and (b) a hypersaline pond with a conductivity reading of 660 mS/cm near Quemado, New Mexico, USA [42] (Tetraselmis QNM1). GSL samples were taken in conjunction with the Great Salt Lake Institute, which holds a permit for sampling on Utah state lands, granted by the Utah Department of Natural Resources, Division of Forestry, Fire and State Lands. Water sampling at the New Mexico site was conducted on public lands administered by the Bureau of Land Management, and did not require a permit nor involve endangered or protected species. Both Tetraselmis isolates have been submitted to the University of Texas (UTEX) algal culture collection.

Isolates were routinely cultured in f/2 medium amended with Booth Bay sea water (National Center for Marine Algae and Microbiota, NCMA), at pH 8.0 [43] and 3.5% of salinity. Where indicated, salinities were increased to 5.5% or 7.0% w/v with NaCl addition. Cultures were maintained at 29°C, without agitation at a constant illumination of ~30 μmol m^{-2} s^{-1} of photosynthetically active radiation (PAR) by cool-white fluorescent lights. Cell counts were assessed using a Z2 Coulter cell and particle counter (Beckman-Coulter).

C. reinhardtii strain CC124 (nit^-, mt^-) was obtained from the Chlamydomonas Genetic Center (http://www.chlamy.org/) and grown in tris–acetate–phosphate (TAP) medium pH 7.2 [44], and shaken at 120 rpm under constant fluorescent irradiance (80 μmol m^{-2} s^{-1} of PAR by GE Ecolux 6500K T5 bulbs). Cells were harvested during mid-logarithmic growth (16–20 μg Chl/ml) for measuring in vitro hydrogenase activities and fermentative H_2 production.

Chlorophyll and total protein determination

Total chlorophyll was determined spectrophotometrically by extraction in 100% methanol for the Tetraselmis strains and 95% ethanol for C. reinhardtii [44]. Tetraselmis cells were washed with 2 volumes of MilliQ water to remove salt prior to pigment extraction. Total chlorophyll was selected as the standard in normalizing hydrogenase activity with the light-absorbing capacity of isolates.

Total protein content was analyzed using a Modified Lowry Protein Assay (Pierce) according to the manufacture's instructions. Cell pellets were washed with 2 volumes of MilliQ water and then solubilized in 0.5% SDS. Total protein was quantified using BSA solubilized in 0.5% SDS to generate a standard curve.

Anaerobic induction

For H_2-photoproduction measurements, 75 ml of mid-log phase cell cultures were grown at the indicated NaCl levels (3.5%, 5.5% and 7.0% w/v), concentrated by centrifugation at 3716 × g for 15 min at 25°C, resuspended in 1 ml of f/2 medium (at the same salinity used for culturing) and transferred to 16-ml glass serum vials covered with aluminum foil to exclude light. For fermentative metabolite analyses, dark H_2-production and CO_2-evolution measurements, 50 ml of mid-log phase cell cultures were harvested, resuspended in 1 ml of fresh medium, and transferred to 16-ml glass serum vials covered with aluminum foil. For in vitro hydrogenase activity assays (see below), 1 ml of mid-log liquid cell cultures was directly transferred to anaerobic vials. For C. reinhardtii, in vitro hydrogenase activity and fermentative H_2 production, 5 ml of cells from mid-log cultures were harvested by centrifugation (3190 × g for 10 min) and resuspended in 1 ml of anaerobic induction buffer (AIB; 50 mM potassium phosphate buffer, pH 7.2, 3 mM $MgCl_2$), then transferred to 13-ml glass serum vials covered with aluminum foil. All vials were sealed with septa, purged for 30 min with ultra-high purity argon and kept sealed in the dark for 4 h or 24 h, as indicated.

H_2-photoproduction measurements

Maximum in vivo H_2-photoproduction rates were determined using a custom-built Ag/AgCl polarographic electrode system (ALGI). H_2- and O_2-photoproduction rates were measured simultaneously with two YSI 5331A electrodes (YSI Incorporated, Yellow Springs, OH, USA), poised at +/− 0.6 V, in a water-jacketed (25°C) assay chamber. O_2 and H_2 electrodes were calibrated between each measurement using f/2 medium (at the respective salinity of tested cells) saturated by atmospheric O_2 or by ultra-high purity 5.3% H_2 (Ar balance), respectively. Pure Ar purging was used to determine electrode baselines and to sparge the assay chamber containing 0.8 ml of f/2 medium of O_2. 0.2 ml of 4 h and 24 h anaerobically induced cells were then introduced into deoxygenated buffer in the sample chamber. After a 30 s dark acclimation, cells were illuminated for 30 s, using saturating LED (Luxeon III Star, Lumileds) irradiance of 2000 μmol photons m^{-2} s^{-1}. H_2-photoproduction rates were calculated from the initial

slope during the first 10 s of illumination from the H_2-dependent current increase.

In vitro hydrogenase activity

In vitro Tetraselmis GSL1 and QNM1 H_2-production activity assays were performed by transferring 1 ml of 2X methyl viologen (MV) buffered solution (10 mM MV, 50 mM potassium phosphate, pH 6.9, and 0.2% triton X-100) and 0.2 ml of reduced sodium dithionite solution (100 mM in 30 mM NaOH) to 1 ml of cells grown in f/2 at the indicated salinities and acclimated to anoxic conditions in f/2 medium at the same salt levels used for culturing for 4 h or 24 h in sealed, Ar-purged 16-ml vials. For the data in Table S1, the in vitro hydrogenase activity protocol was modified for direct comparison of Tetraselmis in vitro hydrogenase activity to the in vitro hydrogenase activity from the fresh water alga C. reinhardtii using final MV assay solutions that were equivalent in salt concentrations for the different species. To obtain the same final assay buffer composition, C. reinhardtii cells grown in TAP medium, were resuspended in 1 ml of AIB and acclimated to anoxic conditions for 4 or 24 h in sealed, Ar-purged 13-ml vials. 1 ml of either a 2X MV solution (10 mM MV, 50 mM potassium phosphate, pH 6.9, and 0.2% triton X-100), used as a control, or 2X MV-f/2 adjusted solutions (10 mM MV, 50 mM potassium phosphate, pH 6.9, and 0.2% triton X-100 dissolved in f/2 medium and adjusted to 3.5%, 5.5% or 7.0% NaCl) was added to measure hydrogenase activity. To 1 ml of the Tetraselmis cells grown and anaerobically induced in f/2 medium at 3.5%, 5.5% or 7.0% NaCl, 1 ml of 2X MV-AIB (10 mM MV, 100 mM potassium phosphate, pH 6.9, 3 mM $MgCl_2$) was added. 0.2 ml of reduced sodium dithionite (100 mM in 30 mM NaOH) was then added to initiate hydrogenase mediated H_2 production in all assays. The reactions were incubated (37°C) in a shaking water bath and H_2 evolution measured for C. reinhardtii, and the Tetraselmis strains by gas chromatography (GC) using a Hewlett Packard Series II 5890 instrument fitted with a Restek 5 Å Molecular Sieve 80/100 6′ 1/8″ column and a thermal conductivity detector with Ar as the carrier gas. The resulting signal was integrated using ChemStation software and H_2 was quantified using a standard curve generated from known quantities of H_2.

Dark fermentative H_2, CO_2 production

Following acclimation of cells to dark, anoxic conditions for 4 or 24 h, H_2 production was measured by withdrawing 0.2 ml of headspace gas and analyzing by GC for both C. reinhardtii and the Tetraselmis strains. CO_2 production was also measured from cells acclimated to dark, anoxic conditions (0.5, 4 and 24 h). To sealed vials containing acclimated cells, 1 ml of 1 M HCl was added. The acidified cell suspension was then shaken vigorously to liberate CO_2 into the vial headspace, and CO_2 (0.2 ml injection) was quantified by GC (Hewlett Packard 5890 series II) using a Supelco column (80/100 PORAPAK) coupled to a thermal conductivity detector using He as the carrier gas. The resulting signal was integrated using ClassVP software, and the gas was quantified using a standard curve generated from known quantities of CO_2.

Dark fermentative metabolite analyses and intracellular sugar content

After 4 or 24 h of dark-anoxic acclimation, fermentative products were analyzed by high pressure liquid chromatography (HPLC). Samples were collected after centrifugation of acclimated cells (3 min at 17000 × g) and the resulting supernatant filtered through a silicon filter (0.45 µm). Filtrate (25 µl) was injected (thermostated sample tray held at 10°C) onto an HPLC column (fermentation monitoring column (BioRad), 150×7.8 mm, 8 mM H_2SO_4 as eluent, flow rate of 0.5 ml/min, column operating temperature of 45°C, refractive index (RI) detector operating temperature 50°C, in parallel with a photodiode array detector (PAD) at 210 nm). Resulting signals were integrated and metabolites quantified using a standard curve generated from standards for each metabolite detected. The remaining cell pellet was used for determining cellular dry weights and the reducing carbohydrate content. Cell pellets were resuspended in the same volume of MilliQ water, with 100 µl used for total quantification by the anthrone assay as described previously [25], and the remaining cells used for dry weight determination.

Genomic DNA, total RNA isolations and sequencing

Genomic DNA from Tetraselmis GSL1 and Tetraselmis QNM1 was isolated from 15 ml of cell culture using a phenol:chloroform extraction protocol as described previously [45]. Total RNA was isolated from 20 ml of 100-fold concentrated mid-log Tetraselmis GSL1 cells grown in f/2 at 3.5% salinity and anaerobically induced in 60 ml sealed, Ar-purged vials for 4 h. Fermentative H_2 production was confirmed by GC before RNA isolation. Briefly, a cell pellet was obtained by centrifugation (3716 × g for 10 min at 25°C), washed with 2 volumes of MilliQ water followed by centrifugation, then resuspended in 5 ml of Plant RNA Reagent (Invitrogen) with RNA isolated according to the manufacturer's instructions for small scale RNA isolation, with the exception that all reagent volumes were multiplied by a factor of 10. Total RNA was concentrated using the RNeasy MinElute Cleanup Kit (Qiagen), according to the manufacturer's instructions. RNA quality was confirmed via 2% agarose gel electrophoresis and quantified using a NanoDrop® ND-1000 (Thermo scientific), as well as by fluorescence using Quant-iT™ RiboGreen® RNA Reagent and Kit (Invitrogen). All purification steps were done with RNase free reagents.

Total RNA was submitted for sequencing to the National Center for Genome Resources (NCGR, Santa Fe, NM) as part of the Marine Microbial Eukaryote Transcriptome Project (Gordon and Betty Moore Foundation). RNA libraries were prepared from total RNA isolated using the standard Tru-Seq™ RNA protocol - poly-A+ selection (Illumina) with an insert size of ~200 bp and sequenced from both ends (paired-end reads 2×50-nt) on the Illumina Hi-Seq 2000. The total sequence data generated for each sample (MMETSP0419_1 & 2) was approximately 2.5 Gbp. Reads were filtered for quality (Q15) and read length (0.5).

Transcriptome Assembly

AbySS [46] was used to generate 20 assemblies across a k-mer sweep from 26 to 50 nt. These assemblies were then subjected to gap closing with GapCloser v 1.10 (Short Oligonucleotide Analysis Package, SOAPdenovo [47]). Gap closed assemblies from the k-mer sweep were reconciled into one assembly using miraEST [48].

Identification of hydrogenase structural and maturation genes

Hydrogenase structural and maturation genes within the Tetraselmis GSL1 transcriptome assembly were identified using tBLASTn (NCBI). HYDA, HYDEF and HYDG from Chlamydomonas reinhardtii (CAC83731, AAS92601, AAS92602, respectively) and Chlorella variabilis NC64A sequences (AEA34989, EFN57384, EFN57653, respectively) were used as search queries. Assemblies of all identified homologs were manually inspected.

RNAseq reads were mapped back to these assemblies using GSNAP (Genomic Short-read Nucleotide Alignment Program) to determine coverage and transcript variation. Mapped reads were reassembled with Geneious (v.5.5.7, Biomatters) to validate the AbySS assembly.

To verify the presence of an unfused HYDE gene, PCR amplification of genomic Tetraselmis GSL1 DNA was used to amplify a region of the unfused, independent HYDE from the 3′-coding region (EU-F1 5′CGACAAGAAGGCCCACCTG-GAGA3′) to the 3′UTR of HYDE (EU-R1 5′ GCGTACCTCGCCTGCCCTTACTA 3′), which spans the unfused HYDE stop codon. To verify the presence of the HYDEF fusion in gDNA, primers corresponding to the 3′-region of the HYDE segment in the HYDEF fusion (EF-F1 5′ GTCCCGCTACCTTGTCCGCATTG 3′) and to the 5′-region of HYDF in HYDEF (EF-R2 5′GAATGTGTGCC-GAGCTGTGCT 3′) were used, which spans the HYDEF fusion sequence and does not contain a stop codon after the HYDE gene segment. PCR conditions included: polymerase activation: 95°C 2 min, 40 cycles: denaturing 95°C 20 s, annealing 60°C 20 s, elongation 72°C 30 s, and a final elongation at 72°C for 5 min using the KOD DNA polymerase and master mix (Promega). Amplified products were sequenced using the Davis DNA sequencing facility (Davis Sequencing). All retrieved sequences have been deposited in GenBank under the accession numbers: KC820787-KC820794, and KC832401.

Molecular phylogeny

DNA was isolated from algal colonies grown on agar using the UltraClean Soil DNA Isolation Kit (MoBio Laboratories). Partial 18S SSU rRNA genes (>1350 and 1120 bp, respectively), for Tetraselmis GSL1 and Tetraselmis QNM1 were amplified and sequenced from each alga using the eukaryote-specific primers 360FE and 1492RE [49]. Sequences were aligned using the NCBI BLAST algorithm queried against the nr/nt database. The complete Tetraselmis GSL1 18S SSU rRNA gene (1802 bp) was attained from transcriptome data and deposited in GenBank (accession no. KC820794).

The phylogenetic position of HYDA relative to representatives available in databases [50] was determined using maximum likelihood approaches similar to those described previously [7], [51]. Briefly, HYDA homologs were aligned using the Gonnet substitution matrix specifying a gap opening penalty of 13 and a gap extension penalty of 0.05. The alignment block was trimmed to contain only the aligned positions corresponding to the H-cluster only homolog, HYDA1, from C. reinhardtii (CAC83731). The phylogenetic position of HYDA from Tetraselmis GSL1 was determined using PhyML (ver. 3.0) [52] specifying the LG substitution model with gamma distributed rate variation and a proportion of invariable sites, as recommended by ProtTest (ver. 3.2.1) [53]. A HYDA paralog, i.e., Nar1, from Saccharomyces cerevisiae, served as the outgroup in the phylogenetic analysis of HYDA.

To further increase the resolution of our phylogenetic analysis of the FeFe-hydrogenase identified in the transcriptome of Tetraselmis GSL1, we compiled homologs of HYDA, HYDE, HYDF, and HYDG from all eukaryotes with available genomes. All homologs were aligned and trimmed as described above. Alignment blocks were concatenated using base functions within PAUP (ver. 4.0) [54] and the phylogenetic position of the HYDAEFG concatenated alignment was determined using PhyML as described above. HYDAEFG homologs from Bacteroides thetaiotaomicron VPI-5482, served as the outgroup in this phylogenetic analysis.

Results

Identification of hydrogenase activity in halophilic strains of Tetraselmis

To assess whether algae with hydrogenase activity are present in hypersaline environments, water samples were collected from a variety of GSL sites with salinities ranging from 3.5–25%, and unialgal isolates from these water samples were obtained using flow cytometry. Hydrogenase activity screens of over 40 unialgal isolates recovered from GSL using the reduced MV assay revealed that the most robust hydrogenase activity was detected from a tetraflagellate alga that morphology and 18S rRNA gene analysis indicated to be a novel strain of Tetraselmis (Tetraselmis strain GSL1), isolated from a roadside pool bordering GSL with a salinity of 6.0% w/v. Notable hydrogenase activity was not detected in any of the isolated strains of Dunaliella, which have been shown to be the numerically dominant alga in several GSL environments [55]. We also obtained an axenic culture of another halophilic strain of Tetraselmis (Tetraselmis QNM1), which was isolated from a hypersaline pond in New Mexico and was available in the Colorado Center for Biofuels and Biorefining algal culture collection [42]. Tetraselmis GSL1 and Tetraselmis QNM1 18S rRNA genes are most similar to the recently described Tetraselmis indica, isolated from salt pans in Goa, India [56]. Both Tetraselmis GSL1 and Tetraselmis QNM1 remained viable at NaCl concentrations greater than 10%, but growth was reduced at these NaCl levels. Therefore, subsequent characterization of hydrogenase activities in the Tetraselmis isolates were done at a comparable ocean salinity of 3.5%, as well as at the increased salinities of 5.5% and 7.0% (the later concentrations are similar to the salinity where this taxon was isolated) to determine the effects of elevated NaCl concentrations on hydrogenase activity. As shown in Figure 1, the highest growth rates and cell densities are observed in medium with 3.5% NaCl, with growth rates declining as NaCl concentration is increased. In the case of Tetraselmis QNM1, cells reached stationary phase earlier when cultured at 7.0% NaCl, yet final cell densities were approximately 50% lower.

Hydrogenase activity in vitro as a function of salinity

Given previous data indicating that salt levels impact algal metabolism and protein expression [41], [57–60], hydrogenase activity was assessed after culturing at 3.5%, 5.5% and 7.0% NaCl concentrations. Cells were acclimated in the dark under anoxic conditions for 4 or 24 h prior to measurement of in vitro hydrogenase activities using cell extracts and reduced MV. As shown in Figure 2, significant hydrogenase activity is observed in cultures grown at all three NaCl concentrations, with a diminution of total in vitro activity as extracellular NaCl levels increase for both strains. The in vitro hydrogenase activity measured at 3.5% NaCl is more than an order of magnitude greater than the in vitro hydrogenase activity typically reported on a chlorophyll basis for C. reinhardtii [61]. As the ionic strength of the assay buffer can influence the measured in vitro hydrogenase activity [62], we tested whether the differences in hydrogenase activity can be attributed to the higher ionic strength used to measure the Tetraselmis MV-mediated hydrogenase activity. As shown in Table S1, when both the Tetraselmis strains and C. reinhardtii are assayed using equivalent final MV assay solutions at variable salt levels, the Tetraselmis strains still show in vitro hydrogenase activity that is about an order of magnitude greater than the rates from C. reinhardtii, with the greatest differences emerging at the 24 h time point (up to ~30 fold at 24 h and 1.6% NaCl). We also assessed hydrogenase activity as a function of total protein levels (Table S1), and again hydrogenase activity was approximately an

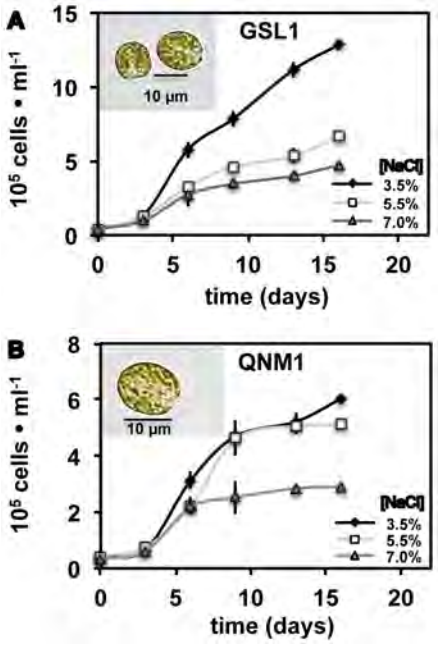

Figure 1. Cell densities in f/2 medium adjusted to 3.5%, 5.5% or 7.0% NaCl (w/v). Tetraselmis GSL1 (A) and Tetraselmis QNM1 (B) cell numbers were determined using a Beckman Z2 Coulter particle counter. Error bars represent standard deviations from 6 experimental repetitions. Representative light microscope images from cells grown at 3.5% NaCl are inset.
doi:10.1371/journal.pone.0085812.g001

order of magnitude greater than is observed from C. reinhardtii after 24 h of anaerobic induction, and ~5 times higher at 4 h of anaerobic induction, when the NaCl levels in the MV assay are equivalent.

Hydrogen photoproduction activities in vivo

Hydrogen photoproduction was assayed using a custom-built, Clark-type electrode [61] (Fig. 3). Both Tetraselmis strains showed significant H_2-photoproduction rates (albeit ~2-fold less than those attained in C. reinhardtii, when rates were normalized to total chlorophyll at 4 h of anoxic acclimation), indicating that hydrogenase activity is coupled to the photosynthetic electron transport chain, as is observed in several species of the Chlorophyceae [50]. In contrast to the results of the MV in vitro hydrogenase assays, H_2 photoproduction in Tetraselmis GSL1 increased slightly as a function of salinity. Given that the in vivo H_2-photoproduction rates are significantly lower (~30 fold) than the measured in vitro (i.e., MV assays) rates, excess enzyme capacity exists under these conditions relative to the amount of reductant supplied by the photosynthetic electron transport chain for H_2 production. These results suggest that although the amount of active enzyme decreases as a function of salinity, the efficiency of hydrogenase coupling to the photosynthetic electron transport chain increases. Interestingly, in C. reinhardtii and other green algae, the in vivo hydrogenase activity levels are frequently similar to the in vivo H_2-photoproduction rates [61], which is not observed in the two Tetraselmis isolates studied. Similar to the in vitro assays, H_2-photoproduction rates increased (~2–3 fold) at 24 h relative to 4 h of dark, anoxic acclimation. H_2-photoproduction rates were higher (~3–4 fold) than those of C. reinhardtii (Table S1) when normalized to total chlorophyll following 24 h of dark, anoxic acclimation [61].

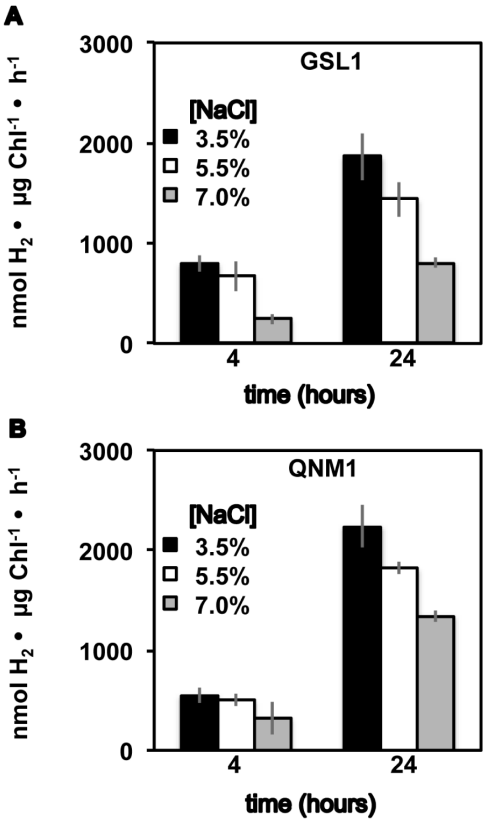

Figure 2. Methyl viologen mediated in vitro hydrogenase activity. Hydrogen production rates from anoxic Tetraselmis GSL1 (A) and Tetraselmis QNM1 (B) cell extracts incubated with reduced dithionite. Cultures were grown and then acclimated to dark, anoxic conditions in f/2 medium at the indicated NaCl levels (w/v). Error bars represent standard deviations from 8 experimental repetitions.
doi:10.1371/journal.pone.0085812.g002

Fermentative metabolite analysis

Fermentative H_2 was detected in the gas phase of cultures of both Tetraselmis GSL1 and Tetraselmis QNM1 following dark, anoxic acclimation (Fig. 4), with H_2 yields being among the highest reported to date for green algae (e.g., ~20 fold higher on a per chlorophyll basis than those observed in C. reinhardtii (Table S1)). Both Tetraselmis strains also accumulated CO_2 in the headspace (Fig. 4) during fermentation, as would be expected if H_2 production was linked to the oxidative decarboxylation of pyruvate by pyruvate-ferredoxin oxidoreducase with subsequent electron transfer from ferredoxin to hydrogenase [63], [64]. The identification of extracellular formate, acetate, and ethanol in the medium following acclimation to dark, anoxic conditions (Fig. 5) suggests that these algae employ a classic heterofermentation pathway, similar to that which has been observed in other green algae [18]. Metabolite analyses indicate up to a 4-fold increase in fermentative product accumulation at 24 h of dark, fermentation relative to 4 h, demonstrating the ability of these Tetraselmis strains to maintain prolonged anoxic metabolism.

Carbohydrate metabolism

Total sugar content was determined using the anthrone assay [25] since it is likely that carbohydrates serve as fermentable substrates in Tetraselmis. As shown in Table 1, concentrations of total reducing sugars increase as a function of higher salinity, consistent with the accumulation of organic osmolytes, as has been

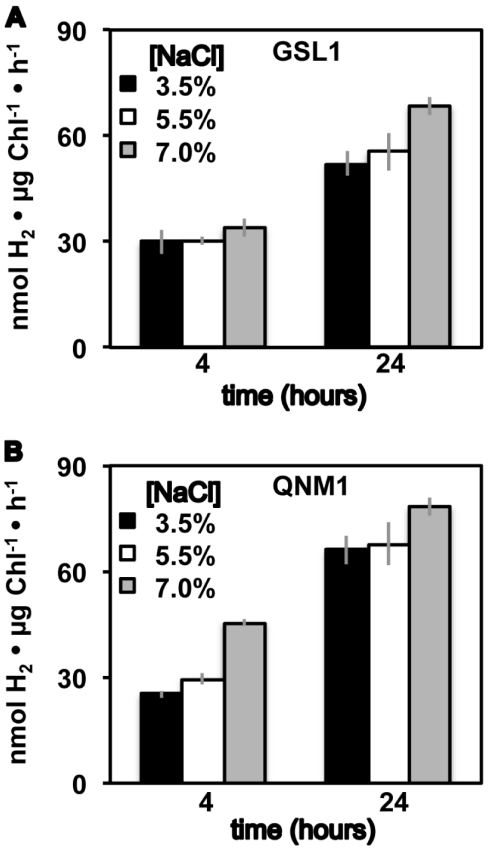

Figure 3. In vivo H_2-photoproduction rates. Hydrogen production rates after illumination of dark, anoxic cultures of Tetraselmis GSL1 (A) and Tetraselmis QNM1 (B). Bar graphs indicate maximal initial H_2-photoproduction rates measured using a custom built Clark-type electrode. Cells were grown and acclimated to dark, anoxic conditions in f/2 medium at the indicated NaCl levels (w/v). Error bars represent standard deviations from 10 experimental repetitions.
doi:10.1371/journal.pone.0085812.g003

observed in other halophilic algae and cyanobacteria [41], [65], [66]. During acclimation to dark anoxia, carbohydrate degradation was observed concomitant with fermentative product secretion. Approximately 30–50% of the carbohydrate accumulated was catabolized at the end of 24 h of anoxia. Paralleling the increase in total carbohydrate as a function of salt concentration, an increase in fermentative metabolites is observed at higher NaCl concentrations, indicative of increased metabolic flux through fermentation. Salt-induced osmotic stress has previously been reported to increase carbohydrate and lipid content in green algae and cyanobacteria, and salt-stress cycling has previously been applied for improving biofuel yields [65], [66].

Transcriptome analysis and hydrogenase gene isolation

Attempts to amplify Tetraselmis GSL1 HYDA1 from genomic DNA or transcript preparations using degenerate primers [7] were unsuccessful. We therefore used whole transcriptome sequencing from Tetraselmis GSL1 after 4 h of anoxic acclimation for gene discovery [67]. From the transcriptome dataset, full length transcripts with homology to the hydrogenase structural gene (HYDA [24]), as well as the hydrogenase maturases (HYDE, HYDEF, and HYDG [68], [69]) were attained. Only one FeFe-hydrogenase gene (HYDA) that encodes an H-cluster domain, but that lacks any F-cluster domains, was identified. For all other green algae exhibiting hydrogenase activity, and with available transcriptome/genome data, at least two FeFe-hydrogenases are present, with Chlorophytes (e.g., Chlamydomonas and Scenedesmus) encoding H-cluster only enzymes and Chlorella NC64A (Trebouxiophyceae) encoding two FeFe-hydrogenases with both the H-cluster domain and additional F-cluster binding domains [25]. There are several explanations that may account for the detection of only one HYDA homolog: (a) Tetraselmis GSL1 contains only a single HYDA isoform, which would be the first report of a single HYDA isoform in a Chlorophyceaen alga; (b) other HYDA isoform(s) exist in the Tetraselmis GSL1 genome but are not expressed at a sufficient level for detection using our assay conditions; or (c) other HYDA isoform(s) are present in the Tetraselmis GSL1 genome but are no longer expressed and therefore not detectable by transcriptome sequencing.

Also unexpected in the transcriptome data was the finding that a HYDE homolog not fused to HYDF is observed as an independent transcript. To date, all other sequenced green algae with hydrogenase activity contain only a HYDEF fusion, and this is the first time that a transcript encoding an independent HYDE has been observed in a green alga. Tetraselmis GSL1 also has a second transcript encoding a gene with HYDE homology that is fused with HYDF (HYDEF). The independent HYDE transcript has a 3′ untranslated region (UTR) and translation stop site, whereas in the HYDEF fusion, the HYDE portion of the gene is fused in frame with the HYDF coding sequence (Fig. S1). The HYDE section of the HYDEF fusion lacks both the last 19 nucleotides found in the independent HYDE coding DNA sequence (CDS), as well as the HYDE 3′ UTR. This CDS deletion effectively removes the translation stop site and the last 6 amino acids at the C-terminus of HYDE. An intronic sequence at the 3′ end of the HYDE region in HYDEF allows an in frame fusion with the 5′ end of the HYDF gene (Fig. S1). The presence of a single HYDF independent of the HYDEF fusion is not supported due to the lack of transcriptional evidence for an independent HYDF 5′UTR and translation start site; however, we cannot eliminate the possibility of a genomic copy of HYDF not expressed under our conditions.

The presence of a single HYDE gene, as well as a HYDEF fusion was verified by PCR using genomic DNA. Primers were designed to amplify only the HYDE gene (sequences complimentary to the C-terminus region of HYDE coding sequence and to the HYDE 3′ UTR downstream of the stop codon); and another primer set to amplify only the HYDEF fusion (primers corresponding to the C-term region of the HYDE coding sequence and the N-terminus region of the HYDF coding sequence). We confirmed that (a) an independent HYDE gene (not fused to HYDF) with a discrete stop codon and 3′UTR and (b) a fused HYDEF that has neither the HYDE 3′UTR, nor a stop codon after the HYDE coding sequence are encoded in the Tetraselmis GSL1 genomic DNA. Sequencing of a gDNA PCR product that spans the region between HYDE and HYDF within the HYDEF fusion revealed an additional intron not present in the independent HYDE that directly connects to an exon of the HYDF coding sequence. In sum, these data are consistent with a simple fusion between what was the 5′ UTR of HYDF to the last exon of a copy of HYDE, effectively eliminating the stop codon and 3′ UTR of this HYDE, which generates a new intron connecting HYDE and HYDF coding sequences. As a negative control, primers were designed corresponding to the 3′UTR of HYDE and the N-terminal coding sequence of HYDF, and as expected no PCR product was obtained.

The relative expression of each transcript was determined and averaged for two biological replicates (Table 2). The hydrogenase

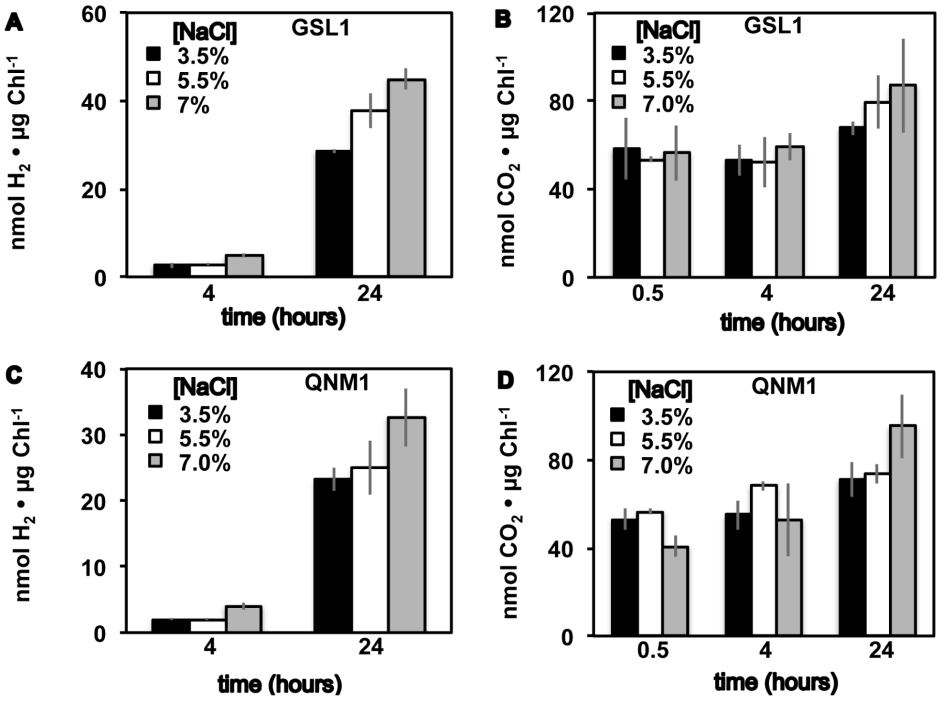

Figure 4. H_2 and CO_2 levels after dark, anoxic acclimation. H_2 (A, C) and CO_2 (B, D) detected from sealed vials during dark, anoxic acclimation of Tetraselmis GSL1 (A, B) and Tetraselmis QNM1 (C, D). Cells were grown and acclimated to anoxia in f/2 medium adjusted to the indicated NaCl levels (w/v). Error bars represent standard deviations from 14 (H_2) and 6 (CO_2) experimental repetitions.
doi:10.1371/journal.pone.0085812.g004

structural gene (HYDA) had the highest expression levels of all hydrogenase related genes and was the 16th most abundant transcript in the entire transcriptome assembly, suggestive of a key role in the anoxic proteome and consistent with the substantial levels of in vitro hydrogenase activity in this alga. Both HYDE and HYDG are expressed at commensurate levels with ~10-fold fewer transcripts than HYDA. Surprisingly HYDEF is only expressed at ~10% of the levels of HYDE and HYDG (100-fold less abundant than HYDA).

Single nucleotide polymorphisms (SNPs) were found in all of the hydrogenase related transcripts (Table 3 and Table S2). The HYDA transcript had the most SNPs detected at 39, while HYDG had only a single SNP. The majority of SNPs are synonymous nucleotide substitutions that result in no amino acid change (Table 3). Of the 34 SNPs detected in the HYDA CDS, only 6 of these result in amino acid changes, all of which occur at the N-terminus end of the peptide and are located outside of active site regions. Genomic sequencing of the fusion region of HYDEF revealed only four SNPs between the HYDE portion of HYDEF relative to the independent HYDE transcript.

Phylogeny of hydrogenase and maturase enzymes

We recently described the presence of two genes encoding HYDA in the green alga Chlorella variabilis NC64A, which is the only representative of the Chlorophyta known to date that has FeFe-hydrogenases containing F-cluster domains [25]. Additionally, this study determined that all algal hydrogenase H-clusters sequenced to date are monophyletic, indicating a single common ancestor for the incorporation of hydrogenase activity in algal metabolism [25]. We also recently sequenced the genome of the marine alga Nannochloropsis gaditana (Eustigmatophyceae) [70] and observed the presence of a single FeFe-hydrogenase encoding both H- and F-cluster domains in this alga [71]. As shown in Figure 6, rigorous phylogenetic analyses demonstrate that the recently obtained algal HYDA sequences from Tetraselmis GSL1 and N. gaditana are also monophyletic with the other algal FeFe-hydrogenases. This is somewhat surprising given the evolutionary distance between Nannochloropsis and Tetraselmis, and indicates a relatively early origin of algal FeFe-hydrogenases, algal H_2 metabolism, and possibly algal fermentation pathways. Additionally, as the Nannochloropsis and Tetraselmis hydrogenases are the first full-length marine/halophilic sequences available, this data indicates that hydrogenases in both salt-water and fresh-water algae are derived from a common ancestor.

As expected, HYDA from Tetraselmis GSL1 nested with the Chlorophyceae, supporting the highest max score and smallest e-value obtained when aligned with C. reinhardtii (392 and 9e-136, respectively), compared to C. variabilis NC64A enzymes (367 and 3e-123) or using blastx CDS alignment (best four results Chlamydomonas moewusii, Volvox carteri, Acutodesmus obliquus, all in the Chlorophyceae). Curiously, while HYDA phylogenetic analyses placed Tetraselmis GSL1 as a sister clade of the Chlorophyceae and placed C. variabilis NC64A basal along with the more ancestral N. gaditana, concatemeric analysis of HYDAEFG sequences suggests a sister clade position for Tetraselmis and Chlorella members; N. gaditana branches basal among algae with genome sequences available. The discrepancy associated with the branching order of Tetraselmis GSL1 and N. gaditana HYD phylogeny when either HYDA is analyzed alone or when HYDAEFG are considered together may arise from differences in the number of available sequences used to construct the trees, leading to bias in the concatenated analysis. Alternatively, these results may suggest slightly different evolutionary histories or selective pressures that have acted on the structural enzyme, HYDA, and the maturases, HYDE, HYDF, HYDG.

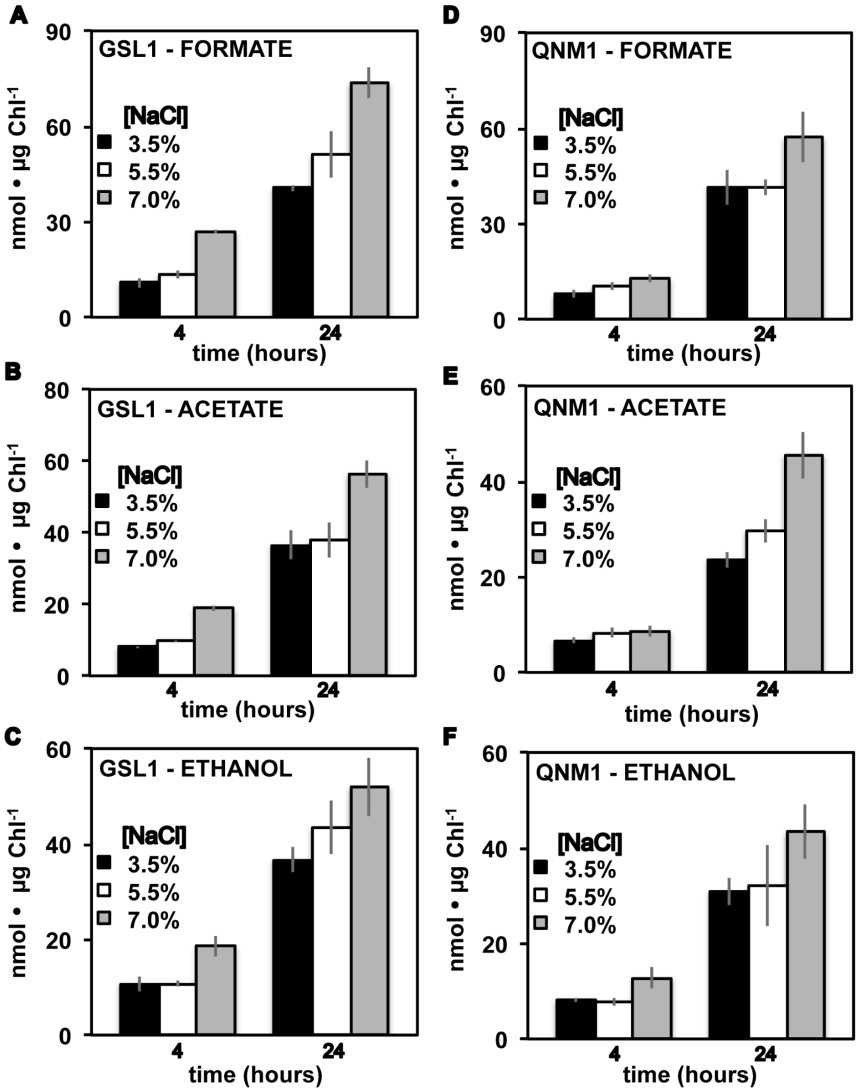

Figure 5. Accumulation of selected metabolites in extracellular medium. Bar graphs indicate the levels of secreted formate, acetate and ethanol from cultures of Tetraselmis GSL1 (A, B, C) and Tetraselmis QNM1 (D, E, F), respectively. Cells were grown and acclimated to dark, anoxic conditions in f/2 medium adjusted to the indicated NaCl levels (w/v). Error bars represent standard deviations from 8 experimental repetitions.
doi:10.1371/journal.pone.0085812.g005

Previously, it was suggested that the multiple HYDA isoforms present in algal genomes are the result of numerous, independent duplication events within each individual lineage (i.e., multiple HYDA isoforms is not an ancestral trait) [25]. The genome of N. gaditana and the transcriptome of Tetraselmis GSL1 suggest that each of these strains encode a single copy of HYDA. When coupled with HYDA phylogenetic data, which indicates that N. gaditana branches at the base of the algal lineages, these results support the notion that the progenitor of H_2 metabolism in algae encoded for only a single HYDA isoform. The observation that HYDA from Tetraselmis GSL1 is nested among algae with multiple HYDA isoforms supports the previous claim that independent duplication events led to the multiple isoforms present in these other strains.

Discussion

Salt water systems have a number of potentially intriguing applications in biological H_2 production using phototrophic microorganisms [72]. Saline water is readily available and salt concentrations can likely be leveraged to influence metabolism. Because little previous research has examined H_2 production in marine or halophilic algae, we undertook an effort aimed at identifying and characterizing hydrogenase activity in halophilic algae, and identified two distinct strains of Tetraselmis with fermentative metabolisms and promising H_2-photoproduction activities. To date, these strains of Tetraselmis are the most robust H_2-producing phototrophs isolated from high-salt environments; however it should be noted that both are relatively slow growing. Marine phototrophs are responsible for a significant portion of global primary productivity, can be cultured in abundant salt water resources, and diverse species of Tetraselmis are present in several saline ecosystems [73], [56]. Moreover, species of Tetraselmis have emerged as biotechnologically relevant organisms for the production of biofuels such as lipids, ethanol, or starch and for the extraction of higher value biocommodities including vitamins and ceramides [74–80], and now H_2.

Table 1. Total reducing sugars detected using the Anthrone Assay.

strain - salinity	Time	μg tot sugars/μg Chl	SD
GSL1 - 3.5%	0 h	55.11	±10.70
	4 h	50.62	±9.12
	24 h	38.00	±7.45
GSL1 - 5.5%	0 h	63.72	±14.52
	4 h	61.13	±12.07
	24 h	39.50	±3.47
GSL1 - 7.0%	0 h	94.73	±9.25
	4 h	85.70	±13.04
	24 h	49.55	±8.21
strain - salinity	**Time**	**μg tot sugars/μg Chl**	**SD**
QNM1 - 3.5%	0 h	58.66	±4.59
	4 h	57.09	±9.54
	24 h	52.10	±2.95
QNM1 - 5.5%	0 h	64.43	±2.12
	4 h	60.62	±8.71
	24 h	52.85	±4.53
QNM1 - 7.0%	0 h	75.90	±8.04
	4 h	51.99	±11.72
	24 h	39.95	±4.59

Intracellular reducing sugar content in cultures of Tetraselmis GSL1 and Tetraselmis QNM1, grown and acclimated to dark, anoxic conditions at the indicated times and NaCl concentrations (w/v).
doi:10.1371/journal.pone.0085812.t001

We confirmed that the halotolerance of Tetraselmis allows its growth in a wide range of salinities. The ability to grow at ocean salinity (3.5%), as well as more saline environments makes these organisms particularly versatile for biotechnological applications. Interestingly, we observed increases in both fermentative and photo- H_2 production as salinity increased, despite decreases in in vitro hydrogenase activities. Further studies are necessary to uncover the mechanistic underpinnings of the increase in H_2 production; however, it is plausible that the higher salt concentrations increase ATP demand, allowing for increased photosynthetic activity in the case of H_2 photoproduction, or increased fermentative activity in the case of dark, anoxic H_2 production. Both of these pathways increase ATP synthesis/utilization via pathways that require anoxic terminal electron acceptors, which may explain the increases in H_2 production. Although further research is necessary to verify or refute this hypothesis, it is clear that salt can be used to increase H_2 production in these Tetraselmis strains.

Five unique features of anoxic metabolism that have not been observed in more established freshwater, model systems were observed in these Tetraselmis isolates. First, hydrogenase activities accumulated to levels that are an order of magnitude greater than is typically observed in C. reinhardtii and other green algae when assayed on a per unit chlorophyll basis. This level of activity greatly exceeds the reducing equivalents delivered to the enzyme by either photosynthetic or fermentative pathways; suggesting that gains in H_2 production can be achieved by increasing reductant to the hydrogenase without having to overexpress the enzyme. Second, robust H_2 production coupled to either the photosynthetic electron transport chain or fermentative pathways can be realized at NaCl concentrations almost two times that of sea water; enabling consideration of salt water resources in efforts to efficiently produce biological H_2 from algae. Third, although increasing salt levels attenuate in vitro enzyme activity, increases in both H_2-photoproduction and dark, fermentative H_2 production are observed as a function of increasing NaCl levels. This demonstrates that salt levels can positively influence H_2 production in algae. Fourth, hydrogenase activity is robust even after 24 h of dark anoxia, which is in contrast to the reduced hydrogenase activities reported for C. reinhardtii at this point in anoxic acclimation [61]. Carbohydrate analysis indicated that well over half of the available reducing sugars remain within the cells at this point of anoxic acclimation, and it may be that these Tetraselmis strains are ''hardwired'' to withstand extended periods of anoxia. Fifth, fermentative H_2 production in the dark is almost 20-fold greater on a per unit chlorophyll basis than reported for C. reinhardtii, suggesting that hydrogenase may be more effectively integrated into fermentative pathways.

In addition to the biotechnological features described, we are also interested in (a) characterizing phototroph metabolism in the dark when anoxia occurs in aquatic ''dead-zones'' and phototrophs rely on fermentation for ATP production and (b) developing a more informed understanding of the evolution of FeFe-hydrogenases in eukaryotic phototrophs to better define why hydrogenase activity is observed in these oxygenic photosynthetic organisms. Eukaryotic phototrophs with hydrogenase activity typically exhibit anoxic heterofermentation activity in the dark, resulting in the secretion of alcohols, organic acids and H_2 [18]. These energy carriers and organic building blocks secreted by the algae are likely used by the consortia of heterotrophic microorganisms that coexists with aquatic phototrophs. These metabolites likely influence the population dynamics of the aquatic microbiota over temporal (diurnal, seasonal cycles) and spatial (vertical depth) gradients. Such features warrant further investigation of

Table 2. HYD gene transcript lengths, relative expression levels and rank with respect to the cellular transcriptome.

Gene	Number of homologs	Transcript length (nt)	Length of predicted protein (AA)	RPKM[a]	Expression rank in transcriptome assembly[b]
HYDA	1	1,825	461	1461±32	16
HYDE	1	2,038	492	118±1.6	655
HYDEF	1	3,446	997	14±3.0	7,088
HYDG	1	2,033	541	113±0.6	631

[a]Transcript expression level in reads per kilobase per million mapped reads. Given is the average expression and range for two biological replicates.
[b]Rank of transcript expression when compared to entire transcriptome assembly, with one being the most expressed transcript out of a total of 31,619 transcripts.
doi:10.1371/journal.pone.0085812.t002

Table 3. Single nucleotide polymorphisms (SNPs) in HYD transcripts.

Genes	SNPs in CDS	AA changes	Avg. Allele 1 Frequency[a]	Avg. Allele 2 Frequency[a]
HYDA	34	6	50.6±6.6	47.6±5.9
HYDE	0	0	-	-
HYDE/EF[b]	4	2	90.1±2.8	8.3±1.8
HYDG	1	1	49.7	48.6

[a]Average frequency, in percentage, of all CDS SNPs of given allele found in sequenced transcriptome. For HYDE/EF Allele 1 represents HYDE and Allele 2 represents HYDEF.
[b]HYDE/EF indicates the comparison of the HYDE region of the HYDE and HYDEF.
doi:10.1371/journal.pone.0085812.t003

phototroph fermentation in order to develop an understanding of the environmental cues influencing metabolism, catalog the products secreted by microbial primary producers, and characterize the effects of fermentative product secretion on microbial population dynamics.

Similar to C. reinhardtii, formate, acetate, and ethanol were secreted into culture media and H_2 and CO_2 were evolved following dark, anoxic acclimation. Other H_2 producing algae can secrete different products such as lactate or glycerol after anoxic acclimation [50]. Although different organic acids and alcohols can be secreted, all H_2 producing algae characterized to date exhibit a form of heterofermentation, which is also observed in the species of Tetraselmis described. Müller et al. recently proposed that a base set of anoxic metabolisms was likely present in the single common eukaryote ancestor, and that most contemporary eukaryotic anoxic metabolisms exhibit at least a subset of these original pathways [81]. Many eukaryotes retain features of these core enzymes, with hallmarks including enzymes such as the FeFe-hydrogenase, pyruvate ferredoxin oxidoreductase, pyruvate formate lyase, lactate dehydrogenase and alcohol dehydrogenase, among other fermentative enzymes enabling the production and secretion of H_2, organic acids and alcohols [82]. Despite greater than a billion years of evolution and ample opportunity to acquire different modes of anoxic metabolism by lateral gene transfer from bacteria and archaea, most eukaryotes with active anoxic metabolisms leverage either fermentation or relatively simple anoxic respiration pathways. This hypothesis is consistent with our observation that Tetraselmis readily activates heterofermentation pathways during anoxia using a subset of the ~50 enzymes posited by Muller et al. to be present in the eukaryote common ancestor [81]. The Tetraselmis GSL1 transcriptome (see below) was attained as part of an effort to obtain transcriptomes from hundreds of eukaryotic algae to mine this information for unique gene content in marine algae. When completed, this project will provide a powerful dataset for use in determining whether evidence exists that eukaryotic phototrophs have acquired other anoxic metabolisms outside of the core proposed by Muller et al. by lateral gene transfer, which does not appear to be a frequent occurrence.

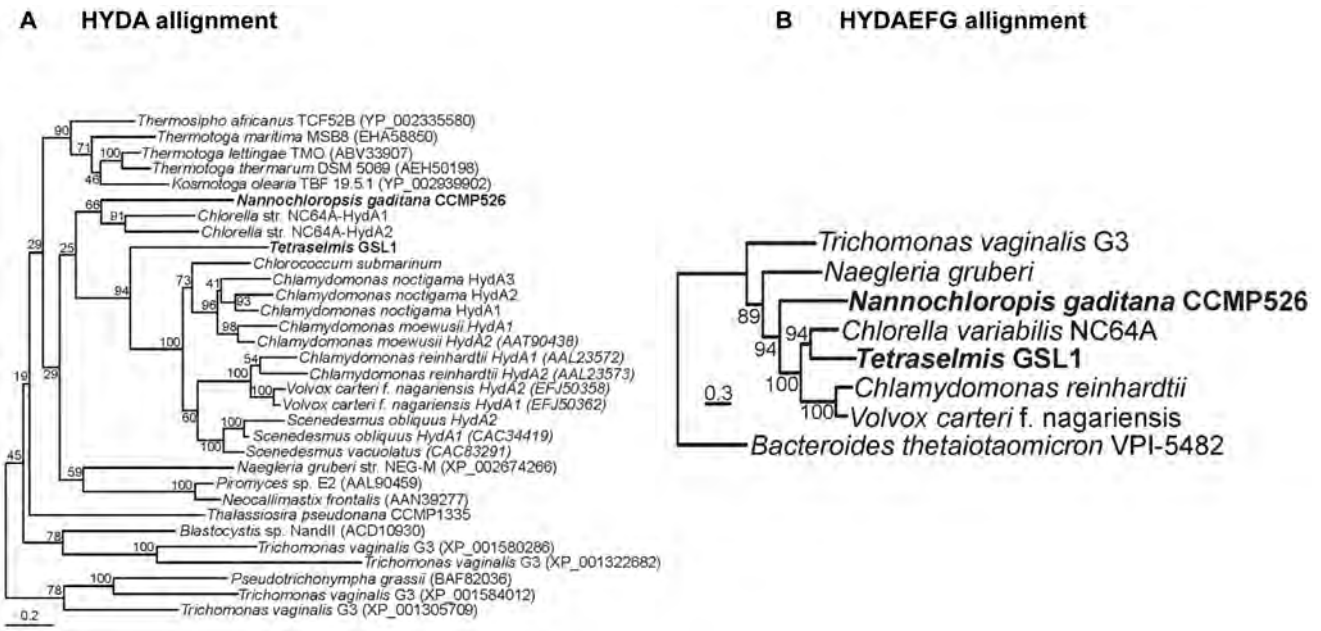

Figure 6. Maximum-likelihood phylogenetic reconstruction of individual HYDA sequences (A) and a concatentation of HYDAEFG (B). Bootstrap support values are indicated at each node. The root in the HYDA (NAR1, paralogs of HYDA) was pruned to conserve space. Given that NAR1 paralogs of HYDEFG do not exist, a different outgroup was chosen (i.e HYDAEFG from Bacteroides thetaiotaomicron) on the basis that the HYDA that it encodes, which branches basal to the eukaryote HYDA lineage.
doi:10.1371/journal.pone.0085812.g006

Phylogenetic analysis of algal hydrogenases sequenced to date show that these enzymes are all monophyletic, indicative of a common ancestor and that distinct lateral gene transfer of hydrogenase among the various algal lineages has not occurred. To determine whether this is also the case for Tetraselmis hydrogenases and to determine if halophiles acquired distinct hydrogenase enzymes from sources that are unrelated to freshwater algae, we performed in depth transcriptome analyses (n = 2) after 4 h of anoxic acclimation using Tetraselmis GSL1. Two surprising features emerged from these analyses that have not previously been described. First, the anoxic transcriptome of Tetraselmis GSL1 suggests a single FeFe-hydrogenase with only the H-cluster binding domain. Without whole genome sequencing, it is impossible to rule out the possibility that other HYDA homologs are present in the Tetraselmis GSL1 genome. However, if other HYDA homologs are present, their expression is sufficiently low after 4 h of anoxia that we could not detect transcripts in our dataset. This is not consistent with other green algae, such as Chlamydomonas, in which both HYDA1 and HYDA2 transcripts increase after exposure to anoxia and have been detected 4 h after anaerobic induction [63]. The depth of coverage obtained by transcriptome sequencing was high enough to capture HYDA precursor mRNA that contained unspliced introns (data not shown), so it seems unlikely that an alternative HYDA homolog is being expressed at substantive levels and not being detected. It seems likely that Tetraselmis encodes only a single FeFe-hydrogenase, and if so, it is the first green alga described that lacks a secondary duplication of this gene. As several SNPs were found in Tetraselmis GSL1 HYDA, we analyzed the SNP frequency. Our results indicate these 34 nucleotide differences are a result of multiploidy, were localized to the putative transit peptide, and resulted in only 6 AA changes (98.7% identical AA). Chlamydomonas reinhardtii is haploid and the HYDA2 isoform in this alga shares only 68% AA identity to HYDA1 [24]. Moreover, the promoter regions of HYDA1 and HYDA2 are unique and lack significant regions of sequence homology, which may suggest differences in the regulation of gene expression, which has been experimentally verified [83]. This phenomenon is not likely to be the case for the two Tetraselmis GSL1 HYDA transcripts that share very high similarity (99.5% nucleotide identity in the CDS), even higher in the promoter region. Moreover, the averaged abundance is very similar for both HYDA alleles (Table 2), suggesting no differential expression for the two allelic transcripts and consistent with a diploid organism.

Second, the Tetraselmis GSL1 transcriptome encodes two homologs to HYDE, one of which exists as a single transcript and the other of which exists as a HYDEF fusion. This represents the first report of the coexistence of 2 HYDE homologs in an algal genome, only one of which is fused inframe to HYDF. A single HYDEF fusion is observed in all other green algae with hydrogenase activity sequenced to date [25]. We speculate that the presence of two HYDE homologs in Tetraselmis GSL1 represents a key evolutionary intermediate pointing to the fusion event that led to the emergence of HYDEF, which may have occurred within the algal lineages as a way to economize protein translocation to the plastid. HYDE was putatively incorporated into algal genomes as a single gene early in the evolution of algae and can still be found as an independent form in Nannochloropsis where HYDE and HYDF remain separate despite being spatially located next to each other in a genomic hydrogenase gene cluster [71]. Analysis of the AA linker region between the HYDE and HYDF regions of fused HYDEF reveals no conserved motifs between currently sequenced algae (data not shown). If the fusion event occurred multiple times in various algal lineages this may account for the lack of any conserved HYDEF linker region because it was not present in the last common algal ancestor. Why Tetraselmis GSL1 retained an independent copy of HYDE is unknown; however, as shown in Table 2, the transcript abundances of HYDE and HYDEF are dramatically different (Table 2). This may be directly correlated to the function of HYDE as the putative source for the dithiolate ligand at the FeFe-hydrogenase active site [84], [85]; whereas, HYDF may function in a catalytic role, consistent with its role as a scaffold protein for active site construction and insertion [86]. It is unclear why HYDE would be fused to HYDF in this scenario.

Intriguing aspects of phylogenetically linked enzymatic adaptations are emerging among the various algal linkages and the sequences reported here provide additional evidence regarding the trajectory of algal hydrogenase acquisition and evolution. To date, eukaryotic algae have only been demonstrated to encode FeFe-hydrogenases [1] which is further supported by our transcriptome analysis. Inconclusive studies indicating the presence of NiFe-hydrogenases have been reported [87], [36]. Although the Bhosale et al. report contends that a NiFe-hydrogenase is present in a strain of Tetraselmis, we find no support of a NiFe-hydrogenase in Tetraselmis GSL1 and only find evidence of FeFe-hydrogenase. Very recently, a partial HYDA CDS from Tetraselmis subcordiformis was submitted to GenBank (Accession number: JQ317304), which has 85% similarity and 50% coverage with respect to the HYDA AA sequence reported here.

Among the Chlorophyceae, all FeFe-hydrogenases encode only the H-cluster binding domain and the presence of a hydrogenase with F-cluster binding domains has yet to be reported in this class. To date, these truncated H-cluster only hydrogenases are exclusively restricted to the Chlorophyceaen algae. It is unclear why these truncated variants emerged in evolution, but the presence of an H-cluster only enzyme in a halophilic specie of Tetraselmis (Chlorophyceae) is consistent with the presence of H-cluster only enzymes early in the evolution of the Chlorophyceae, and indicates that both fresh water and salt water members metabolically incorporate the H-cluster only enzyme variant. Currently, the most robust H_2-photoproduction activity is observed in the Chlorophyceae and truncation may enable more efficient coupling to the photosynthetic electron transport chain [25]. There are now full-length algal FeFe-hydrogenase sequences for two algae outside of the Chlorophyceae [25], [71] and interestingly these organisms both encode enzymes with H-cluster and F-cluster domains and exhibit comparatively lower H_2-photoproduction rates. The Trebouxiophyte, Chlorella variabilis NC64A contains two F-cluster FeFe-hydrogenases [25], whereas marine Nannochloropsis strains encode only a single F-cluster containing FeFe-hydrogenase [69].

Phylogenetic analyses of algal FeFe-hydrogenases demonstrate that the freshwater strains with sequenced transcriptomes/genomes contain at least two hydrogenase isoforms that are most similar to each other with respect to the other algal hydrogenases, indicating gene duplication within each of these individual algal lineages [25]. The marine organisms with available transcriptomes/genomes (Tetraselmis and Nannochloropsis [71], [88]) encode only a single HYDA isoform and both encode a copy of HYDE that is not fused to HYDF. Such observations may imply that marine organisms were not subject to the same evolutionary pressures that resulted in the hydrogenase duplication events observed in fresh water strains. The single HYDE protein is more difficult to interpret as Tetraselmis GSL1 also has HYDEF.

In sum, strains of Tetraselmis are promising candidates for the efficient production of H_2 in saline systems and salt can be leveraged as a means to positively influence H_2 production. The

results of HYDA transcriptome sequencing and phylogenetic analyses are consistent with speculation that FeFe-hydrogenases emerged in algal genomes only a single time, perhaps as far back as the primary endosymbiotic event, and that only a single FeFe-hydrogenase with H-cluster and F-cluster domains was present [51], [25]. The FeFe-hydrogenase was likely a component of a suite of fermentation enzymes present in an ancestral eukaryote that functioned in adaptation to anoxia and was subsequently evolved to couple to the photosynthetic electron transport chain under some conditions. During evolution, the Chlorophyceae selected a truncated H-cluster only enzyme, and the green algae generated a HYDEF fusion by translocating the 5′-UTR of a single HYDF into the end of HYDE 3′-coding sequence to generate a new intron with in frame splicing to generate a HYDEF fusion. Freshwater algae then experienced selective pressures to duplicate the HYDA sequence, although for unknown reasons. Although additional research is required to better define and improve H_2 production from halophilic species of Tetraselmis and new genome information is required to attain more definitive insights into the origins and evolution of hydrogenase in algae, the strains of Tetraselmis described here help to fill existing knowledge gaps in both of these areas.

Supporting Information

Figure S1 Schematic representation of the independent HYDE and fused HYDEF transcripts obtained from transcriptome sequencing. The percent nucleotide identity of each transcript to each other is given. Detected SNPs between HYDE and HYDEF are also indicated. The insert shows a detailed view of the genomic differences (determined by PCR) between the two genes, specifically the loss of the stop codon and 3′UTR plus the addition of an intron in the HYDEF gene.
(PDF)

Table S1 Hydrogenase activity comparisons between Tetraselmis strains and C. reinhardtii. In vivo and in vitro activities of hydrogenase from halophilic strains of Tetraselmis and the fresh water alga C. reinhardtii are indicated.
(PDF)

Table S2 Single nucleotide polymorphisms (SNPs) present in GSL1 HYD genes. Detailed list of all SNPs found in HYD genes, nucleotide positions, allele frequencies and amino acid (AA) changes, if they occurred.
(PDF)

Acknowledgments

We express gratitude to Laura Beer for the initial survey of hydrogenase activity in the GSL strain collection, Andrea Messer for sample collection at the Great Salt Lake, and Lee Elliott for samples from the C2B2 algal culture collection.

Author Contributions

Conceived and designed the experiments: SD MCP. Performed the experiments: SD. Analyzed the data: SD REJ ESB. Contributed reagents/materials/analysis tools: MCP JWP. Wrote the paper: SD MCP. Isolated the strain: SB BB.

References

1. Vignais PM, Billoud B (2007) Occurrence, classification, and biological function of hydrogenases: an overview. Chem Rev 107: 4206–4272.
2. Barz M, Beimgraben C, Staller T, Germer F, Opitz F, et al. (2010) Distribution analysis of hydrogenases in surface waters of marine and freshwater environments. PLoS One 5.
3. Chou CJ, Jenney FE Jr, Adams MW, Kelly RM (2008) Hydrogenesis in hyperthermophilic microorganisms: implications for biofuels. Metab Eng 10: 394–404.
4. Schwarz C, Poss Z, Hoffmann D, Appel J (2010) Hydrogenases and hydrogen metabolism in photosynthetic prokaryotes. In: Hallenbeck PC, editor. Advances in Experimental Medicine and Biology Recent Advances in Phototrophic Prokaryotes: Springer Science+Business Media, LLC. pp. 305–348.
5. Jenney FE Jr, Adams MW (2008) Hydrogenases of the model hyperthermophiles. Ann N Y Acad Sci 1125: 1–373.
6. Thauer RK, Kaster AK, Goenrich M, Schick M, Hiromoto T, et al. (2010) Hydrogenases from methanogenic archaea, nickel, a novel cofactor, and H_2 storage. Annu Rev Biochem 79: 507–536.
7. Boyd ES, Spear JR, Peters JW (2009) FeFe-hydrogenase genetic diversity provides insight into molecular adaptation in a saline microbial mat community. Appl Environ Microbiol 75: 4620–4623.
8. Boyd ES, Hamilton TL, Spear JR, Lavin M, Peters JW (2010) FeFe-hydrogenase in Yellowstone National Park: evidence for dispersal limitation and phylogenetic niche conservatism. ISME J 4: 1485–1495.
9. Spear JR, Walker JJ, McCollom TM, Pace NR (2005) Hydrogen and bioenergetics in the Yellowstone geothermal ecosystem. Proc Natl Acad Sci U S A 102: 2555–2560.
10. Brazelton WJ, Nelson B, Schrenk MO (2012) Metagenomic evidence for H(2) oxidation and H(2) production by serpentinite-hosted subsurface microbial communities. Front Microbiol 2: 268.
11. Burow LC, Woebken D, Bebout BM, McMurdie PJ, Singer SW, et al. (2012) Hydrogen production in photosynthetic microbial mats in the Elkhorn Slough estuary, Monterey Bay. ISME J 6: 863–874.
12. Hoehler TM, Albert DB, Alperin MJ, Bebout BM, Martens CS, et al. (2002) Comparative ecology of H_2 cycling in sedimentary and phototrophic ecosystems. Antonie Van Leeuwenhoek 81: 575–585.
13. Hoehler TM, Bebout BM, Des Marais DJ (2001) The role of microbial mats in the production of reduced gases on the early Earth. Nature 412: 324–327.
14. Cai G, Jin B, Monis P, Saint C (2011) Metabolic flux network and analysis of fermentative hydrogen production. Biotechnol Adv 29: 375–387.
15. Ghirardi ML, Dubini A, Yu J, Maness PC (2009) Photobiological hydrogen-producing systems. Chem Soc Rev 38: 52–61.
16. Eroglu E, Melis A (2011) Photobiological hydrogen production: recent advances and state of the art. Bioresource Technology 102: 8403–8413.
17. McKinlay JB, Harwood CS (2010) Photobiological production of hydrogen gas as a biofuel. Curr Opin Biotechnol 21: 244–251.
18. Posewitz MC, Dubini A, Meuser JE, Seibert M, Ghirardi ML (2009) Hydrogenases, hydrogen production, and anoxia. In: DB S, editor. The Chlamydomonas Sourcebook: Organellar and Metabolic Processes. pp. 217–255.
19. Peters JW, Boyd ES, D'Adamo S, Mulder DW, Therien J, et al. (2013) Hydrogenases, nitrogenases, anoxia, and H_2 production in water-oxidizing phototrophs. In: Michael A. Borowitzka NRM, editor. Algae for biofuels and energy developments in Applied Phycology Springer. pp. 37–75.
20. Allakhverdiev SI, Thavasi V, Kreslavski VD, Zharmukhamedov SK, Klimov VV, et al. (2010) Photosynthetic hydrogen production. Journal of Photochemistry and Photobiology C: Photochemistry Reviews 11: 87–99.
21. Beer LL, Boyd ES, Peters JW, Posewitz MC (2009) Engineering algae for biohydrogen and biofuel production. Curr Opin Biotechnol 20: 264–271.
22. Stern DB (2009) The Chlamydomonas Sourcebook: Organellar and Metabolic Processes, Volume 2; Harris E, editor: Elsevier.
23. Prince RC, Kheshgi HS (2005) The photobiological production of hydrogen: potential efficiency and effectiveness as a renewable fuel. Crit Rev Microbiol 31: 19–31.
24. Forestier M, King P, Zhang L, Posewitz MC, Schwarzer S, et al. (2003) Expression of two [Fe]-hydrogenases in Chlamydomonas reinhardtii under anaerobic conditions. Eur J Biochem 270: 2750–2758.
25. Meuser JE, Boyd ES, Ananyev G, Karns D, Radakovits R, et al. (2011) Evolutionary significance of an algal gene encoding an FeFe-hydrogenase with F-domain homology and hydrogenase activity in Chlorella variabilis NC64A. Planta 234: 829–843.
26. Mulder DW, Shepard EM, Meuser JE, Joshi N, King PW, et al. (2011) Insights into FeFe-hydrogenase structure, mechanism, and maturation. Structure 19: 1038–1052.
27. Melis A, Happe T (2004) Trails of green alga hydrogen research - from hans gaffron to new frontiers. Photosynth Res 80: 401–409.
28. Esquivel MG, Amaro HM, Pinto TS, Fevereiro PS, Malcata FX (2011) Efficient H_2 production via Chlamydomonas reinhardtii. Trends in Biotechnology 29: 595–600.
29. Melis A, Zhang L, Forestier M, Ghirardi ML, Seibert M (2000) Sustained photobiological hydrogen gas production upon reversible inactivation of oxygen evolution in the green alga Chlamydomonas reinhardtii. Plant Physiol 122: 127–136.
30. Antal TK, Krendeleva TE, Rubin AB (2011) Acclimation of green algae to sulfur deficiency: underlying mechanisms and application for hydrogen production. Appl Environ Microbiol 89: 3–15.
31. Srirangan K, Pyne ME, Perry Chou C (2011) Biochemical and genetic engineering strategies to enhance hydrogen production in photosynthetic algae and cyanobacteria. Bioresource Technology 102: 8589–8604.

32. Kosourov SN, Seibert M (2009) Hydrogen photoproduction by nutrient-deprived Chlamydomonas reinhardtii cells immobilized within thin alginate films under aerobic and anaerobic conditions. Biotechnol Bioeng 102: 50–58.
33. Kruse O, Hankamer B (2010) Microalgal hydrogen production. Curr Opin Biotechnol 21: 238–243.
34. Skjånes K, Knutsen G, Källqvist T, Lindblad P (2008) H_2 production from marine and freshwater species of green algae during sulfur deprivation and considerations for bioreactor design. International Journal of Hydrogen Energy 35: 511–521.
35. Yan F, Chen Z, Li W, Cao X, Xue S, et al. (2011) Purification and characterization of a hydrogenase from the marine green alga Tetraselmis subcordiformis. Process Biochemistry 46: 1212–1215.
36. Bhosale SH, Pant A, Khan MI (2009) Purification and characterization of putative alkaline NiFe-hydrogenase from unicellular marine green alga, Tetraselmis kochinensis NCIM 1605. Microbiological Research 164: 131–137.
37. Weiss RF (1970) The solubility of nitrogen, oxygen and argon in water and seawater. Deep Sea Research and Oceanographic Abstracts 17: 721–735.
38. Lambertz C, Leidel N, Havelius KG, Noth J, Chernev P, et al. (2011) O_2 reactions at the six-iron active site (H-cluster) in FeFe-hydrogenase. J Biol Chem 286: 40614–40623.
39. Greenbaum E, Lee JW (1999) Photosynthetic hydrogen and oxygen production by green algae. Biohydrogen 31: 235–241.
40. Reed RH, Borowitzka LJ, MacKay MA, Chudek JA, Foster R, et al. (1986) Organic solute accumulation in osmotically stressed cyanobacteria. FEMS Microbiology Letters 39: 51–56.
41. Chen H, Jiang JG (2009) Osmotic responses of Dunaliella to the changes of salinity. J Cell Physiol 219: 251–258.
42. Elliott LG, Feehan C, Laurens LML, Pienkos PT, Darzins A, et al. (2012) Establishment of a bioenergy-focused microalgal culture collection. Algal Research 1: 102–113.
43. Guillard RR, Rhyter J (1962) Studies of marine planktonic diatoms. I. Cyclotella nana Hustedt, and Detonula confervacea (cleve) Gran. Can J Microbiol 8: 229–239.
44. Harris EH (1989) The Chlamydomonas Sourcebook. San Diego Academic Press.
45. Newman SM, Boynton JE, Gillham NW, Randolph-Anderson BL, Johnson AM, et al. (1990) Transformation of chloroplast ribosomal RNA genes in Chlamydomonas: molecular and genetic characterization of integration events. Genetics 126: 875–888.
46. Simpson JT, Wong K, Jackman SD, Schein JE, Jones SJM, et al. (2009) ABySS: A parallel assembler for short read sequence data. Genome Res 19: 1117–1123.
47. Luo R LB, Xie Y, Li Z, Huang W, Yuan J, et al. (2012) SOAPdenovo2: an empirically improved memory-efficient short-read de novo assembler. Giga Science 1: Epub.
48. Chevreux B, Pfisterer T, Drescher B, Driesel AJ, Müller WEG, et al. (2004) Using the miraEST assembler for reliable and automated mRNA transcript assembly and SNP detection in sequenced ESTs. Genome Res 14: 1147–1159.
49. Dawson SC, Pace NR (2002) Novel kingdom-level eukaryotic diversity in anoxic environments. Proceedings of the National Academy of Sciences 99: 8324–8329.
50. Meuser JE, Ananyev G, Wittig LE, Kosourov S, Ghirardi ML, et al. (2009) Phenotypic diversity of hydrogen production in chlorophycean algae reflects distinct anaerobic metabolisms. J Biotechnol 142: 21–30.
51. Mulder DW, Boyd ES, Sarma R, Lange RK, Endrizzi JA, et al. (2010) Stepwise FeFe-hydrogenase H-cluster assembly revealed in the structure of HydA(DeltaEFG). Nature 465: 248–251.
52. Guindon S, Dufayard JF, Lefort V, Anisimova M, Hordijk W, et al. (2010) New Algorithms and methods to estimate maximum-likelihood phylogenies: assessing the performance of PhyML 3.0. Systematic Biology 59: 307–321.
53. Darriba D, Taboada GL, Doallo R, Posada D (2011) ProtTest 3: fast selection of best-fit models of protein evolution. Bioinformatics 27: 1164–1165.
54. Swofford DL (2002) PAUP*. Phylogenetic Analysis Using Parsimony (*and Other Methods). Sinauer Associates.
55. Meuser JE, Baxter BK, Spear JR, Peters JW, Posewitz MC, et al. (2013) Contrasting patterns of community assembly in the stratified water column of Great Salt Lake, Utah. Microb Ecol. Epub.
56. Arora M, Anil AC, Leliaert F, Delany J, Mesbahi E (2013) Tetraselmis indica (Chlorodendrophyceae, Chlorophyta), a new species isolated from salt pans in Goa, India. Eur J Phycol 48: 61–78.
57. Narváez-Zapata JA, Rojas-Herrera R, López-Uc Y, Sánchez-Estudillo L (2011) Different physiological responses influenced by salinity in genetically related Dunaliella salina isolates. Biotechnol Lett 33: 1021–1026.
58. Alkayal F, Albion RL, Tillett RL, Hathwaik LT, Lemos MS, et al. (2010) Expressed sequence tag (EST) profiling in hyper saline shocked Dunaliella salina reveals high expression of protein synthetic apparatus components. Plant Sci 179: 437–449.
59. Chen H, Lao YM, Jiang JG (2011) Effects of salinities on the gene expression of a (NAD^+)-dependent glycerol-3-phosphate dehydrogenase in Dunaliella salina. Sci Total Environ 409: 1291–1297.
60. Jahnke LS, White AL (2003) Long-term hyposaline and hypersaline stresses produce distinct antioxidant responses in the marine alga Dunaliella tertiolecta. Journal of Plant Physiology 160: 1193–1202.
61. Meuser JE, D'Adamo S, Jinkerson RE, Mus F, Yang W, et al. (2012) Genetic disruption of both Chlamydomonas reinhardtii FeFe-hydrogenases: insight into the role of HYDA2 in H2 production. Biochemical and Biophysical Research Communications 417: 704–709.
62. Roessler PG, Lien S. (1984) Purification of hydrogenase from C. reinhardtii. Plant Physiol 75: 705–709.
63. Mus F, Dubini A, Seibert M, Posewitz MC, Grossman AR (2007) Anaerobic acclimation in Chlamydomonas reinhardtii anoxic gene expression, hydrogenase induction, and metabolic pathways. JBC 282: 25475–25486.
64. Catalanotti C, Dubini A, Subramanian V, Yang W, Magneschi L, et al. (2012) Altered fermentative metabolism in Chlamydomonas reinhardtii mutants lacking pyruvate formate lyase and both pyruvate formate lyase and alcohol dehydrogenase. Plant Cell 24: 692–707.
65. Carrieri D, Momot D, Brasg IA, Ananyev G, Lenz O, et al. (2010) Boosting autofermentation rates and product yields with sodium stress cycling: application to production of renewable fuels by cyanobacteria. Appl Environ Microbiol 76: 6455–6462.
66. Ananyev G, Carrieri D, Dismukes GC (2008) Optimization of metabolic capacity and flux through environmental cues to maximize hydrogen production by the Cyanobacterium "Arthrospira (Spirulina) maxima". Appl Environ Microbiol 74: 6102–6113.
67. Jinkerson RE, Subramanian V, Posewitz MC (2011) Improving biofuel production in phototrophic microorganisms with systems biology. Biofuels 2: 125–144.
68. Posewitz MC, King PW, Smolinki SL, Zhang L, Ghirardi ML (2004) Discovery of two novel radical S-adenosylmethionine proteins required for the assembly of an active Fe- hydrogenase. JBC 279: 25711–25720.
69. Posewitz MC, King PW, Smolinski SL, Smith RD, Ginley AR, et al. (2005) Identification of genes required for hydrogenase activity in Chlamydomonas reinhardtii. Biochem Soc Trans 33: 102–104.
70. Jinkerson RE, Radakovits R, MC P (2013) Genomic insights from the oleaginous model alga Nannochloropsis gaditana. Bioengineered 4: 37–43.
71. Radakovits R, Jinkerson RE, Fuerstenberg SI, Tae H, Settlage RE, et al. (2012) Draft genome sequence and genetic transformation of the oleaginous alga Nannochloropis gaditana. Nat Commun 3: 686.
72. Work VH, Bentley FK, Scholz MJ, D'Adamo S, Gu H, et al. (2013) Biocommodities from photosynthetic microorganisms. Environmental Progress & Sustainable Energy 32: 989–1001.
73. Montoya H (2009) Algal and cyanobacterial saline biofilms of the Grande Coastal Lagoon, Lima, Peru. Natural Resources and Environmental Issues 15: 127–134.
74. Bondioli P, Della Bella L, Rivolta G, Chini Zittelli G, Bassi N, et al. (2012) Oil production by the marine microalgae Nannochloropsis sp. F&M-M24 and Tetraselmis suecica F&M-M33. Bioresource Technology 114: 567–572.
75. Xu D, Gao Z, Li F, Fan X, Zhang X, et al. (2012) Detection and quantitation of lipid in the microalga Tetraselmis subcordiformis (Wille) Butcher with BODIPY 505/515 staining. Bioresource Technology 127: 386–390.
76. Araujo GS, Matos LJBL, Gonçalves LRB, Fernandes FAN, Faria WRL (2011) Bioprospecting for oil producing microalgal strains: evaluation of oil and biomass production for ten microalgal strains. Bioresource Technology 102: 5248–5250.
77. Yao C, Ai J, Cao X, Xue S, Zhang W (2012) Enhancing starch production of a marine green microalga Tetraselmis subcordiformis through nutrient limitation. Bioresource Technology 118: 438–444.
78. Lim DKY, Garg S, Timmins M, Zhang ESB, Thomas-Hall SR, et al. (2012) Isolation and evaluation of oil-producing microalgae from subtropical coastal and brackish waters. PLoS One 7.
79. Arakaki A, Iwama D, Liang Y, Murakami N, Ishikura M, et al. (2013) Glycosylceramides from marine green microalga Tetraselmis sp. Phytochemistry 85: 107–114.
80. Carballo-Càrdenas EC, Tuan PM, Janssen M, Wijffels R (2003) Vitamin E (α-tocopherol) production by the marine microalgae Dunaliella tertiolecta and Tetraselmis suecica in batch cultivation. Biomolecular Engineering 20: 139–147.
81. Müller M, Mentel M, van Hellemond JJ, Henze K, Woehle C, et al. (2012) Biochemistry and evolution of anaerobic energy metabolism in eukaryotes. Microbiol Mol Biol Rev 76: 444–495.
82. Atteia A, van Lis R, Tielens AG, Martin WF (2013) Anaerobic energy metabolism in unicellular photosynthetic eukaryotes. Biochim Biophys Acta 1827: 210–223.
83. Whitney LA, Loreti E, Alpi A, Perata P (2011) Alcohol dehydrogenase and hydrogenase transcript fluctuations during a day-night cycle in Chlamydomonas reinhardtii: the role of anoxia. New Phytol 190: 488–498.
84. Shepard EM, Boyd ES, Broderick JB, Peters JW (2011) Biosynthesis of complex iron-sulfur enzymes. Curr Opin Chem Biol 15: 319–327.
85. Nicolet Y, Rubach JK, Posewitz MC, Amara P, Mathevon C, et al. (2008) X-ray structure of the FeFe-hydrogenase maturase HydE from Thermotoga maritima. J Biol Chem 283: 188861–118872.
86. McGlynn SE, Shepard EM, Winslow MA, Naumov AV, Duschene KS, et al. (2008) HydF as a scaffold protein in FeFe-hydrogenase H-cluster biosynthesis. FEBS Lett 582: 2183–2187.
87. Zinn T, Schnackenberg J, Haak D, Römer S, Schulz R, et al. (1994) Evidence for nickel in the soluble hydrogenase from the unicellular green alga Scenedesmus obliquus. Z Naturforsch C 49: 33–38.
88. Vieler A, Wu G, Tsai CH, Bullard B, Cornish AJ, et al. (2012) Genome, functional gene annotation, and nuclear transformation of the heterokont oleaginous alga Nannochloropsis oceanica CCMP1779. PLoS Genet 8: Epub.

This document is confidential and is proprietary to the American Chemical Society and its authors. Do not copy or disclose without written permission. If you have received this item in error, notify the sender and delete all copies.

[FeFe]-hydrogenase oxygen inactivation is initiated by the modification and degradation of the H cluster 2Fe subcluster

Journal:	*Journal of the American Chemical Society*
Manuscript ID:	ja-2014-079078
Manuscript Type:	Article
Date Submitted by the Author:	01-Aug-2014
Complete List of Authors:	Swanson, Kevin; Montana State University, Biochemistry Ratzloff, Michael; National Renewable Energy Laboratory, Biosciences Center Mulder, David; National Renewable Energy Laboratory, Biosciences Center Artz, Jacob; Montana State University, Biochemistry Ghose, Shourjo; Montana State University,, Biochemistry Hoffman, Andrew; Montana State University, Biochemistry White, Spencer; Montana State University, Biochemistry Zadvornyy, Oleg; Montana State University, Biochemistry Bothner, Brian; Montana State University, Biochemistry Broderick, Joan; Montana State University, Biochemistry King, Paul; National Renewable Energy Laboratory, Biosciences Center Peters, John; Montana State University, Biochemistry

SCHOLARONE™
Manuscripts

[FeFe]-hydrogenase oxygen inactivation is initiated by the modification and degradation of the H cluster 2Fe subcluster

Kevin D. Swanson,[§†] Michael W. Ratzloff,[§‡] David W. Mulder,[‡] Jacob H. Artz,[†] Shourjo Ghose,[†] Andrew Hoffman,[†] Spencer White,[†] Oleg A. Zadvornyy,[†] Joan B. Broderick,[†] Brian Bothner,[†] Paul W. King*,[‡] and John W. Peters*,[†]

†Department of Chemistry and Biochemistry, Montana State University, Bozeman, Montana 59717, United States

‡Biosciences Center, National Renewable Energy Laboratory, Golden, Colorado 80401, United States

ABSTRACT: The [FeFe]-hydrogenase catalytic site H cluster is a complex iron sulfur cluster assembly that is sensitive to oxygen (O_2). The O_2 sensitivity is a significant barrier for production of hydrogen as an energy source in water-splitting, oxygenic systems. Oxygen reacts directly with the H cluster, which results in rapid enzyme inactivation and eventual degradation. To investigate the progression of O_2-dependent [FeFe]-hydrogenase inactivation and the process of H cluster degradation, the highly O_2 sensitive [FeFe]-hydrogenase HydA1 from the green algae *Chlamydomonas reinhardtii* was exposed to defined concentrations of O_2 while monitoring the loss of activity and accompanying changes in H cluster spectroscopic properties. The results indicate that H cluster degradation proceeds through a series of reactions, the rate and extent of which depend on the initial enzyme reduction/oxidation state. The degradation process begins with O_2 binding and reacting with the 2Fe subcluster, leading to degradation of the 2Fe subcluster and leaving an inactive [4Fe-4S] subcluster state. In addition, Cys 169 that has been implicated as part of the proton transfer pathway was observed to have reacted with a reactive oxygen species to form sulfenic acid. This final inactive degradation product could be reactivated *in vitro* by incubation with 2Fe subcluster maturation machinery, specifically $HydF^{EG}$, which was observed by recovery of enzyme activity.

■ INTRODUCTION

[FeFe]-hydrogenases are found in bacteria and lower eukaryotes, and are commonly involved in the recycling of reduced electron carriers that accumulate during anaerobic metabolism.[1] [FeFe]-hydrogenases catalyze reversible H_2 activation at very high rates and thus are attractive targets for bioengineering efforts aimed at coupling microbial H_2 production to oxygenic photosynthesis[2,3] However, [FeFe]-hydrogenases are rapidly inactivated upon exposure to O_2, the byproduct of water oxidation.[4] In [FeFe]-hydrogenases, proton reduction occurs at a complex bridged FeS cluster termed the H cluster. The H cluster exists as a regular [4Fe-4S] subcluster bridged to an organometallic, 2Fe subcluster through a protein cysteine thiolate. The 2Fe subcluster is coordinated by unique non-protein ligands including CO, CN, and dithiomethylamine (Figure 1).[5-9] The O_2 sensitivity has been attributed to redox reactions with O_2, and subsequent destruction of the H cluster by reactive

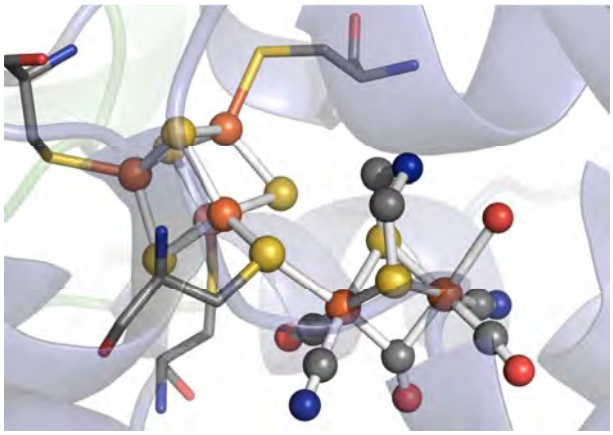

Figure 1. H cluster ball-and-stick representation with carbon, nitrogen, oxygen, sulfur, and iron atoms colored grey, blue, red, yellow, and rust respectively (PDB 3C8Y).

oxygen species (ROS), rendering the enzyme irreversibly inactivated.[10]

Although all of the characterized [FeFe]-hydrogenases have been shown to be sensitive to O_2 inactivation. The enzymes from different sources have varying sensitivity to O_2, which has been attributed largely to differences in the access of the active sites to O_2.[4,11-15] Computational studies have revealed putative channels that are proposed to function in the diffusion of gases, including O_2, to and from the active site.[11] It was also discovered through computational analysis and enzymatic assays of site-directed variants that constricting the gas channels can decrease the sensitivity of the [FeFe]-hydrogenase to O_2 but not to a significant enough degree to be useful for applications in technology.[11,13-15] A random mutagenesis approach was used to screen thousands of [FeFe]-hydrogenase variants leading to isolation of a more O_2 tolerant variant with several site substitutions. The effect of each mutation was individually tested, and showed that each contributed to an additive effect on the overall O_2 tolerance of the [FeFe]-hydrogenase.[15]

Theoretical studies of inactivation have measured the thermodynamics of O_2 binding and reactivity with the H cluster, and probed the subsequent reaction steps that ultimately lead to enzyme degradation. The models suggest that initiation of O_2 interaction with hydrogenase catalytic is dependent on the oxidation state, coordination environment and redox activity of the Fe sites.[16-20] In the H cluster reaction models, O_2 binds at the distal Fe, which is assigned to the (I) oxidation state for H_{ox} with a loosely bound water. Reaction of the bound O_2 with Fe(I) leads to formation of a terminally bound -OOH or $-O_2^-$ species. Further reaction cycles of the terminal "O" species with H^+ generates H_2O_2 or iron-peroxide as end-products.[19] Alternatively, 2Fe subcluster oxidation, or O atom insertion into the distal Fe terminal CO ligand can release CO_2.[19] The exact chemical nature of the O-species produced from O_2 reactions at the H cluster remain to be experimentally validated.

Structural and biophysical studies on how O_2 reacts with the H cluster to cause inactivation are challenging, and there are limited experimental studies on this process.[21,22] A mechanism of H cluster degradation by O_2 has been proposed from the results of X-ray absorption spectroscopy (XAS) studies in which reactive O_2 species produced at the 2Fe subcluster result in enzyme inactivation by destruction of the [4Fe-4S] subcluster.[10,23] Those results contrast with previous models whereby O_2 accesses and binds to the 2Fe subcluster to form ROS or other end-products that can readily degrade the 2Fe subcluster followed by loss of enzyme activity.[19] Thus, in order to reexamine the mechanistic process of O_2 inactivation of [FeFe]-hydrogenases, we have exposed the [FeFe]-hydrogenase from *Chlamydomonas reinhardtii* (CrHydA1) to low titers of O_2 while monitoring changes in the biochemical activity and changes in Fourier transform infrared (FTIR) and Ultraviolet–visible (UV-Vis) spectroscopic properties. The FTIR results indicate that H cluster reacts with O_2 and undergoes a series of reactions to produce a mixture of intermediates, the populations of which depend on the initial reduction/oxidation state of the H cluster. Ultimately, oxidative destruction results in the loss of the 2Fe subcluster and formation of a [4Fe-4S] subcluster state observed with UV-Vis and in the X-ray crystal structure. This inactivation/degradation end product could be reactivated *in vitro* by incubation with the 2Fe subcluster specific maturation machinery, as observed by enzyme activity assays.

■ EXPERIMENTAL SECTION

Protein Preparation. Heterologous expression and purification of CrHydA1 in *Escherichia coli* was done as previously described.[24,25] The protein was purified under anaerobic conditions in a MBraun anaerobic chamber (MBraun USA). All buffers were degassed under vacuum before purification. CrHydA1 isolation from cell extracts was performed using a two-step chromatography process of ion-exchange over diethylaminoethanol (DEAE, GE Lifesciences) Sepharose followed by affinity capture on Strep-Tactin (IBA) resin.[25] Strep-Tactin bound enzyme was eluted in 50 mM Tris buffer (pH 8.0) containing 300 mM NaCl, 5% glycerol, 5 mM sodium dithionite (NaDT), and 2 mM desthiobiotin. Purity was verified by sodium dodecyl sulfate polyacrylamide gel electrophoresis (SDS-PAGE), and the concentration determined by Bradford assay. CrHydA1 was prepared in the H_{ox} state by serial concentration and dilution in NaDT-free buffer until the FTIR spectra consisted primarily of H_{ox}. CrHydA1 was prepared in the H_{ox}-CO state by brief sparging under 100% CO gas, and 10 min incubation, in a sealed serum vial. Aliquots of CrHydA1 were prepared in H_{red}-H_2 by 10 evacuation flush cycles with 100% H_2 on a Schlenk line fitted with an O_2 trap.

HydF was obtained by expression of *hydF* in the background of HydE and HydG ($HydF^{EG}$) in *E. coli* strain BL21 (DE3). The *hydE*, *hydF*, and *hydG* from *Clostridium acetobutylicum* were individually cloned into pET-Duet, pRSF-Duet, and pCDF-Duet, respectively.[26] The cloned copy of *hydF* contained a N-terminal 6xHis tag.[26] Cells were grown in LB Miller growth medium supplemented with streptomycin (50 mg L^{-1}), kanamycin (30 mg L^{-1}), ampicillin (100 mg L^{-1}), 0.5% w/v glucose (~25 mM), 2 mM ferric ammonium citrate and 50 mM phosphate buffer (final pH of medium was 7.4). All cultures were grown aerobically at 25 °C until an OD_{600} of 0.5. Cultures were sparged with 100% argon for 20 min, and induced with 1.5 mM isopropyl β-D-1-thiogalactopyranoside (IPTG). Cysteine (2 mM) and sodium fumarate (25 mM) were added immediately after IPTG addition. Cultures were sparged with argon at 25°C overnight.

$HydF^{EG}$ was purified in an anaerobic chamber (Coy Labs, Grass Lake MI) as previously described.[26] Cells were harvested by centrifugation and cell pellets stored at -80 °C. Cells were lysed by resuspension in buffer composed of 10 mM HEPES, pH 7.4, 0.5 M KCl, 5% glycerol, 1 mM dithiothreitol, 20 mM imidazole, 20 mM $MgCl_2$, 1 mM PMSF, 1% Triton X-100, 140 μg ml^{-1} DNAse and RNAse, and 120 μg ml^{-1} lysozyme. The cell lysate was stirred for

1 h at room temp, and centrifuged in gas tight bottles at 38,000 x *g* for 30 min. The His-HydF^{EG} was purified from the supernatant by immobilized metal chromatography on a TALON cobalt column (GE Life Sciences). The column was loaded and washed with 15 column volumes of 20 mM HEPES pH 7.4, 0.5 M KCl, 5% glycerol, 1 mM dithiothreitol, and 20 mM imidazole. Purified HydF^{EG} was eluted with wash buffer containing 200 mM imidazole. HydF^{EG} was collected and concentrated anaerobically with 30 kDa Amicon Ultra-15 centrifugal concentrators (Millipore). The HydF^{EG} was loaded onto a G25 PD-10 desalting column (GE Life Sciences) to remove imidazole and eluted with 50 mM HEPES pH 7.4, 0.5 M KCl, 5% glycerol, and 1 mM dithiothreitol. HydF^{EG} was flash frozen in liquid N_2 and stored at –80 °C or in liquid N_2 until further use.

Preparation of Oxygen Treated CrHydA1. O_2 gas standards were prepared using septum-sealed 123 ml Wheaton vials. Dilutions were prepared using a gas-tight syringe (Hamilton) to remove gas from a 100% O_2 standard (equilibrated to atmospheric pressure) and injecting the O_2 into vials containing 100% N_2 at atmospheric pressure. Standards of 100%, 4%, 1%, and 0.1% O_2 were used for all of the O_2 additions. Samples used to measure the FTIR spectra of O_2 treated CrHydA1 were prepared as follows: HydA1 at 30-70 mg ml^{-1} was pipetted into a septum-sealed 825 µl conical vial on ice, and O_2 (final partial pressure concentrations of 0.01-24.2%) was added by gas tight syringe with magnetic stirring. A 5.5 µl aliquot of CrHydA1 was removed by syringe and the FTIR spectra were collected in a custom gas-tight FTIR sample cell.[27] For the O_2 reaction characterization by UV-Vis spectroscopy, O_2 was injected in a low volume sealed quartz cuvette and the reaction was scanned once per-min, for 200-300 min.

FTIR Spectroscopy. Spectra were collected as described previously with a Nicolet 6700 FTIR spectrometer (Thermo Fisher Scientific) equipped with a Globar IR source, a CaF_2 beam splitter, and a liquid-nitrogen-cooled mercury cadmium telluride (MCT) detector.[27] All of the spectra were collected at room temperature (21 °C). The OMNIC software was configured to report absorbance spectra, and absorbance baselines were fit to these data using a manually adjusted spline.

Ultraviolet-Visible Spectroscopy. A 100 µl aliquot of H_{ox} CrHydA1 was prepared in the glove box under 100% N_2, transferred into low volume 1 cm path-length quartz cuvette and septum sealed. The O_2 reaction was initiated by injecting O_2 with a gas-tight syringe into the cuvette with the enzyme solution under magnetic stirring at 4°C and cooled with a peltier cooler. The reaction of CrHydA1 with O_2 was monitored by UV-Vis every min by scanning over a 250-750 nm range at 1 nm intervals. UV-Vis spectra were recorded on a Cary 4000 UV-Visible spectrophotometer.

Activity Assays. Activities of CrHydA1 were assayed by H_2 evolution from reduced methyl viologen. Reaction volumes of 0.6 or 2 ml were placed in 3 or 10 ml Wheaton vials, respectively, which contained 5 mM methyl viologen (MV), 10 mM NaDT, 50 mM Tris, 300 mM NaCl, 5% glycerol, and between 25 ng-4 µg of enzyme per assay. Hydrogen production was detected by gas chromatography (Agilent Technologies).

Mass Spectrometry. Protein digests were performed with 1.5 mg ml^{-1} CrHydA1, 12.5 ug ml^{-1} Trypsin Gold (Promega), 50 mM Tris-HCl pH 8, 300 mM NaCl, and 5% glycerol. Reactions were allowed to proceed overnight in a 37 °C heat block, and complete digestion was verified by sodium dodecyl sulfate polyacrylamide gel electrophoresis (SDS-PAGE). Reactions were transferred into septum sealed vials with a N_2 headspace. The digestion product was diluted up to a 1000 fold in 50/50 water/Acetonitrile and transferred to screw capped auto sampler vials for LCMS.

An Agilent 1100 series HPLC system coupled to an Agilent Chip Cube integrated microfluidics reverse-phase nano-HPLC system was used. Trapping and analytical separations were performed with an Agilent C18 HPLC-Chip (G4240-62001, 40 nl trap column and 75 µm x 43 mm analytical). Chromatography solvents were H_2O with 0.1% (v/v) formic acid for channel "A" and acetonitrile for channel "B". The HPLC program was held at 7% B from 0.0 to 2.0 min, then ramped from 7 to 35% B from 2.0 to 20.0 min. The gradient was then ramped from 35 to 95% B from 22 to 27 min. The mass spectrometer was an Agilent 6520 Q-TOF with a dual-ESI source: resolution approximately 20,000 and accuracy 3 ppm. Spectra were collected in positive mode from 50 to 1700 m/z at 2 Hz for both MS and MS/MS, with adaptive acquisition time for highly-abundant ions.

The resulting MS/MS data were analyzed using the PEAKS 6.0 software package and searching the CrHydA1 protein sequence. Peptide mass tolerance was 10 ppm and fragment mass tolerance 0.5 Da. Variable modifications were set to sulfonic acid 47.97, sulfinic acid 31.98, and oxidation or hydroxylation of cysteine 15.99.

Crystallization and Structure Determination. CrHydA1 was crystallized anaerobically in a MBraun glove box at room temperature using micro-capillary batch diffusion with a precipitation solution of 25.5% polyethylene glycol 8000 as precipitate and 0.085 M sodium cacodylate (pH 6.5), 0.17 M sodium acetate trihydrate, and 1 mM dithionite. After allowing the crystals to form for 2-3 weeks, they were mounted on cryo-loops and flash frozen in liquid nitrogen. Data were collected at the Stanford Synchrotron Radiation Lightsource (SSRL) on beam line BL12-1 at 1.75 Å wavelength. The data was processed using XDS,[28] and scaled with Pointless and Aimless.[29] The structure was solved using molecular replacement using AutoMR (CCP4 suite of programs) with CrHydA1 (PDB ID, 3LX4).[30] The structure was built using COOT with further refinement using REFMAC5 using NCS and B factor restraints. The final model was solved to 2.23 Å with an R factor of 20.7% and an R free of 25.2% (Table S1). Atomic coordinates were deposited in the PDB (code 4ROV).

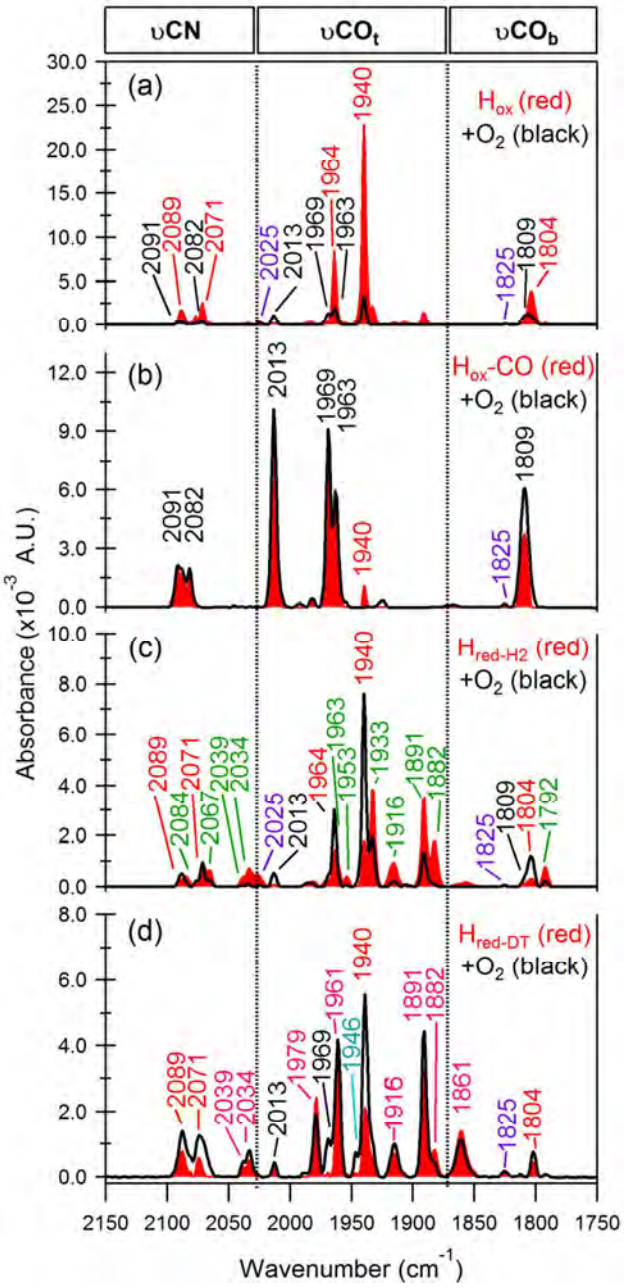

Figure 2. FTIR spectra of CrHydA1 samples exposed to O_2. The solid red spectra are prior to O_2 injection, and black traces after 2 h exposure to O_2. (a) H_{ox}, ~0.01% O_2; (b) H_{ox}-CO, ~2.4% O_2; (c) H_{red}-H_2, ~0.01% O_2; (d) H_{red}-NaDT, ~0.01% O_2. Wavenumbers in red, H_{ox}; black, H_{ox}-CO; green, H_{red}-H_2; magenta H_{red}-NaDT; purple, oxidative damage and cyan, unassigned.

***In vitro* Reactivation of O_2 Inactivated CrHydA1.** Reactivation of the O_2 inactivated CrHydA1 was performed with the addition of N-terminal His tagged-HydF^{EG} at different molar ratios to obtain a 300 µl total volume in 3 ml crimp sealed anaerobic Wheaton vials. CrHydA1 was allowed to reactivate at 37 °C in a water bath for 1 h, and reactivation was followed by measuring the H_2 production activity as described above.

■ RESULTS

FTIR Analysis and Comparison of H_{ox}, H_{red}-NaDT, H_{red}-H_2 and H_{ox}-CO. To investigate how differences in the oxidation state and/or site occupancy of the 2Fe subcluster of CrHydA1 affect the process of O_2 damage, reducing agents NaDT and H_2, and the competitive inhibitor CO were each added to oxidized (H_{ox}) CrHydA1. These enzyme samples were then exposed to O_2 and monitored by FTIR. CrHydA1 was initially prepared in the H_{ox} state with major peaks observed at 1804, 1940, 1964, 2071 and 2089 cm^{-1} (Figure 2a, red). Exposure of the H_{ox} CrHydA1 to ~0.01% O_2 (Figure 2a black spectrum) for 2 h resulted in the loss of H_{ox} features and an increase in features assigned to H_{ox}-CO and the O_2-damaged cluster, discussed in more detail in the time course discussion.

CrHydA1 in the H_{ox} state was exposed to CO to make H_{ox}-CO (Figure 2b, red spectrum). The expected shift of *ν*CO and *ν*CN peaks to higher wavenumbers were observed as previously reported for CO-inhibited [FeFe]-hydrogenases, with *ν*CO peaks at 1809, 1963, 1969, 2013, and *ν*CN peaks at 2082, and 2091 cm^{-1}.[31-33] The enzyme was then exposed to ~2.4% O_2. H_{ox}-CO was exposed to larger percentages of oxygen in order to see if any attenuation of FTIR signal could be observed. After 2 h of O_2 exposure, the FTIR spectrum indicated the peaks assigned to H_{ox}-CO remained relatively unchanged (Figure 2b, red vs. black spectrum). Small peaks appeared, which are attributed to degradation of some residual H_{ox} species, and this may have also contributed to the slight increase in H_{ox}-CO signal intensity after O_2 exposure. Enzyme in the H_{ox}-CO state was also treated with higher amounts of O_2 (up to ~24.2%, Figure S2), and the resulting FTIR spectra again showed significantly less degradation compared to oxidized and reduced preparations, consistent with other observations that H_{ox}-CO is stable to oxidative reactions with O_2.[4,10,34]

Equilibration of H_{ox} CrHydA1 under 100% H_2 led to a collective shift in the *ν*CO peaks, consistent with ligand exchange and electronic transitions at the H cluster associated with H_2 activation.[27,35] Figure 2c shows the spectrum of H_2-reduced CrHydA1 with principle *ν*CO peaks, assigned to a mixed population of reduced intermediates, observed at 1792, 1882, 1891, 1916, 1933, 1953, and 1963 cm^{-1} (Figure 2c, red spectrum).[27,35,36] Additional peaks associated with H_{ox}-CO were also seen in the starting sample, possibly arising from a slight amount of O_2 exposure during H_2 treatment. Exposure of H_{red}-H_2 CrHydA1 to ~0.01% O_2 for 2 h, in the presence of 100% H_2 atmosphere led to attenuation of the 1792, 1882, 1891, 1916, and 1933 cm^{-1} peaks (Figure 2c, red vs. black spectrum). This was accompanied by an increase in peak intensities assigned to H_{ox} at 1804, 1940, and 1964 cm^{-1} together with a small increase in peak intensities assigned to H_{ox}-CO at 1969 and 2013 cm^{-1}. Thus, degradation of the H_2-reduced CrHydA1 is likely to involve initial formation of H_{ox}, with subsequent interaction with O_2 leading to formation of H_{ox}-CO and eventual 2Fe subcluster degradation.

When H_{ox} CrHydA1 was treated with NaDT (20 mM final concentration, a 20-fold excess), the initial spectrum

(Figure 2d, red spectrum) showed *ν*CO peaks previously assigned to reduced intermediates at 1861, 1882, 1891, 1916, 1961, and 1979 cm^{-1}.[27] Compared to H_{ox} (Figure 2a), the NaDT-treated CrHydA1 showed less signal attenuation after exposure to O_2 (Figure 2d, red vs. black spectra), with only a small loss of 2Fe subcluster signal after 2 h of exposure to ~0.01% O_2. Regarding *ν*CO peak intensities, the O_2 treatment produced new peaks at 1946 cm^{-1} and 1969 cm^{-1}, a slight increase in peak intensities at 1916, and 2013 cm^{-1}, and larger increases in peak intensities at 1804 and 1940 cm^{-1}. The increases at 1804 and 1940 cm^{-1} are assigned to an increase in the population of H_{ox}, and the changes at 1969 and 2013 cm^{-1} are assigned to an increase in the population of H_{ox}-CO. The appearance of H_{ox} is similar to the sequence observed for O_2 exposure of H_2-reduced CrHydA1, again consistent with O_2 inactivation involving at least one H_{ox}-dependent reaction pathway.

FTIR time series of O_2 exposed H_{ox} CrHydA1. In order to observe O_2-induced transitions in the 2Fe subcluster by FTIR on the timescales of full spectral collection (512 scans, ~8 min), CrHydA1 prepared in the H_{ox} state (with νCO modes at 1804, 1940, 1964 cm^{-1}) was incubated under a low (~0.01%) O_2 partial pressure at 4 °C, and FTIR spectra were collected at approximately ~25 min intervals (Figure 3). Under these conditions, the H_{ox} signal gradually attenuated and transitioned to H_{ox}-CO, with primary *ν*CO peaks at 1809, 1963, and 2013 cm^{-1}. A near complete transition of H_{ox} to H_{ox}-CO was observed after ~200 min of O_2 exposure. The decay rates of H_{ox} specific *ν*CO signals at 1940 and 1964 cm^{-1} were calculated from normalized absorbance measurements to be $k_{\Delta Hox} \approx 10^{-4}$ s^{-1} μM^{-1} (Table 1). These rates matched well to the inactivation rates $k_{inact} \approx 10^{-4}$ s^{-1} μM^{-1} of H_2 evolution activity (Table 1). We also measured the change in the FTIR spectra of *Clostridium acetobutylicum* HydA (CaI) prepared in H_{ox} and exposed to a ~30-fold higher concentration (~0.28%) of O_2. This enzyme is ~100-fold less sensitive to O_2 inactivation than CrHydA1,[4] thus was expected to have slower kinetics of O_2-induced changes in FTIR spectral features. A time-course spectrum (Figure S1) of CaI exposed to ~0.28% O_2 shows a slower decay rate of H_{ox} peak intensities, and subsequent appearance of H_{ox}-CO signals, than for CrHydA1 (Table 1). These differences match to the comparatively slower (~100-fold) inactivation rate of CaI versus CrHydA1 (Table 1). As observed for CrHydA1 there is good agreement between the rate of loss of H_{ox} signal intensity, $k_{\Delta Hox} \approx 10^{-6}$ s^{-1} μM^{-1}, and the inactivation rate of H_2 evolution activity by O_2, $k_{inact} \approx 10^{-6}$ s^{-1} μM^{-1}.

Table 1. Rate constants for O_2 induced changes in CrHydA1 and CaI H_{ox} *ν*CO peak intensities, and H_2 evolution activities.

Enzyme	[1] $k_{\Delta Hox}$ ΔIR signal, (s^{-1} μM^{-1})		[1] k_{inact} H_2 evolution activity (s^{-1} μM^{-1})	[2] Ref. k_{inact} (s^{-1} μM^{-1})
CrHydA1	(Δ1940) 3.0×10^{-4}	(Δ1964) 2.0×10^{-4}	2.0×10^{-4}	4.3×10^{-4} (a) 2.2×10^{-3} (b)
CaI	(Δ1945) 9.0×10^{-6}	(Δ1800) 1.2×10^{-6}	6.4×10^{-6}	5.1×10^{-6} (b)

1 $k = -[\ln(y/y_o)]/t$ (s^{-1} μM^{-1})

2 (a) Goldet, G., et al. 2009. *JACS*. 131:14979; (b) Stripp, S.T., et al. 2009. *PNAS*. 106(41):17331.

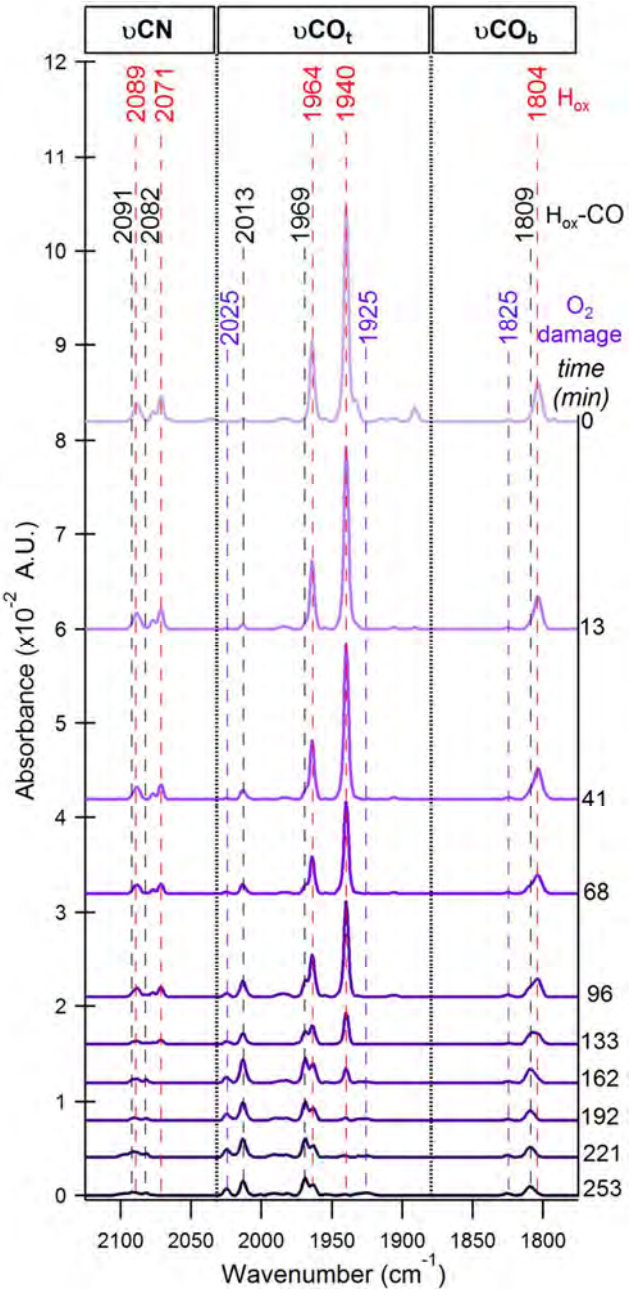

Figure 3. Time course of the FTIR spectra of H_{ox} CrHydA1 exposed to ~0.01% O_2. The initial H_{ox} signal (1804, 1940, 1964, 2071, and 2089 cm^{-1}) gradually decays, and the spectrum transitions to a characteristic H_{ox}-CO signal with *ν*CO peaks at 1809, 1963, 1969, and 2013 cm^{-1}. Signals assigned to O_2 damaged clusters are shown in purple.

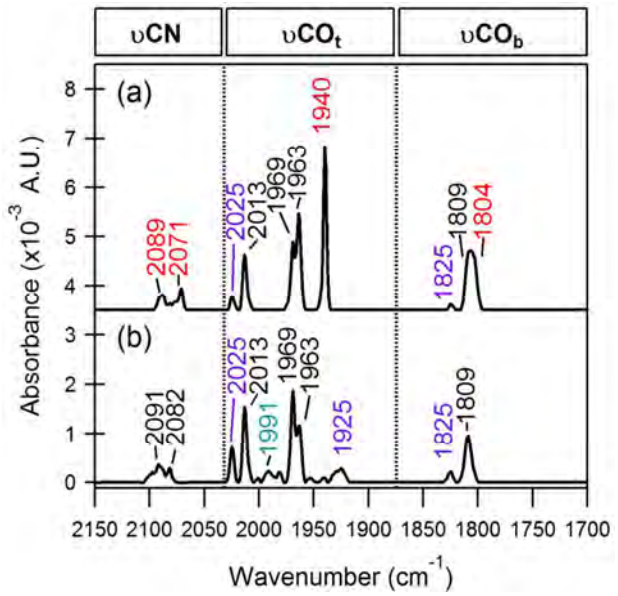

Figure 4. FTIR spectra of H_{ox} CrHydA1 after long-term exposure to 0.01% O_2. Scans taken at (a) 133 min, and (b) 253 min, after exposure to O_2. Wavenumber coloring is as described in Figure 2.

The percentage of H_{ox}-CO formed after O_2 exposure of H_{ox} (change in primary *ν*CO peaks from 1804, 1940, and 1964 cm^{-1} to 1809, 1963 and 1969 cm^{-1}) was estimated by using standardized values for *ν*CO peak heights, normalized to mg of enzyme, for an anaerobically prepared CrHydA1 H_{ox}-CO sample (Figure 2b, red spectrum). The amount of O_2-treated H_{ox} CrHydA1 that converted to H_{ox}-CO was determined based on normalizing the *ν*CO peak intensities in the O_2-treated sample to the Hox-CO standard. The amount of CrHydA1 that converted to H_{ox}-CO was ~20% after 133 min (Figure 4a) of ~0.01% O_2 exposure, where the rest of the signal loss is likely due to complete degradation of the 2Fe subcluster, which is observed at 253 min (Figure 4b). The O_2-induced H_{ox}-CO signal appeared simultaneously with the loss of H_{ox}, and slowly decreased in intensity after 133 min (Figure 3). After a longer period of exposure, the loss of H_{ox}-CO was accompanied by the appearance and perturbations of new *ν*CO peaks at 1825, 1925 and 2025 cm^{-1} (Figure 4b). These peaks seem to be specific for oxidatively damaged H cluster, but since the overall 2Fe subcluster signal is degrading and other states are growing in (H_{ox}-CO) and decaying (H_{ox}), it is not currently possible to determine whether these peaks arise from a single or multiple H cluster state(s).

UV-Vis of O_2 exposed CrHydA1. Ultraviolet visible (UV-Vis) spectroscopy was employed to monitor the [4Fe-4S] cluster during O_2 exposure. The absorption spectra of holo-CrHydA1, CrHydA1 expressed in the absence of HydE, HydF and HydG and lacking the 2Fe subcluster (CrHydA1$^{\Delta EFG}$), and the O_2 inactivated CrHydA1 all showed a broad 415-420 nm absorbance feature associated with S→Fe charge transfer bands of FeS clusters. CrHydA1$^{\Delta EFG}$ contains only a [4Fe-4S] subcluster inserted by *E. coli's* FeS cluster assembly machinery.[37,38] The difference between the spectra of CrHydA1$^{\Delta EFG}$ and holo-CrHydA1 (Figure 5, red and blue trace, respectively) shows that the spectra for CrHydA1$^{\Delta EFG}$ appears to be red-shifted and the difference in signal at 450 nm accounts for 11% of the total absorbance. This absorbance difference could be due to CrHydA1$^{\Delta EFG}$ being in a more oxidized state, differences in Fe-loading per-mol of enzyme, or the presence of the 2Fe subcluster causing a blue shift of the 450 nm absorbance peak in holo-CrHydA1.

Inactivation of CrHydA1 by exposure to ~0.001% O_2 for 2 h was monitored by H_2 evolution activity and UV-Vis spectroscopy. Since the amount of enzyme was about 10-fold lower for UV-Vis experiments, 10-fold less O_2 was added as compared to FTIR experiments. The initial activity was 500 μmol min^{-1}mg^{-1}, which declined after the 2 h O_2 treatment to 12 μmol min^{-1} mg^{-1}. The blue trace in Figure 5 is the starting spectrum of holo-CrHydA1, and the black trace is after 2 h incubation with O_2. The difference spectra between holo-CrHydA1 (Figure 5a, blue trace) and O_2 inactivated CrHydA1 (Figure 5a, black trace) did not reveal significant differences (data not shown), suggesting that most of the S→Fe charge transfer absorption is maintained after O_2 inactivation This result is consistent with stability of the [4Fe-4S] cluster against O_2 damage.

***In-vitro* activation of O2 inactivated CrHydA1.** CrHydA1 that had been O_2 inactivated could be *in vitro* activated with HydF^{EG} (Figure S3) and activity could be recovered to ~80% of as purified activity. The remaining population of enzyme that was inactivateable is likely due to degradation products that were further degraded to possibly [3Fe-4S] cluster, [2Fe-2S] cluster, or completely stripped of cluster.[39] This data suggests there is a residual population of enzyme containing [4Fe-4S] after O_2 exposure. It had been previously shown that HydF^{EG} is sufficient for activating CrHydA1$^{\Delta EFG}$,[26] and that activation of CrHydA1$^{\Delta EFG}$ requires the assembly of a preformed [4Fe-4S] cluster.[37]

Structural characterization of O_2 inactivated CrHydA1. CrHydA1 inactivated by O_2 readily crystallized and the structure was determined to 2.3Å resolution. The resulting structure was very similar to the previously characterized structure of purified CrHydA1 expressed in the absence of [FeFe]-hydrogenase maturases HydE, HydF, and HydG with an overall r.m.s. deviation between the two structures of 0.29 Å.[37] The structure revealed a vacant 2Fe subcluster site and an intact [4Fe-4S] subcluster (Figure 5b) and an open channel leading from the surface to the site left vacant in absence of the 2Fe subcluster. This suggests that the O_2 inactivated CrHydA1 is the appropriate conformation and is consistent with the observation that oxygen inactivated CrHydA1 can be reactivated by the H cluster maturation machinery. In addition, the structure revealed three Cys residues (amino acids 88, 169, and 238) to have additional electron density around the sulfur atoms which can be modeled and refined suggesting sulfenic acid (R-SOH) at positions Cys 169 (which functions in proton-transfer to the H cluster[40]) and Cys 238 (surface localized) and sulfinic acid

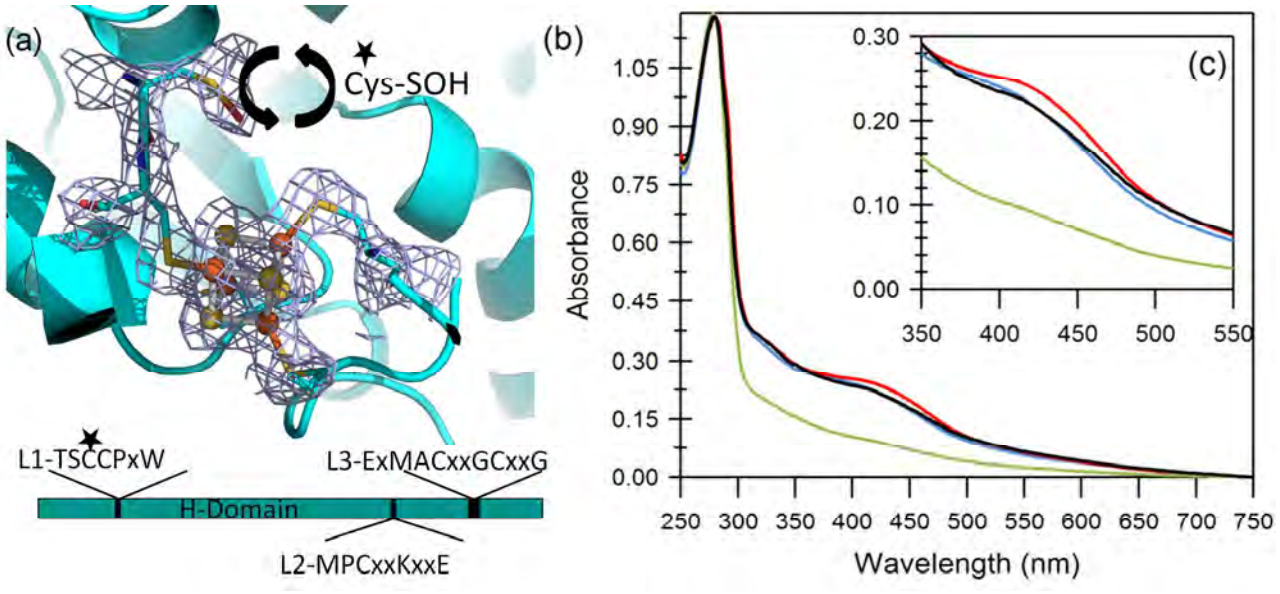

Figure 5. Crystal structure and UV-Vis of O_2 inactivated CrHydA1. (a) Electron density map contoured at 2σ showing extra electron density in the H cluster environment including oxidized Cys 169. The conserved [FeFe]-hydrogenase motifs are depicted below the ribbon diagram with Cys 169 (starred). (b) The full spectrum of reduced immature CrHydA1$^{\Delta EFG}$ (—), and of holo-CrHydA1 (—) after inactivation with 0.001% O_2 2 h (—), or with 3 atm of 100% O_2 for 3 h (—). (c) A close-up view of the 350-550 nm region.

(R-SOOH) at position Cys 88 (surface localized). No modifications of the four Cys residues that function to coordinate the H cluster (Cys 170, 225, 417, and 421) were detected. The extra electron density at Cys 169 is best explained as a reaction product of the sulfur group with ROS, which might arise from O_2 binding at the 2Fe subcluster as indicated by the FTIR results. It is possible that the modifications of the surface Cys 88 and 238 might arise from diffusion of ROS out of the catalytic site. MS analysis confirmed the presence of sulfenic and sulfinic acid at the Cys positions observed in the X-ray structure (data not shown). Although O_2 damage is evident from the X-ray and analytical structures, the [4Fe-4S] subcluster was intact with no evidence of O2 damage.

■ DISCUSSION

The results of recent studies in which X-ray Absorption Spectroscopy (XAS) was used to monitor O_2 damage of CrHydA1 were interpreted to indicate that after O_2 binding and reaction with the 2Fe subcluster, the initial target of H cluster degradation was the [4Fe-4S] subcluster.[10,23] These studies were conducted with high concentrations of O_2 and in one study with the additional presence of high concentrations of NaDT. For example, Stripp *et al.* exposed ~ 30 nmol of CrHydA1 equilibrated in the H_{ox} state to ~20% O_2 over a period of 15 min,[10] whereas in Lambertz *et al.* exposed 8 nmol of NaDT reduced CrHydA1 to air saturated buffer (~330 μM or 21% O_2) for ~17 min.[23] In contrast, for the comparative study with FTIR we monitored H_{ox} 2Fe subcluster degradation with slightly more enzyme (68 nmol), but exposed to ~2500x less (~0.137 μM in solution as determined by Henry's Law or ~0.01% headspace partial pressure) concentrated O_2 in solution over a ~17x longer time period. Similar experimental setups were done to also allow the use of additional analytical techniques (biochemical assays, and UV-Vis spectroscopies, mass spectrometry, and X-ray crystallography) to follow the fate of the 2Fe subcluster and [4Fe-4S] subcluster during the inactivation process.

FTIR analysis of CrHydA1 incubated in the presence of ~0.01% O_2 in the absence of exogenously added reducing agents exhibited attenuation of the H_{ox} state. The attenuation of the H_{ox} signal tracked nearly 1:1 with loss of enzyme hydrogen production activity and is strong evidence that the 2Fe subcluster of the H cluster is the initial site of O_2 inactivation. In addition to the loss of H_{ox} signal due to O2, signals commonly associated with H_{ox}-CO state appeared. This observation suggests that O_2 degrades the 2Fe subcluster, liberating CO, and that the proportion of H cluster that transitions to the H_{ox}-CO state is a result of the free CO binding to remaining intact clusters. CO liberation and CO binding to intact enzyme in H_{ox} is also thought to occur during photoillumination of the [FeFe]-hydrogenases.[31] These observations are consistent with free CO being a potent inhibitor (k_i≈0.1 μM)[4] of [FeFe]-hydrogenases, and O_2 liberating CO that binds free H_{ox} is consistent with the prior EPR studies of O_2 treated CpI showing formation of a H_{ox}-CO axial EPR signal.[41]

The changes that occur when CrHydA1 is exposed to O_2 appear to occur to a greater extent and at a higher rate when poised in the H_{ox} state. Enzyme poised in H_{ox}-CO, H_{red}-H_2, and H_{red}-NaDT were less prone to O_2-dependent decay. CrHydA1 equilibrated under H_2 or NaDT reduced also showed limited degradation compared to H_{ox}, with a majority of 2Fe subcluster signal being maintained at 1.2%

to 2% O_2 respectively after 2 h (data not shown). The data suggests that an H cluster that is coordinately saturated with an occupied distal Fe ligand exchangeable site is more resistant to O_2 damage and provide strong support of this site as the initial site of O_2 binding and attack along the pathway of H cluster degradation.[4,27,34,35] The addition of CO had the greatest protective effect with no observable decay of H_{ox}-CO up to 24.2% O_2 (Figure S2) over 2 h of exposure, consistent with previous electrochemical observations.[4,10] The H_2 and NaDT treated CrHydA1 exposed to O_2 initially transitions into H_{ox} prior to degradation indicated by the observed appearance of the 1940 cm^{-1} feature. Subsequently, similar degradation products are observed in the NaDT- and H_2-treated CrHydA1 samples as were observed with H_{ox} samples, with the transient appearance of H_{ox}-CO specific FTIR features.

The O_2 inactivated CrHydA1 was capable of being reactivated by the addition of $HydF^{EG}$ suggesting that the inactivated enzyme has a damaged or absent 2Fe subcluster. Further, as described above, both UV-Vis spectroscopy and structural characterization indicated the presence of an intact [4Fe-4S] subcluster that was stable long after activity attenuated. Interestingly, the X-ray crystal structure and UV-Vis of O_2 inactivated CrHydA1 strongly resembled CrHydA1 expressed in the absence of maturases ($CrHydA1^{\Delta EFG}$). Previous studies probing H cluster degradation using comparatively higher concentrations of O_2 either with[23] or without[10] NaDT proposed that the degradation of the [4Fe-4S] subcluster preceded 2Fe subcluster degradation, whereby ROS was generated by O_2 binding and reaction at the 2Fe subcluster. Under the conditions of our study in which CrHydA1 was exposed to O_2 in the absence of NaDT, the [4Fe-4S] subcluster seems fairly resistant to degradation. We do however see evidence for the oxidation of the non-coordinating active site Cys (Cys 169) perhaps through the formation of ROS.[42] Exposure of either the O_2 degradation intermediate observed here or $CrHydA1^{\Delta EFG}$ to high concentrations of O_2 resulted in the eventual destruction of the [4Fe-4S] subcluster, as evidenced by reduction and eventual loss of the S→Fe charge transfer bands at ~420 nm.

■ CONCLUSION

The inactivation of [FeFe]-hydrogenase by O_2 is defined by steps that involve the diffusion of gases into close proximity of the catalytic site, followed by redox/chemical steps of O_2 reaction with the H cluster. Our results are consistent with theoretical models[19] and indicate that the latter process proceeds *via* oxidative breakdown of the 2Fe subcluster, initially releasing CO that can bind to secondary targets (e.g., other enzymes). Further exposure results in the eventual formation of a stable break-down product with an intact [4Fe-4S] subcluster and a vacant 2Fe subcluster site capable of being reactivated by 2Fe subcluster specific maturation machinery. Long-term and/or high concentration O_2 exposure is required for oxidative damage of the [4Fe-4S] subcluster and complete H cluster degradation as evidenced by the previous XAS/EXAFS studies.[10,23] Based on our results, [FeFe]-hydrogenase inactivation from O_2 exposure essentially reverses the maturation pathway of H cluster insertion into immature CrHydA1, and suggests that H clusters inactivated by low concentration O_2 exposure *in vitro* could be substrates for reactivation by $HydF^{EG}$.

■ ASSOCIATED CONTENT

Supporting Information.

Additional FTIR spectra of O2-treated CaI and O2-treatment of CO-inhibited CrHydA1, CrHydA1 activity and HydF titration data, and crystallographic data collection and refinement statistics for O2-exposed CrHydA1

■ AUTHOR INFORMATION

Corresponding Author

paul.king@nrel.gov
john.peters@chemistry.montana.edu

Author Contributions

The manuscript was written through contributions of all authors. / All authors have given approval to the final version of the manuscript. / [§]These authors contributed equally.

Notes

The authors declare no competing financial interest.

■ ACKNOWLEDGMENT

This work on the mechanism of oxygen sensitivity was supported by Air Force Office of Scientific Research grant FA-9550-11-1-0218 to J.W.P. Authors M.W.R., D.W.M., and P.W.K. gratefully acknowledge funding support for CrHydA1 and CaI preparation and FTIR spectra measurements from the U.S. Department of Energy, Division of Chemical Sciences, Geosciences, and Biosciences, Office of Basic Energy Sciences; and support of the U.S. Department of Energy under Contract no. DE-AC36-08-GO28308 with the National Renewable Energy Laboratory. The work on reactivation of damaged CrHydA1 with purified HydF was supported by the U.S. Department of Energy grant DE-FG02-10ER16194 (to J.B.B., and J.W.P.) Use of the Stanford Synchrotron Radiation Lightsource, SLAC National Accelerator Laboratory, is supported by the U.S. Department of Energy, Office of Science, Office of Basic Energy Sciences under Contract No. DE-AC02-76SF00515. The SSRL Structural Molecular Biology Program is supported by the DOE Office of Biological and Environmental Research, and by the National Institutes of Health, National Institute of General Medical Sciences (including P41GM103393). The mass spectrometry facility at MSU receives funding from the Murdock Charitable Trust and NIH 5P20RR02437 of the Cobre program. The contents of this publication are solely the responsibility of the authors and do not necessarily represent the official views of NIGMS or NIH. Atomic coordinates were deposited in the PDB (code 4ROV).

■ REFERENCES

(1) Vignais, P. M.; Billoud, B. *Chem. Rev.* **2007**, *107*, 4206.

(2) Turner, J.; Sverdrup, G.; Mann, M. K.; Maness, P. C.; Kroposki, B.; Ghirardi, M. L.; Evans, R. J.; Blake, D. *Int. J. Hydrogen Energ.* **2008**, *32*, 379.

(3) McKinlay, J. B.; Harwood, C. S. *Curr. Opin. Biotech.* **2010**, *21*, 244.

(4) Goldet, G.; Brandmayr, C.; Stripp, S. T.; Happe, T.; Cavazza, C.; Fontecilla-Camps, J. C.; Armstrong, F. A. *J. Am. Chem. Soc.* **2009**, *131*, 14979.

(5) Peters, J. W.; Lanzilotta, W. N.; Lemon, B. J.; Seefeldt, L. C. *Science* **1998**, *282*, 1853.

(6) Nicolet, Y.; Piras, C.; Legrand, P.; Hatchikian, C. E.; Fontecilla-Camps, J. C. *Struct. Fold. Des.* **1999**, *7*, 13.

(7) Pandey, A. S.; Harris, T. V.; Giles, L. J.; Peters, J. W.; Szilagyi, R. K. *J. Am. Chem. Soc.* **2008**, *130*, 4533.

(8) Silakov, A.; Wenk, B.; Reijerse, E.; Lubitz, W. *Phys. Chem. Chem. Phys.* **2009**, *11*, 6592.

(9) Berggren, G.; Adamska, A.; Lambertz, C.; Simmons, T. R.; Esselborn, J.; Atta, M.; Gambarelli, S.; Mouesca, J. M.; Reijerse, E.; Lubitz, W.; Happe, T.; Artero, V.; Fontecave, M. *Nature* **2013**, *499*, 66.

(10) Stripp, S. T.; Goldet, G.; Brandmayr, C.; Sanganas, O.; Vincent, K. A.; Haumann, M.; Armstrong, F. A.; Happe, T. *P. Natl. Acad. Sci. U.S.A.* **2009**, *106*, 17331.

(11) Cohen, J.; Kim, K.; King, P. W.; Seibert, M.; Schulten, K. *Structure* **2005**, *13*, 1321.

(12) King, P. W.; Svedruzic, D.; Cohen, J.; Schulten, K.; Seibert, M.; Ghirardi, M. L. 2006; Vol. 6340, p 63400Y.

(13) Ghirardi, M. L.; Cohen, J.; King, P. W.; Schulten, K.; Kim, K.; Seibert, M. 2006; Vol. 6340, p 63400X.

(14) Lautier, T.; Ezanno, P.; Baffert, C.; Fourmond, V.; Cournac, L.; Fontecilla-Camps, J. C.; Soucaille, P.; Bertrand, P.; Meynial-Salles, I.; Leger, C. *Faraday Discuss.* **2011**, *148*, 385.

(15) Bingham, A. S.; Smith, P. R.; Swartz, J. R. *Int. J. Hydrogen Energ.* **2012**, *37*, 2965.

(16) Lyon, E. J.; Shima, S.; Boecher, R.; Thauer, R. K.; Grevels, F.-W.; Bill, E.; Roseboom, W.; Albracht, S. P. J. *J. Am. Chem. Soc.* **2004**, *126*, 14239.

(17) Bruska, M. K.; Stiebritz, M. T.; Reiher, M. *J. Am. Chem. Soc.* **2011**, *133*, 20588.

(18) Stiebritz, M. T.; Finkelmann, A. R.; Reiher, M. *Eur. J. Inorg. Chem.* **2011**, *2011*, 1163.

(19) Stiebritz, M. T.; Reiher, M. *Chem. Sci.* **2012**, *3*, 1739.

(20) Kubas, A.; De Sancho, D.; Best, R. B.; Blumberger, J. *Angew. Chem.* **2014**, *126*, 4165.

(21) Baffert, C.; Demuez, M.; Cournac, L.; Burlat, B.; Guigliarelli, B.; Bertrand, P.; Girbal, L.; Léger, C. *Angew. Chem. Int. Edit* **2008**, *47*, 2052.

(22) Liebgott, P.-P.; Leroux, F.; Burlat, B.; Dementin, S.; Baffert, C.; Lautier, T.; Fourmond, V.; Ceccaldi, P.; Cavazza, C.; Meynial-Salles, I.; Soucaille, P.; Fontecilla-Camps, J. C.; Guigliarelli, B.; Bertrand, P.; Rousset, M.; Léger, C. *Nat Chem Biol* **2010**, *6*, 63.

(23) Lambertz, C.; Leidel, N.; Havelius, K. G. V.; Noth, J.; Chernev, P.; Winkler, M.; Happe, T.; Haumann, M. *J. Biol. Chem.* **2011**, *286*, 40614.

(24) King, P. W.; Posewitz, M. C.; Ghirardi, M. L.; Seibert, M. *J. Bacteriol.* **2006**, *188*, 2163.

(25) Yacoby, I.; Tegler, L. T.; Pochekailov, S.; Zhang, S.; King, P. W. *PLoS ONE* **2012**, *7*, e35886.

(26) McGlynn, S. E.; Shepard, E. M.; Winslow, M. A.; Naumov, A. V.; Duschene, K. S.; Posewitz, M. C.; Broderick, W. E.; Broderick, J. B.; Peters, J. W. *FEBS Lett.* **2008**, *582*, 2183.

(27) Mulder, D. W.; Ratzloff, M. W.; Shepard, E. M.; Byer, A. S.; Noone, S. M.; Peters, J. W.; Broderick, J. B.; King, P. W. *J. Am. Chem. Soc.* **2013**, *135*, 6921.

(28) Kabsch, W. *Acta Acta Crystallogr D* **2010**, *66*, 125.

(29) Evans, P. *Acta Crystallogr D* **2006**, *62*, 72.

(30) Vagin, A.; Teplyakov, A. *J. Appl. Crystallogr.* **1997**, *30*, 1022.

(31) Pierik, A. J.; Hulstein, M.; Hagen, W. R.; Albracht, S. P. J. *Eur. J. Biochem.* **1998**, *258*, 572.

(32) Chen, Z. J.; Lemon, B. J.; Huang, S.; Swartz, D. J.; Peters, J. W.; Bagley, K. A. *Biochemistry* **2002**, *41*, 2036.

(33) Roseboom, W.; De Lacey, A. L.; Fernandez, V. M.; Hatchikian, E. C.; Albracht, S. P. J. *J. Biol. Inorg. Chem.* **2006**, *11*, 102.

(34) Bennett, B.; Lemon, B. J.; Peters, J. W. *Biochemistry* **2000**, *39*, 7455.

(35) Adamska, A.; Silakov, A.; Lambertz, C.; Rüdiger, O.; Happe, T.; Reijerse, E.; Lubitz, W. *Angew. Chem. Int. Edit.* **2012**, *51*, 11458.

(36) Silakov, A.; Kamp, C.; Reijerse, E.; Happe, T.; Lubitz, W. *Biochemistry* **2009**, *48*, 7780.

(37) Mulder, D. W.; Ortillo, D. O.; Gardenghi, D. J.; Naumov, A. V.; Ruebush, S. S.; Szilagyi, R. K.; Huynh, B.; Broderick, J. B.; Peters, J. W. *Biochemistry* **2009**, *48*, 6240.

(38) Mulder, D. W.; Boyd, E. S.; Sarma, R.; Lange, R. K.; Endrizzi, J. A.; Broderick, J. B.; Peters, J. W. *Nature* **2010**, *465*, 248.

(39) Nicolet, Y.; Rohac, R.; Martin, L.; Fontecilla-Camps, J. C. *P. Natl. Acad. Sci. U.S.A.* **2013**, *110*, 7188.

(40) Cornish, A. J.; Gärtner, K.; Yang, H.; Peters, J. W.; Hegg, E. L. *J. Biol. Inorg. Chem.* **2011**, *286*, 38341.

(41) Kowal, A. T.; Adams, M. W.; Johnson, M. K. *J. Biol. Chem.* **1989**, *264*, 4342.

(42) Kettenhofen, N. J.; Wood, M. J. *Chem. Res. Toxicol.* **2010**, *23*, 1633.

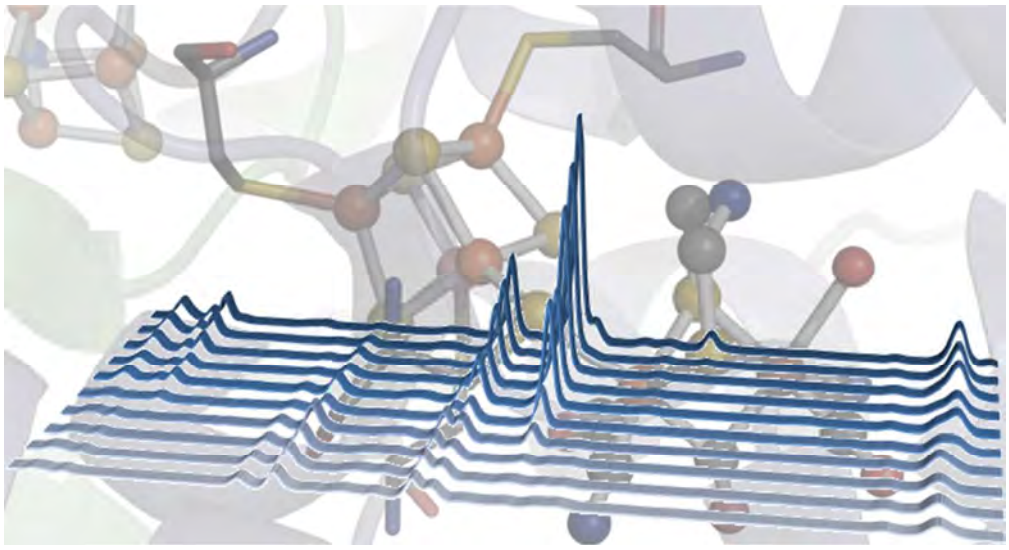

44x23mm (600 x 600 DPI)

This document is confidential and is proprietary to the American Chemical Society and its authors. Do not copy or disclose without written permission. If you have received this item in error, notify the sender and delete all copies.

Investigations on the Role of Proton-Coupled Electron Transfer in Hy-drogen Activation by [FeFe]-hydrogenase

Journal:	*Journal of the American Chemical Society*
Manuscript ID:	Draft
Manuscript Type:	Article
Date Submitted by the Author:	n/a
Complete List of Authors:	Mulder, David; National Renewable Energy Laboratory, Ratzloff, Michael; National Renewable Energy Laboratory, Biosciences Center Bruschi, Maurizio; University of Milan-Bicocca, Department of Environmental and Heart Sciences Greco, Claudio; University of Milan-Bicocca, Department of Biotechnology and Biosciences Koonce, Evangeline; Montana State University, Chemistry and Biochemistry Peters, John; Montana State University, Director, Astrobiology Biogeocatalysis Research Center & Thermal Biology Institute King, Paul; National Renewable Energy Laboratory, Biosciences Center

SCHOLARONE™
Manuscripts

Investigations on the Role of Proton-Coupled Electron Transfer in Hydrogen Activation by [FeFe]-hydrogenase

David W. Mulder,[†] Michael W. Ratzloff,[†] Maurizio Bruschi,[‡] Claudio Greco,[‡] Evangeline Koonce,[§] John W. Peters,[§] and Paul W. King[*,†]

[†]Biosciences Center, National Renewable Energy Laboratory, Golden, Colorado 80401, United States

[‡]University of Milano-Bicocca, Department of Earth and Environmental Sciences, Piazza della Scienza 1, Milan, Italy

[§]Montana State University, Department of Chemistry and Biochemistry, Bozeman, Montana 59717, United States

ABSTRACT: Proton-coupled electron transfer (PCET) is a fundamental process at the core of oxidation-reduction reactions for energy conversion. The [FeFe]-hydrogenases catalyze the reversible activation of molecular H_2 through a unique metallocofactor (H-cluster) that is finely tuned by the surrounding protein environment to undergo fast PCET transitions. The coordination of electronic and structural transitions at the H-cluster with proton-transfer (PT) steps has not been closely examined experimentally. Here, we explore how disruption of the conserved PT network via a Cys-to-Ser mutation proximal to the H-cluster of *Chlamydomonas reinhardtii* [FeFe]-hydrogenase (CrHydA1) affects the H-cluster using electron paramagnetic resonance (EPR) and Fourier transform infrared (FTIR) spectroscopy. Despite a substantial decrease in catalytic activity, the EPR and FTIR spectra reveal different H-cluster catalytic states under reducing and oxidizing conditions. Under H_2 or sodium dithionite reductive treatments, the EPR spectra show signals that are consistent with a reduced $[4Fe\text{-}4S]_H^{1+}$ subcluster. The FTIR spectra showed upshifts of νCO modes to energies that are consistent with an increase in oxidation state of the diiron subcluster, which was corroborated by Density Functional Theory analysis. In contrast to wild-type CrHydA1, spectra associated with H_{red} and $H_{sred,}$ states are less populated in the Cys→Ser variant, demonstrating that the exchange of -SH to -OH alters how the H-cluster equilibrates among different reduced states of the catalytic cycle under steady-state conditions.

INTRODUCTION

Hydrogen (H_2) gas is an appealing energy carrier for the future, which has inspired efforts to develop biological based approaches for renewable H_2 production.[1,2] The [NiFe]- and [FeFe]-hydrogenases are enzymes that catalyze the reversible activation of molecular H_2 through the reaction, $H_2 \leftrightarrows 2H^+ + 2e^-$. Because they accomplish this reaction near the thermodynamic potential of the H_2/H^+ couple[3] at high rates using base transition metals, the active-sites of these enzymes, and the mechanisms of H_2 activation, provide models to help guide synthetic efforts.[4-9]

The catalytic site H-cluster of [FeFe]-hydrogenase consists of two subclusters, $[4Fe\text{-}4S]_H$ and $[2Fe]_H$, which are linked through a conserved cysteine (Cys) residue.[10,11] The $[2Fe]_H$ subcluster is ligated by strong field CO and CN^- ligands along with a bridging azadithiolate (adt) ligand.[12,13] Altogether, the H-cluster is designed to carry out H_2 activation via proton-coupled electron transfer (PCET) reactions; the $[4Fe\text{-}4S]_H$ functions as an electronic relay[14-17] between either accessory FeS clusters (F-clusters) or external redox carriers,[18] and adt functioning to shuttle protons between PT networks and $[2Fe]_H$[19,20,13] during H_2 activation and proton reduction.[21-23] Mechanistic details on how PCET steps are accomplished in [FeFe]-hydrogenases are not fully described, thus there is a need to closely examine how active site chemistry is functionally coupled to, and controls, the H-cluster electronic transitions during catalysis.

Several proton-transfer (PT) pathways connecting the protein surface to the H-cluster in [FeFe]-hydrogenases have been proposed based on x-ray structure and biochemical analysis.[10,11,24,25] The importance of PT for efficient H_2 activation has, in general, been shown by incorporation of proton relays in molecular catalysts that are a critical design component for improving catalytic performance.[26] In [FeFe]-hydrogenase the primary PT channel consists of coordinated water molecules that form an H-bond network with conserved residues (e.g., Glu, Ser).[27] Pathway models show that protons are transferred along this pathway to either one of two strictly conserved residues, Cys or Lys, that are within H-bond distance of the H-cluster.[25,28,29] The H-cluster proximal Cys in CrHydA1

(Cys169) is within H-bonding distance of the adt ligand and modeled to function in PT to the bridgehead amine[27-29] (Figure 1). Mutagenesis studies demonstrate that this Cys residue is critical for full catalytic activity, and exchange of the -SH group of Cys to a more basic -OH group of Ser or nonpolar side chains like Ala and Ile leads to severe reduction in H_2 evolution and H_2 uptake activity.[27,30-32] The Lys stabilizes H-cluster binding through H-bonding with the terminal CN^- ligand[10,33] and can also be modeled to promote H-transfer directly to the Fe atoms of $[2Fe]_H$.[34,22] Substitutions of the conserved Lys result in a more severe defect and were found to lack a $[2Fe]_H$ subcluster, consistent with the function of H-bonding to CN^-.[31]

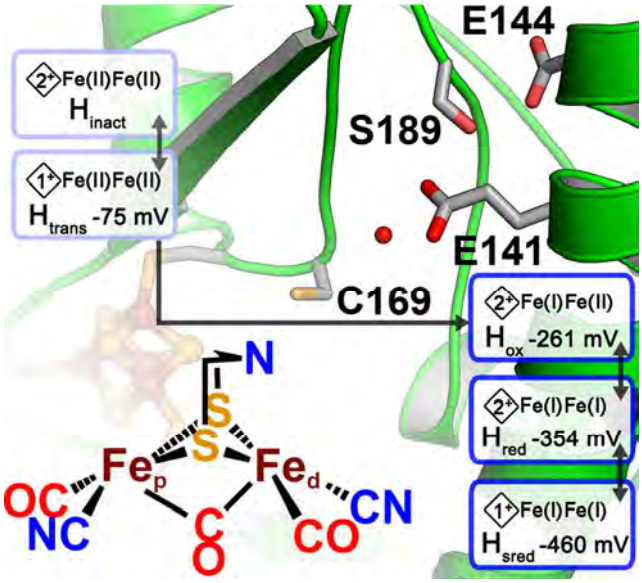

Figure 1. H-cluster schematic and primary conserved proton transport pathway in [FeFe]-hydrogenase. Numbering of amino acids is based on the sequence of CrHydA1 and the secondary structure is from PDB ID 3LX4.[35] Midpoint potentials for defined redox states[36,37,14] are from DdH (H_{inact}, H_{trans}, H_{ox}, and H_{red})[38] and CrHydA1 (H_{sred}).[39] Oxidation states of the Fe atoms of $[2Fe]_H$ are shown adjacent to the diamond which represents the $[4Fe\text{-}4S]_H$ subcluster.

An initial study of a Cys-to-Ser substitution in CrHydA1 (Cys169Ser) and *Clostridium acetobutylicum* (CaI, Cys298Ser) result in a complete loss of catalytic activity, which was associated with alterations in the H-cluster spectroscopic properties.[31] Though the H-cluster was fully intact, the EPR and FTIR spectra indicated it was "trapped" in a state with properties similar to H_{trans} (Figure 1) that had been only previously observed in the [FeFe]-hydrogenase from *Desulfovibrio desulfuricans* (DdH).[31] This state is *trans*iently formed during reductive activation (e.g., under H_2 or electrochemical reduction)[40,41,36,37,42] of the oxidized inactive form of DdH (Figure 1).[43,20,38,39] The observation that Cys169Ser was able to equilibrate into H_{trans} was based on the Cys→Ser substitution resulting in an inactive enzyme, and/or was due to a modification of the H-cluster redox properties and H_2 binding environment.[31]

Amino acid substitutions that disrupt PT pathways can be used to explore in more depth how H-cluster electronic transitions are coupled to protonation steps involved in H_2 activation. Here we examine effects of a Cys169Ser substitution in CrHydA1 under steady-state conditions by EPR and FTIR spectroscopies, and evaluated the electronic properties of this variant by complementary Density Functional Theory (DFT) calculations. Our results show that spectral features assigned to different oxidation states of WT CrHydA1[15] are also observed in the Cys169Ser variant, however, at significantly altered intensities. Under reduction, Cys169Ser exhibited EPR spectra consistent with the presence of a $[4Fe\text{-}4S]_H^{1+}$ subcluster (Figure 1)[39,14] that strongly correlated with higher frequency *ν*CO peaks in the accompanying FTIR spectra. DFT analysis of a Cys169Ser H-cluster model complex were used to calculate IR vibrational frequencies of CO/CN^- ligands and to help assign the oxidation state of $[2Fe]_H$. Isotope and exogenous CO binding effects on the spectroscopic signals were further explored to help characterize the nature of H-cluster intermediates.

EXPERIMENTAL METHODS

Expression Plasmids and Site-directed Mutagenesis. The pETDuet based plasmid constructs for co-expression of either CrHydA1 from *C. reinhardtii* or CaI from *C. acetobutylicum* along with Hyd maturases (*hydE*, *hydF*, *hydG*) from *C. acetobutylicum* have been described previously.[44,45] Site-directed mutagenesis of the Cys residue implicated in PT in both CrHydA1 (Cys169) and CaI (Cys298) were carried out using the XL site-directed mutagenesis kit (Stratagene). Plasmid constructs were confirmed by DNA sequencing before transformation into *Escherichia coli* NovaBlue (Novagen) for propagation.

Cys169Ser CrHydA1 and Cys298Ser CaI Expression and Purification. Expression and purification of Cys169Ser CrHydA1 and Cys298S CaI were carried out with slight modifications to a previously described procedure.[45] Protein expression was induced by addition of IPTG (1.5 mM final) and the following supplements were added sequentially: cysteine (2 mM final), ammonium ferric citrate (4 mM final), glucose (0.5% v/v final), and sodium fumarate (10 mM final). Induction was carried out in 2 L narrow necked flasks (Kimax, Kimble) sealed with rubber stoppers and proceeded for 12-16 h at 30 °C under a continuous argon sparge with an outlet needle (18 gauge). Cells were broken using a French Press (American Instrument Company) at 1,000 psi. Purification over DEAE Sepharose Fast Flow (GE Healthcare) and Strep-Tactin Superflow high capacity (IBA) resins were carried out in a LABmaster Glove Box Workstation (Mbraun) using anaerobic buffers supplemented with NaDT (5 mM final). The H_2 evolution activity of the purified enzymes was measured by addition of a methyl viologen solution (5 mM final) reduced with NaDT (10 mM final). Higher con-

centrations of methyl viologen (10, 20, 40 mM final) and NaDT (20, 40, 80 mM final) were also used in some cases for further analysis. Purified Cys169Ser CrHydA1 was stored at 4 °C in 50 mM Tris, pH 8.0, 300 mM NaCl, 5% glycerol, 5 mM NaDT (buffer A) and Cys298Ser CaI was stored at 4 °C in 50 mM Tris, pH 8.0, 200 mM NaCl, 5% glycerol, 5 mM NaDT (buffer B).

[FeFe]-hydrogenase Sample Preparation. All samples were prepared in an Mbraun glove box under a nitrogen atmosphere. Samples were concentrated using a 10 MWCO Microcon centrifugal filter device (Millipore). As-isolated samples were either prepared in buffer A (Cys169Ser CrHyA1) or Buffer B (Cys298Ser CaI). Reduced samples were prepared in buffer A with either additional NaDT (50 mM final) or 100% UHP H_2 (General Air, Denver, CO USA) flush for 10 cycles on a Schlenk line. The H_2 inlet had an O_2 trap (Big O_2 Trap, Agilent Technologies, Inc., Santa Clara, CA USA) between the gas cylinder and the Schlenk line. For the H_2 sample, high pressure/vacuum EPR tubes (Wilmad-LabGlass) were used and samples were frozen under a slight over-pressure of H_2. FTIR of samples treated with 100% H_2 were prepared by a similar procedure and a septum-sealed 0.3 mL conical vial containing a 10 µL aliquot of enzyme was flushed with H_2 on a Schlenk line for 10 cycles while it was kept on ice. The sample was then equilibrated for 2 h at 4 °C in the Mbraun glove box prior to obtaining the FTIR spectrum. Auto-oxidized, defined previously,[15] samples were prepared by exchange using a G-25 column (GE Healthcare) into buffer A prepared in the absence of NaDT followed by incubation for 7 to 14 days at 4 °C in the Mbraun glove-box. In some a cases oxidized methyl viologen was added (2 mM final) to achieve more complete formation of H_{ox}. As-isolated, NaDT, and auto-oxidized samples were treated with 100% CO gas by either: sparge for 30 s, 5 min incubation on ice, sparge for 15 s, and a final 10 min incubation on ice; or by 10 vacuum/100% CO flush cycles on a Schlenk line. Typical sample concentrations ranged from 12 – 20 mg/mL and from 100 – 150 mg/mL for higher concentrated samples.

For isotope studies, the NaDT/H_2O sample was prepared in buffer A with additional NaDT (100 mM final; final protein concentration: 150 mg/mL) and equilibrated for 1 h at 4 °C in the MBraun glove box prior to obtaining the IR spectrum. The NaDT reduced sample in D_2O was prepared by G-25 column exchange into D_2O buffer of 50 mM Tris, pH 8.0, 300 mM NaCl, 5% glycerol with NaDT at 100 mM (final protein concentration, 112 mg/mL). The sample was equilibrated for 30 min at room temperature in the MBraun glove box prior to obtaining the FTIR spectrum. The H_2/H_2O was prepared by treating as-isolated Cys169Ser (120 mg/mL) with 100% H_2 by 10 flush cycles on a Schlenk line. The sample was in a septum-sealed conical vial and kept on ice during treatment and was followed by incubation for 2 h at 4 °C in the refrigerator in the MBraun glove box prior to collecting the FTIR spectrum. The D_2/D_2O sample (124 mg/mL) was prepared by G25-column exchange into D_2O buffer of 50 mM Tris, pH 8.0, 300 mM NaCl, 5% glycerol. After 5 days equilibration at 4 °C, the sample was loaded into a septum-sealed conical vial and sparged for 1 min with D_2 (99.7% D_2, Matheson Tri-Gas, Newark, CA USA). An outlet needle prevented over pressurization and allowed for gas flow. After sparging, the sample equilibrated overnight (~24 h) at 4 °C in the MBraun glove box prior to obtaining the FTIR spectrum.

EPR Spectroscopy. EPR spectra were recorded on a Bruker ELEXSYS E500 CW spectrometer system outfitted with an Oxford Instruments liquid helium cryostat (ESR900), automatic transfer line (LLT750), temperature controller (ITC503) and cylindrical Bruker resonator (SHQ). The magnetic field was calibrated with a 2,2-diphenyl-1-picrylhydrazyl (DPPH) standard from Bruker. Temperatures of recorded spectra ranged from ±2 K. Simulations were carried out in Easy Spin.[46] Double integration of the spectra was carried out in Origin (OriginLab) for determination of relative intensities, and fractional contributions of the different signals comprising the overall spectra. Analysis of the power saturation data was prepared by plotting log ($S/\sqrt{P}$) against log P, where S is signal amplitude and P is power. In these plots, the line slopes towards the abscissa with increasing concentration.[47,48] Power saturation data collected at 11 K were fitted to the equation $S = \sqrt{P}/(1+P/P_{½})^{0.5b}$, where $P_{½}$ is that half-saturation power and b is the inhomogeneity parameter.

FTIR Spectroscopy. FTIR spectra were recorded on a Nicolet 6700 FTIR Spectrometer (Thermo Fisher Scientific). The spectrometer was purged with N_2 gas passed through a Drierite-filled glass desiccant tube and two miniature desiccant air dryers (Twin Tower Engineering) with pre- and post-desiccant filters. The spectrometer uses a Globar IR source, with a CaF_2 beam splitter and a liquid-nitrogen cooled mercury-cadmium telluride (MCT) detector.

The custom sample cell consisted of a set of CaF_2 windows with a spacer with a path-length of approximately 12 µm. The sample volume was approximately 5.0 µL. A final spectrum consisted of 512 scans at 2 cm^{-1} resolution, collected by the OMNIC software program (Thermo Fisher Scientific). Buffer solution served as the reference spectrum, where appropriately treated buffer solution containing protein served as the sample spectrum. All spectra were collected at room temperature (21 °C). The OMNIC software was configured to report absorbance spectra, and the final format for the figures was generated using manually adjusted spline baseline fitting. Occasionally, spurious water absorption peaks would be seen due to slight changes in water vapor concentration in the N_2 purge gas. These water absorption peaks could be removed using a built-in atmospheric suppression algorithm in OMNIC, or with manual subtraction of a water vapor spectrum.

Computational Model of CrHydA1. The starting structure for the DFT calculations was based on the x-ray geometry of the *Desulfovibrio desulfuricans* [FeFe]-hydrogenase (PDB ID 1HFE)[11] in which the water molecule bridging Fe_d and Fe_p (Figure 1), was replaced by a CO group, and the bridging propanedithiolate (pdt) ligand was replaced by adt.[12,13] Calculations were carried out on models of WT CrHydA1 and the Cys169Ser variant, in which the -SH group of Cys169 was replaced with the -OH group of Ser (Figure S1).

A main difference between CrHydA1 and DdH is the lack, in the former, of an accessory domain containing the conserved cysteine-rich motifs for the binding of the two [4Fe-4S] auxiliary F-clusters.[11,33] However, the residues forming the hydrophobic pocket surrounding the active site, as well as the residues involved in the putative PT chain, are well conserved among all [FeFe]-hydrogenases.[27-29] In addition, *ν*CO and *ν*CN stretching frequencies of well-characterized states, such as H_{ox} and H_{ox}-CO of CrHydA1, CpI and DdH are similar, indicating that the structural differences in H-cluster environments between these enzymes do not significantly affect *ν*CO and *ν*CN IR frequencies.[49] The computational model, which is schematically shown in Figure S1, includes the bimetallic $[2Fe]_H$ cluster, and selected residues of the second coordination sphere. In the following discussion, the residues are numbered according to the sequence of CrHydA1.

The cysteine residue linking $[4Fe\text{-}4S]_H$ to $[2Fe]_H$ (Cys421 in CrHydA1) was truncated at the Cα atom. The $[4Fe\text{-}4S]_H$ cluster in the oxidized (+2) or reduced (+1) forms was modelled by a thiol, or thiolate ligand, respectively, as we showed that protonation of the sulphur atom of Cys421 mimics coordination of the $[4Fe\text{-}4S]_H^{+2}$ cluster, whereas a thiolate better represents coordination of the $[4Fe\text{-}4S]_H$ cluster in its +1 redox state.[50]

The second coordination sphere of the metal cluster includes side chains of residues Cys169/Ser169, Lys228, Ser193, Glu231, Phe290, Met223, Ser133, and Glu141, and selected backbone atoms of Pro194, Gln195, Pro93 and Ala94. The truncated residues were saturated with hydrogens. The model also contains a water molecule H-bonded to Cys169/Ser169 and Glu141 as a part of the PT chain.[10,11,24,25] A detailed list of the atoms composing the model is shown in Table S1. Notice that when states featuring a protonated bridgehead amine are taken into account, the latter group behaves as a H-bond donor, the acceptor being Cys169/Ser169; the chain of hydrogen bonds then extends up to Glu141, the side chain of which attains the anionic COO^- state in this case (*see* Figure S1). On the other hand, when the bridgehead amine is in the deprotonated (neutral) form in the model, the directionality of hydrogen bonds in the chain is inverted, which calls for the introduction of Glu141 residue in its neutral (COOH) form. During geometry optimizations, selected atoms were kept fixed at their crystallographic positions, in order to avoid unrealistic distortions at the boundary of the model. These atoms are also indicated in Table S1.

Lys228, Glu231 and Asp13 were included in the model since they form a network of H-bonds, which ends at one CN^- ligand. Amide hydrogens of Ala94 and Gln195 also form H-bonds with the two CN^- ligands. Met223 and Phe290 are in the hydrophobic pocket surrounding the active site, and they can be crucial in favoring the conformation of the $[2Fe]_H$ cluster with a bridged CO. Finally, Cys169 (Ser169), Glu141, Ser133 and the water molecule are involved in the PT pathway to shuttle protons from/to the bridgehead amine.

All residues included in the model are conserved in CrHydA1 and DdH as well as in other [FeFe]-hydrogenases[51] emphasizing the possible relevance of these residues in the catalytic mechanism of the enzyme. An exception is Gln195, which is replaced by Ile in DdH. However, only backbone atoms of this residue are included in our model.

DFT Calculations. Quantum mechanics (QM) calculations were carried out in the DFT framework with the TURBOMOLE 6.4 suite of programs[52] by using the BP86 functional[53,54] in conjunction with the resolution-of-the-identity (RI) technique[55] and an all-electron valence triple-ζ basis set with polarization functions TZVP for all atoms.[56]

Vibrational analyses were carried out for all species in their minimum on the potential energy hypersurface using the same level of theory. Due to the atoms constrained at the original positions, several very small negative eigenvalues of the Hessian were computed. However, these imaginary frequencies should not affect the (much higher in energy) *ν*CO and *ν*CN stretching modes. CO frequencies were scaled according to the scaling factor:[50]

$$\nu CO_{(Scal.)} = 1.023 \cdot \nu CO_{(Cal.)} - 49$$

Deuterium isotopic effects on the CO frequencies were investigated by replacing the hydrogen terminally coordinated to Fe_d with deuterium and re-calculating vibrational frequencies from the hessian. In some forms of the enzyme, an additional frequency was identified in the range of the CO and CN^- stretching frequencies. This frequency can be assigned to a N-H stretching mode of Lys228 associated to the hydrogen involved in the H-bond with Glu231. In fact, this N-H distance is unusually large, and the corresponding NH---O_{Glu} distance unusually small, explaining the considerable shift to lower wavenumbers of this stretching mode, which is probably an artefact of the model used for the computational analysis. Since this mode can be coupled to the *ν*CO and *ν*CN stretching modes, thus possibly affecting their frequency values, we also considered to replace this hydrogen with deuterium in order to shift the N-H stretching frequency well outside the region of the *ν*CO and *ν*CN stretching modes; notably, the additional set of calculations on such deuterated models did not allow us to observe any significant

change in the computed *v*CO and *v*CN stretching frequencies, as compared to the parent models.

RESULTS AND DISCUSSION

Biochemical Properties of Purified CrHydA1 Cys169Ser. The specific activity (U), defined as 1 μmol H_2 produced min^{-1} mg^{-1}, ranged between 15 and 30 U for Cys169Ser CrHydA1. Although active, the level of H_2 evolution activity represents a significant decrease (30-40 fold) compared to wild-type CrHydA1. Use of increased concentrations of methyl viologen (MV, 80 mM) and NaDT (160 mM) resulted in increased H_2 evolution activity to a V_{max} of 84 U, further demonstrating that the Cys→Ser variant retains catalytic function, albeit at reduced levels. Despite the reduced activity, both EPR and FTIR spectra of Cys169Ser displayed strong spectroscopic signals, indicating that H-cluster incorporation was minimally affected during *in vivo* biosynthesis. This is consistent with the previous initial characterization of the Cys169Ser CrHydA1 variant,[31] however for those studies this substitution was reported to be completely deficient in H_2 evolution and H_2 oxidation activities.

Spectroscopic Properties of As-Isolated Cys169Ser. We showed previously that when WT CrHydA1 was purified in NaDT buffer, a major fraction equilibrated into the H_{ox} state, with minor contributions from other reduced states.[15]. This was evident from a strong g=2.1 H_{ox} EPR signal assigned to the mixed-valent Fe(II)Fe(I) $[2Fe]_H$ and diamagnetic $[4Fe\text{-}4S]_H^{2+}$ subclusters, with minor contributions from other reduced states.[15] In contrast, the EPR spectrum of an as-isolated sample of Cys169Ser in buffer containing 5 mM NaDT primarily displayed a strong rhombic 2.07 signal (g = 2.068, 1.943, 1.881, T_{opt} = 11 K) along with an overlapping rhombic 2.06 signal (g = 2.065, 1.969, 1.906, T_{opt} = 23 K) (Figure 2A). The rhombic 2.07 signal decreased in intensity with increasing temperature and was nearly silent at 36 K (Figure S2). Above 36 K, the rhombic 2.06 signal became more resolved and could be observed up to 50 K without much broadening. The temperature profiles of these two signals are most consistent with either a S=½ $[4Fe\text{-}4S]_H^{1+}$ cluster (rhombic 2.07) or a S=½ $[2Fe]_H$ cluster (rhombic 2.06). These profiles are nearly identical to the rhombic 2.08 (g = 2.077, 1.935, 1.880) and 2.06 (g = 2.061, 1.968, 1.900) signals, respectively, we previously reported for reduced WT CrHydA1.[15] The broad shoulder near g = 2.1, more evident at elevated temperatures (23 K), indicates a small contribution of H_{ox} to the overall spectrum, which produces a rhombic 2.1 signal (g = 2.100, 2.039, 1.990).[57]

The FTIR spectrum of the as-isolated Cys169Ser (Figure 2A) displayed numerous peaks in regions where CO (~1775-2030 cm^{-1}, 8 peaks) and CN^- stretching modes (~2030-2100 cm^{-1}, 4 peaks) are detected, indicating the presence of multiple intermediates. The peaks assigned to *v*CO modes at 1860, 1869, 1960, 1967, 1977, and 1984 cm^{-1} and *v*CN modes at 2074 and 2080 cm^{-1} most likely correlate with the two rhombic 2.07 and 2.06 signals of the reduced H-cluster. The peaks observed at 1800, 1936, 1969, 2067, and 2087 cm^{-1} are assigned to the H_{ox} state,[15] and are consistent with the EPR spectrum having a g = 2.1 H_{ox} signal. The as-isolated sample, showed IR peaks at 1967 and 1969 cm^{-1} that are assigned to the reduced and oxidized H-cluster, respectively, based on comparison of NaDT-treated to auto-oxidized samples *(vide infra)*. At higher concentrations, a *v*CO peak at 1896 cm^{-1} was observed (Figure 2E) that is assigned to the H_{red} state with a $[4Fe\text{-}4S]_H^{2+}$-Fe(I)Fe(I)-[H] H-cluster.[20] A similar set of peaks at 1878, 1891, and 1900 cm^{-1} were also observed in the corresponding CaI variant Cys298Ser (Figure S3). The slight differences in *v*CO/*v*CN peak intensities and energies between Cys169Ser and Cys298Ser indicate the H-cluster in the two enzymes populate similar intermediates, but at fractional levels. These differences are likely due to long-range electronic and ET effects of F-clusters present in CaI, but not CrHydA1, on the H-cluster electronic state.[58]

Spectroscopic Properties of Oxidized Cys169Ser. The oxidation of as-isolated Cys169Ser was carried out by an auto-oxidization procedure, which involves exchange and equilibration into buffer without NaDT.[15] This procedure requires enzyme turnover to achieve equilibration into H_{ox}, therefore to account for the much lower turnover frequency of the Cys169Ser variant this procedure was carried out for 7 to 14 days at 4 °C. The resulting EPR spectra yielded almost total attenuation of the rhombic 2.07 signal along with the appearance of a weak, but well resolved rhombic 2.1 signal (g = 2.099, 2.040, 1.996, T_{opt} = 20 K) of the H_{ox} state (Figure 2B, dark shade). The rhombic 2.06 EPR signal was also present at a similar intensity to the as-isolated sample as determined by double-spin integration of the signal. Depending on the sample, weak intensities of the rhombic 2.07 signal remained present (Figure 2B, light shade). There was a minimal contribution of the CO inhibited state (H_{ox}-CO) to the spectra, which is indicative of H-cluster degradation. Further oxidation by methyl viologen gave an increase in signal intensity of the rhombic 2.1 signal along with appearance of an axial g = 2.05 signal that can be assigned to H_{ox}-CO (Figure S4). As also pointed out earlier,[31] the evidence for EPR silent species formed upon auto-oxidation is consistent with the weak spectral intensity, which was 20% (Figure 2B) compared to the as-isolated overall signal at 23 K. In the earlier report, no EPR signal was detected in the absence of NaDT. Several defined H-cluster states such as H_{red} and H_{inact} (Figure 1) have been shown to be EPR silent.[40-42,39]

The FTIR spectrum of auto-oxidized Cys169Ser showed *v*CO peaks at 1798 (μ-CO), 1936 and 1969 cm^{-1} (terminal), and *v*CN peaks at 2067, and 2087 cm^{-1}, which are assigned to the H_{ox} state. Enrichment of the H_{ox} signal in the IR spectrum correlates nicely with the appearance of the EPR rhombic 2.1 signal assigned to H_{ox} (Figure 2B). Additional IR peaks at 1944, 1985 (*v*CO), and 2072 cm^{-1} (*v*CN) indicate the presence of other intermediates.

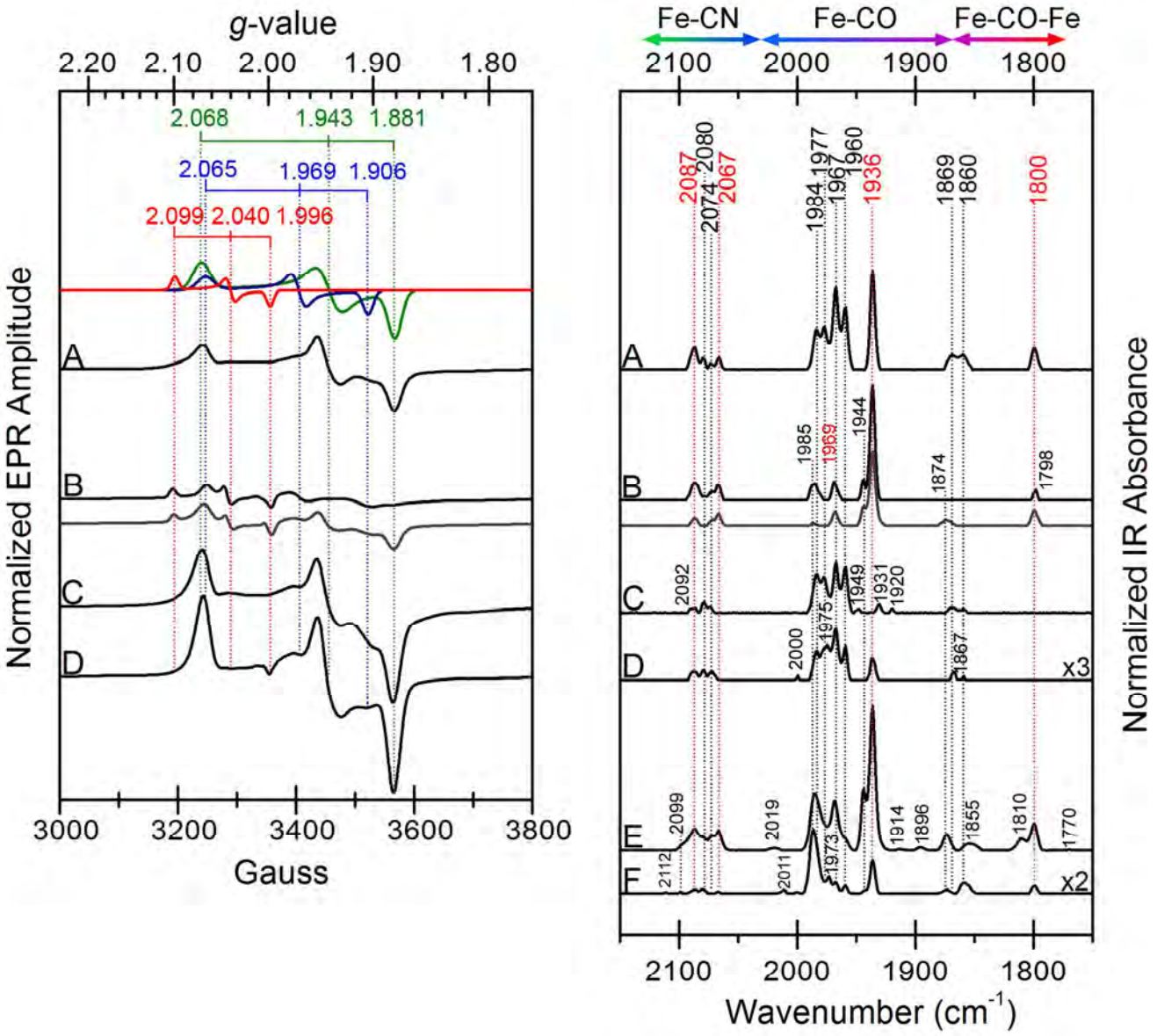

Figure 2. EPR and FTIR of Cys169Ser under steady-state reducing and oxidizing conditions. Panels show EPR (left) and FTIR (right) spectra of Cys169Ser samples. (A) As-isolated. (B) Auto-oxidized sample 1 dark shade, sample 2 light-shade. (C) NaDT. (D) 100% H_2 treated. (E) High concentration as-isolated sample (120 mg/mL). (F) High concentration 100% H_2 treated sample (120 mg/mL). Simulations of EPR signals (left panel) are shown on top: red, rhombic 2.1 (H_{ox}); blue, rhombic 2.06; green, rhombic 2.07. The *v*CN and *v*CO peaks of FTIR spectra (right panel) assigned to H_{ox} are in red, and reduced or unassigned signals are in black. FTIR spectra were collected at room temperature. EPR spectrometer settings: temperature, 11 K; microwave power, 1.0 mW, microwave frequency, 9.38 – 9.39 GHz; modulation frequency, 100 kHz; modulation amplitude, 10.0 G; time constant, 327.68 ms.

The peak at 1985 cm^{-1} mostly correlated with the presence of the rhombic 2.06 signal and the peaks at 1944 and 2072 cm^{-1} more likely correlate to an EPR silent species, since the latter peaks have only been observed for oxidized samples.

Spectroscopic Properties of NaDT and H_2 Reduced CrHydA1 Cys169Ser. Reduction of Cys169Ser with excess NaDT (Figure 2C) primarily yielded the rhombic 2.07 signal, which was more sharp and intense than in the as-isolated Cys169Ser sample. Treatments with H_2 yielded similar spectra (Figure 2D), also primarily composed of the sharp rhombic 2.07 signal. This differed from the WT samples under H_2, which displayed a broadened signal (g = 2.3-2.07) compared to the rhombic 2.07 (Table S2).[15] Also present in Cys169Ser under NaDT and H_2 reduction was a second, overlapping rhombic 2.06 signal, present at a similar intensity as for the as-isolated and auto-oxidized samples. For the H_2 sample, the feature at g = 1.997 indicates a small presence of H_{ox} that likely did not react with H_2. Simulations show that the overall spectra of reduced

samples consist of 86% of the 2.07 signal and 14% of the 2.06 signal. The power saturation dependency of the rhombic 2.07 signal was nearly identical to the WT rhombic 2.08 signal, and saturated with increasing power at 11 K more quickly than at 23 K, indicating a similar source for the two signals (Figure S5).

The source of the rhombic 2.07 signal in Cys169Ser is assigned to a S = ½, $[4Fe\text{-}4S]_H^{1+}$ cluster and is highly related to the rhombic 2.08 signal observed in the WT CrHydA1.[15] The assignment of rhombic 2.06, however, has two possibilities; either it originates from a S = ½, $[2Fe\text{-}2S]^{1+}$ (*vide infra*) based on the temperature saturation[15] or a S = ½, $[4Fe\text{-}4]_H^{1+}$ that is similar to $[4Fe\text{-}4S]_H^{1+}$ of the H_{trans} state of DdH.[40-42] The EPR signal assigned to H_{trans} shows similar g-values (g = 2.06, 1.96, 1.89) and temperature properties ($[2Fe\text{-}2S]^{1+}$-like) to rhombic 2.06 of Cys169Ser. For the H_{trans} signal, Mössbauer studies assigned the H-cluster oxidation state to $[4Fe\text{-}4S]_H^{1+}$ paired with a diamagnetic Fe(II)Fe(II) $[2Fe]_H$ subcluster.[36,37] An H_{trans} state was also reported for the as-isolated Cys169Ser by Knörzer *et al.*,[31] however, this assignment was based on an EPR signal with g-values of 2.067, 1.94, 1.88. Those g-values more closely align with the g = 2.07 signal (2.068, 1.943, 1.881) we observed for Cys169Ser. They suggested that changes in redox properties could allow a nearby H_2O to react with Fe_d to produce a terminal -OH ligand as modeled by earlier DFT studies of H_{trans} and also H_{inact},[59,60] although this ligand has not yet been observed experimentally.[38] Thus, the two overlapping 2.07 and 2.06 EPR signals of Cys169Ser (and 2.08/2.06 for wild-type CrHydA1)[15] represent discrete states, and are distinguished by slight differences in g-tensor, and temperature and power properties. We propose these states arise from changes at $[2Fe]_H$ that lead to each state having a unique terminal ligand, electronic spin and charge distribution, coordination environment and/or protonation state of adt.

The FTIR spectra of Cys169Ser reduced with NaDT (Figure 2C) or H_2 gas (Figure 2D) showed complexity in the terminal νCO region (1900-2030 cm^{-1}), but at higher energy positions compared to WT CrHydA1. In addition, there were several νCO peaks in a region consistent with a "semi-bridging" (~1850-1880 cm^{-1}) assignment. Overall, under reduction with NaDT, 13 peaks were observed at 1860, 1870, 1920, 1931, 1949, 1960, 1967, 1978, 1984, 2074, 2079, 2087, and 2092 cm^{-1}. Likewise, reduction with H_2 also produced a complex IR spectrum with 12 peaks at 1859, 1867, 1937, 1960, 1967, 1975, 1984, 2000, 2073, 2079, 2086, 2088 cm^{-1}. The slight shift of the 1969 cm^{-1} peak assigned to H_{ox} WT, to 1967 cm^{-1} in Cys169Ser, may reflect minor rearrangements of $[2Fe]_H$ during reduction. Through analysis of these spectra and other data not shown, it appears that νCO peaks at 1860, 1977, and 1984 cm^{-1} and peaks at 1867, 1960, and 1967 cm^{-1} can be assigned to two discrete states. It is possible that these two sets of signals correlate to the rhombic 2.06 and 2.07 EPR signals, however the potential presence of EPR silent species along with the different temperatures for data collection between EPR (11-60 K) and FTIR (room temperature), complicates these correlations. For higher concentrated Cys169Ser samples treated with H_2 (Figure 2F), residual H_{ox} was observed by the presence of peaks at 1800, 1936, and 1969 cm^{-1}, whereas additional peaks at 1874, 1944, 1960, 1968, 1973, 1987, 2001, 2011, 2067, 2080, 2087, 2099 2112 cm^{-1} are similar to the lower concentrated sample. This may indicate a decreased ability for the Cys169Ser variant to react with H_2 or incomplete H_2 treatment, since residual H_{ox} peaks are also observed for H_2 treated wild-type CrHydA1.[15]

Observation of Hydrogen/Deuterium Isotope-Sensitive FTIR Peaks in Reduced Cys169Ser. A mechanism for H_2 activation by [FeFe]-hydrogenases has been proposed based on crystallographic and FTIR analysis of reduced DdH and CrHydA1, whereby the μ-CO is proposed to alternate between bridging (H_{ox}) and terminal (H_{red}-hydride) orientations as the H-cluster transitions through a catalytic cycle.[11,20,38,39,14] This shift of the μ-CO is assumed to occur along with formation of terminal hydride on $[2Fe]_H$.[59,61] It has been shown for metal-carbonyl organometallic complexes that terminal hydrides exert a strong trans-influence on the trans-ligand, in this case the μ-CO of $[2Fe]_H$. This can result in mixing of the νFeH with νCO modes and causes an hydrogen/deuterium isotope effect on the position of νCO in the IR spectrum.[62] Notably, the H/D isotope effect induces a shift of νCO to lower energies after H→D substitution, with only small to negligible effect on *cis* CO ligands.[63-65] Thus, reduction of [FeFe]-hydrogenases in H- or D-enriched buffers can be used to assign νCO peaks to the μ-CO ligand based on a isotope induced shift, and provide indirect evidence for an H-species bound to the terminal position on $[2Fe]_H$.

As shown in Figure 3 (detailed spectra, Figure S6), reduction of Cys169Ser by NaDT or H_2 produces νCO peaks in the 1860-1870 cm^{-1} region, which are consistent with a "semi-bridging" assignment. After exchange from H_2O→D_2O enriched buffers followed by reduction with NaDT or D_2, these peaks shifted to slightly lower energies. Specifically, the 1860 and 1868 cm^{-1} peaks shifted to 1853 and 1864 cm^{-1} after reduction with NaDT, and the peak observed at 1859 cm^{-1} under 100% H_2-treatment in H_2O, shifted to 1853 cm^{-1} under 100% D_2 in D_2O buffer (Figure 3). These shifts are consistent with a change in mass of a terminal ligand on Fe_d that is positioned trans to the semi-bridging CO, and supports a terminal H-species (e.g., hydride) coordinated to the Fe_d atom of $[2Fe]_H$ in these reduced states. The DFT calculations shown in Figure 3 on the reduced H-cluster in Cys169Ser simulated with either H or D terminal ligands also show a similar H→D induced downshift in the μ-CO peak.

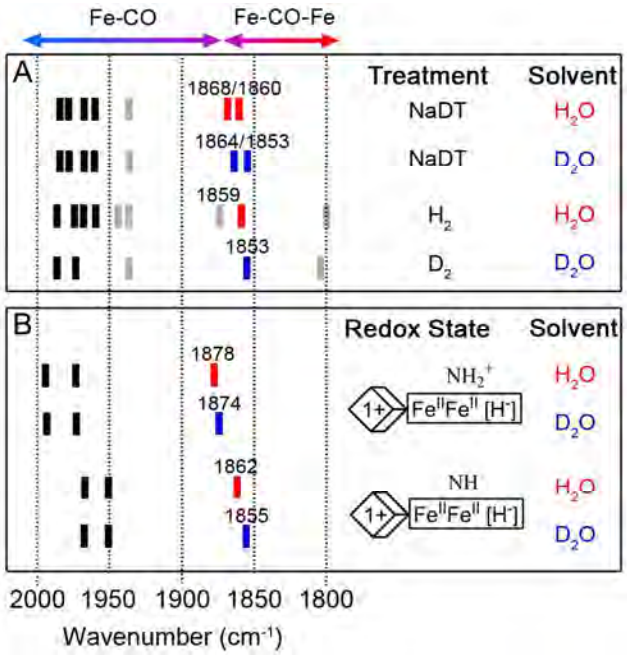

Figure 3. Comparison of experimental FTIR bands of CrHydA1 Cys169Ser after reduction to calculated FTIR bands from a DFT model of Cys169Ser. (A) Experimental FTIR bands in *v*CO region from CrHydA1 Cys169Ser enzyme reduced with either NaDT, H_2, or D_2 in buffer prepared with either H_2O or D_2O. (B) DFT calculated FTIR bands in the *v*CO region based on the Cys169Ser H-cluster model prepared in H_2O or D_2O solvent. Bands indicated in red (H_2O) are observed to shift to slightly lower energies under D_2O (blue). Bands in light gray are either assigned to the H_{ox} state or are unassigned.

DFT calculations of the vCO frequencies in reduced Cys169Ser and WT enzymes. The observation of the H→D exchange effect on the μ–CO bands called for a detailed DFT analysis of adducts featuring a terminal hydride *trans* to the μ-CO on Fe_d. In addition, a comparison of the FTIR spectrum of WT CrHydA1 to the Cys169Ser variant after treatment with 100% H_2 shows the principle *v*CO peaks shift to higher energies (Figure S7), suggesting that binding H_2 to H_{ox} induces a further oxidation of the $[2Fe]_H$ subcluster from a mixed-valent Fe(II)Fe(I) to a diferrous state. Notably, DFT vibrational analysis performed on Cys169Ser species, in which the $[2Fe]_H$ subcluster attains the Fe(II)Fe(II) state, and the $[4Fe\text{-}4S]_H$ cluster is in the reduced $[4Fe\text{-}4S]_H^{1+}$ state, shows that the principle *v*CO peaks occur at 1878, 1971, and 1992 cm^{-1} or 1862, 1951, and 1965 cm^{-1}, depending on the protonation state of the adt ligand (**3b** and **4b** in Figure 4 and Table 1). In particular, the assignments of *v*CO frequencies reported in Table 1 for **3b** and **4b** are associated to mean absolute errors (MAE) as low as 9 and 5 cm^{-1}, respectively, compared to the experimental frequencies that correlate with the rhombic 2.06 and 2.07 EPR signals (*vide infra*). This suggests that these two states might actually differ in the protonation state of the adt ligand. As far as the effects of H→D substitution on theoretical vibrational spectra are concerned, the presence of a D^- terminal ligand in the model leads to a significant downshift in the μ-CO energies, in agreement with experiments (see Figure 3).

A very good match between computed and experimental values can also be found when WT CrHydA1 is taken into account: in particular, the comparison between theoretical frequencies of model **4a** and the available experimental data highlights a MAE as low as 9 cm^{-1}. The latter result suggests that the higher oxidation state intermediate also forms in the WT form of the enzyme. This conclusion is further supported by the EPR spectra for which similar rhombic signals are observed in both Cys169Ser and WT under reduction (*vide infra*). Multiple theoretical studies have predicted formation of a $[2Fe]_H$ intermediate with Fe(II)Fe(II) oxidation states upon H_2 binding and activation at the H-cluster.[19,59,50] Experimental evidence from x-ray absorption studies on CrHydA1 also indicated a slight oxidation of $[2Fe]_H$ upon H_2 binding by H_{ox},[66] consistent with the transition of $[2Fe]_H$ from Fe(II)Fe(I) to Fe(II)Fe(II).

Table 1. Calculated and experimental CO vibrational frequencies for the H-cluster model intermediates described in this study (Figure 4).

	CO Vibrational Frequencies (cm^{-1})	
Model	DFT	Experimental
1a	1841, 1949, 1989	1802, 1940, 1964[a]
1b	1831, 1948, 1995	1798, 1936, 1969
2a	1905, 1991, 2011	not observed
2b	1902, 1992, 2012	not observed
3a	1879, 1972, 1992	1861, 1961, 1979[a,b]
3b	1878, 1971, 1992	1860, 1977, 1984[c]
4a	1862, 1951, 1964	1861, 1961, 1979[a,b]
4b	1862, 1951, 1965	1867, 1960, 1967[c]
5a	1803, 1891, 1904	1792, 1891, 1915[a]

[a]WT signals are reported from a previous analysis of CrHydA1.[15] [b]Experimental assignment of these CO peaks cannot be distinguished between models **3a** and **4a**. [c]Experimental assignment of these CO peaks cannot be distinguished between models **3b** and **4b**.

Disruption of PT in Cys169Ser Causes a Shift in the Steady-state Equilibria of H-cluster Redox States. The strong bias for CrHydA1 Cys169Ser to equilibrate into a $[4Fe\text{-}4S]^{1+}$-Fe(II)Fe(II) oxidation state is again consistent with the Cys-to-Ser substitution disrupting fast PT during the catalytic cycle of the H-cluster. The *v*CO peaks observed in the reduced WT CrHydA1 that occur at 1882, 1891, 1919, 1920 and 1954 cm^{-1} are significantly weaker in the FTIR of reduced Cys169Ser. Our initial assignments of WT CrHydA1 EPR signals observed under NaDT reduction (rhombic 2.08) and H_2 reduction (broad 2.3-2.07) were H_{sred} or $[4Fe\text{-}4S]_H^{1+}$-Fe(I)Fe(I) and $[4Fe\text{-}4S]_H^{1+}$-

Fe(II)Fe(II) state, respectively.[15] A more comprehensive analysis that considers the results presented here for Cys169Ser suggests the rhombic 2.07/2.08 signals better correlate to a $[4Fe\text{-}4S]_H^{1+}$-Fe(II)Fe(II) assignment. The contribution of the broad signal is strongest in the WT EPR spectrum when the 1883, 1891, 1916, and 1933 cm^{-1} *v*CO peaks dominate the FTIR spectrum,[15] suggesting these might be assigned to a $[4Fe\text{-}4S]_H^{1+}$-Fe(I)Fe(I) H-cluster. Likewise, the rhombic 2.08 signal in WT CrHydA1 correlated best with the occurrence of 1861, 1961 and 1979 cm^{-1} *v*CO peaks,[15] which matches with the rhombic 2.07 signal and higher energy *v*CO peaks of Cys169Ser (Figure 2). By comparison the H_{sred} state of WT CrHydA1 described by Adamaska *et al.*[14] as $[4Fe\text{-}4S]_H^{1+}$-Fe(I)Fe(I) was formed under reduction by NaDT and 100% H_2 with *v*CO peaks at 1954, 1919 and 1882 cm^{-1}, and a rhombic EPR signal with properties most similar to the rhombic 2.07/2.08 signals we observed in Cys169Ser and WT, respectively (Figure 2, Table S2). Although the catalytic relevance of H_{sred} has recently been questioned,[67] these studies indicate that formation of H_{red} and H_{sred} require functional PT, and that reduction of the $[2Fe]_H$ subcluster to the Fe(I)Fe(I) level is accomplished via a PCET mechanism.

Disruption of PT pathway and the subsequent prevention of electronic transitions at the H-cluster may also explain accumulation of a $[4Fe\text{-}4S]_H^{1+}$ subcluster signal in the EPR spectrum of reduced Cys169Ser. Intramolecular electron transfer between the $[4Fe\text{-}4S]_H$ and $[2Fe]_H$ subclusters is facilitated by strong spin coupling exchange through the bridging Cys thiolate.[36,37,61,68-70] This coupling may be disrupted when PT and ET steps are decoupled in Cys169Ser, further demonstrating that the electronic properties of the H-cluster are tightly coupled to its surrounding protein framework.[69,71-73,31,74,75]

In addition, the substitution of a more electronegative group like -OH for -SH just 3.5 Å away from the bridgehead amine could alter H-cluster interaction and cause changes to the electronic distribution. Model studies on $[2Fe]_H$ compounds show that electron-delocalization extends into the adt ligand suggesting that nearby changes such as H-bonding or differences in protonation state of the bridgehead amine could result in different H-cluster properties.[76] The latter observation is consistent with the calculations here, which give different *v*CO frequencies for H-cluster states where the only difference is the protonation state of the bridgehead (Figure 4). Interestingly, the upward *v*CO shifts observed in this study compare nicely to FTIR of a NaDT reduced CrHydA1 that was reconstituted with a synthetic $[2Fe]_H$ mimic containing an O atom in the form of pdt in place of N at the bridgehead position.[13]

Spectroscopic Properties of CO Treated Cys169Ser. CO is known to inhibit [FeFe]-hydrogenase catalytic activity by binding reversibly to the terminal site on Fe_d of the oxidized $[2Fe]_H$ subcluster,[77] which results in distinctive H_{ox}-CO signals in both EPR[78,57,42] and FTIR spectra.[43,79] Thus, the requirement for an open site on Fe_d for exogenous CO binding together with the unique spectral signatures provide a means to probe the coordination sphere and occupancy of Fe_d.

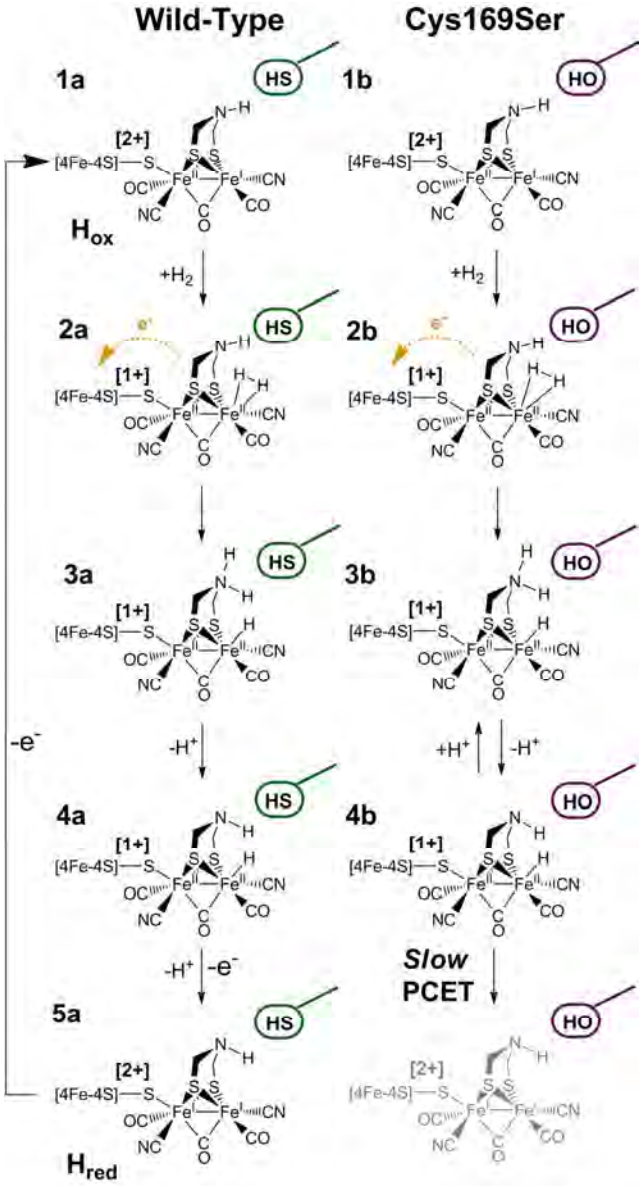

Figure 4. Schematic of model for H_2 activation by WT and Cys169Ser variant of CrHydA1 based on experimental results and DFT calculations. The respective thiol and hydroxyl side chains of nearby Cys and Ser residues are noted in green and purple.

The interaction of CO with Cys169Ser was explored by treating differently prepared Cys169Ser samples with 100% CO gas. As reported by Knörzer et al.,[31] the treatment of as-isolated, or NaDT reduced Cys169Ser with 100% CO did not give rise to the characteristic H_{ox}-CO EPR axial signal of CrHydA1 (data not shown).[39,15]

By comparison, treatment of auto-oxidized Cys169Ser with CO yielded an axial 2.05 signal (g = 2.047, 2.005, 2.007) assigned to formation of H_{ox}-CO (Table S2). This signal coincided with the complete replacement (or at-

tenuation) of the rhombic 2.1 H_{ox} signal (Figure 5). However, the intensity of the rhombic 2.06 signal present in the auto-oxidized EPR spectrum remained unchanged after CO exposure (Figure 5) indicating that this H-cluster species does not readily react with CO. The observations that the H_{ox} state in Cys169Ser occurs only after prolonged auto-oxidation, that CO requires an open coordination site on Fe_d to induce formation of H_{ox}-CO,[80] and that the state that gives rise to the rhombic 2.06 signal does not readily react with CO, are consistent with Cys169Ser equilibrating into a reduced state that harbors a terminally bound H-species.

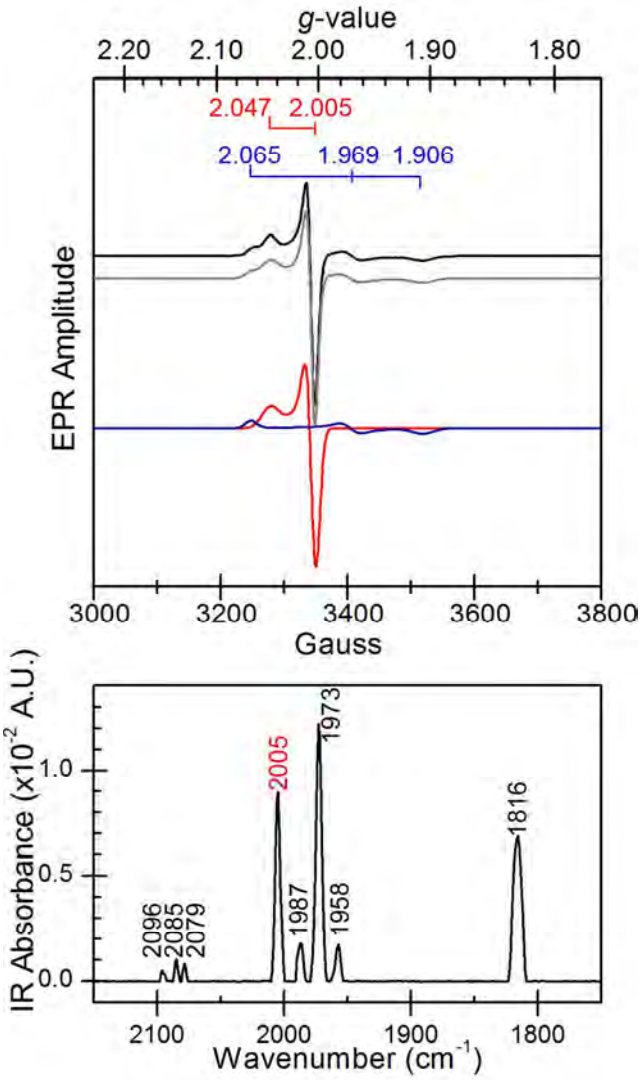

Figure 5. EPR (top panel) and FTIR (bottom panel) of auto-oxidized Cys169Ser treated with 100% CO. The EPR spectrum collected at 23 K (black) can be simulated (gray) with a combination of 45% rhombic 2.06 (blue) and 55% axial 2.05 (red) components. Sample concentration, 12 mg/mL. Other spectrometer settings as Figure 2 caption.

Likewise, the FTIR spectrum of Cys169Ser sample also showed the strongest H_{ox}-CO signal after auto-oxidization and CO treatment. The H_{ox}-CO spectrum of Cys169Ser was similar to WT showing an upshift of μ-CO from 1802→1816 cm^{-1}, with an additional *ν*CO peak at 2005 cm^{-1} from binding and vibrational coupling of a terminal exogenous CO (Figure 5). For WT CrHydA1, binding of an exogenous CO to the terminal site of $[2Fe]_H$ gives rise to a peak at 2013 cm^{-1}. The 7 cm^{-1} difference of this *ν*CO peak in Cys169Ser versus WT may arise from slight differences in coordination of other CO and CN^- ligands, or H-bonding and charge distribution around the H-cluster.

Accumulation of a Reduced Intermediate with a Hydrogen Species Bound to $[2Fe]_H$ of Cys169Ser. The observation that Cys169Ser forms a reduced state that does not easily react easily with CO suggests that the CO binding site, located at the open coordination site at Fe_d of $[2Fe]_H$,[77] is occupied by another terminal ligand. While the possibility for altered redox properties of the H-cluster in Cys169Ser[31] might affect the reactivity with CO, it is also possible that an H-species is stabilized at the distal site of this state due to disruption of PT. Since H_2 formation and oxidation is a two proton process, an intermediate such as $[4Fe\text{-}4S]_H^{1+}$-Fe(II)Fe(II)-H might accumulate, which is consistent with EPR/FTIR spectra and the observed isotope sensitive *ν*CO modes. Similar spectral features are observed in reduced WT CrHydA1, but at lower intensities compared to Cys169Ser. We hypothesize the differences are due to a shift in the equilibrium of reduced states from the disruption of a PT-dependent step (summarized in Figure 4), and/or a shifts in the mid-point potentials of reduced states as presented in Figure 1.[37,38]

Buildup of H_2-derived species at Fe_d fits the model of catalysis for which protons are shuttled between the enzyme surface and catalytic site with the terminal step of the primary PT pathway being proton exchange between Cys169 and adt. Substitution of Cys-to-Ser is likely to slow this step, and indirectly limit the exchange of protons between Fe_d of $[2Fe]_H$ and adt and possibly by disrupting the H-bonding network of the pathway.[28] While the Cys residue belongs to the primary PT pathway, several other PT networks have been identified[27] that perhaps function as a secondary pathway in Cys169Ser. This may explain the observations in this study that although Cys169Ser has much lower catalytic activity, it still exhibits spectral properties of H-cluster electronic and structural transitions.

CONCLUSIONS

Using EPR and FTIR spectroscopy in conjunction with DFT calculations we have provided evidence that disruption of the primary PT pathway by the Cys169→Ser substitution in CrHydA1 substantially reduces catalytic activity, and alters steady-state equilibration of the H-cluster among catalytic states. We hypothesize this effect arises from decoupling of PT and ET steps, and/or changes in mid-point potentials with the exchange of Cys→Ser. We demonstrated that under reduction, Cys169Ser was biased towards H-cluster states consisting of a S=½, $[4Fe\text{-}4S]_H^{1+}$

subcluster, signifying the importance of intramolecular ET to catalysis by [FeFe]-hydrogenase. Likewise, the FTIR spectra and DFT calculations showed that the $[2Fe]_H$ subcluster of Cys169Ser was biased more strongly towards a Fe(II)Fe(II) redox state. The fact that one of these diferrous states (rhombic 2.06) was unreactive with CO and showed an H→D sensitive, semi-bridging μ-CO is consistent with the presence of an exchangeable, terminal H-species trans to μ-CO. The properties of these $[4Fe\text{-}4S]_H^{1+}$-Fe(II)Fe(II) H-cluster states agree well with activation model of H_2 by the H-cluster. Indeed, DFT calculations on the model used in this work show that activation of H_2 in a $[4Fe\text{-}4S]^{2+}$-Fe(II)Fe(II) H-cluster is slightly exothermic by -2 kcal/mol, whereas activation on the corresponding $[4Fe\text{-}4S]^{2+}$-Fe(II)Fe(I) is endothermic by +5 kcal/mol. A diferrous activation state was also proposed earlier by Fan and Hall,[19] and supported by recent results on a H-cluster model where heterolytic cleavage of H_2 by the diiron subsite was stimulated by initial oxidation to the diferrous state by a covalently attached ferrocene.[7]

ASSOCIATED CONTENT

Supporting Information. Table, Schematic and Figures describing the computational model of the H-cluster. Table and Figures of EPR signals, temperature profiles, and power saturation data. FTIR Figures of isotope spectra, Cys298Ser CaI spectrum, and difference spectra of WT and Cys169Ser CrHydA1 treated with H_2.

AUTHOR INFORMATION

Corresponding Author

* paul.king@nrel.gov

ACKNOWLEDGMENT

(D.W.M, M.W.R., and P.W.K. gratefully acknowledge funding support from the U.S. Department of Energy, Division of Chemical Sciences, Geosciences, and Biosciences, Office of Basic Energy Sciences; and support of the U.S. Department of Energy under Contract No. DE-AC36-08-GO28308 with the National Renewable Energy Laboratory for the hydrogenase purification, biochemical and spectroscopy studies. M.B. and C.G. acknowledge the University of Milano-Bicocca (FAR 2013) for support of studies on H-cluster models and DFT calculations. E.K. and J.W.P. thank the Air Force Office of Scientific Research (grant FA-9550-11-1-0218) for funding support.

REFERENCES

(1) Lee, H. S.; Vermaas, W. F.; Rittmann, B. E. *Trends Biotechnol.* **2010**, *28*, 262.
(2) Sakurai, H.; Masukawa, H.; Kitashima, M.; Inoue, K. *J. Photochem. Photobiol., C* **2013**, *17*, 1.
(3) Vincent, K. A.; Parkin, A.; Armstrong, F. A. *Chem. Rev.* **2007**, *107*, 4366.
(4) Tard, C.; Liu, X.; Ibrahim, S. K.; Bruschi, M.; De Gioia, L.; Davies, S. C.; Yang, X.; Wang, L.-S.; Sawers, G.; Pickett, C. J. *Nature* **2005**, *433*, 610.
(5) DuBois, M. R.; DuBois, D. L. *Chem. Soc. Rev.* **2009**, *38*, 62.
(6) Gloaguen, F.; Rauchfuss, T. B. *Chem. Soc. Rev.* **2009**, *38*, 100.
(7) Camara, J. M.; Rauchfuss, T. B. *Nat. Chem.* **2012**, *4*, 26.
(8) Chenevier, P.; Mugherli, L.; Darbe, S.; Darchy, L.; DiManno, S.; Tran, P. D.; Valentino, F.; Iannello, M.; Volbeda, A.; Cavazza, C. *C. R. Chim.* **2013**, *16*, 491.
(9) Hsieh, C. H.; Ding, S.; Erdem, O. F.; Crouthers, D. J.; Liu, T.; McCrory, C. C.; Lubitz, W.; Popescu, C. V.; Reibenspies, J. H.; Hall, M. B.; Darensbourg, M. Y. *Nat. Commun.* **2014**, *5*, 3684.
(10) Peters, J. W.; Lanzilotta, W. N.; Lemon, B. J.; Seefeldt, L. C. *Science* **1998**, *282*, 1853.
(11) Nicolet, Y.; Piras, C.; Legrand, P.; Hatchikian, C. E.; Fontecilla-Camps, J. C. *Struct. Fold. Des.* **1999**, *7*, 13.
(12) Silakov, A.; Wenk, B.; Reijerse, E.; Lubitz, W. *Phys. Chem. Chem. Phys.* **2009**, *11*, 6592.
(13) Berggren, G.; Adamska, A.; Lambertz, C.; Simmons, T.; Esselborn, J.; Atta, M.; Gambarelli, S.; Mouesca, J.-M.; Reijerse, E.; Lubitz, W. *Nature* **2013**, *499*, 66.
(14) Adamska, A.; Silakov, A.; Lambertz, C.; Rudiger, O.; Happe, T.; Reijerse, E.; Lubitz, W. *Angew. Chem. Int. Ed.* **2012**, *51*, 11458.
(15) Mulder, D. W.; Ratzloff, M. W.; Shepard, E. M.; Byer, A. S.; Noone, S. M.; Peters, J. W.; Broderick, J. B.; King, P. W. *J. Am. Chem. Soc.* **2013**, *135*, 6921.
(16) Adamska-Venkatesh, A.; Krawietz, D.; Siebel, J.; Weber, K.; Happe, T.; Reijerse, E.; Lubitz, W. *J Am Chem Soc* **2014**, *136*, 11339.
(17) Lambertz, C.; Chernev, P.; Klingan, K.; Leidel, N.; Sigfridsson, K. G.; Happe, T.; Haumann, M. *Chem. Sci.* **2014**.
(18) Florin, L.; Tsokoglou, A.; Happe, T. *J. Biol. Chem.* **2001**, *276*, 6125.
(19) Fan, H. J.; Hall, M. B. *J. Am. Chem. Soc.* **2001**, *123*, 3828.
(20) Nicolet, Y.; de Lacey, A. L.; Vernede, X.; Fernandez, V. M.; Hatchikian, E. C.; Fontecilla-Camps, J. C. *J. Am. Chem. Soc.* **2001**, *123*, 1596.
(21) Siegbahn, P. E.; Tye, J. W.; Hall, M. B. *Chem. Rev.* **2007**, *107*, 4414.
(22) Finkelmann, A. R.; Stiebritz, M. T.; Reiher, M. *Chem. Sci.* **2014**, *5*, 215.
(23) Fourmond, V.; Greco, C.; Sybirna, K.; Baffert, C.; Wang, P.-H.; Ezanno, P.; Montefiori, M.; Bruschi, M.; Meynial-Salles, I.; Soucaille, P. *Nat. Chem.* **2014**, *6*, 336.
(24) Fontecilla-Camps, J. C.; Volbeda, A.; Cavazza, C.; Nicolet, Y. *Chem. Rev.* **2007**, *107*, 4273.
(25) Hong, G.; Cornish, A.; Hegg, E.; Pachter, R. *Biochim. Biophys. Acta, Bioenerg.* **2011**, *1807*, 510.
(26) Dutta, A.; Lense, S.; Hou, J.; Engelhard, M. H.; Roberts, J. A.; Shaw, W. J. *J. Am. Chem. Soc.* **2013**, *135*, 18490.
(27) Cornish, A. J.; Gärtner, K.; Yang, H.; Peters, J. W.; Hegg, E. L. *J. Biol. Chem.* **2011**, *286*, 38341.
(28) Ginovska-Pangovska, B.; Ho, M.-H.; Linehan, J. C.; Cheng, Y.; Dupuis, M.; Raugei, S.; Shaw, W. J. *Biochim. Biophys. Acta, Bioenerg.* **2014**, *1837*, 131.
(29) Long, H.; King, P. W.; Chang, C. H. *J. Phys. Chem. B* **2014**.
(30) Lautier, T.; Ezanno, P.; Baffert, C.; Fourmond, V.; Cournac, L.; Fontecilla-Camps, J. C.; Soucaille, P.; Bertrand, P.; Meynial-Salles, I.; Léger, C. *Faraday Discuss.* **2011**, *148*, 385.
(31) Knörzer, P.; Silakov, A.; Foster, C. E.; Armstrong, F. A.; Lubitz, W.; Happe, T. *J. Biol. Chem.* **2012**, *287*, 1489.
(32) Morra, S.; Giraudo, A.; Di Nardo, G.; King, P. W.; Gilardi, G.; Valetti, F. *PloS one* **2012**, *7*, e48400.
(33) Mulder, David W.; Shepard, Eric M.; Meuser, Jonathan E.; Joshi, N.; King, Paul W.; Posewitz, Matthew C.; Broderick, Joan B.; Peters, John W. *Structure* **2011**, *19*, 1038.
(34) Zampella, G.; Greco, C.; Fantucci, P.; De Gioia, L. *Inorg. Chem.* **2006**, *45*, 4109.
(35) Mulder, D. W.; Boyd, E. S.; Sarma, R.; Lange, R. K.; Endrizzi, J. A.; Broderick, J. B.; Peters, J. W. *Nature* **2010**, *465*, 248.
(36) Popescu, C. V.; Münck, E. *J. Am. Chem. Soc.* **1999**, *121*, 7877.
(37) Pereira, A. S.; Tavares, P.; Moura, I.; Moura, J. J. G.; Huynh, B. H. *J. Am. Chem. Soc.* **2001**, *123*, 2771.
(38) Roseboom, W.; De Lacey, A. L.; Fernandez, V. M.; Hatchikian, E. C.; Albracht, S. P. J. *J. Biol. Inorg. Chem.* **2006**, *11*, 102.

(39) Silakov, A.; Kamp, C.; Reijerse, E.; Happe, T.; Lubitz, W. *Biochemistry* **2009**, *48*, 7780.
(40) Patil, D. S.; Moura, J. J. G.; He, S. H.; Teixeira, M.; Prickril, B. C.; Dervartanian, D. V.; Peck, H. D.; Legall, J.; Huynh, B. H. *J. Biol. Chem.* **1988**, *263*, 18732.
(41) Pierik, A. J.; Hagen, W. R.; Redeker, J. S.; Wolbert, R. B.; Boersma, M.; Verhagen, M. F.; Grande, H. J.; Veeger, C.; Mutsaers, P. H.; Sands, R. H.; Dunham, W. R. *Eur. J. Biochem.* **1992**, *209*, 63.
(42) Albracht, S. P. J.; Roseboom, W.; Hatchikian, E. C. *J. Biol. Inorg. Chem.* **2006**, *11*, 88.
(43) Pierik, A. J.; Hulstein, M.; Hagen, W. R.; Albracht, S. P. *Eur. J. Biochem.* **1998**, *258*, 572.
(44) King, P. W.; Posewitz, M. C.; Ghirardi, M. L.; Seibert, M. *J. Bacteriol.* **2006**, *188*, 2163.
(45) Yacoby, I.; Tegler, L. T.; Pochekailov, S.; Zhang, S.; King, P. W. *PloS one* **2012**, *7*, e35886.
(46) Stoll, S.; Schweiger, A. *J. Magn. Reson.* **2006**, *178*, 42.
(47) Beinert, H.; Orme-Johnson, W. In *Magnetic Resonance in Biological Systems*; Ehrenberg, A., Malmström, B., Vänngård, T., Eds.; Pergamon Press Ltd.: 1967, p 221.
(48) Rupp, H.; Rao, K. K.; Hall, D. O.; Cammack, R. *Biochim. Biophys. Acta* **1978**, *537*, 255.
(49) Myers, W. K.; Stich, T. A.; Suess, D. L. M.; Kuchenreuther, J. M.; Swartz, J. R.; Britt, R. D. *J. Am. Chem. Soc.* **2014**.
(50) Yu, L.; Greco, C.; Bruschi, M.; Ryde, U.; De Gioia, L.; Reiher, M. *Inorg. Chem.* **2011**, *50*, 3888.
(51) Happe, T.; Kaminski, A. *Eur. J. Biochem.* **2002**, *269*, 1022.
(52) Ahlrichs, R.; Bär, M.; Häser, M.; Horn, H.; Kölmel, C. *Chem. Phys. Lett.* **1989**, *162*, 165.
(53) Perdew, J. P. *Phys. Rev. B* **1986**, *33*, 8822.
(54) Becke, A. D. *Phys. Rev. A* **1988**, *38*, 3098.
(55) Eichkorn, K.; Treutler, O.; Öhm, H.; Häser, M.; Ahlrichs, R. *Chem. Phys. Lett.* **1995**, *240*, 283.
(56) Schäfer, A.; Huber, C.; Ahlrichs, R. *J. Chem. Phys.* **1994**, *100*, 5829.
(57) Adams, M. *J. Biol. Chem.* **1987**, *262*, 15054.
(58) Greco, C.; Bruschi, M.; Fantucci, P.; Ryde, U.; De Gioia, L. *J. Am. Chem. Soc.* **2011**, *133*, 18742.
(59) Liu, Z.-P.; Hu, P. *J. Am. Chem. Soc.* **2002**, *124*, 5175.
(60) Tye, J. W.; Darensbourg, M. Y.; Hall, M. B. *Inorg. Chem.* **2008**, *47*, 2380.
(61) Fiedler, A. T.; Brunold, T. C. *Inorg. Chem.* **2005**, *44*, 9322.
(62) Kaesz, H. D.; Saillant, R. B. *Chemical Reviews* **1972**, *72*, 231.
(63) Vaska, L. *J. Am. Chem. Soc.* **1966**, *88*, 4100.
(64) Kubas, G. J.; Burns, C. J.; Khalsa, G. R. K.; Van Der Sluys, L. S.; Kiss, G.; Hoff, C. D. *Organometallics* **1992**, *11*, 3390.
(65) van der Vlugt, J. I.; Rauchfuss, T. B.; Whaley, C. M.; Wilson, S. R. *J. Am. Chem. Soc.* **2005**, *127*, 16012.
(66) Stripp, S.; Sanganas, O.; Happe, T.; Haumann, M. *Biochemistry* **2009**, *48*, 5042.
(67) Hajj, V.; Baffert, C.; Sybirna, K.; Meynial-Salles, I.; Soucaille, P.; Bottin, H.; Fourmond, V.; Léger, C. *Energy Environ. Sci.* **2014**, *7*, 715.
(68) Schwab, D. E.; Tard, C.; Brecht, E.; Peters, J. W.; Pickett, C. J.; Szilagyi, R. K. *Chem. Commun. (Cambridge, U. K.)* **2006**, 3696.
(69) Greco, C.; Bruschi, M.; Heimdal, J.; Fantucci, P.; De Gioia, L.; Ryde, U. *Inorg. Chem.* **2007**, *46*, 7256.
(70) Silakov, A.; Reijerse, E. J.; Albracht, S. P. J.; Hatchikian, E. C.; Lubitz, W. *J. Am. Chem. Soc.* **2007**, *129*, 11447.
(71) Bruschi, M.; Greco, C.; Kaukonen, M.; Fantucci, P.; Ryde, U.; De Gioia, L. *Angew. Chem. Int. Ed.* **2009**, *48*, 3503.
(72) Trohalaki, S.; Pachter, R. *Int. J. Hydrogen Energy* **2010**, *35*, 5318.
(73) Giles, L. J.; Grigoropoulos, A.; Szilagyi, R. K. *Eur. J. Inorg. Chem.* **2011**, *2011*, 2677.
(74) Miyake, T.; Bruschi, M.; Cosentino, U.; Baffert, C.; Fourmond, V.; Léger, C.; Moro, G.; De Gioia, L.; Greco, C. *J. Biol. Inorg. Chem.* **2013**, *18*, 693.
(75) Winkler, M.; Esselborn, J.; Happe, T. *Biochim. Biophys. Acta, Bioenerg.* **2013**, *1827*, 974.
(76) Erdem, Ö. F.; Stein, M.; Kaur-Ghumaan, S.; Reijerse, E. J.; Ott, S.; Lubitz, W. *Chem. Eur. J.* **2013**, *19*, 14566.
(77) Lemon, B. J.; Peters, J. W. *Biochemistry* **1999**, *38*, 12969.
(78) Erbes, D. L.; Burris, R.; Orme-Johnson, W. *Proc. Natl. Acad. Sci. U. S. A.* **1975**, *72*, 4795.
(79) Chen, Z.; Lemon, B. J.; Huang, S.; Swartz, D. J.; Peters, J. W.; Bagley, K. A. *Biochemistry* **2002**, *41*, 2036.
(80) Bennett, B.; Lemon, B. J.; Peters, J. W. *Biochemistry* **2000**, *39*, 7455.

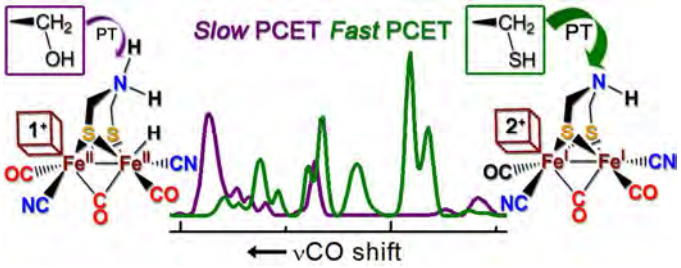
Slow PCET Fast PCET
CH2
OH
PT
H
N
H
1+
S
S
H
OC
Fe
Fe
CN
NC
C
O
CO
CH2
SH
PT
2+
vCO shift

[FeFe]- and [NiFe]-Hydrogenase Diversity, Mechanism, and Maturation

John W. Peters[1,5*], Gerrit J. Schut[2,5], Eric S. Boyd[3,5], David W. Mulder[4,5], Eric S. Shepard[1], Joan B. Broderick[1], Paul W. King[4,5], and Michael W. W. Adams[2,5]

[1]Department of Chemistry and Biochemistry, Montana State University, Bozeman, MT 59717;

[2]Department of Biochemistry and Molecular Biology, University of Georgia, Athens, GA 30602;

[3]Department of Microbiology and Immunology, Montana State University, Bozeman, MT 59717;

[4]National Renewable Energy Laboratory, Golden CO 80401;

[5]The Biological Electron Transfer and Catalysis Energy Frontiers Research Center

* Corresponding Author – John W. Peters, john.peters@chemistry.montana.edu, VOICE 406-994-7212, FAX 406-994-5407.

Abstract

The [FeFe]- and [NiFe]-hydrogenases catalyze the formal interconversion between hydrogen and protons and electrons, possess characteristic non-protein ligands at their catalytic sites and thus share common mechanistic features. Despite the similarities between these two types of hydrogenases, they clearly have distinct evolutionary origins and likely emerged from different selective pressures. [FeFe]-hydrogenases are widely distributed in fermentative anaerobic microorganisms and likely evolved under selective pressure to couple hydrogen production to the recycling of electron carriers that accumulate during anaerobic metabolism. In contrast, many [NiFe]-hydrogenases catalyze hydrogen oxidation as part of energy metabolism and were likely key enzymes in early life and arguably represent the predecessors of modern respiratory metabolism. Although the reversible combination of protons and electrons to generate hydrogen gas is the simplest of chemical reactions, the [FeFe]- and [NiFe]-hydrogenases have distinct mechanisms and differ in the fundamental chemistry associated with proton transfer and control of electron flow that also help to define catalytic bias. A unifying feature of these enzymes is that hydrogen activation itself has been restricted to one solution involving diatomic ligands (carbon monoxide and cyanide) bound to an Fe ion. On the other hand, and quite remarkably, the biosynthetic mechanisms to produce these ligands are exclusive to each type of enzyme. Furthermore, these mechanisms represent two independent solutions to the formation of complex bioinorganic active sites for catalyzing the simplest of chemical reactions, reversible hydrogen oxidation. As such, the [FeFe]- and [NiFe]-hydrogenases are arguably the most profound case of convergence evolution.

Introduction

The enzyme hydrogenase utilizes hydrogen (H_2) as a substrate or produces H_2 by the reduction of protons. The two main types of hydrogenases are classified by the nature of the metal clusters at their catalytic sites and are termed [FeFe]- and [NiFe]-hydrogenases. Their active sites have structural characteristics in common including the presence of carbon monoxide (CO) and cyanide (CN^-) groups bound to the iron (Fe) ions. The [FeFe]-hydrogenase active site cluster is termed the H cluster, and exists as a regular [4Fe-4S] subcluster bridged to a 2Fe subcluster unit through a bridging cysteine thiolate. The 2Fe subcluster is also coordinated by the non-protein ligands carbon monoxide, cyanide and dithiomethylamine, thereby giving it a distinctly organometallic character. The Fe atom at the active site of the [NiFe]-hydrogenase has a similar architecture as one of the Fe ions of the 2Fe subcluster with CO and CN^- ligation but it is bridged to a Ni atom through bridging cysteine thiolates. The Ni atom is in turn terminally coordinated by two additional cysteine thiolates. In some hydrogenases one of the two terminal cysteines is replaced by selenocysteine and these so-called [NiFeSe]-hydrogenases are considered variations of [NiFe]-hydrogenases. Both [FeFe]- and [NiFe]-hydrogenases typically contain multiple iron-sulfur clusters that exist as either cysteine coordinated [4Fe-4S] or [2Fe-2S] clusters and in some cases there is mixed coordination with a His substituting for one of the Cys residues. As conduits between the catalytic metal sites and external electron donors and acceptors, the composition of these iron-sulfur clusters varies among different phylogenetic clades that in large part delineate hydrogenases on the basis of physiological function.

In the case of both [FeFe]- and [NiFe]-hydrogenases, the CO and CN^- ligands at their catalytic sites function as strong π-acceptor ligands that facilitate low-spin, II/I oxidation states of the Fe atoms. In all cases, the hydrogenases require efficient proton-transfer (PT), and proton-

coupled electron transfer (PCET) to achieve fast H_2 activation rates of turnovers of ~10^3-10^4 s^{-1} [1-4]. This functional necessity is satisfied by a secondary coordination sphere that includes conserved polar residues with exchangeable sites for transferring protons to the redox-active bimetallic clusters [5-8]. In addition, these conserved residues can also participate in H-bonding interactions to stabilize cofactor orientations and tune electronic properties. Altogether these extended interactions are critical for creating a catalytic reaction coordinate that minimizes high-energy steps, or kinetic barriers that would otherwise constrain enzymatic function and efficiency.

For the most part, hydrogenases function in recycling reduced electron carriers that accumulate during anaerobic fermentation through proton reduction or in coupling H_2 oxidation to energy yielding processes. The [FeFe]-hydrogenases are typically associated with proton reduction and [NiFe]-hydrogenases with H_2 oxidation, although there are a number of exceptions [9, 10]. Despite sharing the unique features of CO and CN- ligands to active site Fe ions, the [FeFe]- and [NiFe]-hydrogenases are not evolutionarily related and show no sequence similarity [11, 12]. In general, [FeFe]-hydrogenases are found in anaerobic bacteria and are especially prevalent among the fermentative organisms (e.g., firmicutes). They are also found in a number of lower eukaryotes including algae and protists but surprisingly they have yet to be found in cyanobacteria or in the archaeal domain. In contrast, [NiFe]-hydrogenases, are frequently found associated with cyanobacteria and archaea, in addition to their common occurrence in a large number of bacteria. A variety of organisms harbor multiple hydrogenases [11-14]. In some cases, this may provide functional redundancy but it is thought in general they likely have different roles. Some bacteria, again largely firmicutes and sulfate reducing bacteria, even harbor both [NiFe]- and [FeFe]-hydrogenases [11, 12].

The [FeFe]-hydrogenases are closely related to a protein found only in eukaryotes termed Nar1 or Narf [15, 16]. This protein has been implicated in having a role in cytoplasmic iron-sulfur cluster biosynthesis and/or repair, and appears to resemble a minimal [FeFe]-hydrogenase that lacks a 2Fe subcluster. Homology models of Narf suggest the presence of an open cavity adjacent to the [4Fe-4S] cubane that could accommodate the 2Fe subcluster [17]. We have proposed [18] that Narf proteins and [FeFe]-hydrogenases have a common ancestor that more likely resembles the simpler Narf-like protein and that the biosynthetic pathway for assembly and insertion of the 2Fe subcluster evolved, at least in part, in response to the characteristics of the vacant cavity present in the ancestral enzyme and fill it with a organometallic cluster capable of catalyzing new biochemistry. Whatever the merits of this proposal, in general [FeFe]-hydrogenases do not occur universally in deeply rooted lineages of ribosomal RNA-based phylogenetic reconstructions and they are not commonly associated with metabolisms considered by many to be ancestral (e.g., chemolithotrophy or methanogenesis). This indicates that it unlikely that [FeFe]-hydrogenases were a property of the Last Universal Common Ancestor (LUCA) and are perhaps not old from an evolutionary perspective [18].

As discussed below and in contrast to the [FeFe]-enzymes, the [NiFe]-hydrogenases are encoded in the genomes of many Bacteria and Archaea and are frequently detected in deeply rooted lineages of both domains. For this reason, one can make an argument that [NiFe]-hydrogenases played a key role in the metabolism of the LUCA [19]. The closest evolutionarily relative of [NiFe]-hydrogenases are proteins involved in respiratory Complex I / NADH dehydrogenase [20, 21]. Subunits comprising NADH dehydrogenase are close relatives of the so-called group 4 membrane bound [NiFe]-hydrogenases that couple the oxidation of ferredoxin (Fd) to proton reduction which is in turn coupled to generating a membrane potential through ion

pumping. This mechanism is analogous to the mechanism of Complex I in coupling NADH oxidation and ubiquinone reduction to proton pumping. This suggests that ion pumping membrane [NiFe]-hydrogenases are the ancestors of modern respiratory Complex I and chemiosmosis.

Given that both [FeFe]- and [NiFe]-hydrogenases have independently evolved essentially the same unique solution to catalyzing reversible H_2 oxidation chemistry (carbon monoxide and cyanide ligands to Fe ions) is somewhat of a surprise. However evidence for independent evolutionary origins is also supported in the stark difference in the mechanisms by which these unique carbon monoxide and cyanide ligands are synthesized in their respective cluster maturation pathways [22-27]. The process by which the CO, CN^-, and other nonprotein ligands are synthesized, coordinated to iron, and are inserted into the active sites of [FeFe]- and [NiFe]-hydrogenases to yield the mature enzymes clearly represents two different paradigms in metal cluster biosynthetic pathways. These two independent paths for the evolution of these unrelated enzymes perhaps represents one of the most profound cases of convergence evolution and one that is supported by differences in the taxonomic distribution of these enzymes, the pathways required to synthesize active site co-factors, and their physiological roles.

Diversity

Our recent screening of 2919 complete bacterial and archaeal genomes available in July 2014 (Boyd, E.S., *unpublished data*) indicate the presence of [FeFe]-hydrogenase homologs in 265 of those genomes (9.1% of total) while 778 (26.7% of total) of those genomes encode homologs of [NiFe]-hydrogenases. Like previous studies [11, 12, 14], we found that [FeFe]- and

[NiFe]-hydrogenase homologs are discretely distributed at the domain, phylum, and order levels of taxonomic classifications. While [FeFe]-hydrogenases are encoded in the genomes of anaerobic bacteria and anaerobic or phototrophic eukaryotes, they are not encoded by archaea. In contrast, [NiFe]-hydrogenases are encoded by both aerobic and anaerobic bacteria and archaea but eukarya (**Fig. 1**).

Genes encoding homologs of [FeFe]-hydrogenase were identified in the genomes of anaerobic members of several phyla (**Fig. 1**), including the *Actinobacteria* (7 / 301 genomes), *Firmicutes* (160 / 622 genomes), *Bacteroides* (9 / 94 genomes), *Chloroflexi* (11 / 24 genomes), *Proteobacteria* (28 /1240 genomes), *Spirochaetes* (20 / 65 genomes), *Dictyoglomi* (2 / 2 genomes), *Ignavibacteriae* (2 / 2 genomes), and *Thermotogae* (18 /18 genomes). In addition, [FeFe]-hydrogenase homologs were identified, albeit infrequently, among members of *Synergistetes*, *Verrucomicrobia*, *Nitrospirae*, and *Fusobacteria*. Intriguingly, homologs were not identified among the *Chlamydia* (109 genomes), *Chlorobi* (11 genomes), *Cyanobacteria* (79 genomes), *Deinococcus-Thermus* (21 genomes), *Tenericutes* (89 genomes), or *Planctomycetes* (8 genomes). Among eukaryotes, [FeFe]-hydrogenase were identified in the genomes of several anaerobic protists (*Trichomonas*, *Nyctotherus*), Fungi (*Neocallimastix*, *Sclerotinia*), and green algae (*Volvox*, *Chlamydomonas*).

Genes encoding homologs of [NiFe]-hydrogenase were more evenly distributed among bacterial and archaeal phyla when compared to [FeFe]-hydrogenase (**Fig. 1**). Among archaea, the genomes of all members of the crenarchaeal, euryarchaeal, and korarchaeal taxonomic orders contain at least one [NiFe]-hydrogenase homolog while genomes from members of the *Nanoarchaea* and *Thaumarchaea* do not. Among the *Crenarchaea*, homologs were identified in 13 of the 35 genomes, whereas 70 of the 110 euryarchaeal genomes encoded [NiFe]-hydrogenase

homologs. Among bacterial phyla, [NiFe]-hydrogenase homologs were common in the *Actinobacteria* (72 / 303 genomes), *Aquificae* (13 / 14 genomes), *Chlorobi* (10 / 11 genomes), *Chloroflexi* (30 / 35 genomes), *Cyanobacteria* (43 / 79 genomes), *Firmicutes* (86 / 622 genomes), and *Proteobacteria* (497 / 1240 genomes). In addition, homologs were identified among members of the *Acidobacteria*, *Chrysiogenetes*, *Deferribacteres*, *Deinococcus-Thermus*, *Dictyoglomi*, *Elusimicrobia*, *Nitrospirae*, *Planctomycetes*, *Synergistetes*, *Thermodesulfobacteria*, *Thermotogae*, and *Verrucomicrobia*. [NiFe]-hydrogenase homologs were not identified in members of the *Chlamydia* (109 genomes), *Fusobacteria* (8 genomes), *Spirochaetes* (65 genomes), or *Tenericutes* (89 genomes). As previously noted [12], the presence of both [FeFe]- and [NiFe]-hydrogenase in the same genome is rare and is found among members of the bacterial phyla *Actinobacteria*, *Bacteroidetes*, *Chloroflexi*, *Dictyoglomi*, *Firmicutes*, *Nitrospirae*, *Proteobacteria*, *Thermodesulfobacteria*, and *Thermotogae*, suggesting unique functional roles for these enzymes in the metabolism of each organism.

Phylogenetic and Functional Diversity of [FeFe]-hydrogenases

[FeFe]-hydrogenase are delineated from paralogous proteins present in eukaryotes, such as Nar1, by the presence of three conserved cysteine-containing motifs that coordinate the active site H-cluster. These consist of TS**C**CPxW (L1), MP**C**xxKxxE (L2) and ExMx**C**xxG**C**xxG (L3) in [FeFe]-hydrogenase, and although some sequence variation does occur in these motifs, the bolded cysteine residues are essential for coordination of the H-cluster [11]. In addition to variation in the cluster binding motifs, previous studies have noted substantial sequence variation in the motifs that contain the cysteine residues that bind the N- and C-terminal Fe-S cluster and accessory cofactor binding domains [13, 14] (Fig. 2), suggesting potential interactions with a

variety of redox partners. Due to the substantial N and C-terminal cluster variation, only the H-cluster is included in phylogenetic reconstructions of the catalytic subunit, which is termed HydA. Although the branching order of some H-cluster lineages mirror that of taxonomic reconstructions, most organisms with *hydA* encode multiple copies that often belong to divergent lineages, implying a number of gene duplications and horizontal gene transfers during the functional diversification of this protein class. As an example, individual clostridial genomes each encode for up to 13 divergent *hydA* homologs, suggesting that these enzymes have unique functional roles in these organisms. In addition to variation at the level of primary sequence, disparities in the number of [FeFe]-hydrogenase subunits and their tertiary structure have been identified [13, 14].

The best characterized [FeFe]-hydrogenases are monomeric, ferredoxin-dependent enzymes [12]. Examples include the hydrogenases from eukaryotic algae, such as *Chlamydomonas reinhardtii,* and clostridial species, such as *Clostridium pasteurianum*. *C. reinhardtii* [FeFe]-hydrogenase HydA1 (*Cr*HydA1) contains only the H-cluster and no additional iron-sulfur clusters [14]. Like bacteria, algae often encode multiple homologs of [FeFe]-hydrogenase. However, unlike bacteria, homologs in a given algal taxon are monophyletic relative to other algal or bacterial HydA, implying independent gene duplications in each of the algal lineages [28]. Given the structural simplicity of the *C. reinhardtii* hydrogenase it has become the model for active site maturation studies ([18, 29, 30]). Phylogenetic analyses indicate that the H-cluster domain of algal [FeFe]-hydrogenase is not likely to be ancestral, rather it is likely that the ancestral enzyme had a single ferredoxin binding domain at the N-terminus which was lost when these genes were laterally transferred to algae [18]. The simple algal enzyme containing only the H-cluster is thought to function during the fermentation of carbohydrate

reserves [31, 32] although photosynthetic H_2 production was recently demonstrated under fully aerobic conditions in the alga *Chlorella vulgaris* [33].

C. pasteurianum contains [FeFe]-hydrogenases of the ferredoxin (Fd)-dependent monomeric (M3) structural category [34] (**Fig. 2**). *C. pasteurianum* ferments 3 mol glucose to 2 mol acetate, 2 mol butyrate, 4 mol CO_2 and 8 mol H_2. In addition, reduced ferredoxin (Fd_{red}) is generated by the bifurcating butyryl-CoA dehydrogenase, which helps to explain how 8 moles of H_2 are produced instead of the 6 mol that would be expected based on thermodynamic considerations [35]. The Fd-dependent [FeFe] hydrogenases are widespread in anaerobic bacteria, in particular in the order *Firmicutes* [11, 13]. More complex, multimeric [FeFe]-hydrogenases have been identified in *Thermotoga maritima*, *Thermoanaerobacter tengcongensis* and *Desulfovibrio fructosovorans* and these have been implicated as NAD(P)H-linked H_2 producing enzymes [36-38]. The trimeric hydrogenase of *T. maritima* was shown not to couple H_2 formation with the oxidation of reduced Fd or of NADH when each was used as the sole electron donor. However, the presence of both reduced Fd and NADH promoted efficient H_2 production [39]. The key to the formation of H_2 from Fd and NADH simultaneously is the coupling of their energetics; the exergonic reduction of protons by electrons derived from Fd allows the endergonic reduction of protons by electrons from NADH. This type of reaction mechanism is called electron bifurcation and represents the third form of energy conservation [35, 39].

Energy conservation by electron bifurcation was first proposed in 2008 [40] and is defined as an exergonic reaction driving an endergonic reaction without the involvement of an ion gradient. The clostridial cytoplasmic enzyme complex butyryl-CoA dehydrogenase catalyzes the reduction of crotonyl-CoA ($E^{0'}$ = -10 mV) to butyryl-CoA with NADH ($E^{0'}$ = -320 mV) as

the electron donor and this is coupled to the endergonic reduction of Fd (E_m = -410 mV) by NADH [40, 41]. Reduced Fd is then recycled to produce H_2 ($E^{0'}$ = -420 mV). As a consequence of this pair of linked redox reactions, the oxidation of NADH can be coupled to H_2 production and this ultimately leads to the formation of additional ATP. The discovery of electron bifurcation can explain important reactions in anaerobic microbes, such as in clostridia and methanogens [42].

The heterotrimeric [FeFe]-hydrogenase from *T. maritima* (T_{opt} 80°C) utilizes the exergonic oxidation of Fd [(E_m = -453 mV (at 80°C), [43, 44]] to drive the unfavorable oxidation of NADH (E°' = -320 mV) to produce H_2 ($E^{0'}$ = -420 mV). The overall reaction is:

$$NADH + 2Fd_{red} + 3H^+ \rightarrow 2H_2 + NAD^+ + 2\,Fd_{ox}$$

This bifurcating hydrogenase provided new insights into H_2 production by anaerobes. For example, *Caldicellusiruptor* and other *Thermoanaerobacteriales* contain two types of hydrogenase, a soluble multimeric [FeFe]-hydrogenase similar to the *T. maritima* bifurcating hydrogenase and a group 4 membrane bound Fd-dependent [NiFe]-hydrogenase. These enzymes were proposed to function together to evolve H_2 during sugar metabolism [37]. However, genetic analyses of *T. saccharolyticum* showed that the membrane bound [NiFe]-hydrogenase appeared not to be involved in H_2 production while deletion of the multimeric [FeFe]-hydrogenase resulted in decreased H_2 production [45]. This indicates that these organisms also utilize a bifurcating [FeFe]-hydrogenase for H_2 production and the non-bifurcating [NiFe]-hydrogenase could have a secondary metabolic role.

Bifurcating [FeFe]-hydrogenases also play a central role in energy conservation in acetogens [46]. *Acetobacterium woodii* uses a respiratory system for electron transfer between Fd and NAD as the main energy-conserving mechanism for autotrophic growth on H_2 and carbon

dioxide [47, 48]. However, the mechanism for how reduced Fd is generated from H_2 only became clear through the characterization of its bifurcating [FeFe]-hydrogenase, which functions to couple H_2 oxidation to the simultaneous production of reduced Fd and NADH [46].

Bifurcating [FeFe]-hydrogenases can in principle function *in vivo* in both the production and oxidation of H_2, as was recently shown for a reversible bifurcating hydrogenase in *Moorella thermoacetica* [49]. During growth on glucose, *M. thermoacetica* can intermittingly produce H_2 from Fd and NADH via the bifurcating hydrogenase. Likewise, this same hydrogenase can utilize produced H_2 and CO_2 to perform acetogenesis generating 3 mol of acetate per glucose molecule. Although *M. thermoacetica* does not grow well autotrophically on H_2 and CO_2, it uses the bifurcating hydrogenase to produce reduced Fd to drive acetogenesis. In addition to Fd- and NADH-dependent hydrogenases, a Fd- and NADPH-dependent enzyme was characterized from *Clostridium autoethanogenum* cultured on CO and it was proposed that this hydrogenase functions in the formation of H_2 [50]. Moreover, the genome of *C. autoethanogenum* encodes for two additional bifurcating [FeFe]-hydrogenases that could function in providing reduced Fd and NADH during autotrophic growth on H_2 and CO_2 [51]. Bifurcating hydrogenases might also play an important role in the gut microbiota. *Ruminoccoccus* species, which are involved in the degradation of recalcitrant biomass, contain [FeFe]-hydrogenases very similar to the bifurcating hydrogenase of *T. maritima* [52]. Anaerobic gut-dwelling protists and fungi involved in biomass degradation also encode [FeFe]-hydrogenases to recycle their electron carriers that bear a similarity to the bifurcating [FeFe]-hydrogenases of anaerobic bacteria [53-55]

Phylogenetic and Functional Diversity of [NiFe]-hydrogenases

[NiFe]-hydrogenases from a variety of microorganisms have been biochemically characterized [56, 57]. These enzymes are comprised of at least two subunits, with the large subunit (LSU) containing the NiFe-catalytic site and the small subunit (SSU) containing three highly conserved iron-sulfur clusters that serve to shuttle electrons between the external electron carrier and the NiFe site. Based on comparison of the sequence motifs that coordinate the active site, [NiFe]-hydrogenases can be separated into four distinct functional groups that in general correspond to their putative physiological role [12]. Intriguingly, phylogenetic reconstructions of representatives of these enzymes also reveal patterns of clustering that correspond to variations in NiFe cluster binding motifs and their inferred physiological role [12, 13] (**Fig. 3**).

Group 1

Enzymes within this group are typically membrane-bound hydrogenases and are found in organisms that use H_2 as an energy source. A cytochrome *b* is often also present to anchor the hydrogenase complex to the membrane and allow electron transfer to the quinone pool. These enzymes couple the oxidation of H_2 to the reduction of electron acceptors such as oxygen, nitrate, sulfate, CO_2 or oxidized sulfur compounds [12]. *E. coli* contains 2 homologs of this group and one of these (Hya) is thought to oxidize H_2 and transfer electrons to the quinone pool to provide the cell with additional energy [58]. The sulfate reducing bacterium *Desulfovibrio gigas* encodes two [NiFe]-hydrogenases. One is a membrane bound Ech-type group 4 enzyme while the other is a periplasmic group 1 enzyme (HynAB). By mutational analysis it was shown that the periplasmic hydrogenase is essential for growth on H_2 with sulfate and functions to donate electrons from H_2 to the quinone pool via a periplasmic cytochrome c [59]. *Aquifex*

aolicus is one the most thermophilic bacteria known and it gains energy by oxidizing H_2 using low concentrations of oxygen or oxidized sulfur compounds as electron acceptors [60]. Its genome encodes two trimeric uptake (group 1) [NiFe]-hydrogenases (MbhI and MbhII) and these have distinct physiological functions [61]. MbhI is involved in the oxidation of H_2 linked to oxygen reduction while H_2 oxidation by MbhII is coupled to elemental sulfur reduction [62]. A similar H_2-oxidizing and elemental sulfur reducing respiratory system was described in the archaeon *Acidianus ambivalens* [63] but its genome sequence is not available and so the diversity of its hydrogenases is currently not resolved.

Group 2

Group 2a: This subgroup includes hydrogenases of cyanobacteria that fix dinitrogen (N_2) using nitrogenase. These organisms contain a dimeric uptake hydrogenase (HupSL) to recapture energy lost as H_2 during the reduction of N_2 [64]. Electrons from H_2 are then channeled into the quinone pool or function to reduce O_2 that deactivates the oxygen sensitive nitrogenase enzyme [65, 66]. Mutation of the HupLS genes in the diazotroph *Anabaena siamensis* abolished H_2 uptake activity and led to an increase in light-dependent H_2 production, presumably due to the lack of recapture of H_2 produced by nitrogenase enzyme in the absence of the uptake hydrogenase [67].

Group 2b: Group 2b consists of H_2-sensing regulatory hydrogenases that function to signal the availability of H_2 to the transcriptional regulation of metabolic hydrogenases, which themselves are most often affiliated with Group 1 H_2 oxidizing enzymes [11]. A very well studied model is the H_2 oxidizing aerobe *Ralstonia eutropha,* which contains three different hydrogenases. In this

case its H_2 sensing hydrogenase HoxBC regulates the expression of the membrane bound (HoxKGZ) and the cytoplasmic NAD-dependent (HoxFUYH) enzymes [68].

Group 3

Group 3a: The F_{420} reducing hydrogenases (Frh) are exclusively found in methanogenic archaea where they function in coupling the oxidation of H_2 to the reduction of cofactor F_{420}, thereby supplying reductant for two steps in the reduction of CO_2 to methane [11]. These enzymes consist of a large subunit (FrhA), a small subunit (FrhG), and a FAD containing-subunit (FrhB) for electron transfer to F_{420} [69, 70].

Group 3b: Group 3b enzymes are tetrameric (αβγδ) and are found primarily in thermophilic archaea. Their α and δ subunits represent the minimal [NiFe]-hydrogenase structure, with the two other subunits (β and γ) containing iron-sulfur clusters and a NAD(P)/FAD binding domain [12]. The enzyme from the hyperthermophilic archaeon *Pyrococcus furiosus* has been well characterized and shown to function as an uptake hydrogenase to provide NADPH for biosynthesis, although mutational analysis has shown that it is not required for growth or for supplying NADPH to other metabolic processes under usual laboratory growth conditions [71-73].

Group 3c: Some archaea, primarily methanogens, encode a trimeric methylviologen reducing hydrogenase (MvhAGD). MvhAGD forms a complex with heterodisulfide dehydrogenase (HdrABC) that in turn provides the physiological electron acceptor heterodisulfide CoM-S-S-CoB [74]. With the discovery of electron bifurcation it became clear that the MvhADG/HdrABC complex catalyzes the reduction of heterodisulfide and Fd simultaneously with H_2 as reductant at high specific activity, while in the absence of Fd only low rates are

observed [75]. The complex thus appears to couple the endergonic reduction of Fd (E' ≈−500 mV) to the exergonic reduction of CoM-S-S-CoB (E'_0= −140 mV) with H_2 (E'_0= −414 mV) as the electron donor, providing a putative mechanism by which methanogens conserve energy [42, 76].

Group 3d: This subgroup consists of bidirectional heteromultimeric [NiFe]-hydrogenases (HoxHY) that are associated with an additional NADH oxidoreductase (diaphorase) module, which shows distinct homology to the NADH input module of Complex I [12]. The bidirectional hydrogenases are found in aerobic H_2-utilizing organisms such as *Ralstonia eutropha*, in which they most likely catalyze H_2 oxidation and supply reducing equivalents (NADH) to Complex I for energy generation or provide reductant for biosynthesis [77]. These bidirectional hydrogenases are also found in many cyanobacteria where they function to dispose of excess electrons derived from fermentation and photosynthesis [65]. In the cyanobacterium *Synechocystis* spp. PCC 6803 it was shown that the bidirectional hydrogenase could also directly accept electrons from Fd or flavodoxin, which explains the production of H_2 by over-reduction of the Fd pool in the light or fermentative metabolism under anoxic dark conditions [78].

Group 4

Group 4 [NiFe]-hydrogenases are all membrane-bound and are mostly Fd-dependent enzymes. These enzymes cluster distinctly from all the other hydrogenases indicating that they have a separate evolutionary history [11]. The members of this group fall into 3 major subgroups: *1)* six subunit reversible ion-translocating enzymes termed Ech (energy converting hydrogenase), which are found in various orders of bacteria and a few archaea [20], *2)* a thirteen (or even more) subunit membrane bound and ion-translocating enzyme (Mbh) with subunits homologous to

Na^+/H^+ antiporters (Mrp) and these Mrp-Mbh enzymes are common in the thermophilic archaea [79], and *3)* a variant of the Mrp-Mbh (Eha/ Ehb) present in hydrogenotrophic methanogens that contains additional subunits (17-20 subunits) and uses an ion gradient to reduce Fd with H_2 [80]. The group 4 hydrogenases also include a number of distinct H_2-evolving multienzyme complexes such as the formate hydrogen lyase of *E. coli* and *Thermococcus onnurineus* that oxidizes formate and evolves H_2 [81, 82], and the CO-induced hydrogenases of *T. onnurineus* and *Carboxydothermus hydrogenoformans*, which are involved in generating energy from the oxidation of CO to CO_2 coupled with the production of H_2 [83, 84]. The six-subunit energy converting hydrogenase (EchA-F) was originally characterized in *Methanosarcina barkeri* where it was found to be required for its growth on acetate [85]. This hydrogenase can reversibly generate H_2 from reduced Fd with the concomitant generation/utilization of a proton gradient; homologs of this enzyme are found among anaerobic bacteria and few archaea. The Mrp-Mbh-type energy-converting H_2-producing enzymes were first described in the hyperthermophilic archaeon *P. furiosus* [79, 86, 87]. The striking difference between Mrp-Mbh and Ech is the presence of the Mrp-like H^+/Na^+ antiporter module in the Mrp-Mbh complex and the subsequent generation of a sodium gradient rather than a proton gradient. This Fd-dependent enzyme is linked to the glycolytic pathway found in heterotrophic archaea that is unique in that Fd is the only electron carrier (NADH is not produced). This allows for the efficient production of 4 moles of H_2 per mole of glucose [88] The energy converting hydrogenases of hydrogenotrophic methanogens (Eha and Ehb), are thought to provide reduced Fd for biosynthesis and to balance the first step of methanogenesis, the Fd-dependent reduction of CO_2 to form formylmethanofuran [80, 89].

The group 4 hydrogenases also contain a subunit core that has close homologs in three non-hydrogenase enzyme complexes. These are termed cofactor F_{420} oxidoreductase (Fpo) found in methanogenic archaea, a membrane oxidoreductase (Mbx) involved in sulfur reduction by hyperthermophilic archaea such as *P. furiosus*, and NADH quinone oxidoreductase (Complex I, Nuo) found in aerobic bacteria and eukaryotes [21, 39]. In particular, the close relationship between group 4 hydrogenases and components of Complex I of the ubiquitous aerobic respiratory chain indicates an intricate evolutionary history between H_2 and oxygen respiration [21, 39].

Group 5

Recently a group 5 [NiFe]-hydrogenase was proposed based on genome sequence, phylogenetic reconstructions, and biochemical characterization of an enzyme from *Streptomyces spp*. that is capable of oxidizing very low (<1 ppm) levels of H_2 [90, 91]. This was corroborated with the characterization of several *Streptomyces* soil isolates [92]. These group 5 hydrogenases are similar in structure to the group 1 enzymes in that they also consist of a small and large subunit but a potential cytochrome containing membrane anchor is not obvious. Thus, while appearing to be biochemically similar to group 1 H_2-oxidizing enzymes, the group 5 enzymes are distinct from the group 1 enzymes and their [NiFe] binding motifs are different [90].

Hydrogenase Mechanism

[NiFe(Se)]-hydrogenases

Catalytic site structure, coordination sphere and H_2 activation mechanism

X-ray structures of both [NiFe]- and [NiFeSe]-hydrogenases poised in various active and inactive states have been collected and these have provided detailed insights into cofactor arrangements and coordination environments [9, 93-101]. The bimetallic cofactor of [NiFe(Se)] hydrogenase is composed of Ni and Fe atoms bridged by a pair of Cys thiolates. Two CN- and one CO complete the coordination of the iron ion to create a subsite resembling the 2Fe subcluster of the [FeFe]-hydrogenase H cluster (**Fig. 4**). A second pair of Cys thiolates completes the coordination of the Ni atom, one of which is replaced by selenocysteine in [NiFe(Se)] hydrogenases. Surrounding the Ni-Fe cluster are conserved Arg, His and Glu residues, the functional groups of which create a network of exchangeable sites near or within H-bonding distance to the Ni-Fe cluster illustrated in **Fig. 4A**. Mutagenesis of the nearby Arg, Glu and His residues leads to loss or attenuation of catalytic activity, consistent with their proposed function in proton transfer (PT) and/or H-bonding interactions with the [NiFe] cluster [102, 103]. In addition, electron nuclear double resonance (ENDOR) spectroscopy and high-resolution crystallography have shown that the Se/S groups that coordinate Ni can function as a base to accept protons during PT and H_2 activation [104].

[NiFe(Se)-hydrogenase oxidation states under H_2 activation

Detailed summaries and overview of the various crystallographic, paramagnetic (e.g., EPR, ENDOR), and infrared (IR) spectroscopic properties of catalytic intermediates of [NiFe(Se)]-hydrogenases have recently been extensively reviewed [10, 104-106]. There are several reasonably defined catalytic states observed in the different classes of [NiFe(Se)]-hydrogenases (Table 1). Notwithstanding the significant experimental and theoretical studies

applied to the mechanism of [NiFe(Se)]-hydrogenases, definitive experimental evidence for the site of H_2 binding is lacking, though most models support Ni in this function [89, 90]. Reaction intermediates isolated under catalytic conditions have been modeled into a mechanism of activation, but many of the details are unresolved [104, 105, 107, 108].

Table 1. States identified in [NiFe(Se)]-hydrogenases under H_2.

Catalytic State	Oxidation State		EPR (*g*-values)	FTIR (cm^{-1})		Ligand
	Ni	Fe		νCO	νCN	
[a]Ni-SI	II	II	Silent	1943	2075, 2086	H_2O
Ni-C	III	II	2.21, 2.15, 2.01	1961	2074, 2085	H^-
Ni-R	II	II	Silent	1948	2061, 2074	H
[b]Ni-L	I	II	2.28, 2.11, 2.05	1911	2048, 2062	H^+

[a] Ni-TR for [NiFeSe] hydrogenases.
[b] Photoproduct observed after illumination at <200K.

In the resting state of [NiFe(Se)]-hydrogenases, Ni-SI, the Fe center lies within H-bonding distance of the Ni, whereby H_2 binding and heterolytic cleavage at Ni^{II} would be facilitated by PT to result in a μ-hydride intermediate (**Fig. 5**) [109]. Alternatively, experimental and theoretical models propose initial H_2 binding and activation can occur at the Fe site, when the Ni is modeled as high spin Ni^{II} [107, 108, 110]. Cleavage is proposed to result in PT to one of the coordinating thiolate or selenate groups, and subsequently to nearby conserved Glu [102]. The resulting hydride is bound to the Ni-C (or Ni-R) intermediate and based on spectroscopic analysis together with density functional theory (DFT) calculations, it is proposed to adopt a bridging conformation between the Ni and Fe atoms [109, 111, 112]. Much of the detail on reaction intermediates of [NiFe]-hydrogenases have relied on studies of a subset of the [NiFe(Se)]-hydrogenases. Thus, it is quite possible for unique aspects to emerge from future studies of a more diverse array of enzymes.

[FeFe]-hydrogenases

Catalytic site structure and coordination sphere

Two x-ray crystal structures of [FeFe]-hydrogenases from *Clostridium pasteurianum* (*Cp*I) and *Desulfovibrio desulfuricans* (*Dd*H) revealed the active site H cluster (**Fig. 4B**), a unique [6Fe-6S] organometallic cluster comprised of a [4Fe-4S] subcluster and 2Fe subcluster, which are linked through a protein cysteine thiolate ligand [113, 114]. The geometric and electronic properties of the 2Fe subcluster are closely connected to the [4Fe-4S] subcluster by strong spin coupling exchange through the Cys thiolate ligand between the two subclusters [115-120].

Reduction of protons to H_2 occurs at the 2Fe subcluster site, which includes a proximal Fe atom (Fe_p) and distal Fe atom (Fe_d) (in relation to the [4Fe-4S] cubane), each bound to a terminal CO and CN- ligand, bridging/semi-bridging CO ligand, and a bridging dithiolate ligand. A ligand exchangeable coordination site also resides at Fe_d and is a potential site for the formation of hydride intermediates [121]. The CO and CN- ligands promote reversible heterolytic H_2 cleavage and stabilize low spin states of the two Fe atoms of the subcluster [122, 123]. The CN- ligands further fine-tune the energy levels of the frontier orbitals of the [4Fe-4S] and 2Fe subcluster moieties, which helps make possible fast electron transfer (ET) between the two subclusters during catalysis [124]. The functional bridgehead group of the dithiolate ligand was recently confirmed as an amine [125, 126], an assignment previously suggested from analysis of *Dd*H [127] and advanced EPR methods [115], and theoretical models to function in PT to Fe_d during H_2 activation [128].

In the enzyme, the H cluster resides in a hydrophobic pocket where nearby residues

participate in H-bonding interactions to the diatomic ligands of the 2Fe subcluster [113, 114, 129]. The surrounding protein framework finely-tunes the H-cluster and is considered to play an important role in regulating its catalytic activity, electronic properties, and potential hydride binding sites [8, 118, 130-134]. Within the catalytic site are several conserved, charged residues that form the secondary coordination sphere, with exchangeable groups proposed to function in the transfer of protons, water coordination, and bonding interactions with the H cluster (**Fig. 4B**) [8, 121, 129, 133, 135].

Table 2. Redox states identified in [FeFe]-hydrogenases under H_2.

Catalytic State	**Oxidation State**			**EPR (*g*-values)**	**FTIR (cm^{-1})**		**Fe_d Terminal Ligand**
	2Fe		**[4Fe-4S]**				
	Fe_p	**Fe_d**			**νCO**	**νCN**	
[a]H_{ox}	II	I	2+	2.10, 2.04, 1.99	1964, 1940, 1802	2089, 2071	H_2O
[b]H_{ox}	I	II	2+	2.10, 2.04, 1.99	1964, 1940, 1800	2088, 2072	H_2O
[c]H_{red}	I	I	2+	Silent	1916, 1891, 1792	2038, 2034	H^+
[d]H_{red}	I	I	2+	Silent	1935, 1891, 1793	2083, 2070	Open (H)
[e]H_{red}	I	I	2+	Silent	1965, 1916, 1894	2079, 2041	H^+
[f]H_{sred}	I	I	1+	ND	1955, 1932, 1883	NA	NA
[g]H_{sred}	I	I	1+	2.08, 1.94, 1.88	1954, 1919, 1882	2070, 2026	H^+
[h]H_{sred}	I	I	1+	Broad 2.3-2.07	1933, 1883, ?	2085, ?	H^+

[a] Based on [136-140]. [b] Based on [115, 141, 142]. [c] Based on [139]. [d] Based on [8, 143-145]. [e] Based on [123, 140, 143-145]. [f] Based on [140]. [g] Based on [143, 144]. [h] Based on [139], "?" signifies unresolved assignments for CO/CN modes.

The emerging role of [4Fe-4S] in the [FeFe]-hydrogenase catalytic cycle

Recent spectroscopic investigations of the minimal algal [FeFe]-hydrogenase *Cr*HydA, have put focus on the [4Fe-4S] and its role as an ET relay during catalysis (**Fig. 6,** and Table 2). Initial spectroelectrochemical FTIR and EPR investigations on *Dd*H led to identification of a "super-reduced" [140], or H_{sred}, H cluster state, which was later confirmed in *Cr*HydA and assigned as a $[4Fe\text{-}4S]^{1+}$-$Fe^{I}Fe^{I}$ [141, 146]. Further EPR and FTIR studies of *Cr*HydA under reducing conditions provided evidence for multiple H cluster intermediates containing a reduced $[4Fe\text{-}4S]^{1+}$ during both catalytic H_2 activation and proton reduction. This implicated a role as an electron mediator between 2Fe and Fd [147]. X-ray spectroscopy along with DFT on *Cr*HydA found that for a complete model of the H-cluster, the LUMO resides over the [4Fe-4S] subcluster and is close in energy to the HOMO localized on Fe_d of 2Fe, further supporting its role as an initial relay into the 2Fe subcluster during H_2 activation [148].

These forms of H-cluster reduced states with $[4Fe\text{-}4S]^{1+}$ have led to revisions [141, 147] of earlier models for H_2 activation by [FeFe]-hydrogenases [149]. Formally, H_2 activation was principally based on PT/ET transitions between the H_{ox} ($[4Fe\text{-}4S]^{2+}$-$Fe^{II}Fe^{I}$) and H_{red} ($[4Fe\text{-}4S]^{2+}$-$Fe^{I}Fe^{I}$) states. These two redox states of the H cluster were assigned from early spectroscopic studies of more complex [FeFe]-hydrogenases containing additional FeS cofactors, or "F clusters" [150-153]. Thus, it is possible that trapping of $[4Fe\text{-}4S]^{1+}$ intermediates in these enzymes was prevented by ET between the H cluster and F clusters during H_2 activation. Alternatively, it is possible that some of these intermediates that have been observed in CrHydA1 might be unique to this enzyme due to its lack of F clusters.

The role of H_{sred} as a catalytic intermediate has come under question recently based on

protein film voltammetry (PFV) studies of *Cr*HydA. In one case, *Cr*HydA was observed to inactivate at low potentials, leading to the hypothesis that H_{sred} might not be catalytically relevant [140, 154]. This observation differs from the high catalytic currents of enzymes at the low reduction potentials (<500 mV vs. NHE) [141, 155, 156], conditions that enrich for the H_{sred} state in spectroelectrochemical FTIR [144]. Clearly, identification of a $[4Fe\text{-}4S]^{1+}$ in *Cr*HydA under different reducing conditions indicates that oxidation of H_2 is a tightly coupled two-electron, two-proton reaction, and facile intramolecular ET steps to F clusters of more complex [FeFe] hydrogenases likely prevented the earlier detection of a $[4Fe\text{-}4S]^{1+}$ oxidation state. Mutants where PT is blocked or disrupted could be a useful strategy towards capturing reduced states and transient intermediates during catalysis [149].

H_2 binding and activation at the H cluster; activation at Fe_d^{II}

The resting state of the H clusters in *Cp*I, *Dd*H and *Cr*HydA are formally assigned to a mixed-valent 2Fe subcluster paired to a diamagnetic $[4Fe\text{-}4S]^{2+}$ subcluster based on the collective EPR/FTIR spectra of oxidized states (H_{ox}) of various enzymes (Table 2). Oxidation state assignments of the Fe_d / Fe_p pair in the H_{ox} state, and the localization of the unpaired spin, are currently under debate [115, 120, 157] (**Fig. 6**). Nevertheless, there is agreement that the initial step of H_2 binding occurs at the open coordination site of Fe_d in the Fe^{II} oxidation state. Evidence in support of this comes from spectroscopic studies on ^{57}Fe labeled *Dd*H poised in H_{ox} and CO-inhibited states [115]. The effect of CO on H_{ox} was used to interpret the effect of H_2 binding on the H cluster electronic state. CO binding induced stronger couplings between the [4Fe-4S] cubane and the 2Fe subcluster, consistent with a shift of the unpaired spin from the 2Fe

subcluster toward [4Fe-4S] (e.g., electron exchange from $Fe_d \rightarrow Fe_p$). More recently pulse EPR studies on isotopically labeled H cluster with $^{13}C^{15}N$ ligands support assignment of the unpaired spin in the H_{ox} state to Fe_d and delocalization of the spin over both Fe ions upon CO binding, a picture also consistent with a shift of unpaired spin toward [4Fe-4S] [157]. A completely synthetic H cluster mimic has also been shown to proceed via a $Fe^I \rightarrow Fe^{II}$ transition of a diiron/dithiolate subsite to accomplish H_2 binding and activation [158]. In this example of bio-inspired chemistry, the diferrous state was induced via oxidation by a covalently attached ferrocene (e.g., $[4Fe\text{-}4S]^{2+}$). The intramolecular ET step led to binding and activation of H_2 at the open coordination site of the Fe_d^{II} site, similar to the mechanism based on enzyme studies as proposed in **Fig. 6**, Scheme B.

Common functional themes

Catalytic bias and electron-transfer reactions

Under electrochemical PFV or biochemical assays with redox dyes of varying potentials, different hydrogenases have been shown to possess differences in catalytic bias, or reaction directionality [10, 159, 160]. The degree of reaction bias, or extent that H_2 production or oxidation is favored, is intrinsic to each particular hydrogenase [159, 161-163]. This property has implications in the function of hydrogenase in a metabolic network, which is how the H_2 activation step is coupled to specific redox partners. Most or all members of each enzyme class have been shown by PFV to operate near to the thermodynamic potential of the $H_2/2H^+$ redox couple. Structural factors that control enzyme reaction bias, and to what degree these are enzyme specific, remain ongoing areas of investigation. Several hypotheses have been proposed for how

bias might be controlled based on differences in the enzyme structures. One model for bias control is based on the differences in the potential of the electrons entering the catalytic site [162, 164]. Thus, the evolution of enzyme and accessory cluster diversity has a significant role in tuning the catalytic function of the particular hydrogenase to couple to a given metabolic pathway. Other possible controlling factors of reaction bias are proton availability [8], midpoint potentials of the $1e^-$ oxidized/reduced forms of bimetallic clusters, role of secondary sphere coordination environment [165] and the accessibility of metal oxidation states and electronic structures [160].

Low spin, low-valent Fe(CO)(CN) centers and H_2 activation

A functional theme that has emerged from hydrogenase active site theoretical and model compound studies is the role of a square planar $Fe^{I/II}$(CO)(CN) center in enzymes that function in H_2 binding and activation. The functional importance of the Fe site in [NiFe]-hydrogenases is perhaps less obvious than for the [FeFe]-hydrogenases where H_2 binding and activation occur directly at a Fe(CO)(CN) subsite. For both enzyme families, inclusion of this organometallic functional group as a component of the bimetallic catalytic sites is likely required to keep the respective metal centers in low-spin, low valence states, where the reaction coordinate for H_2 activation is thermodynamically favored [166-168].

Maturation

[NiFe]-Hydrogenase Active Site Assembly

Six *hyp* genes denoted *hypA – hypF* (and their associated homologs) are required for biosynthesis and insertion of the $NiFe(CN)_2CO$ catalytic cluster into the large subunit of [NiFe]-hydrogenases.

The Synthesis of Thiocyanate: HypE and HypF

HypC, D, E, and F proteins are involved in $Fe(CN)_2CO$ biosynthesis and are absolutely required for maturation of [NiFe]-hydrogenases [169-171]. The cyanide ligands of the active site cluster are derived from carbamoylphosphate in a series of reactions involving HypE and HypF (Figure 7) [172]. HypF utilizes carbamoylphosphate as substrate and first converts it to carbamate and then to carbamoyladenylate (in an ATP-dependent step) before finally transferring the carbamoyl functional group to the C-terminal cysteine residue of HypE (Figure 7, I – V) [172, 173]. The intermediates that are produced by HypF are quite unstable, however, a mechanism for their formation is suggested by the HypE-HypF complex, a heterotetrameric structure comprised of a HypE dimer flanked by two HypF molecules [174]. The structure supports a mechanism in which the N-terminal, HypF acylphosphatase domain hydrolyzes carbamoylphosphate to carbamate and inorganic phosphate; carbamate is transferred through an internal channel to the YrdC domain where ATP is bound and carbamoyladenylate formation occurs with release of pyrophosphate [174, 175]. Carbamoyl group transfer to the C-terminal cysteine of HypE, with the liberation of AMP, occurs within the C-terminal Kae1-like domain [174]. The Kae1-like domain of HypF binds a mononuclear Fe ion via two His and two Asp, in similar fashion to other ASKHA superfamily members like Kae1 and TobZ [174, 176-178]. In HypF, this Fe ion coordinates the carbamoyladenylate moiety, promoting the transferase reaction [174].

The thiocarboxamide group bound to HypE's terminal Cys is converted to thiocyanate in a manner reminiscent of reactions catalyzed by formylglycinamide ribonucleotide amidotransferase (PurL) and aminoimidazole ribonucleotide synthetase (PurM); HypE, PurL, and PurM all utilize ATP to form phosphoryl anhydride intermediates [179-181]. In the case of HypE, the thiocarboxamide oxygen group is within van der Waals distance of the γ – phosphate group of ATP and is optimally positioned for in-line attack [182]. The thiocarboxamide group is proposed to become activated via deprotonation by an active site H_2O molecule. This H_2O hydrogen bonds to Lys134 which in turn is in close proximity to an Arg residue that decreases its effective pKa to approximately 5.1, allowing Lys134 to act as a general base [182]. Following the in-line attack of ATP, ADP is released and a thiocarbamic phosphoryl anhydride species is formed [181, 182]. This iminophosphate intermediate is then activated for dephosphorylation via deprotonation of the imino nitrogen by a conserved Glu272 residue [182]. The resulting thiocyanate bound to Cys at the C-terminus of HypE is on a flexible loop that not only permits the insertion of the critical cysteine residue near the carbamoylation active site in the Kae1 domain of HypF, but then also facilitates delivery of the thiocyanate to the HypC-HypD complex where delivery of CN^- to iron occurs (Figure 8) [172, 181, 183].

$Fe(CN)_2CO$ Cofactor Biosynthesis: HypC and HypD

Proteins in the HypC family of proteins are approximately 10 kDa in size and associate with HypD and a precursor form of the hydrogenase large subunit, and also form a ternary complex with HypD and HypE [22, 184-189]. HypC is structurally simple, being comprised of a C-terminal α-helix joined to a β-barrel in what is known as an OB-fold [188, 190, 191]. HypD proteins are approximately 40 kDa in size and contain a unique C-terminal $CX_{14}CX_6CX_{16}C$

motif in domain III that coordinates a [4Fe-4S] cluster, whereas domains I and II are both characterized as Rossmann folds [186, 191, 192]. The cluster environment in domain III shares similarities with the ferredoxin:thioredoxin reductase system wherein a redox cascade is created that involves the [4Fe-4S] cluster and a pair of cysteine residues that are in close proximity to it, although these Cys residues are not absolutely conserved in all HypD isoforms [189, 191, 193]. The redox cascade is extended to four other conserved motifs in HypD (CGXHXH, GPGCPVCX_2P, GFETT, and PXHVSX_3G) and this conduit has been proposed to play a role in the mechanism of iron cyanation [187, 188, 191].

Co-expression studies revealed that substoichiometric amounts of HypE were associated with a HypC–HypD complex and that this complex accepted CN^- from HypE; CN^- was not transferred to either HypC or HypD when they were expressed singly, suggesting that the HypC–HypD complex shared coordination of the CN^- group (Figure 8) [186]. The exact details of diatomic ligand coordination to Fe at this stage of maturation are not fully resolved and a consensus model has not yet been attained. Structural characterization of the HypC–D–E ternary complex provides a picture for how the conserved motifs of HypD create the scaffold for Fe–cyanation; a model is proposed wherein Cys38 from HypD and Cys2 of HypC (*Thermococcus kodakarensis* numbering) bind an Fe ion along with two CN^- ligands and two unresolved moieties [188]. Spectroscopic characterization of anaerobic preparations of HypC–HypD complexes containing substoichiometric amounts of HypE from *E. coli* [187] and HypC–HypD complexes from both *Ralstonia eutropha* and *E. coli* [189] show FTIR bands that correspond to an $Fe(CN)_2CO$ species similar to that observed in [NiFe]-hydrogenase. Importantly, the characterization of the HypC–HypD complex reported by Soboh et al. revealed the existence of two labile Fe ions in addition to the [4Fe-4S] cluster, and also showed an IR

feature at 2337 cm^{-1} assigned to νCO_2; Cys41 in HypD was shown to be required for the coordination of CN^-, CO, and CO_2, presumably to one of the labile Fe ions [187]. Analysis of anaerobically purified HypD showed that it contained FTIR bands associated with a CO and two CN^- groups, consistent with the presence of an $Fe(CN)_2CO$ moiety; no 2337 cm^{-1} CO_2 feature was present (Figure 8) [194].

Insight into the significance of CO_2 was provided in a subsequent report that examined individually purified HypC along with its *E. coli* homolog HybG [195]. Characterization revealed that under anaerobic conditions the proteins contained ~ 0.3 mol Fe per mol protein and exhibited single FTIR bands arising from CO_2. Evaluation of variant HypC proteins conclusively demonstrated that both Cys2 and His51 were absolutely required for Fe and CO_2 coordination [195]. This observation coupled with the presence of the 2337 cm^{-1} feature in the HypC–HypD complex suggests that HypC delivers Fe–CO_2 to HypD where the CO_2 is reduced to CO (Figure 8) [187, 195]. Importantly, these results and others suggest that metabolic CO_2 is the source of the CO ligand, although this has yet to be experimentally demonstrated [195, 196].

In the case of HypD, Cys41, Cys69, and Cys72 are all critical for synthesis of the intermediate $Fe(CN)_2CO$ cluster [194]. Collectively, these data suggest a model wherein Cys2 and His51 of HypC and Cys41 and His44 of HypD (*E. coli* numbering) come together to coordinate a precursor Fe ion in a tetrahedral environment; addition of the CO and the CN^- ligands results in HypC dissociation and addition of His201 to accomplish formation of the octahedrally coordinated $Fe(CN)_2CO$ unit on HypD (Figure 8) [194, 195]. The assignment of His44 and His201 as the fourth and fifth ligands is not established and it is also possible that Cys69 and Cys72 perform this function [194].

Insertion of Ni^{2+}: HypA and HypB

Two of the *hyp* gene products, HypA and HypB, are involved in acquiring and inserting Ni^{2+} and studies have shown that these proteins are not absolutely required because addition of Ni^{2+} during anaerobic growth restores hydrogenase activity in mutant cell lines [170, 171, 197, 198]. The insertion of Ni^{2+} into the large subunit occurs only after the $Fe(CN)_2CO$ moiety is present (Figure 8) [22, 199]. HypA is a 140 amino acid protein that exists in both monomeric and dimeric states [200]. HypA coordinates a single Ni^{2+} ion with micromolar affinity via an N-terminal MHE motif [200-202], and also binds Zn^{2+} through the cysteine thiolates of a zinc finger motif [200]. While the Ni^{2+} and Zn^{2+} binding domains are independent of one another, the presence of Ni^{2+} appears to help dictate the orientation of these two domains, likely as a mechanism to mediate protein-protein interactions [193, 200, 202]. Moreover, HypA exhibits low sequence conservation outside of the Ni^{2+} and Zn^{2+} motifs; this mirrors the sequence diversity in both HypB and [NiFe]-hydrogenase, all three of which putatively interact during Ni^{2+} delivery [193].

HypB is a Ni^{2+}-metallochaperone that has GTPase activity, which is essential to achieve complete hydrogenase maturation [22, 203, 204]. Several HypB homologs exist with varying sequence-based metal binding properties. For example, *E. coli* HypB contains a high affinity, Ni^{2+} binding N-terminal CXXCGC motif (which is not absolutely conserved) and a C-terminal GTPase domain that can bind either Ni^{2+} or Zn^{2+} [205-207]. HypB dimerization is Ni^{2+}–dependent and its GTPase activity is modulated by metal binding [208]. The structure of the nucleotide bound *Methanocaldococcus jannaschii* enzyme shows two Zn^{2+} ions bound at the dimer interface, utilizing a combination of cysteine thiolate, histidine imidazole, and H_2O as ligands [206]. Structural analysis of the nucleotide bound form of *Helicobacter pylori* HypB, on

the other hand, reveals a single Ni^{2+} ion bound at the dimer interface via the tetrathiolate coordination of Cys106 and Cys142 from each monomer, whereas in the absence of nucleotide His107 becomes a metal ligand [209]. Cys142 is part of the GTPase Switch II motif and is likely a ligand to both Ni^{2+} and Zn^{2+} bound forms of HypB regardless of the nucleotide bound state [209]. This enables Cys142 to couple GTP hydrolysis with metal binding and delivery, potentially providing a mechanism wherein HypB distinguishes between Ni^{2+}– and Zn^{2+}–loaded forms, precluding delivery of zinc to the large subunit during maturation [206, 209, 210].

While the molecular mechanism for Ni^{2+} transfer to the large catalytic subunit is not yet fully resolved, delivery of nickel *in vivo* is likely modulated by protein-protein interactions and evidence for HypA, HypB, SlyD (a Ni^{2+} metallochaperone in *E. coli*), and HycE (the large subunit of hydrogenase 3 in *E. coli*) complexes have been reported (Figure 8) [211-216]. HypB's interaction with the large subunit requires the presence of HypA, providing support for HypA being the docking protein between HypB and HycE in the nickel delivery step [202, 211, 212]. Moreover, HypA selectively removes Ni^{2+} from the GTPase domain of HypB and this metal release appears to be stimulated by GTP hydrolysis [217]. Despite the observation that Ni^{2+} binding to HypB partially inhibits the GTPase activity of HypB [209], it is presumed that complex formation *in vivo* alleviates this retardation and promotes nickel mobilization [217]. Along these lines, it has been demonstrated that in *E. coli*, SlyD delivers Ni^{2+} to HypB and heterodimer formation between these proteins promotes GTP hydrolysis by HypB [218]. This provides a mechanism whereby SlyD acts to mediate the delivery of Ni^{2+} to the large subunit via the GTPase activity of HypB; the favorable interaction between SlyD and the GDP-bound form of HypB may help drive the Ni^{2+} insertion process and overcome any thermodynamic barriers associated with metal ion delivery [207, 213, 218].

Ni^{2+} Dependent Proteolysis and Active Site Closure

In a final step to accomplish maturation of the large catalytic subunit, a peptide on the C-terminus is processed (Figure 8). Peptide length varies somewhat among different hydrogenases; a peptide of approximately 15 residues is most commonly cleaved although maturation of *E. coli* hydrogenase 3 results in the removal of 32 residues [183]. The peptide extension of the large subunit is necessary for interaction with HypC, and its presence helps keep the large subunit in an open conformation for both Ni^{2+} and $Fe(CN)_2CO$ insertion [184, 185, 219]. The endopeptidases in *E. coli* that mature the three cognate [NiFe]-hydrogenases are HyaD (hydrogenase 1), HybD (hydrogenase 2), and HycI (hydrogenase 3) [220]. These enzymes recognize the DPCXXCXXH/R consensus motif that helps coordinate the active site metal center in [NiFe]-hydrogenase; the proteases cleave between the basic His/Arg and the nonpolar Met/Ile/Val/Ala residues [221-224]. Nickel promotes the recognition of the binding motif by the proteases and explains why cleavage only occurs after Ni^{2+} has been inserted [225]. Structural characterization of HycI suggests that two conserved Asp residues may be critical for Ni^{2+} coordination, implying that HycI functions via metal-based activation wherein the Ni^{2+} ion polarizes the carbonyl oxygen of the peptide bond, which in turn fosters hydrolysis by H_2O [183, 226]. Upon cleavage of the C-terminal peptide, a conformational change in the active site environment is induced which effectively internalizes the $NiFe(CN)_2CO$ moiety and affords the active enzyme [22].

[FeFe]-Hydrogenase Active Site Assembly

Identification of the Maturation Machinery

Three genes denoted *hydE*, *hydF*, and *hydG* are found in all organisms expressing [FeFe]-hydrogenase (HydA) and the expression of active HydA in *E. coli* requires coexpression with HydE, HydF, and HydG [26, 227]. Activation of HydA expressed singly ($HydA^{\Delta EFG}$) is accomplished via addition of *E. coli* lysate mixtures containing HydE, HydF, and HydG together; H_2(g) generation under these experimental conditions does not require exogenous small molecules, leading to the conclusion that the maturase enzymes utilize ubiquitous small molecules present in the cellular matrix to assemble the H-cluster [24, 227]. Sequence annotation coupled with preliminary biochemical characterization demonstrated that HydE and HydG both belong to the radical *S*-adenosyl-L-methionine (SAM) enzyme superfamily, while HydF is an FeS cluster binding GTPase [26, 227-229]. Point mutations in the radical SAM motifs of HydE and HydG, as well as the FeS cluster and GTPase regions of HydF, all proved to be deleterious to achieving $HydA^{\Delta EFG}$ activation, meaning that HydE, HydF, and HydG functionalities are indispensable for proper H-cluster synthesis [227].

Activation of $HydA^{\Delta EFG}$ Requires a Preformed [4Fe-4S] Cluster

Spectroscopic and structural characterization of the monomeric [FeFe]-hydrogenase of the green algae *Chlamydomonas reinhardtii* (*Cr*) has provided important insights into the maturation process. The enzyme $HydA^{\Delta EFG}$, obtained from a strain that lacks the genes encoding the three maturation proteins HydEFG, contains the [4Fe-4S] cubane of the H-cluster [230, 231]. Importantly, *Cr* $HydA^{\Delta EFG}$ is readily activated by *E. coli* lysate containing HydE, HydF, and

HydG. Moreover, the metal-free form of the protein must first be chemically reconstituted with iron and sulfide prior to successful activation by lysate [230]. These results show that activation by the maturase enzymes requires a preformed [4Fe-4S] cluster that is presumably synthesized by the endogenous iron sulfur cluster assembly machinery of the cell, and also suggest that HydE, HydF, and HydG come together to synthesize the 2Fe subcluster component of the H-cluster [230, 231]. *In vitro* labeling studies provide additional support for this model, as activation of $HydA^{\Delta EFG}$ by ^{57}Fe-labeled HydE, HydF, and HydG lysates demonstrate the incorporation of ^{57}Fe into only the 2Fe subcluster of the H-cluster [232].

Comparison of the *Cr* $HydA^{\Delta EFG}$ structure to that of *Cp*I HydA provides insight into 2Fe subcluster insertion [231]. An electropositive channel filled with H_2O molecules runs from the protein surface to the active site cavity of *Cr* $HydA^{\Delta EFG}$; this channel is absent in the mature *Cp*I HydA structure, which contains two ordered loop regions that effectively shield the H-cluster from solvent. The loop regions in *Cr* $HydA^{\Delta EFG}$ are splayed open, providing clear access to the active site cavity for 2Fe subcluster insertion, which may either be electrostatically- or entropically-driven [231, 233].

HydF is an Iron Sulfur Cluster Binding GTPase

HydF is a 47 kDa monomeric protein that binds FeS clusters and hydrolyzes GTP to GDP [229, 234]. The purified state of this protein is a composite mixture of dimers and tetramers and structural characterization of the metal-free enzyme has suggested that FeS cluster(s) bind at subunit interfaces [235]. Both FeS- and GTP-binding motifs are essential for maturation in the *Ca* system [227]. Moreover, among the three maturase enzymes, only purified HydF when expressed in a genetic background of HydE and HydG ($HydF^{EG}$) could activate $HydA^{\Delta EFG}$. This

activation was achieved in the absence of exogenously added proteins or small molecules, suggesting that HydF bound a precursor form of the H-cluster needed to achieve maturation [236].

Spectroscopic comparison of $HydF^{EG}$ to $HydF^{\Delta EG}$ revealed that both proteins bound [4Fe-4S]$^{+}$ clusters, but $HydF^{EG}$ samples contained additional LMCT features in UV-Vis spectra and an overlapping axial component in EPR spectra that are thought to arise from a [2Fe-2S]$^{+}$ cluster [234, 236]. Preparations of *Ca* $HydF^{EG}$ revealed the existence of Fe–CN^{-}, Fe–CO, and Fe–CO–Fe species via FTIR spectroscopy [234, 237]. These moieties were absent in $HydF^{\Delta EG}$, suggesting that HydE and HydG modified a [2Fe-2S] cluster precursor bound to $HydF^{\Delta EG}$ to produce the 2Fe subcluster of the H-cluster [27, 234].

The FeS cluster states of both wild type and variant forms of HydF have been examined from various species and all of the results provide evidence for [4Fe-4S] cluster binding to HydF [229, 234, 237-242]. The coordination environment for the [4Fe-4S] cluster utilizes three conserved cysteine residues; the fourth coordination site appears to be variable, either being a histidine in the case of *Ca* HydF or a labile/exchangeable ligand in *Thermotoga maritima* (*Tm*) and *Thermotoga neopolitana* (*Tn*) HydF [235, 239, 241-243]. The observation and significance of [2Fe-2S]$^{+}$ cluster binding by HydF is still an open issue. While similar overlapping axial signals to those initially reported [234] have now been observed in reduced preparations of both *Ca* and *Tn* samples, it has been suggested this signal arises from a radical in close proximity to the [4Fe-4S]$^{+}$ cluster [241, 242, 244]. Regardless, multiple lines of evidence support the notion that the 2Fe subcluster bound by HydF resembles the H-cluster, and may potentially even be directly linked to the [4Fe-4S] cubane present on HydF [238, 244].

While the exact role of GTP hydrolysis in [FeFe]-hydrogenase maturation remains unresolved, it is clear that the GTPase activity of HydF is not associated with the activation step of $HydA^{\Delta EFG}$ by $HydF^{EG}$ [234]. In a manner reminiscent of HypB [209], the GTPase activity of HydF is gated by different monovalent cations and these regulate GTP hydrolysis by ~ 40–fold. HydF therefore belongs to a subclass of GTPase enzymes wherein an alkali metal substitutes for the "arginine finger" of the partner GTPase activating protein [234]. The ability of $HydF^{EG}$ to mature $HydA^{\Delta EFG}$ is unaltered by HydF being in either a "GTPase–on" or a "GTPase–off" state, as established by accomplishing the activation in various alkali containing buffers [234]. However, it was observed that the rate of GTP hydrolysis was stimulated when HydF was assayed in the presence of either HydE or HydG, leading to the hypothesis that the production of GDP could be coupled to gating the protein–protein interactions associated with 2Fe subcluster assembly [234]. Experiments designed to probe protein–protein interactions between the maturases revealed that HydE and HydG do not bind to HydF concurrently, suggesting that the radical SAM enzymes associate with the same binding site on HydF [245]. Moreover, HydE and HydF bind to one another with an order of magnitude higher affinity than HydG binds to HydF and addition of GTP during dissociative phases causes enhanced detachment rates for both HydE–HydF and HydG–HydF complexes. [245]. Collectively, these results implicate GTP binding and hydrolysis as providing a mechanism for gating the interactions between HydE and HydG with the scaffold/carrier HydF, and this may be linked to nucleotide dependent structural changes in HydF.

While the majority of reports provide support for the indispensable nature of HydF during maturation [24, 26, 227, 234, 236, 237], results with *Shewanella oneidensis* maturases suggest that HydF is nonessential. Specifically, the *in vitro* $HydA^{\Delta EFG}$ activation studies with this

system concluded that HydG is the only maturase enzyme absolutely required [240]. Interestingly, $HydA^{\Delta EFG}$ activation experiments using compounds designed to mimic the 2Fe subcluster show that these analogs can not only be loaded into a [4Fe-4S] cluster containing form of *Tm* HydF, but that this charged HydF can then fully mature $HydA^{\Delta EFG}$ [246]. A subsequent study demonstrated that the 2Fe biomimetic analogs could load into $HydA^{\Delta EFG}$ in the absence of HydF, showing that HydF is not required for *in vitro* activation [247].

HydG and Diatomic Ligand Biosynthesis from Tyrosine

HydG contains a CX_3CX_2C N-terminal motif identifying it as a member of the radical SAM superfamily of enzymes [26, 248]. This 55 kDa monomeric protein exhibits high similarity to ThiH, an enzyme involved in thiamine pyrophosphate synthesis that cleaves L-tyrosine into *p*-cresol and dehydroglycine (DHG) [248, 249]. Like ThiH, HydG also utilizes L-tyrosine as substrate and forms *p*-cresol (Figure 9) [250]. HydG is differentiated from ThiH, however, in the existence of a 90 amino acid C-terminal extension containing a $CX_2CX_{22}C$ motif that harbors an accessory [4Fe-4S] cluster. The presence of the C-terminal [4Fe-4S] cluster is essential for [FeFe]-hydrogenase maturation, and the formation of the diatomic products CO and CN^- [23, 227, 251, 252]. Diatomic ligand production during HydG catalysis was demonstrated both by derivatizing CN^- into a 1-cyanobenz[f]isoindole adduct [23] and by trapping CO via binding to deoxyhemoglobin [251]. Both of these diatomic species formed on the same time scale and it was hypothesized that they could be formed in a single step via a decarbonylation reaction involving DHG [23].

Analysis of HydG variant proteins demonstrated the absolute requirement of the C-terminal [4Fe-4S] cluster for formation of CO, although CN^- was still detected in variants

containing either single or double point mutations to residues in the $CX_2CX_{22}C$ motif [253, 254]. Assessment of a variant in which the three cysteines of the CX_3CX_2C N-terminal motif were altered to alanine revealed that SAM coordination to the enzyme occurs exclusively at the N-terminal cluster, despite the apparent site-differentiated nature of the C-terminal [4Fe-4S] cluster [254]. Evaluation of ΔCTD HydG, a variant that is missing the C-terminal domain, shows that the enzyme still acts as a tyrosine lyase [253-255]. Collectively, the results show that SAM binding and cleavage, with subsequent H-atom abstraction from tyrosine, and the generation of *p*-cresol and DHG, all occur within the core TIM barrel fold [244, 254].

Spectroscopic characterization of intermediate species formed during catalysis provided direct evidence for heterolytic Cα–Cβ tyrosine bond cleavage, with generation of a *p*-cresolate radical and DHG (Figure 9) [256]. Stopped-flow FTIR studies were used to monitor the fate of DHG to formation of either Fe–CO–CN or Fe–$(CO)_2$CN moieties. It was assumed that these species formed at the site differentiated Fe of the accessory [4Fe-4S] cluster although there is no direct experimental evidence for this [252]. In separate experiments, ^{57}Fe was used to track iron transfer from HydG to HydA, suggesting that the C-terminal [4Fe-4S] cluster in HydG becomes cannibalized to form the Fe–CO–CN building blocks of the 2Fe subcluster [252]. Furthermore, it is known that all five diatomic ligands of the H-cluster are derived from tyrosine [257], suggesting that multiple rounds of HydG catalysis are necessary for 2Fe subcluster formation. The mechanistic details of this process are unknown but must be resolved to delineate the role of HydF as a scaffold/carrier protein during biosynthesis [244].

An Undefined Role in H-cluster Biosynthesis: HydE

In contrast to the extensive experimental data supporting the proposed roles of HydF and HydG in H-cluster biosynthesis, the role of HydE, a member of the radical SAM superfamily of enzymes, is still unknown. It has been suggested that HydE functions in an observatory role during maturation, possibly acting as a chaperone and assisting HydF during translocation of the 2Fe subcluster species [240]. It seems much more likely, however, that HydE utilizes a common metabolite and synthesizes the bridging dithiomethylamine ligand (Figure 9). Evidence in support of this comes from the absolute requirement of HydE to achieve [FeFe]-hydrogenase activity in *E. coli* lysate experiments [24, 26, 227, 230] and the difficult chemistries often associated with radical SAM enzymes [248]. HydE is a 42 kDa monomer and contains a CX_3CX_2C N-terminal motif, like other radical SAM enzymes [26, 248]. However, it shows high sequence similarity to the methylornithine synthase PylB [228, 244, 258], rather than to enzymes like BioB that catalyze a sulfur insertion reaction [259]. While the significance of HydE's relationship to PylB is difficult to currently gauge, it is possible that it is an indication that these enzymes exhibit mechanistic parallels.

Multiple X-ray crystal structures of HydE exist and these include SAM and 5'-deoxyadenosine/methionine bound states [259-261]. The global architecture of HydE shows the existence of an internal electropositive cavity spanning the breadth of the $(\beta\alpha)_8$ TIM barrel fold. Three anion binding sites were observed within the internal cavity and SCN^- also binds here, potentially representing a pathway whereby a small molecule product(s) traverses from the top to the bottom of the barrel where delivery to a maturation partner protein occurs [259]. Surface plasmon resonance experiments indicate that HydE and HydF bind to one another with high affinity and even exist as a fused gene product in some organisms [26, 245]. Regardless of these experimental findings, the substrate and mechanism of HydE in H-cluster biosynthesis remain

unresolved. Although it is somewhat tenuous to assign it a role in dithiomethylamine synthesis, this seems the most likely given the precedence in the literature for the chemistries associated with HydF and HydG [244]. An intriguing aspect of HydE's presumed chemistry relates to the source of the sulfurs in the 2Fe subcluster. Future work will hopefully resolve if the sulfurs are derived from HydE's substrate or if they are cannibalized from HydG's C-terminal cluster.

Mechanistic Parallels and Differences Between [NiFe]– and [FeFe]–Hydrogenase Biosynthesis

[NiFe]– and [FeFe]–hydrogenases are a superb example of convergent evolution and it follows that their biosynthetic pathways exhibit both commonalities and differences. Generally, it is straightforward to see that both active site assembly pathways require multiple maturation proteins involved in intricate chemical transformations. Moreover, each system utilizes a key scaffold protein that belongs to the same subclass of GTPase enzymes, which are activated by alkali metals. The formation and transfer of Fe-diatomic species among proteins is also an intriguing aspect shared by these systems, despite the fact that the source of these diatomic ligands is disparate. [FeFe]-hydrogenase assembly requires the involvement of two radical SAM enzymes, a feature that noticeably distinguishes it from [NiFe]-hydrogenase maturation.

Future Frontiers of Hydrogenase Research

Hydrogenases are unique enzymes and the recent insights into their diversity, mechanism, and maturation have revealed many surprises that represent highly unique aspects of bioinorganic chemistry, as summarized here. Although a number of questions have been answered through the surge of recent work in this area, these exciting new discoveries also serve

to open the door for perhaps more lines of inquiry than they have closed. It is likely that hydrogenases will have a central role in clarifying the newly discovered mechanism of energy conservation termed electron bifurcation ([35]). In many systems these bifurcating reactions are likely key points for controlling and balancing electron flow in metabolism and a better fundamental understanding of these processes could potentially provide the basis for proactively controlling electron flow for the production of biofuels in engineered systems.

The striking functional diversity of [FeFe]-hydrogenases and [NiFe]-hydrogenases has interesting evolutionary implications and the further characterization of representatives of the various diverse classes of these enzymes will lead to more fascinating evolutionary insights. Most would agree that aspects of hydrogen metabolism must have been a component of the metabolism of early life and this appears to be supported for the [NiFe]-hydrogenases but arguably not for the [FeFe]-hydrogenases. The traditional dogma and natural impetus is that hydrogenase must be ancient or even must be primordial because of the perceived importance of hydrogen metabolism for early life. However, in the case of [FeFe]-hydrogense,the available data including their taxonomic occurrence among extant organisms is inconsistent with an ancient origin. This begs the question of whether [NiFe]-hydrogenases and [FeFe]-hydrogenases are both ancient, or primordial, and what the selective pressures might have been to independently evolve so-called functionally redundant enzymes. Further analysis of hydrogenase diversity in the context of their modes of metabolism could provide important new clues into hydrogenase ancestry as well as the ancestry of chemiosmosis and respiration. One driving force will likely be the close evolutionary relationship between one specific type of [NiFe]-hydrogenase (the group 4 energy-conserving enzymes) and the ubiquitous complex I of

the aerobic respiratory chain. How did the latter evolve from a presumably H_2-metabolizing ancestor?

Additional insight gained into the relationship between sequence variations and the respective physiological roles for hydrogenases have potential to further identify the key structural determinants for catalysis. Hydrogenases are intriguing models for proton coupled electron transfer reactions and these are in some regards very special enzymatic reactions. We are taught in general chemistry of the separation between thermodynamics and kinetics in chemical reactions and that catalysts by definition exert the influence solely on the rates of reactions and don't influence reaction thermodynamics. However for enzymes involved in proton coupled electron transfer reactions there is clear evidence that the properties of the enzymes themselves can influence the thermodynamics of reactions by influencing the local concentration of substrates and/or products. The chemical character and availability of proton donors and acceptor groups in the active site and the oxidation-reduction potential of active site metal and accessory clusters can essentially tune the concentration of protons and electrons and influence the thermodynamics of hydrogenase reactions. The extent of this influence is not well understood and the simplicity of the hydrogenase reaction makes this an ideal model system for delineating the degree of this control, potentially significantly impacting biotechnology particularly in the area of biofuel production.

For [NiFe]- and [FeFe]-hydrogenases, as detailed in this review, there have been significant advances in our understanding of nonprotein ligand biosynthesis and protein maturation. There is, however, still much more work to be done. The illumination of the pathways for nonprotein ligand biosynthesis can be linked to a classic metabolic pathway elucidation problem in which the substrates are not defined and as such present significant challenges to researchers.

Advances over the last decade have succeeded in identifying the substrates for carbon monoxide and cyanide synthesis but there are still a lot of mechanistic details that need to be resolved. For the [NiFe]-hydrogenase diatomic ligand biosynthesis, the existence of Fe–CO_2 FTIR bands both in HypC alone and when HypC is in a complex with HypD has led to the recent hypothesis that HypC delivers an Fe–CO_2 group to HypD where the CO_2 is reduced to CO. Experimental validation is needed, both for the transfer and delivery of this species from HypC to HypD, as well as to the source of the CO ligand being CO_2. For [FeFe]-hydrogenase diatomic ligand biosynthesis the presence of Fe–CO/CN species which form during HydG catalysis leads to the hypothesis that the C-terminal cluster is cannibalized in this process and that the iron-diatomic group(s) are then mobilized to HydF. Clearly for [FeFe]-hydrogenase H cluster biosynthesis there are conflicting results and differing perspectives on many aspects of the mechanism of H cluster assembly. Some of these likely reflect differences in experimental design, in particular how these maturation proteins are expressed and analyzed. It will be the challenge of the next generation of maturation studies to delineate the relevant insights being gleaned for all the expected approaches in the context of physiological or in vivo assembly.

The culmination of the new insights into hydrogenase diversity, mechanism, and maturation presented herein should have one convinced of the amazing qualities of hydrogenases as complex iron sulfur enzymes that span evolutionary time and which played a key role in the physiological diversification of life. These enzymes provide a one stop model system for studies of the evolution of early life processes, control of biological electron flow in metabolism, proton coupled electron transfer reactions in biological systems, complex metal cluster assembly, and the origin of modern day aerobic respiration.

Acknowledgements

The authors would like to acknowledge the following funding sources: Air Force Office of Scientific Research grant FA-9550-11-1-0218 to J.W.P., NASA Exobiology and Evolutionary Biology (NNX13AI11G) to E.S.B., and the U.S. Department of Energy, Division of Chemical Sciences, Geosciences, and Biosciences, Office of Basic Energy Sciences (DE-AC36-08-GO28308 to P.W.K., DE-FG05-95ER20175 to M.W.W.A., FG02-10ER16194 to J.B.B. and J.W.P.). The Biological Electron Transfer and Catalysis Energy Frontiers Research Center funded by the Department of Energy, Office of Science.

References

[1] A.K. Jones, E. Sillery, S.P.J. Albracht, F.A. Armstrong, Direct comparison of the electrocatalytic oxidation of hydrogen by an enzyme and a platinum catalyst, Chemical Communications, (2002) 866-867.

[2] P.-P. Liebgott, F. Leroux, B. Burlat, S. Dementin, C. Baffert, T. Lautier, V. Fourmond, P. Ceccaldi, C. Cavazza, I. Meynial-Salles, P. Soucaille, J.C. Fontecilla-Camps, B. Guigliarelli, P. Bertrand, M. Rousset, C. Léger, Relating diffusion along the substrate tunnel and oxygen sensitivity in hydrogenase, Nat Chem Biol, 6 (2010) 63-70.

[3] C. Madden, M.D. Vaughn, I. Díez-Pérez, K.A. Brown, P.W. King, D. Gust, A.L. Moore, T.A. Moore, Catalytic Turnover of [FeFe]-Hydrogenase Based on Single-Molecule Imaging, Journal of the American Chemical Society, 134 (2011) 1577-1582.

[4] H.R. Pershad, J.L.C. Duff, H.A. Heering, E.C. Duin, S.P.J. Albracht, F.A. Armstrong, Catalytic Electron Transport in Chromatium vinosum [NiFe]-Hydrogenase: Application of Voltammetry in Detecting Redox-Active Centers and Establishing That Hydrogen Oxidation Is Very Fast Even at Potentials Close to the Reversible H+/H2 Value†, Biochemistry, 38 (1999) 8992-8999.

[5] A.J. Cornish, K. Gärtner, H. Yang, J.W. Peters, E.L. Hegg, Mechanism of Proton Transfer in [FeFe]-Hydrogenase from Clostridium pasteurianum, Journal of Biological Chemistry, 286 (2011) 38341-38347.

[6] B. Ginovska-Pangovska, A. Dutta, M.L. Reback, J.C. Linehan, W.J. Shaw, Beyond the Active Site: The Impact of the Outer Coordination Sphere on Electrocatalysts for Hydrogen Production and Oxidation, Accounts of Chemical Research, (2014).

[7] B. Ginovska-Pangovska, M.-H. Ho, J.C. Linehan, Y. Cheng, M. Dupuis, S. Raugei, W.J. Shaw, Molecular dynamics study of the proposed proton transport pathways in [FeFe]-hydrogenase, Biochimica et Biophysica Acta (BBA) - Bioenergetics, 1837 (2014) 131-138.

[8] P. Knörzer, A. Silakov, C.E. Foster, F.A. Armstrong, W. Lubitz, T. Happe, Importance of the protein framework for catalytic activity of [FeFe]-hydrogenases, Journal of Biological Chemistry, 287 (2012) 1489-1499.

[9] M.C. Marques, R. Coelho, A.L. De Lacey, I.A.C. Pereira, P.M. Matias, The Three-Dimensional Structure of [NiFeSe] Hydrogenase from Desulfovibrio vulgaris Hildenborough: A Hydrogenase without a Bridging Ligand in the Active Site in Its Oxidised, "as-Isolated" State, Journal of Molecular Biology, 396 (2010) 893-907.

[10] K.A. Vincent, A. Parkin, F.A. Armstrong, Investigating and Exploiting the Electrocatalytic Properties of Hydrogenases, Chemical Reviews, 107 (2007) 4366-4413.

[11] P.M. Vignais, B. Billoud, Occurrence, classification, and biological function of hydrogenases: an overview, Chem Rev, 107 (2007) 4206-4272.

[12] P.M. Vignais, B. Billoud, J. Meyer, Classification and phylogeny of hydrogenases, FEMS Microbiol Rev, 25 (2001) 455-501.

[13] M. Calusinska, T. Happe, B. Joris, A. Wilmotte, The surprising diversity of clostridial hydrogenases: a comparative genomic perspective, Microbiology, 156 (2010) 1575-1588.

[14] J. Meyer, [FeFe] hydrogenases and their evolution: a genomic perspective, Cell Mol Life Sci, 64 (2007) 1063-1084.

[15] J. Balk, A.J. Pierik, D.J.A. Netz, U. Mühlenhoff, R. Lill, The hydrogenase-like Nar1p is essential for maturation of cytosolic and nuclear iron–sulphur proteins, The EMBO Journal, 23 (2004) 2105-2115.

[16] D.S. Horner, B. Heil, T. Happe, T.M. Embley, Iron hydrogenases – ancient enzymes in modern eukaryotes, Trends in Biochemical Sciences, 27 (2002) 148-153.

[17] D.S. Horner, B. Heil, T. Happe, T.M. Embley, Iron hydrogenases--ancient enzymes in modern eukaryotes., Trends Biochem. Sci, 27 (2002) 148-153.

[18] D.W. Mulder, E.S. Boyd, R. Sarma, R.K. Lange, J.A. Endrizzi, J.B. Broderick, J.W. Peters, Stepwise [FeFe]-hydrogenase H-cluster assembly revealed in the structure of $HydA^{DEFG}$, Nature, 465 (2010) 248-251.

[19] E.S. Boyd, G.J. Schut, M.W.W. Adams, J.W. Peters, Hydrogen metabolism and the evolution of biological respiration, Microbe, In Press (2014).

[20] R. Hedderich, Energy-converting [NiFe] hydrogenases from archaea and extremophiles: ancestors of complex I, J Bioenerg Biomembr, 36 (2004) 65-75.

[21] G.J. Schut, E.S. Boyd, J.W. Peters, M.W. Adams, The modular respiratory complexes involved in hydrogen and sulfur metabolism by heterotrophic hyperthermophilic archaea and their evolutionary implications, FEMS Microbiol Rev, 37 (2013) 182-203.

[22] A. Bock, P.W. King, M. Blokesch, M.C. Posewitz, Maturation of hydrogenases, Adv.Microb.Physiol, 51 (2006) 1-71.

[23] R.C. Driesener, M.R. Challand, S.E. McGlynn, E.M. Shepard, E.S. Boyd, J.B. Broderick, J.W. Peters, P.L. Roach, [FeFe]-hydrogenase cyanide ligands derived from S-adenosylmethionine-dependent cleavage of tyrosine, Angew Chem Int Ed Engl, 49 (2010) 1687-1690.

[24] S.E. McGlynn, S.S. Ruebush, A. Naumov, L.E. Nagy, A. Dubini, P.W. King, J.B. Broderick, M.C. Posewitz, J.W. Peters, In vitro activation of [FeFe] hydrogenase: new insights into hydrogenase maturation, J.Biol.Inorg.Chem., 12 (2007) 443-447.

[25] C. Pinske, R.G. Sawers, The importance of iron in the biosynthesis and assembly of [NiFe]-hydrogenases, in: BioMolecular Concepts, 2014, pp. 55.

[26] M.C. Posewitz, P.W. King, S.L. Smolinski, L. Zhang, M. Seibert, M.L. Ghirardi, Discovery of two novel radical S-adenosylmethionine proteins required for the assembly of an active [Fe] hydrogenase, J.Biol.Chem., 279 (2004) 25711-25720.

[27] E.M. Shepard, E.S. Boyd, J.B. Broderick, J.W. Peters, Biosynthesis of complex iron-sulfur enzymes, Curr Opin Chem Biol, 15 (2011) 319-327.

[28] J.E. Meuser, E.S. Boyd, G. Ananyev, D. Karns, R. Radakovits, U.M. Narayana Murthy, M.L. Ghirardi, G.C. Dismukes, J.W. Peters, M.C. Posewitz, Evolutionary significance of an algal gene encoding an [FeFe]-hydrogenase with F-domain homology and hydrogenase activity in Chlorella variabilis NC64A, Planta, 234 (2011) 829-843.

[29] C.M. English, C. Eckert, K. Brown, M. Seibert, P.W. King, Recombinant and in vitro expression systems for hydrogenases: new frontiers in basic and applied studies for biological and synthetic H_2 production, Dalton Trans, (2009) 9970-9978.

[30] M.C. Posewitz, D.W. Mulder, J.W. Peters, New frontiers in hydrogenase structure and biosynthesis Curr Chem Biol, 2 (2008) 178-199.

[31] B. Ghysels, D. Godaux, R.F. Matagne, P. Cardol, F. Franck, Function of the chloroplast hydrogenase in the microalga Chlamydomonas: the role of hydrogenase and state transitions during photosynthetic activation in anaerobiosis, PLoS One, 8 (2013) e64161.

[32] J. Noth, D. Krawietz, A. Hemschemeier, T. Happe, Pyruvate:ferredoxin oxidoreductase is coupled to light-independent hydrogen production in Chlamydomonas reinhardtii, J Biol Chem, 288 (2013) 4368-4377.

[33] J.H. Hwang, H.C. Kim, J.A. Choi, R.A. Abou-Shanab, B.A. Dempsey, J.M. Regan, J.R. Kim, H. Song, I.H. Nam, S.N. Kim, W. Lee, D. Park, Y. Kim, J. Choi, M.K. Ji, W. Jung, B.H. Jeon, Photoautotrophic hydrogen production by eukaryotic microalgae under aerobic conditions, Nat Commun, 5 (2014) 3234.

[34] J.W. Peters, W.N. Lanzilotta, B.J. Lemon, L.C. Seefeldt, X-ray crystal structure of the Fe-only hydrogenase (CpI) from Clostridium pasteurianum to 1.8 angstrom resolution, Science, 282 (1998) 1853-1858.

[35] W. Buckel, R.K. Thauer, Energy conservation via electron bifurcating ferredoxin reduction and proton/Na^+ translocating ferredoxin oxidation, Biochim Biophys Acta, 1827 (2013) 94-113.

[36] S. Malki, I. Saimmaime, G. De Luca, M. Rousset, Z. Dermoun, J.P. Belaich, Characterization of an operon encoding an NADP-reducing hydrogenase in Desulfovibrio fructosovorans, J Bacteriol, 177 (1995) 2628-2636.

[37] B. Soboh, D. Linder, R. Hedderich, A multisubunit membrane-bound [NiFe] hydrogenase and an NADH-dependent Fe-only hydrogenase in the fermenting bacterium Thermoanaerobacter tengcongensis, Microbiology, 150 (2004) 2451-2463.

[38] M.F. Verhagen, M.W. Adams, Fe-only hydrogenase from Thermotoga maritima, Methods Enzymol, 331 (2001) 216-226.

[39] G.J. Schut, M.W. Adams, The iron-hydrogenase of Thermotoga maritima utilizes ferredoxin and NADH synergistically: a new perspective on anaerobic hydrogen production, J Bacteriol, 191 (2009) 4451-4457.

[40] G. Herrmann, E. Jayamani, G. Mai, W. Buckel, Energy conservation via electron-transferring flavoprotein in anaerobic bacteria, J Bacteriol, 190 (2008) 784-791.

[41] F. Li, J. Hinderberger, H. Seedorf, J. Zhang, W. Buckel, R.K. Thauer, Coupled ferredoxin and crotonyl coenzyme A (CoA) reduction with NADH catalyzed by the butyryl-CoA dehydrogenase/Etf complex from Clostridium kluyveri, J Bacteriol, 190 (2008) 843-850.

[42] R.K. Thauer, A.K. Kaster, H. Seedorf, W. Buckel, R. Hedderich, Methanogenic archaea: ecologically relevant differences in energy conservation, Nat Rev Microbiol, 6 (2008) 579-591.

[43] E.T. Smith, J.M. Blamey, Z.H. Zhou, M.W. Adams, A variable-temperature direct electrochemical study of metalloproteins from hyperthermophilic microorganisms involved in hydrogen production from pyruvate, Biochemistry, 34 (1995) 7161-7169.

[44] R. Sterner, Ferredoxin from Thermotoga maritima, Methods Enzymol, 334 (2001) 23-30.

[45] A.J. Shaw, D.A. Hogsett, L.R. Lynd, Identification of the [FeFe]-hydrogenase responsible for hydrogen generation in Thermoanaerobacterium saccharolyticum and demonstration of increased ethanol yield via hydrogenase knockout, J Bacteriol, 191 (2009) 6457-6464.

[46] K. Schuchmann, V. Muller, A bacterial electron-bifurcating hydrogenase, J Biol Chem, 287 (2012) 31165-31171.

[47] E. Biegel, V. Muller, Bacterial Na^+-translocating ferredoxin:NAD^+ oxidoreductase, Proc Natl Acad Sci USA, 107 (2010) 18138-18142.

[48] V. Hess, K. Schuchmann, V. Muller, The ferredoxin:NAD^+ oxidoreductase (Rnf) from the acetogen Acetobacterium woodii requires Na^+ and Is reversibly coupled to the membrane potential, J Biol Chem, 288 (2013) 31496-31502.

[49] S. Wang, H. Huang, J. Kahnt, R.K. Thauer, A reversible electron-bifurcating ferredoxin- and NAD-dependent [FeFe]-hydrogenase (HydABC) in Moorella thermoacetica, J Bacteriol, 195 (2013) 1267-1275.

[50] S. Wang, H. Huang, J. Kahnt, A.P. Mueller, M. Kopke, R.K. Thauer, NADP-specific electron-bifurcating [FeFe]-hydrogenase in a functional complex with formate dehydrogenase in Clostridium autoethanogenum grown on CO, J Bacteriol, 195 (2013) 4373-4386.

[51] J.M. Bruno-Barcena, M.S. Chinn, A.M. Grunden, Genome sequence of the autotrophic acetogen Clostridium autoethanogenum JA1-1 strain DSM 10061, a producer of ethanol from carbon monoxide, Genome Announc, 1 (2013).

[52] S.C. Leahy, W.J. Kelly, R.S. Ronimus, N. Wedlock, E. Altermann, G.T. Attwood, Genome sequencing of rumen bacteria and archaea and its application to methane mitigation strategies, Animal, 7 Suppl 2 (2013) 235-243.

[53] A. Brune, Symbiotic digestion of lignocellulose in termite guts, Nat Rev Microbiol, 12 (2014) 168-180.

[54] E.A. Davidson, M. van der Giezen, D.S. Horner, T.M. Embley, C.J. Howe, An [Fe] hydrogenase from the anaerobic hydrogenosome-containing fungus Neocallimastix frontalis L2, Gene, 296 (2002) 45-52.

[55] X. Ze, F. Le Mougen, S.H. Duncan, P. Louis, H.J. Flint, Some are more equal than others: the role of "keystone" species in the degradation of recalcitrant substrates, Gut Microbes, 4 (2013) 236-240.

[56] J.C. Fontecilla-Camps, Structure and function of [NiFe]-hydrogenases, Met Ions Life Sci, 6 (2009) 151-178.

[57] H. Ogata, W. Lubitz, Y. Higuchi, [NiFe] hydrogenases: structural and spectroscopic studies of the reaction mechanism, Dalton Trans, (2009) 7577-7587.

[58] K. Trchounian, C. Pinske, R.G. Sawers, A. Trchounian, Characterization of Escherichia coli [NiFe]-hydrogenase distribution during fermentative growth at different pHs, Cell Biochem Biophys, 62 (2012) 433-440.

[59] F.O. Morais-Silva, C.I. Santos, R. Rodrigues, I.A. Pereira, C. Rodrigues-Pousada, Roles of HynAB and Ech, the only two hydrogenases found in the model sulfate reducer Desulfovibrio gigas, J Bacteriol, 195 (2013) 4753-4760.

[60] R. Huber, T. Wilharm, D. Huber, A. Trincone, S. Burggraf, H. Konig, R. Rachel, I. Rockinger, H. Fricke, K.O. Stetter, Aquifex pyrophilus Gen-Nov Sp-Nov represents a novel Group of marine hyperthermophilic hydrogen-oxidizing bacteria, Syst Appl Microbiol, 15 (1992) 340-351.

[61] G. Deckert, P.V. Warren, T. Gaasterland, W.G. Young, A.L. Lenox, D.E. Graham, R. Overbeek, M.A. Snead, M. Keller, M. Aujay, R. Huber, R.A. Feldman, J.M. Short, G.J. Olsen, R.V. Swanson, The complete genome of the hyperthermophilic bacterium Aquifex aeolicus, Nature, 392 (1998) 353-358.

[62] M. Guiral, L. Prunetti, S. Lignon, R. Lebrun, D. Moinier, M.T. Giudici-Orticonit, New insights into the respiratory chains of the chemolithoautotrophic and hyperthermophilic bacterium Aquifex aeolicus, J Proteome Res, 8 (2009) 1717-1730.

[63] S. Laska, F. Lottspeich, A. Kletzin, Membrane-bound hydrogenase and sulfur reductase of the hyperthermophilic and acidophilic archaeon Acidianus ambivalens, Microbiology, 149 (2003) 2357-2371.

[64] I. Berman-Frank, P. Lundgren, P. Falkowski, Nitrogen fixation and photosynthetic oxygen evolution in cyanobacteria, Res Microbiol, 154 (2003) 157-164.

[65] P. Tamagnini, E. Leitao, P. Oliveira, D. Ferreira, F. Pinto, D.J. Harris, T. Heidorn, P. Lindblad, Cyanobacterial hydrogenases: diversity, regulation and applications, FEMS Microbiol Rev, 31 (2007) 692-720.

[66] X. Zhang, D.M. Sherman, L.A. Sherman, The uptake hydrogenase in the unicellular diazotrophic cyanobacterium Cyanothece sp. strain PCC 7822 protects nitrogenase from oxygen toxicity, J Bacteriol, 196 (2014) 840-849.

[67] W. Khetkorn, P. Lindblad, A. Incharoensakdi, Inactivation of uptake hydrogenase leads to enhanced and sustained hydrogen production with high nitrogenase activity under high light exposure in the cyanobacterium Anabaena siamensis TISTR 8012, J Biol Eng, 6 (2012) 19.

[68] O. Lenz, M. Bernhard, T. Buhrke, E. Schwartz, B. Friedrich, The hydrogen-sensing apparatus in Ralstonia eutropha, J Mol Microbiol Biotechnol, 4 (2002) 255-262.

[69] L.A. Alex, J.N. Reeve, W.H. Orme-Johnson, C.T. Walsh, Cloning, sequence determination, and expression of the genes encoding the subunits of the nickel-containing 8-

hydroxy-5-deazaflavin reducing hydrogenase from Methanobacterium thermoautotrophicum delta H, Biochemistry, 29 (1990) 7237-7244.

[70] S. Vitt, K. Ma, E. Warkentin, J. Moll, A.J. Pierik, S. Shima, U. Ermler, The F_{420}-reducing [NiFe]-yydrogenase complex from Methanothermobacter marburgensis, the first X-ray structure of a group 3 family member, J Mol Biol, 426 (2014) 2813-2826.

[71] T. Kanai, R. Matsuoka, H. Beppu, A. Nakajima, Y. Okada, H. Atomi, T. Imanaka, Distinct physiological roles of the three [NiFe]-hydrogenase orthologs in the hyperthermophilic archaeon Thermococcus kodakarensis, J Bacteriol, 193 (2011) 3109-3116.

[72] K. Ma, M.W. Adams, Hydrogenases I and II from Pyrococcus furiosus, Methods Enzymol, 331 (2001) 208-216.

[73] G.J. Schut, W.J. Nixon, G.L. Lipscomb, R.A. Scott, M.W. Adams, Mutational analyses of the enzymes involved in the metabolism of hydrogen by the hyperthermophilic archaeon Pyrococcus furiosus, Front Microbiol, 3 (2012) 163.

[74] A. Stojanowic, G.J. Mander, E.C. Duin, R. Hedderich, Physiological role of the F_{420}-non-reducing hydrogenase (Mvh) from Methanothermobacter marburgensis, Arch Microbiol, 180 (2003) 194-203.

[75] A.K. Kaster, J. Moll, K. Parey, R.K. Thauer, Coupling of ferredoxin and heterodisulfide reduction via electron bifurcation in hydrogenotrophic methanogenic archaea, Proc Natl Acad Sci USA, 108 (2011) 2981-2986.

[76] R.K. Thauer, A.K. Kaster, M. Goenrich, M. Schick, T. Hiromoto, S. Shima, Hydrogenases from methanogenic archaea, nickel, a novel cofactor, and H_2 storage, Annu Rev Biochem, 79 (2010) 507-536.

[77] R. Cramm, Genomic view of energy metabolism in Ralstonia eutropha H16, J Mol Microbiol Biotechnol, 16 (2009) 38-52.

[78] K. Gutekunst, X. Chen, K. Schreiber, U. Kaspar, S. Makam, J. Appel, The bidirectional NiFe-hydrogenase in Synechocystis sp. PCC 6803 is reduced by flavodoxin and ferredoxin and is essential under mixotrophic, nitrate-limiting conditions, J Biol Chem, 289 (2014) 1930-1937.

[79] R. Sapra, K. Bagramyan, M.W. Adams, A simple energy-conserving system: proton reduction coupled to proton translocation, Proc Natl Acad Sci USA, 100 (2003) 7545-7550.

[80] A. Tersteegen, R. Hedderich, Methanobacterium thermoautotrophicum encodes two multisubunit membrane-bound [NiFe] hydrogenases. Transcription of the operons and sequence analysis of the deduced proteins, Eur J Biochem, 264 (1999) 930-943.

[81] Y.J. Kim, H.S. Lee, E.S. Kim, S.S. Bae, J.K. Lim, R. Matsumi, A.V. Lebedinsky, T.G. Sokolova, D.A. Kozhevnikova, S.S. Cha, S.J. Kim, K.K. Kwon, T. Imanaka, H. Atomi, E.A. Bonch-Osmolovskaya, J.H. Lee, S.G. Kang, Formate-driven growth coupled with H_2 production, Nature, 467 (2010) 352-355.

[82] R.G. Sawers, S.P. Ballantine, D.H. Boxer, Differential expression of hydrogenase isoenzymes in Escherichia coli K-12: evidence for a third isoenzyme, J Bacteriol, 164 (1985) 1324-1331.

[83] H.S. Lee, S.G. Kang, S.S. Bae, J.K. Lim, Y. Cho, Y.J. Kim, J.H. Jeon, S.S. Cha, K.K. Kwon, H.T. Kim, C.J. Park, H.W. Lee, S.I. Kim, J. Chun, R.R. Colwell, S.J. Kim, J.H. Lee, The complete genome sequence of Thermococcus onnurineus NA1 reveals a mixed heterotrophic and carboxydotrophic metabolism, J Bacteriol, 190 (2008) 7491-7499.

[84] B. Soboh, D. Linder, R. Hedderich, Purification and catalytic properties of a CO-oxidizing:H_2-evolving enzyme complex from Carboxydothermus hydrogenoformans, Eur J Biochem, 269 (2002) 5712-5721.

[85] J. Meuer, S. Bartoschek, J. Koch, A. Kunkel, R. Hedderich, Purification and catalytic properties of Ech hydrogenase from Methanosarcina barkeri, Eur J Biochem, 265 (1999) 325-335.

[86] R. Sapra, M.F.J.M. Verhagen, M.W.W. Adams, Purification and characterization of a membrane-bound hydrogenase from the hyperthermophilic archaeon Pyrococcus furiosus, J Bacteriol, 182 (2000) 3423-3428.

[87] P.J. Silva, E.C. van den Ban, H. Wassink, H. Haaker, B. de Castro, F.T. Robb, W.R. Hagen, Enzymes of hydrogen metabolism in Pyrococcus furiosus, Eur J Biochem, 267 (2000) 6541-6551.

[88] C.H. Verhees, S.W.M. Kengen, J.E. Tuininga, G.J. Schut, M.W.W. Adams, W.M. De Vos, J. Van der Oost, The unique features of glycolytic pathways in Archaea, Biochemical J, 377 (2004) 819-822.

[89] T.A. Major, Y. Liu, W.B. Whitman, Characterization of energy-conserving hydrogenase B in Methanococcus maripaludis, J Bacteriol, 192 (2010) 4022-4030.

[90] P. Constant, S.P. Chowdhury, L. Hesse, J. Pratscher, R. Conrad, Genome data mining and soil survey for the novel group 5 [NiFe]-hydrogenase to explore the diversity and

ecological importance of presumptive high-affinity H_2-oxidizing bacteria, Appl Environ Microbiol, 77 (2011) 6027-6035.

[91] P. Constant, S.P. Chowdhury, J. Pratscher, R. Conrad, Streptomycetes contributing to atmospheric molecular hydrogen soil uptake are widespread and encode a putative high-affinity [NiFe]-hydrogenase, Environ Microbiol, 12 (2010) 821-829.

[92] L.K. Meredith, D. Rao, T. Bosak, V. Klepac-Ceraj, K.R. Tada, C.M. Hansel, S. Ono, R.G. Prinn, Consumption of atmospheric hydrogen during the life cycle of soil-dwelling actinobacteria, Environ Microbiol Rep, 6 (2014) 226-238.

[93] A. Volbeda, M.-H. Charon, C. Piras, E.C. Hatchikian, M. Frey, J.C. Fontecilla-Camps, Crystal structure of the nickel-iron hydrogenase from Desulfovibrio gigas, Nature, 373 (1995) 580-587.

[94] Y. Higuchi, H. Ogata, K. Miki, N. Yasuoka, T. Yagi, Removal of the bridging ligand atom at the Ni–Fe active site of [NiFe] hydrogenase upon reduction with H< sub> 2</sub>, as revealed by X-ray structure analysis at 1.4 Å resolution, Structure, 7 (1999) 549-556.

[95] E. Garcin, X. Vernede, E. Hatchikian, A. Volbeda, M. Frey, J. Fontecilla-Camps, The crystal structure of a reduced [NiFeSe] hydrogenase provides an image of the activated catalytic center, Structure, 7 (1999) 557-566.

[96] H. Ogata, Y. Mizoguchi, N. Mizuno, K. Miki, S.-i. Adachi, N. Yasuoka, T. Yagi, O. Yamauchi, S. Hirota, Y. Higuchi, Structural studies of the carbon monoxide complex of [NiFe] hydrogenase from Desulfovibrio vulgaris Miyazaki F: suggestion for the initial activation site for dihydrogen, Journal of the American Chemical Society, 124 (2002) 11628-11635.

[97] A. Volbeda, L. Martin, C. Cavazza, M. Matho, B.W. Faber, W. Roseboom, S.P. Albracht, E. Garcin, M. Rousset, J.C. Fontecilla-Camps, Structural differences between the ready and unready oxidized states of [NiFe] hydrogenases, JBIC Journal of Biological Inorganic Chemistry, 10 (2005) 239-249.

[98] H. Ogata, S. Hirota, A. Nakahara, H. Komori, N. Shibata, T. Kato, K. Kano, Y. Higuchi, Activation process of [NiFe] hydrogenase elucidated by high-resolution X-ray analyses: conversion of the ready to the unready state, Structure, 13 (2005) 1635-1642.

[99] H. Ogata, P. Kellers, W. Lubitz, The Crystal Structure of the [NiFe] Hydrogenase from the Photosynthetic Bacterium< i> Allochromatium vinosum</i>: Characterization of the Oxidized Enzyme (Ni-A State), Journal of molecular biology, 402 (2010) 428-444.

[100] Y. Shomura, K.-S. Yoon, H. Nishihara, Y. Higuchi, Structural basis for a [lsqb] 4Fe-3S [rsqb] cluster in the oxygen-tolerant membrane-bound [lsqb] NiFe [rsqb]-hydrogenase, Nature, 479 (2011) 253-256.

[101] A. Volbeda, P. Amara, C. Darnault, J.-M. Mouesca, A. Parkin, M.M. Roessler, F.A. Armstrong, J.C. Fontecilla-Camps, X-ray crystallographic and computational studies of the O2-tolerant [NiFe]-hydrogenase 1 from Escherichia coli, Proceedings of the National Academy of Sciences, 109 (2012) 5305-5310.

[102] S. Dementin, B. Burlat, A.L. De Lacey, A. Pardo, G. Adryanczyk-Perrier, B. Guigliarelli, V.M. Fernandez, M. Rousset, A Glutamate Is the Essential Proton Transfer Gate during the Catalytic Cycle of the [NiFe] Hydrogenase, Journal of Biological Chemistry, 279 (2004) 10508-10513.

[103] E. Szőri-Dorogházi, G. Maróti, M. Szőri, A. Nyilasi, G. Rákhely, K.L. Kovács, Analyses of the Large Subunit Histidine-Rich Motif Expose an Alternative Proton Transfer Pathway in [NiFe] Hydrogenases, PLoS ONE, 7 (2012) e34666.

[104] W. Lubitz, H. Ogata, O. Rüdiger, E. Reijerse, Hydrogenases, Chemical Reviews, 114 (2014) 4081-4148.

[105] P.E.M. Siegbahn, J.W. Tye, M.B. Hall, Computational Studies of [NiFe] and [FeFe] Hydrogenases, Chemical Reviews, 107 (2007) 4414-4435.

[106] H.S. Shafaat, O. Rüdiger, H. Ogata, W. Lubitz, [NiFe] hydrogenases: A common active site for hydrogen metabolism under diverse conditions, Biochimica et Biophysica Acta (BBA) - Bioenergetics, 1827 (2013) 986-1002.

[107] M. Bruschi, M. Tiberti, A. Guerra, L. De Gioia, Disclosure of Key Stereoelectronic Factors for Efficient H2 Binding and Cleavage in the Active Site of [NiFe]-Hydrogenases, Journal of the American Chemical Society, 136 (2014) 1803-1814.

[108] H. Wu, M.B. Hall, Density functional theory on the larger active site models for [NiFe] hydrogenases: Two-state reactivity?, Comptes Rendus Chimie, 11 (2008) 790-804.

[109] C. Fan, M. Teixeira, J. Moura, I. Moura, H. Huynh Boi, J. Le Gall, H.D. Peck, B.M. Hoffman, Detection and characterization of exchangeable protons bound to the hydrogen-activation nickel site of Desulfovibrio gigas hydrogenase: a proton and deuterium Q-band ENDOR study, Journal of the American Chemical Society, 113 (1991) 20-24.

[110] J.M. Keith, M.B. Hall, Potential Hydrogen Bottleneck in Nickel−Iron Hydrogenase, Inorganic Chemistry, 49 (2010) 6378-6380.

[111] S. Foerster, M. Gastel, M. Brecht, W. Lubitz, An orientation-selected ENDOR and HYSCORE study of the Ni-C active state of Desulfovibrio vulgaris Miyazaki F hydrogenase, JBIC Journal of Biological Inorganic Chemistry, 10 (2005) 51-62.

[112] M. Kampa, W. Lubitz, M. van Gastel, F. Neese, Computational study of the electronic structure and magnetic properties of the Ni–C state in [NiFe] hydrogenases including the second coordination sphere, JBIC Journal of Biological Inorganic Chemistry, 17 (2012) 1269-1281.

[113] J.W. Peters, W.N. Lanzilotta, B.J. Lemon, L.C. Seefeldt, X-ray Crystal Structure of the Fe-Only Hydrogenase (CpI) from Clostridium pasteurianum to 1.8 Angstrom Resolution, Science, 282 (1998) 1853-1858.

[114] Y. Nicolet, C. Piras, P. Legrand, C.E. Hatchikian, J.C. Fontecilla-Camps, Desulfovibrio desulfuricans Iron Hydrogenase: The Structure Shows Unusual Coordination to an Active Site Fe Binuclear Center, Struct. Fold. Des., 7 (1999) 13-23.

[115] A. Silakov, E.J. Reijerse, S.P.J. Albracht, E.C. Hatchikian, W. Lubitz, The Electronic Structure of the H-Cluster in the [FeFe]-Hydrogenase from Desulfovibrio desulfuricans: A Q-band 57Fe-ENDOR and HYSCORE Study, Journal of the American Chemical Society, 129 (2007) 11447-11458.

[116] A.S. Pereira, P. Tavares, I. Moura, J.J.G. Moura, B.H. Huynh, Mössbauer Characterization of the Iron−Sulfur Clusters in Desulfovibrio vulgaris Hydrogenase, Journal of the American Chemical Society, 123 (2001) 2771-2782.

[117] C.V. Popescu, E. Münck, Electronic Structure of the H Cluster in [Fe]-Hydrogenases, Journal of the American Chemical Society, 121 (1999) 7877-7884.

[118] C. Greco, M. Bruschi, J. Heimdal, P. Fantucci, L. De Gioia, U. Ryde, Structural Insights into the Active-Ready Form of [FeFe]-Hydrogenase and Mechanistic Details of Its Inhibition by Carbon Monoxide, Inorganic Chemistry, 46 (2007) 7256-7258.

[119] D.E. Schwab, C. Tard, E. Brecht, J.W. Peters, C.J. Pickett, R.K. Szilagyi, On the electronic structure of the hydrogenase H-cluster, Chemical communications, (2006) 3696-3698.

[120] A.T. Fiedler, T.C. Brunold, Computational Studies of the H-Cluster of Fe-Only Hydrogenases: Geometric, Electronic, and Magnetic Properties and Their Dependence on the [Fe4S4] Cubane, Inorganic Chemistry, 44 (2005) 9322-9334.

[121] Y. Nicolet, B.J. Lemon, J.C. Fontecilla-Camps, J.W. Peters, A novel FeS cluster in Fe-only hydrogenases, Trends in biochemical sciences, 25 (2000) 138-143.

[122] G.J. Kubas, Fundamentals of H_2 binding and reactivity on transition metals underlying hydrogenase function and H_2 production and storage, Chem. Rev., 107 (2007) 4152-4205.

[123] A.J. Pierik, M. Hulstein, W.R. Hagen, S.P.J. Albracht, A low-spin iron with CN and CO as intrinsic ligands forms the core of the active site in [Fe]-hydrogenases, Eur. J. Biochem., 258 (1998) 572-578.

[124] M. Bruschi, C. Greco, L. Bertini, P. Fantucci, U. Ryde, L.D. Gioia, Functionally Relevant Interplay between the Fe4S4 Cluster and CN− Ligands in the Active Site of [FeFe]-Hydrogenases, Journal of the American Chemical Society, 132 (2010) 4992-4993.

[125] G. Berggren, A. Adamska, C. Lambertz, T. Simmons, J. Esselborn, M. Atta, S. Gambarelli, J.-M. Mouesca, E. Reijerse, W. Lubitz, Biomimetic assembly and activation of [FeFe]-hydrogenases, Nature, 499 (2013) 66-69.

[126] J. Esselborn, C. Lambertz, A. Adamska-Venkatesh, T. Simmons, G. Berggren, J. Noth, J. Siebel, A. Hemschemeier, V. Artero, E. Reijerse, Spontaneous activation of [FeFe]-hydrogenases by an inorganic [2Fe] active site mimic, Nature chemical biology, 9 (2013) 607-609.

[127] Y. Nicolet, A.L. de Lacey, X. Vernède, V.M. Fernandez, E.C. Hatchikian, J.C. Fontecilla-Camps, Crystallographic and FTIR Spectroscopic Evidence of Changes in Fe Coordination Upon Reduction of the Active Site of the Fe-Only Hydrogenase from Desulfovibrio desulfuricans, Journal of the American Chemical Society, 123 (2001) 1596-1601.

[128] H.-J. Fan, M.B. Hall, A Capable Bridging Ligand for Fe-Only Hydrogenase: Density Functional Calculations of a Low-Energy Route for Heterolytic Cleavage and Formation of Dihydrogen, Journal of the American Chemical Society, 123 (2001) 3828-3829.

[129] David W. Mulder, Eric M. Shepard, Jonathan E. Meuser, N. Joshi, Paul W. King, Matthew C. Posewitz, Joan B. Broderick, John W. Peters, Insights into [FeFe]-Hydrogenase Structure, Mechanism, and Maturation, Structure, 19 (2011) 1038-1052.

[130] L.J. Giles, A. Grigoropoulos, R.K. Szilagyi, Electron and Spin Density Topology of the H-Cluster and Its Biomimetic Complexes, European Journal of Inorganic Chemistry, 2011 (2011) 2677-2690.

[131] T. Miyake, M. Bruschi, U. Cosentino, C. Baffert, V. Fourmond, C. Léger, G. Moro, L. De Gioia, C. Greco, Does the environment around the H-cluster allow coordination of the pendant amine to the catalytic iron center in [FeFe] hydrogenases? Answers from theory, JBIC Journal of Biological Inorganic Chemistry, 18 (2013) 693-700.

[132] M. Bruschi, C. Greco, M. Kaukonen, P. Fantucci, U. Ryde, L. De Gioia, Influence of the [2Fe] H subcluster environment on the properties of key intermediates in the catalytic cycle of [FeFe] hydrogenases: hints for the rational design of synthetic catalysts, Angewandte Chemie International Edition, 48 (2009) 3503-3506.

[133] M. Winkler, J. Esselborn, T. Happe, Molecular basis of [FeFe]-hydrogenase function: An insight into the complex interplay between protein and catalytic cofactor, Biochimica et Biophysica Acta (BBA)-Bioenergetics, 1827 (2013) 974-985.

[134] S. Trohalaki, R. Pachter, Mechanism of hydrogen production in [Fe–Fe]-hydrogenases: A quantum mechanics/molecular mechanics study, International Journal of Hydrogen Energy, 35 (2010) 5318-5331.

[135] B.J. Lemon, J.W. Peters, Photochemistry at the Active Site of the Carbon Monoxide Inhibited Form of the Iron-Only Hydrogenase (CpI), Journal of the American Chemical Society, 122 (2000) 3793-3794.

[136] Z. Cao, M.B. Hall, Modeling the Active Sites in Metalloenzymes. 3. Density Functional Calculations on Models for [Fe]-Hydrogenase: Structures and Vibrational Frequencies of the Observed Redox Forms and the Reaction Mechanism at the Diiron Active Center, Journal of the American Chemical Society, 123 (2001) 3734-3742.

[137] Z.J. Chen, B.J. Lemon, S. Huang, D.J. Swartz, J.W. Peters, K.A. Bagley, Infrared studies of the CO-inhibited form of the Fe-only hydrogenase from Clostridium pasteurianum I: Examination of its light sensitivity at cryogenic temperatures, Biochemistry, 41 (2002) 2036-2043.

[138] C. Greco, M. Bruschi, P. Fantucci, U. Ryde, L. De Gioia, Mechanistic and Physiological Implications of the Interplay among Iron–Sulfur Clusters in [FeFe]-Hydrogenases. A QM/MM Perspective, Journal of the American Chemical Society, 133 (2011) 18742-18749.

[139] D.W. Mulder, M.W. Ratzloff, E.M. Shepard, A.S. Byer, S.M. Noone, J.W. Peters, J.B. Broderick, P.W. King, EPR and FTIR Analysis of the Mechanism of H2 Activation by [FeFe]-Hydrogenase HydA1 from Chlamydomonas reinhardtii, J. Am. Chem. Soc., 135 (2013) 6921-6929.

[140] W. Roseboom, A.L. De Lacey, V.M. Fernandez, E.C. Hatchikian, S.P.J. Albracht, The active site of the [FeFe]-hydrogenase from Desulfovibrio desulfuricans. II. Redox properties, light sensitivity and CO-ligand exchange as observed by infrared spectroscopy, J. Biol. Inorg. Chem., 11 (2006) 102-118.

[141] A. Adamska, A. Silakov, C. Lambertz, O. Rudiger, T. Happe, E. Reijerse, W. Lubitz, Identification and Characterization of the "Super-Reduced" State of the H-Cluster in [FeFe]

Hydrogenase: A New Building Block for the Catalytic Cycle?, Angew. Chem. Int. Ed., 51 (2012) 11458-11462.

[142] J.C. Fontecilla-Camps, P. Amara, C. Cavazza, Y. Nicolet, A. Volbeda, Structure–function relationships of anaerobic gas-processing metalloenzymes, Nature, 460 (2009) 814-822.

[143] A. Adamska, A. Silakov, C. Lambertz, O. Rüdiger, T. Happe, E. Reijerse, W. Lubitz, Identification and Characterization of the "Super-Reduced" State of the H-Cluster in [FeFe] Hydrogenase: A New Building Block for the Catalytic Cycle?, Angew. Chem. Int. Edit., 51 (2012) 11458-11462.

[144] A. Adamska-Venkatesh, D. Krawietz, J. Siebel, K. Weber, T. Happe, E. Reijerse, W. Lubitz, New Redox States Observed in [FeFe] Hydrogenases Reveal Redox Coupling Within the H-Cluster, Journal of the American Chemical Society, 10.1021/ja503390c (2014).

[145] A. Silakov, C. Kamp, E. Reijerse, T. Happe, W. Lubitz, Spectroelectrochemical Characterization of the Active Site of the [FeFe] Hydrogenase HydA1 from Chlamydomonas reinhardtii, Biochemistry, 48 (2009) 7780-7786.

[146] A. Silakov, C. Kamp, E. Reijerse, T. Happe, W. Lubitz, Spectroelectrochemical characterization of the active site of the [FeFe] hydrogenase HydA1 from Chlamydomonas reinhardtii, Biochemistry, 48 (2009) 7780-7786.

[147] D.W. Mulder, M.W. Ratzloff, E.M. Shepard, A.S. Byer, S.M. Noone, J.W. Peters, J.B. Broderick, P.W. King, EPR and FTIR Analysis of the Mechanism of H2 Activation by [FeFe]-Hydrogenase HydA1 from Chlamydomonas reinhardtii, Journal of the American Chemical Society, 135 (2013) 6921-6929.

[148] C. Lambertz, P. Chernev, K. Klingan, N. Leidel, K.G. Sigfridsson, T. Happe, M. Haumann, Electronic and molecular structures of the active-site H-cluster in [FeFe]-hydrogenase determined by site-selective X-ray spectroscopy and quantum chemical calculations, Chemical Science, (2014).

[149] W. Lubitz, E. Reijerse, M. van Gastel, [NiFe] and [FeFe] hydrogenases studied by advanced magnetic resonance techniques, Chem. Rev., 107 (2007) 4331-4365.

[150] A.J. Pierik, W.R. Hagen, J.S. Redeker, R.B. Wolbert, M. Boersma, M.F. Verhagen, H.J. Grande, C. Veeger, P.H. Mutsaers, R.H. Sands, W.R. Dunham, Redox properties of the iron-sulfur clusters in activated Fe-hydrogenase from Desulfovibrio vulgaris (Hildenborough), Eur. J. Biochem., 209 (1992) 63-72.

[151] C.V. Popescu, E. Münck, Electronic structure of the H cluster in [Fe]-hydrogenases, J. Am. Chem. Soc., 121 (1999) 7877-7884.

[152] D.S. Patil, J.J.G. Moura, S.H. He, M. Teixeira, B.C. Prickril, D.V. Dervartanian, H.D. Peck, J. Legall, B.H. Huynh, EPR-Detecable Redox Centers of the Periplasmic Hydrogenase from Desulfovibrio vulgaris, J. Biol. Chem., 263 (1988) 18732-18738.

[153] A.S. Pereira, P. Tavares, I. Moura, J.J.G. Moura, B.H. Huynh, Mössbauer characterization of the iron−sulfur clusters in Desulfovibrio vulgaris Hydrogenase, J. Am. Chem. Soc., 123 (2001) 2771-2782.

[154] V. Hajj, C. Baffert, K. Sybirna, I. Meynial-Salles, P. Soucaille, H. Bottin, V. Fourmond, C. Leger, FeFe hydrogenase reductive inactivation and implication for catalysis, Energy & Environmental Science, 7 (2014) 715-719.

[155] C. Baffert, K. Sybirna, P. Ezanno, T. Lautier, V. Hajj, I. Meynial-Salles, P. Soucaille, H. Bottin, C. Léger, Covalent Attachment of FeFe Hydrogenases to Carbon Electrodes for Direct Electron Transfer, Analytical Chemistry, 84 (2012) 7999-8005.

[156] A. Parkin, C. Cavazza, J.C. Fontecilla-Camps, F.A. Armstrong, Electrochemical Investigations of the Interconversions between Catalytic and Inhibited States of the [FeFe]-Hydrogenase from Desulfovibrio desulfuricans, Journal of the American Chemical Society, 128 (2006) 16808-16815.

[157] W.K. Myers, T.A. Stich, D.L.M. Suess, J.M. Kuchenreuther, J.R. Swartz, R.D. Britt, The Cyanide Ligands of [FeFe] Hydrogenase: Pulse EPR Studies of 13C and 15N-Labeled H-Cluster, Journal of the American Chemical Society, 10.1021/ja507046w (2014).

[158] J.M. Camara, T.B. Rauchfuss, Combining acid–base, redox and substrate binding functionalities to give a complete model for the [FeFe]-hydrogenase, Nat Chem, 4 (2012) 26-30.

[159] M.W. Adams, L.E. Mortenson, J.-S. Chen, Hydrogenase, Biochimica et Biophysica Acta (BBA)-Reviews on Bioenergetics, 594 (1980) 105-176.

[160] C.L. McIntosh, F. Germer, R. Schulz, J. Appel, A.K. Jones, The [NiFe]-Hydrogenase of the Cyanobacterium Synechocystis sp. PCC 6803 Works Bidirectionally with a Bias to H2 Production, Journal of the American Chemical Society, 133 (2011) 11308-11319.

[161] M.W. Adams, L.E. Mortenson, The physical and catalytic properties of hydrogenase II of Clostridium pasteurianum. A comparison with hydrogenase I, Journal of Biological Chemistry, 259 (1984) 7045-7055.

[162] S.V. Hexter, F. Grey, T. Happe, V. Climent, F.A. Armstrong, Electrocatalytic mechanism of reversible hydrogen cycling by enzymes and distinctions between the major classes of hydrogenases, Proceedings of the National Academy of Sciences, 109 (2012) 11516-11521.

[163] K. Vincent, A. Parkin, O. Lenz, S. Albracht, J. Fontecilla-Camps, R. Cammack, B. Friedrich, F. Armstrong, Electrochemical definitions of O-2 sensitivity and oxidative inactivation in hydrogenases, J. Am. Chem. Soc., 127 (2005) 18179-18189.

[164] M. Adams, E. Eccleston, J.B. Howard, Iron-sulfur clusters of hydrogenase I and hydrogenase II of Clostridium pasteurianum, Proceedings of the National Academy of Sciences, 86 (1989) 4932.

[165] A. Abou Hamdan, S. Dementin, P.-P. Liebgott, O. Gutierrez-Sanz, P. Richaud, A.L. De Lacey, M. Rousset, P. Bertrand, L. Cournac, C. Léger, Understanding and Tuning the Catalytic Bias of Hydrogenase, Journal of the American Chemical Society, 134 (2012) 8368-8371.

[166] M.Y. Darensbourg, E.J. Lyon, X. Zhao, I.P. Georgakaki, The organometallic active site of [Fe]hydrogenase: Models and entatic states, Proceedings of the National Academy of Sciences, 100 (2003) 3683-3688.

[167] C. Tard, C.J. Pickett, Structural and Functional Analogues of the Active Sites of the [Fe]-, [NiFe]-, and [FeFe]-Hydrogenases†, Chemical Reviews, 109 (2009) 2245-2274.

[168] D.L. DuBois, Development of Molecular Electrocatalysts for Energy Storage, Inorganic Chemistry, 53 (2014) 3935-3960.

[169] T. Maier, U. Binder, A. Bock, Analysis of the hydA locus of Escherichia coli: two genes (hydN and hypF) involved in formate and hydrogen metabolism, Arch Microbiol, 165 (1996) 333-341.

[170] A. Jacobi, R. Rossmann, A. Bock, The hyp operon gene products are required for the maturation of catalytically active hydrogenase isoenzymes in Escherichia coli, Arch Microbiol, 158 (1992) 444-451.

[171] S. Lutz, A. Jacobi, V. Schlensog, R. Bohm, G. Sawers, A. Bock, Molecular characterization of an operon (hyp) necessary for the activity of the three hydrogenase isoenzymes in Escherichia coli, Mol Microbiol, 5 (1991) 123-135.

[172] S. Reissmann, E. Hochleitner, H. Wang, A. Paschos, F. Lottspeich, R.S. Glass, A. Bock, Taming of a poison: biosynthesis of the NiFe-hydrogenase cyanide ligands, Science, 299 (2003) 1067-1070.

[173] M. Blokesch, A. Paschos, A. Bauer, S. Reissmann, N. Drapal, A. Bock, Analysis of the transcarbamoylation-dehydration reaction catalyzed by the hydrogenase maturation proteins HypF and HypE, Eur J Biochem, 271 (2004) 3428-3436.

[174] Y. Shomura, Y. Higuchi, Structural basis for the reaction mechanism of S-carbamoylation of HypE by HypF in the maturation of [NiFe]-hydrogenases, J Biol Chem, 287 (2012) 28409-28419.

[175] S. Petkun, R. Shi, Y. Li, A. Asinas, C. Munger, L. Zhang, M. Waclawek, B. Soboh, R.G. Sawers, M. Cygler, Structure of hydrogenase maturation protein HypF with reaction intermediates shows two active sites, Structure, 19 (2011) 1773-1783.

[176] A. Hecker, N. Leulliot, D. Gadelle, M. Graille, A. Justome, P. Dorlet, C. Brochier, S. Quevillon-Cheruel, E. Le Cam, H. van Tilbeurgh, P. Forterre, An archaeal orthologue of the universal protein Kae1 is an iron metalloprotein which exhibits atypical DNA-binding properties and apurinic-endonuclease activity in vitro, Nucleic Acids Res, 35 (2007) 6042-6051.

[177] A. Hecker, R. Lopreiato, M. Graille, B. Collinet, P. Forterre, D. Libri, H. van Tilbeurgh, Structure of the archaeal Kae1/Bud32 fusion protein MJ1130: a model for the eukaryotic EKC/KEOPS subcomplex, EMBO J, 27 (2008) 2340-2351.

[178] C. Parthier, S. Gorlich, F. Jaenecke, C. Breithaupt, U. Brauer, U. Fandrich, D. Clausnitzer, U.F. Wehmeier, C. Bottcher, D. Scheel, M.T. Stubbs, The O-carbamoyltransferase TobZ catalyzes an ancient enzymatic reaction, Angew Chem Int Ed Engl, 51 (2012) 4046-4052.

[179] C. Li, T.J. Kappock, J. Stubbe, T.M. Weaver, S.E. Ealick, X-ray crystal structure of aminoimidazole ribonucleotide synthetase (PurM), from the Escherichia coli purine biosynthetic pathway at 2.5 A resolution, Structure, 7 (1999) 1155-1166.

[180] R. Anand, A.A. Hoskins, J. Stubbe, S.E. Ealick, Domain organization of Salmonella typhimurium formylglycinamide ribonucleotide amidotransferase revealed by X-ray crystallography, Biochemistry, 43 (2004) 10328-10342.

[181] E.S. Rangarajan, A. Asinas, A. Proteau, C. Munger, J. Baardsnes, P. Iannuzzi, A. Matte, M. Cygler, Structure of [NiFe] hydrogenase maturation protein HypE from Escherichia coli and its interaction with HypF, J Bacteriol, 190 (2008) 1447-1458.

[182] T. Tominaga, S. Watanabe, R. Matsumi, H. Atomi, T. Imanaka, K. Miki, Crystal structures of the carbamoylated and cyanated forms of HypE for [NiFe] hydrogenase maturation, Proc Natl Acad Sci U S A, 110 (2013) 20485-20490.

[183] B. Soboh, R.G. Sawers, [NiFe]-Hydrogenase Cofactor Assembly, in: V. Culotta, R.A. Scott (Eds.) Encylopedia of Inorganic and Bioinorganic Chemistry, John Wiley & Sons, Chichester, U.K., 2013, pp. 1-9.

[184] N. Drapal, A. Bock, Interaction of the hydrogenase accessory protein HypC with HycE, the large subunit of Escherichia coli hydrogenase 3 during enzyme maturation, Biochemistry, 37 (1998) 2941-2948.

[185] M. Blokesch, A. Bock, Maturation of [NiFe]-hydrogenases in Escherichia coli: the HypC cycle, J Mol Biol, 324 (2002) 287-296.

[186] M. Blokesch, S.P. Albracht, B.F. Matzanke, N.M. Drapal, A. Jacobi, A. Bock, The complex between hydrogenase-maturation proteins HypC and HypD is an intermediate in the supply of cyanide to the active site iron of [NiFe]-hydrogenases, J Mol Biol, 344 (2004) 155-167.

[187] B. Soboh, S.T. Stripp, E. Muhr, C. Granich, M. Braussemann, M. Herzberg, J. Heberle, R. Gary Sawers, [NiFe]-hydrogenase maturation: isolation of a HypC-HypD complex carrying diatomic CO and CN- ligands, FEBS Lett, 586 (2012) 3882-3887.

[188] S. Watanabe, R. Matsumi, H. Atomi, T. Imanaka, K. Miki, Crystal structures of the HypCD complex and the HypCDE ternary complex: transient intermediate complexes during [NiFe] hydrogenase maturation, Structure, 20 (2012) 2124-2137.

[189] I. Burstel, E. Siebert, G. Winter, P. Hummel, I. Zebger, B. Friedrich, O. Lenz, A universal scaffold for synthesis of the Fe(CN)2(CO) moiety of [NiFe] hydrogenase, J Biol Chem, 287 (2012) 38845-38853.

[190] L. Wang, B. Xia, C. Jin, Solution structure of Escherichia coli HypC, Biochem Biophys Res Commun, 361 (2007) 665-669.

[191] S. Watanabe, R. Matsumi, T. Arai, H. Atomi, T. Imanaka, K. Miki, Crystal structures of [NiFe] hydrogenase maturation proteins HypC, HypD, and HypE: insights into cyanation reaction by thiol redox signaling, Mol Cell, 27 (2007) 29-40.

[192] M. Blokesch, A. Bock, Properties of the [NiFe]-hydrogenase maturation protein HypD, FEBS Lett, 580 (2006) 4065-4068.

[193] S. Watanabe, D. Sasaki, T. Tominaga, K. Miki, Structural basis of [NiFe] hydrogenase maturation by Hyp proteins, Biol Chem, 393 (2012) 1089-1100.

[194] S.T. Stripp, B. Soboh, U. Lindenstrauss, M. Braussemann, M. Herzberg, D.H. Nies, R.G. Sawers, J. Heberle, HypD Is the Scaffold Protein for Fe-(CN)2CO Cofactor Assembly in [NiFe]-Hydrogenase Maturation, Biochemistry, 52 (2013) 3289-3296.

[195] B. Soboh, S.T. Stripp, C. Bielak, U. Lindenstrauss, M. Braussemann, M. Javaid, M. Hallensleben, C. Granich, M. Herzberg, J. Heberle, R.G. Sawers, The [NiFe]-hydrogenase accessory chaperones HypC and HybG of Escherichia coli are iron- and carbon dioxide-binding proteins, FEBS Lett, 587 (2013) 2512-2516.

[196] W. Roseboom, M. Blokesch, A. Bock, S.P. Albracht, The biosynthetic routes for carbon monoxide and cyanide in the Ni-Fe active site of hydrogenases are different, FEBS Lett, 579 (2005) 469-472.

[197] R. Waugh, D.H. Boxer, Pleiotropic hydrogenase mutants of Escherichia coli K12: growth in the presence of nickel can restore hydrogenase activity, Biochimie, 68 (1986) 157-166.

[198] J.W. Olson, N.S. Mehta, R.J. Maier, Requirement of nickel metabolism proteins HypA and HypB for full activity of both hydrogenase and urease in Helicobacter pylori, Mol Microbiol, 39 (2001) 176-182.

[199] L. Forzi, R.G. Sawers, Maturation of [NiFe]-hydrogenases in Escherichia coli, Biometals, 20 (2007) 565-578.

[200] S. Watanabe, T. Arai, R. Matsumi, H. Atomi, T. Imanaka, K. Miki, Crystal structure of HypA, a nickel-binding metallochaperone for [NiFe] hydrogenase maturation, J Mol Biol, 394 (2009) 448-459.

[201] N. Mehta, J.W. Olson, R.J. Maier, Characterization of Helicobacter pylori nickel metabolism accessory proteins needed for maturation of both urease and hydrogenase, J Bacteriol, 185 (2003) 726-734.

[202] M. Blokesch, M. Rohrmoser, S. Rode, A. Bock, HybF, a zinc-containing protein involved in NiFe hydrogenase maturation, J Bacteriol, 186 (2004) 2603-2611.

[203] T. Maier, F. Lottspeich, A. Bock, GTP hydrolysis by HypB is essential for nickel insertion into hydrogenases of Escherichia coli, Eur J Biochem, 230 (1995) 133-138.

[204] N. Mehta, S. Benoit, R.J. Maier, Roles of conserved nucleotide-binding domains in accessory proteins, HypB and UreG, in the maturation of nickel-enzymes required for efficient Helicobacter pylori colonization, Microb Pathog, 35 (2003) 229-234.

[205] M.R. Leach, S. Sandal, H. Sun, D.B. Zamble, Metal binding activity of the Escherichia coli hydrogenase maturation factor HypB, Biochemistry, 44 (2005) 12229-12238.

[206] R. Gasper, A. Scrima, A. Wittinghofer, Structural insights into HypB, a GTP-binding protein that regulates metal binding, J.Biol.Chem., 281 (2006) 27492-27502.

[207] H. Kaluarachchi, K.C. Chan Chung, D.B. Zamble, Microbial nickel proteins, Nat Prod Rep, 27 (2010) 681-694.

[208] A.M. Sydor, J. Liu, D.B. Zamble, Effects of metal on the biochemical properties of Helicobacter pylori HypB, a maturation factor of [NiFe]-hydrogenase and urease, J Bacteriol, 193 (2011) 1359-1368.

[209] A.M. Sydor, H. Lebrette, R. Ariyakumaran, C. Cavazza, D.B. Zamble, Relationship between Ni(II) and Zn(II) coordination and nucleotide binding by the Helicobacter pylori [NiFe]-hydrogenase and urease maturation factor HypB, J Biol Chem, 289 (2014) 3828-3841.

[210] F. Cai, T.T. Ngu, H. Kaluarachchi, D.B. Zamble, Relationship between the GTPase, metal-binding, and dimerization activities of E. coli HypB, J Biol Inorg Chem, 16 (2011) 857-868.

[211] K.C. Chan Chung, D.B. Zamble, Protein interactions and localization of the Escherichia coli accessory protein HypA during nickel insertion to [NiFe] hydrogenase, J Biol Chem, 286 (2011) 43081-43090.

[212] W. Xia, H. Li, X. Yang, K.B. Wong, H. Sun, Metallo-GTPase HypB from Helicobacter pylori and its interaction with nickel chaperone protein HypA, J Biol Chem, 287 (2012) 6753-6763.

[213] M.R. Leach, J.W. Zhang, D.B. Zamble, The role of complex formation between the Escherichia coli hydrogenase accessory factors HypB and SlyD, J.Biol.Chem., 282 (2007) 16177-16186.

[214] K. Stingl, K. Schauer, C. Ecobichon, A. Labigne, P. Lenormand, J.C. Rousselle, A. Namane, H. de Reuse, In vivo interactome of Helicobacter pylori urease revealed by tandem affinity purification, Mol Cell Proteomics, 7 (2008) 2429-2441.

[215] J.W. Zhang, G. Butland, J.F. Greenblatt, A. Emili, D.B. Zamble, A role for SlyD in the Escherichia coli hydrogenase biosynthetic pathway, J Biol Chem, 280 (2005) 4360-4366.

[216] T. Cheng, H. Li, X. Yang, W. Xia, H. Sun, Interaction of SlyD with HypB of Helicobacter pylori facilitates nickel trafficking, Metallomics, 5 (2013) 804-807.

[217] C.D. Douglas, T.T. Ngu, H. Kaluarachchi, D.B. Zamble, Metal transfer within the Escherichia coli HypB-HypA complex of hydrogenase accessory proteins, Biochemistry, 52 (2013) 6030-6039.

[218] H. Kaluarachchi, J.W. Zhang, D.B. Zamble, Escherichia coli SlyD, more than a Ni(II) reservoir, Biochemistry, 50 (2011) 10761-10763.

[219] E. Theodoratou, R. Huber, A. Bock, [NiFe]-Hydrogenase maturation endopeptidase: structure and function, Biochem Soc Trans, 33 (2005) 108-111.

[220] R. Rossmann, T. Maier, F. Lottspeich, A. Bock, Characterisation of a protease from Escherichia coli involved in hydrogenase maturation, Eur J Biochem, 227 (1995) 545-550.

[221] D.J. Gollin, L.E. Mortenson, R.L. Robson, Carboxyl-terminal processing may be essential for production of active NiFe hydrogenase in Azotobacter vinelandii, FEBS Lett, 309 (1992) 371-375.

[222] O. Sorgenfrei, D. Linder, M. Karas, A. Klein, A novel very small subunit of a selenium containing [NiFe] hydrogenase of Methanococcus voltae is postranslationally processed by cleavage at a defined position, Eur J Biochem, 213 (1993) 1355-1358.

[223] N.K. Menon, J. Robbins, M. Der Vartanian, D. Patil, H.D. Peck, Jr., A.L. Menon, R.L. Robson, A.E. Przybyla, Carboxy-terminal processing of the large subunit of [NiFe] hydrogenases, FEBS Lett, 331 (1993) 91-95.

[224] R. Rossmann, M. Sauter, F. Lottspeich, A. Bock, Maturation of the large subunit (HYCE) of Escherichia coli hydrogenase 3 requires nickel incorporation followed by C-terminal processing at Arg537, Eur J Biochem, 220 (1994) 377-384.

[225] E. Theodoratou, A. Paschos, A. Magalon, E. Fritsche, R. Huber, A. Bock, Nickel serves as a substrate recognition motif for the endopeptidase involved in hydrogenase maturation, Eur J Biochem, 267 (2000) 1995-1999.

[226] T. Kumarevel, T. Tanaka, Y. Bessho, A. Shinkai, S. Yokoyama, Crystal structure of hydrogenase maturating endopeptidase HycI from Escherichia coli, Biochem Biophys Res Commun, 389 (2009) 310-314.

[227] P.W. King, M.C. Posewitz, M.L. Ghirardi, M. Seibert, Functional studies of [FeFe] hydrogenase maturation in an Escherichia coli biosynthetic system, J.Bacteriol., 188 (2006) 2163-2172.

[228] J.K. Rubach, X. Brazzolotto, J. Gaillard, M. Fontecave, Biochemical characterization of the HydE and HydG iron-only hydrogenase maturation enzymes from Thermatoga maritima, FEBS Lett., 579 (2005) 5055-5060.

[229] X. Brazzolotto, J.K. Rubach, J. Gaillard, S. Gambarelli, M. Atta, M. Fontecave, The [Fe-Fe]-hydrogenase maturation protein HydF from Thermotoga maritima is a GTPase with an iron-sulfur cluster, J.Biol.Chem., 281 (2006) 769-774.

[230] D.W. Mulder, D.O. Ortillo, D.J. Gardenghi, A.V. Naumov, S.S. Ruebush, R.K. Szilagyi, B. Huynh, J.B. Broderick, J.W. Peters, Activation of HydA(DeltaEFG) requires a preformed [4Fe-4S] cluster, Biochemistry, 48 (2009) 6240-6248.

[231] D.W. Mulder, E.S. Boyd, R. Sarma, R.K. Lange, J.A. Endrizzi, J.B. Broderick, J.W. Peters, Stepwise [FeFe]-hydrogenase H-cluster assembly revealed in the structure of HydA(DeltaEFG), Nature, 465 (2010) 248-251.

[232] J.M. Kuchenreuther, Y. Guo, H. Wang, W.K. Myers, S.J. George, C.A. Boyke, Y. Yoda, E.E. Alp, J. Zhao, R.D. Britt, J.R. Swartz, S.P. Cramer, Nuclear resonance vibrational spectroscopy and electron paramagnetic resonance spectroscopy of 57Fe-enriched [FeFe] hydrogenase indicate stepwise assembly of the H-cluster, Biochemistry, 52 (2013) 818-826.

[233] D.W. Mulder, E.M. Shepard, J.E. Meuser, N. Joshi, P.W. King, M.C. Posewitz, J.B. Broderick, J.W. Peters, Insights into [FeFe]-hydrogenase structure, mechanism, and maturation, Structure, 19 (2011) 1038-1052.

[234] E.M. Shepard, S.E. McGlynn, A.L. Bueling, C.S. Grady-Smith, S.J. George, M.A. Winslow, S.P. Cramer, J.W. Peters, J.B. Broderick, Synthesis of the 2Fe subcluster of the [FeFe]-hydrogenase H cluster on the HydF scaffold, Proc Natl Acad Sci U S A, 107 (2010) 10448-10453.

[235] L. Cendron, P. Berto, S. D'Adamo, F. Vallese, C. Govoni, M.C. Posewitz, G.M. Giacometti, P. Costantini, G. Zanotti, Crystal structure of HydF scaffold protein provides insights into [FeFe]-hydrogenase maturation, J Biol Chem, 286 (2011) 43944-43950.

[236] S.E. McGlynn, E.M. Shepard, M.A. Winslow, A.V. Naumov, K.S. Duschene, M.C. Posewitz, W.E. Broderick, J.B. Broderick, J.W. Peters, HydF as a scaffold protein in [FeFe] hydrogenase H-cluster biosynthesis, FEBS Lett., 582 (2008) 2183-2187.

[237] I. Czech, A. Silakov, W. Lubitz, T. Happe, The [FeFe]-hydrogenase maturase HydF from Clostridium acetobutylicum contains a CO and CN- ligated iron cofactor, FEBS Lett, 584 (2010) 638-642.

[238] I. Czech, S. Stripp, O. Sanganas, N. Leidel, T. Happe, M. Haumann, The [FeFe]-hydrogenase maturation protein HydF contains a H-cluster like [4Fe4S]-2Fe site, FEBS Lett, (2011).

[239] N. Joshi, E.M. Shepard, A.S. Byer, K.D. Swanson, J.B. Broderick, J.W. Peters, Iron-sulfur cluster coordination in the [FeFe]-hydrogenase H cluster biosynthetic factor HydF, FEBS Lett, 586 (2012) 3939-3943.

[240] J.M. Kuchenreuther, R.D. Britt, J.R. Swartz, New insights into [FeFe] hydrogenase activation and maturase function, PLoS One, 7 (2012) e45850.

[241] P. Berto, M. Di Valentin, L. Cendron, F. Vallese, M. Albertini, E. Salvadori, G.M. Giacometti, D. Carbonera, P. Costantini, The [4Fe-4S]-cluster coordination of [FeFe]-hydrogenase maturation protein HydF as revealed by EPR and HYSCORE spectroscopies, Biochim Biophys Acta, 1817 (2012) 2149-2157.

[242] M. Albertini, F. Vallese, M. Di Valentin, P. Berto, G.M. Giacometti, P. Costantini, D. Carbonera, The proton iron-sulfur cluster environment of the [FeFe]-hydrogenase maturation protein HydF from Thermotoga neapolitana, International Journal of Hydrogen Energy, (2014).

[243] G. Berggren, R. Garcia-Serres, X. Brazzolotto, M. Clemancey, S. Gambarelli, M. Atta, J.M. Latour, H.L. Hernandez, S. Subramanian, M.K. Johnson, M. Fontecave, An EPR/HYSCORE, Mossbauer, and resonance Raman study of the hydrogenase maturation enzyme HydF: a model for N-coordination to [4Fe-4S] clusters, J Biol Inorg Chem, 19 (2014) 75-84.

[244] E.M. Shepard, F. Mus, J.N. Betz, A.S. Byer, B.R. Duffus, J.W. Peters, J.B. Broderick, [FeFe]-Hydrogenase Maturation, Biochemistry, 53 (2014) 4090-4104.

[245] F. Vallese, P. Berto, M. Ruzzene, L. Cendron, S. Sarno, E. De Rosa, G.M. Giacometti, P. Costantini, Biochemical analysis of the interactions between the proteins involved in the [FeFe]-hydrogenase maturation process, J Biol Chem, 287 (2012) 36544-36555.

[246] G. Berggren, A. Adamska, C. Lambertz, T.R. Simmons, J. Esselborn, M. Atta, S. Gambarelli, J.M. Mouesca, E. Reijerse, W. Lubitz, T. Happe, V. Artero, M. Fontecave, Biomimetic assembly and activation of [FeFe]-hydrogenases, Nature, 499 (2013) 66-69.

[247] J. Esselborn, C. Lambertz, A. Adamska-Venkatesh, T. Simmons, G. Berggren, J. Noth, J. Siebel, A. Hemschemeier, V. Artero, E. Reijerse, M. Fontecave, W. Lubitz, T. Happe, Spontaneous activation of [FeFe]-hydrogenases by an inorganic [2Fe] active site mimic, Nat Chem Biol, 9 (2013) 607-609.

[248] J.B. Broderick, B.R. Duffus, K.S. Duschene, E.M. Shepard, Radical S-Adenosylmethionine Enzymes, Chem Rev, (2014).

[249] M. Kriek, F. Martins, M.R. Challand, A. Croft, P.L. Roach, Thiamine biosynthesis in Escherichia coli: identification of the intermediate and by-product derived from tyrosine, Angew.Chem.Int.Ed Engl., 46 (2007) 9223-9226.

[250] E. Pilet, Y. Nicolet, C. Mathevon, T. Douki, J.C. Fontecilla-Camps, M. Fontecave, The role of the maturase HydG in [FeFe]-hydrogenase active site synthesis and assembly, FEBS Lett., 583 (2009) 506-511.

[251] E.M. Shepard, B.R. Duffus, S.J. George, S.E. McGlynn, M.R. Challand, K.D. Swanson, P.L. Roach, S.P. Cramer, J.W. Peters, J.B. Broderick, [FeFe]-hydrogenase maturation: HydG-catalyzed synthesis of carbon monoxide, J Am Chem Soc, 132 (2010) 9247-9249.

[252] J.M. Kuchenreuther, W.K. Myers, D.L. Suess, T.A. Stich, V. Pelmenschikov, S.A. Shiigi, S.P. Cramer, J.R. Swartz, R.D. Britt, S.J. George, The HydG enzyme generates an Fe(CO)2(CN) synthon in assembly of the FeFe hydrogenase H-cluster, Science, 343 (2014) 424-427.

[253] Y. Nicolet, L. Martin, C. Tron, J.C. Fontecilla-Camps, A glycyl free radical as the precursor in the synthesis of carbon monoxide and cyanide by the [FeFe]-hydrogenase maturase HydG, FEBS Lett, 584 (2010) 4197-4202.

[254] R.C. Driesener, B.R. Duffus, E.M. Shepard, I.R. Bruzas, K.S. Duschene, N.J. Coleman, A.P. Marrison, E. Salvadori, C.W. Kay, J.W. Peters, J.B. Broderick, P.L. Roach, Biochemical and Kinetic Characterization of Radical S-Adenosyl-l-methionine Enzyme HydG, Biochemistry, (2013).

[255] C. Tron, Cherrier M.V., Amara, P., Martin L., Fauth, F., Fraga, E., Correard, M., Fontecave, M., Nicolet, Y., Fontecilla-Camps, J.C., Further Characterization of the [FeFe]-Hydrogenase Maturase HydG, European Journal of Inorganic Chemistry, (2011) 1121-1127.

[256] J.M. Kuchenreuther, W.K. Myers, T.A. Stich, S.J. George, Y. Nejatyjahromy, J.R. Swartz, R.D. Britt, A radical intermediate in tyrosine scission to the CO and CN- ligands of FeFe hydrogenase, Science, 342 (2013) 472-475.

[257] J.M. Kuchenreuther, S.J. George, C.S. Grady-Smith, S.P. Cramer, J.R. Swartz, Cell-free H-cluster synthesis and [FeFe] hydrogenase activation: all five CO and CN ligands derive from tyrosine, PLoS One, 6 (2011) e20346.

[258] F. Quitterer, A. List, W. Eisenreich, A. Bacher, M. Groll, Crystal structure of methylornithine synthase (PylB): insights into the pyrrolysine biosynthesis, Angew Chem Int Ed Engl, 51 (2012) 1339-1342.

[259] Y. Nicolet, J.K. Rubach, M.C. Posewitz, P. Amara, C. Mathevon, M. Atta, M. Fontecave, J.C. Fontecilla-Camps, X-ray structure of the [FeFe]-hydrogenase maturase HydE from Thermotoga maritima, J.Biol.Chem., 283 (2008) 18861-18872.

[260] Y. Nicolet, P. Amara, J.M. Mouesca, J.C. Fontecilla-Camps, Unexpected electron transfer mechanism upon AdoMet cleavage in radical SAM proteins, Proc Natl Acad Sci U S A, 106 (2009) 14867-14871.

[261] Y. Nicolet, R. Rohac, L. Martin, J.C. Fontecilla-Camps, X-ray snapshots of possible intermediates in the time course of synthesis and degradation of protein-bound Fe4S4 clusters, Proc Natl Acad Sci U S A, 110 (2013) 7188-7192.

[262] A. Volbeda, E. Garcin, C. Piras, A.L. de Lacey, V.M. Fernandez, E.C. Hatchikian, M. Frey, J.C. Fontecilla-Camps, Structure of the [NiFe] Hydrogenase Active Site: Evidence for Biologically Uncommon Fe Ligands⊥, Journal of the American Chemical Society, 118 (1996) 12989-12996.

[263] A.S. Pandey, T.V. Harris, L.J. Giles, J.W. Peters, R.K. Szilagyi, Dithiomethylether as a Ligand in the Hydrogenase H-Cluster, J. Am. Chem. Soc., 130 (2008) 4533-4540.

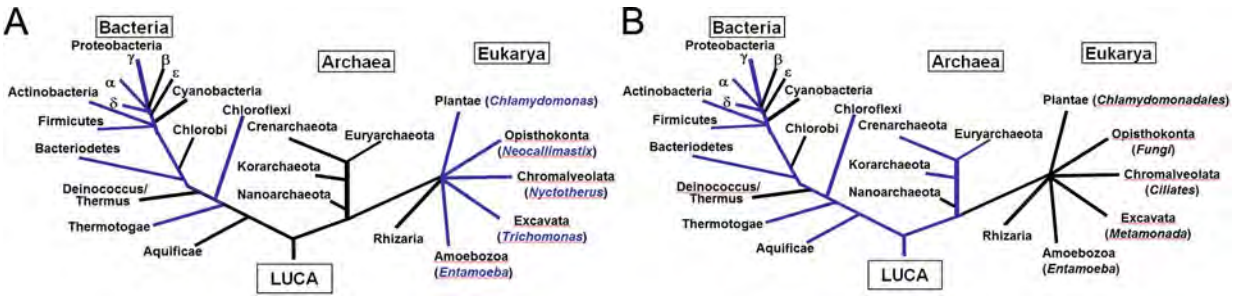

Figure 1. Distribution of [FeFe]-hydrogenase (A) and [NiFe]-hydrogenase mapped on a "universal" taxonomic tree of life. Lineages with at least one homolog of each enzyme are overlaid in blue. Parsimony rules were used to map the ancestral character of extinct lineages (e.g., LUCA).

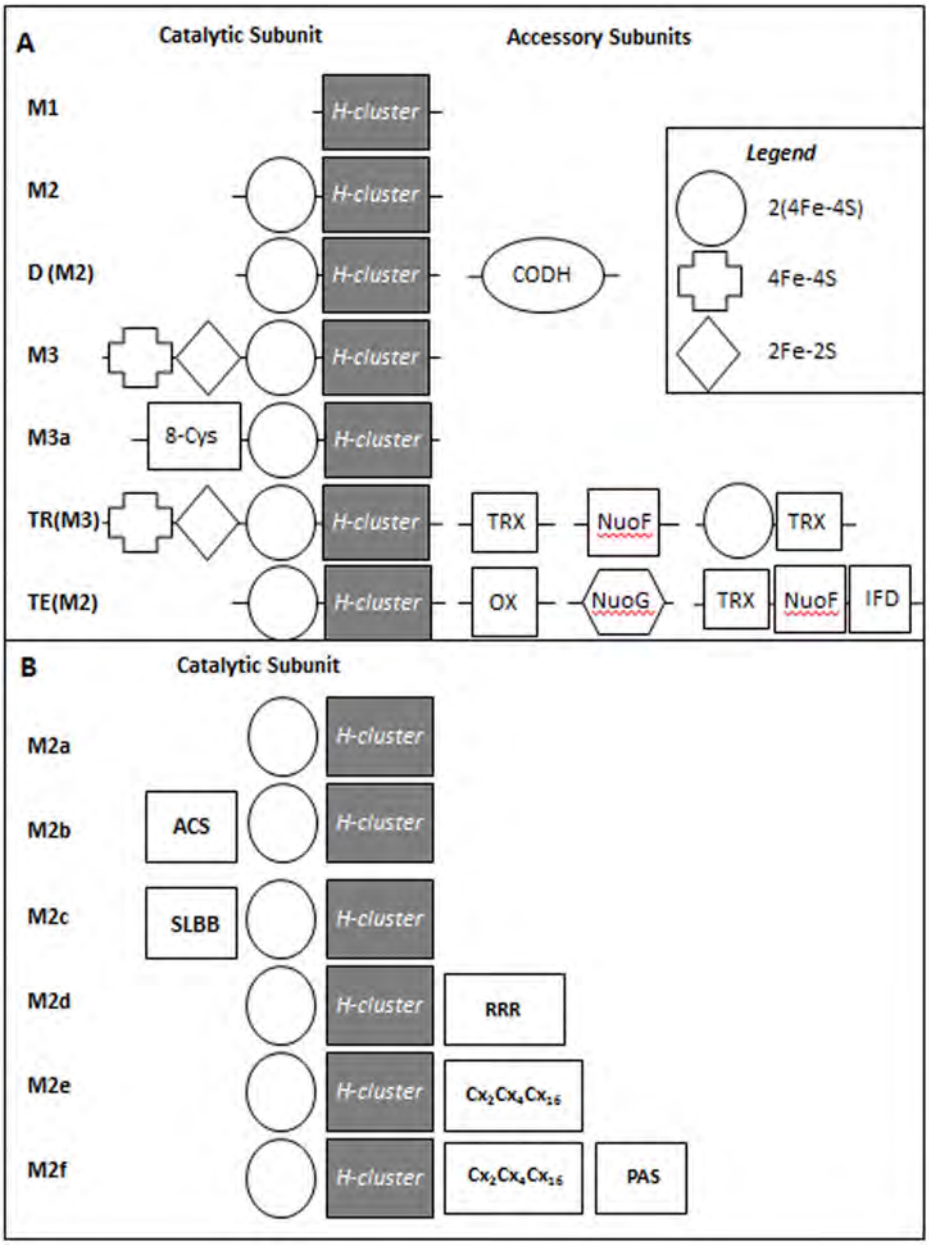

Figure 2. Schematic representation of the structural variation of [FeFe]-hydrogenase homologs present in sequence databases as adapted from Meyer, 2007 and more recently Calusinska et al., 2010. Panel A illustrates the primary structural classes while panel B illustrates the remarkable structural variation in within the M2 structural subclass. Abbreviations: CODH, carbon monoxide dehydrogenase; TRX: Thioredoxin domain; NuoF: homolog subunit F of NADH dehydrogenase; OX: oxidoreductase domain; NuoG: homolog of subunit G of NADH dehydrogenase; IDF: Indolepyruvate:ferredoxin domain; ACS: Acetyl CoA dehydrogenase; SLBB: soluble-ligand-binding b-grasp fold domain; RRR: Rubredoxin-rubrerhythrin-rubredoxin domain; PAS: PAS/PAC domain.

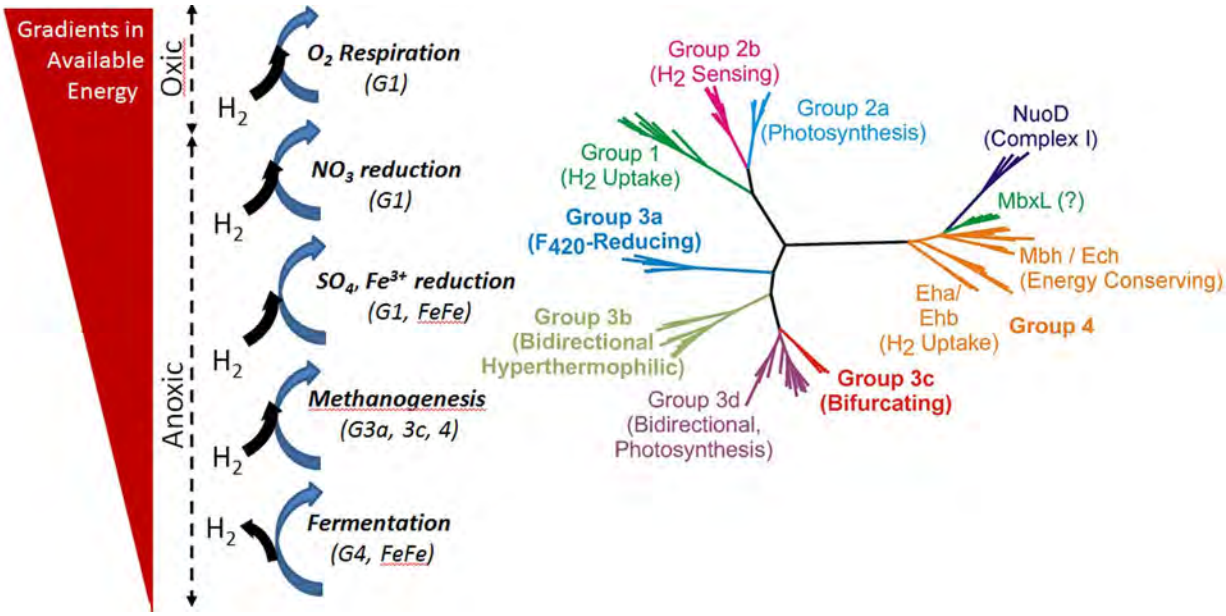

Figure 3. Hypothetical depiction of the distribution specific groups of organisms and associated [FeFe]- and [NiFe]-hydrogenases (designated by "G") that function to couple the oxidation or reduction of substrates along a gradient in the availability of oxidants. **(B)** Phylogenetic reconstruction of representatives of [NiFe]-hydrogenase and related paralogs (NuoBD, MbxJL) with group designations indicated. Figure adapted from Boyd et al., 2014.

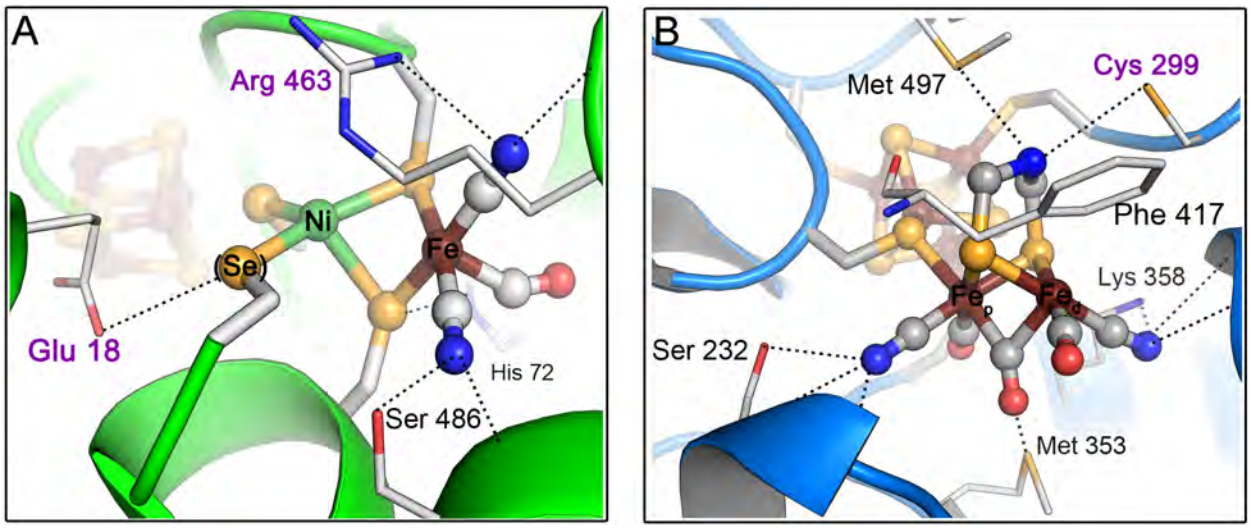

Figure 4. X-ray structures of binuclear cofactors of the hydrogenase catalytic sites. (A) The Ni-Fe cluster of [NiFe(Se)]-hydrogenases. (B) The 2Fe subcluster of the [FeFe]-hydrogenase H cluster. Images rendered from PDB codes 2FRV ([NiFe] hydrogenase) [262] and 3C8Y ([FeFe] hydrogenase *Cp*I from *Clostridium pasteurianum*).[263] The H-bonding interactions (dashed lines, black font) and conserved, exchangeable groups (dashed lines, purple font) are labeled. Ni, nickel; Se, selenium; Fe, iron.

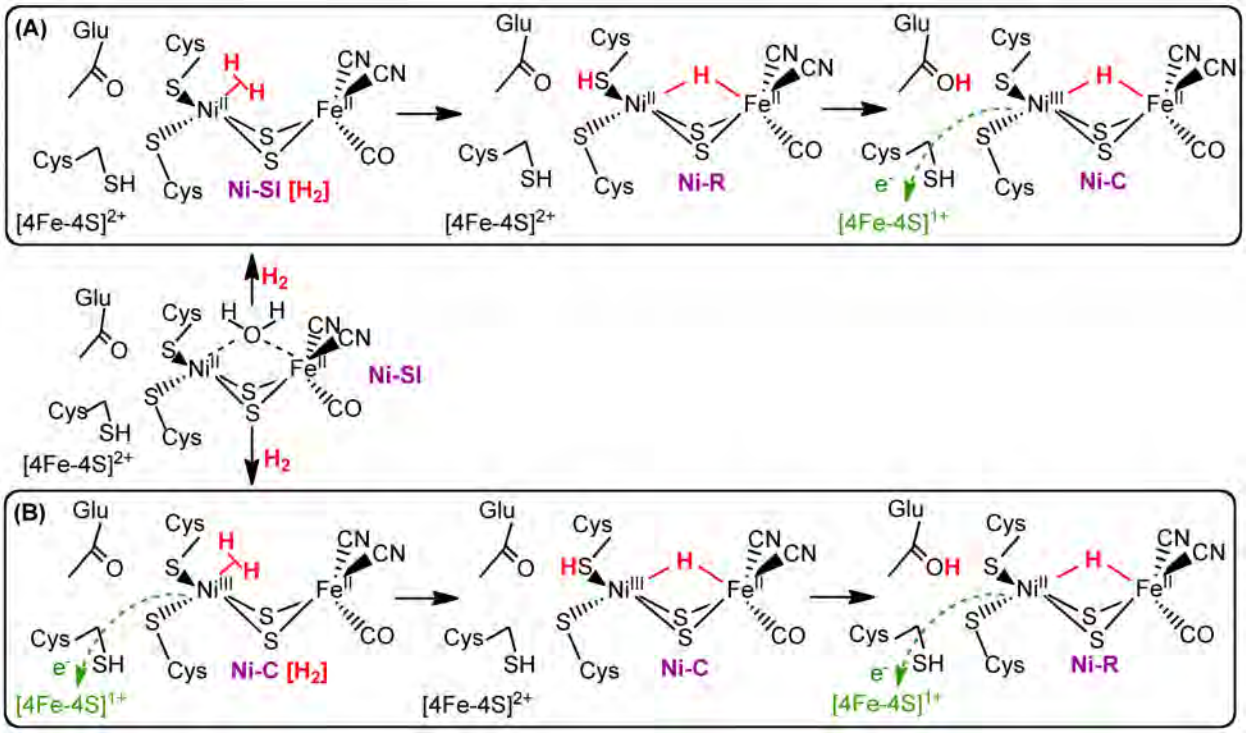

Figure 5. Model of the H_2 binding, and the initial activation steps, catalyzed by [NiFe(Se)] hydrogenases. Scheme (A) proposed by Bruschi, M., et al. [107]. Scheme (B) is a summary of activation proposed by Wu and Hall [108]. Green signifies electron transfer reactions.

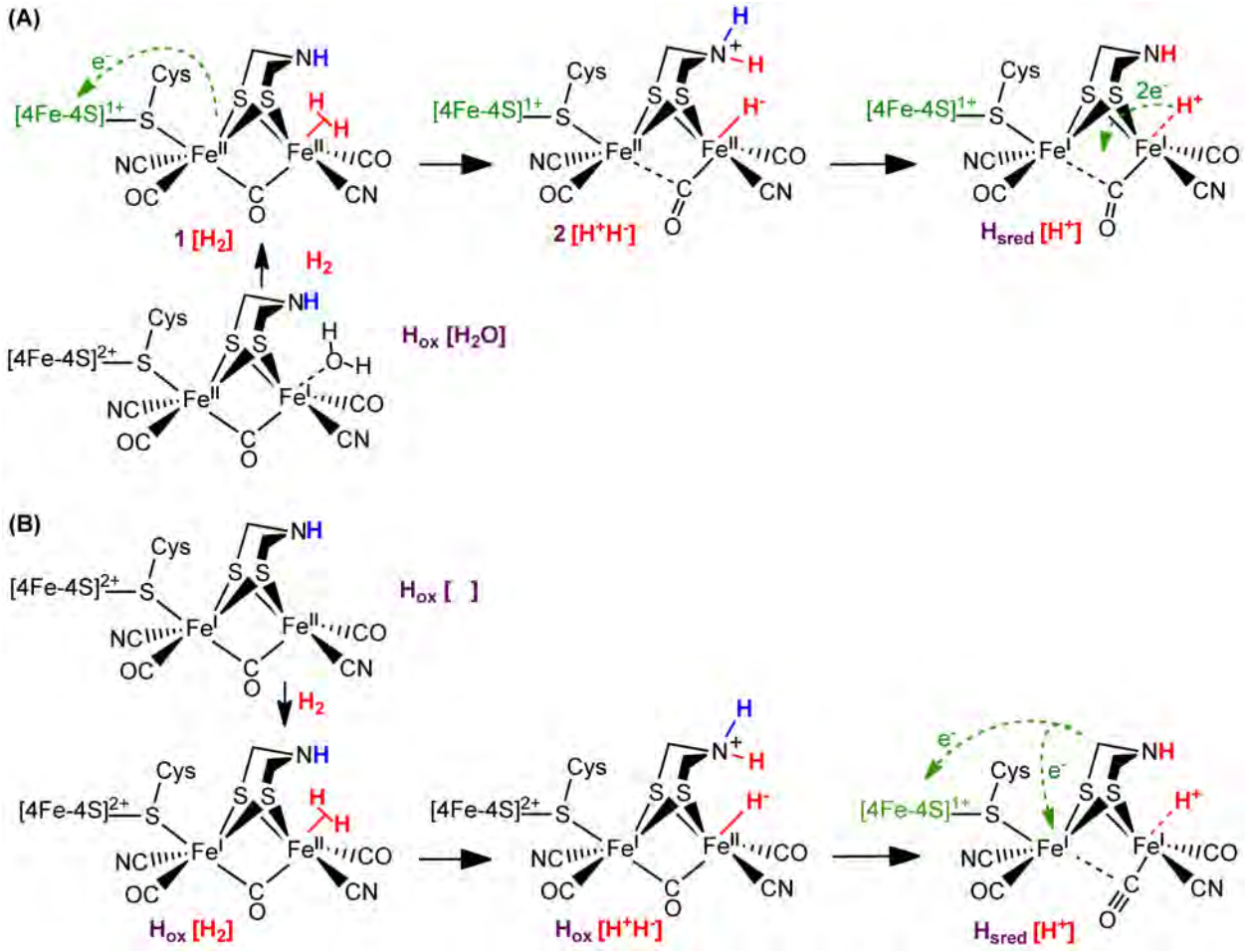

Figure 6. Model for the H_2 binding and activation steps by [FeFe]-hydrogenases. Two alternative schemes are presented based on DFT and spectroscopic studies of [FeFe]-hydrogenases. Scheme (A), the resting H_{ox} state is assigned as a $[4Fe\text{-}4S]^{2+}$ subcluster and a 2Fe subcluster as Fe_p^{II} / Fe_d^{I} based on FTIR and EPR spectra and DFT calculations of oxidized *Cp*I and *Cr*HydA [120, 137, 139, 140], and involves a diferrous 2Fe intermediate for H_2 binding and activation. Scheme (B), the resting H_{ox} state is assigned as $[4Fe\text{-}4S]^{2+}$ and 2Fe as Fe_p^{I} / Fe_d^{II} [104, 115, 141, 144], where H_2 binding and activation occurs on a mixed valent 2Fe at the Fe^{I} site. Green identifies intramolecular ET steps. The initial PT step of H_2 activation from Fe_d to the bridgehead amine ligand is shown in red.

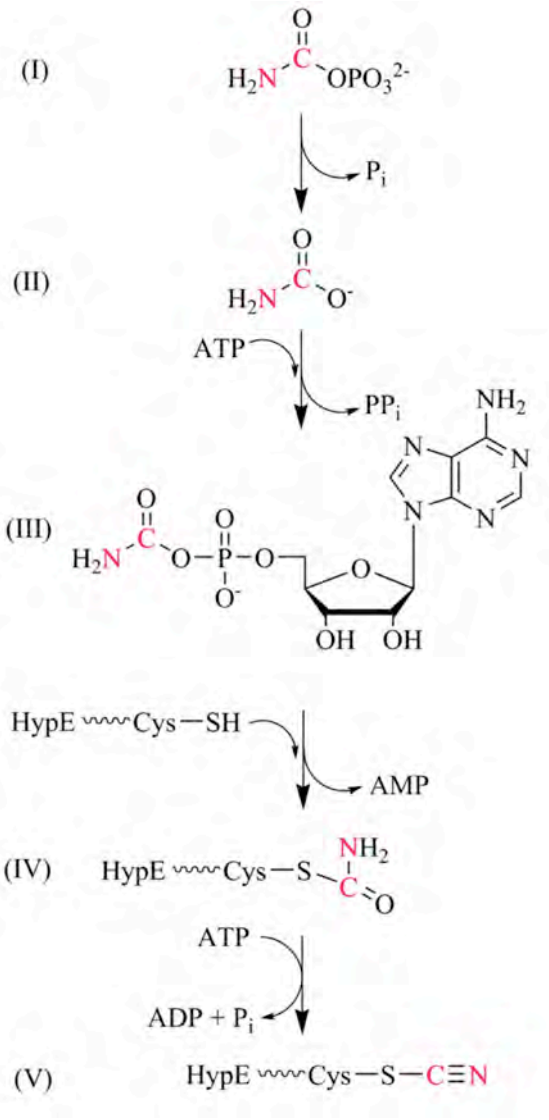

Figure 7. Thiocyanate biosynthesis in [NiFe]-hydrogenase maturation. HypF acts on carbamoylphosphate (I), converting it first to carbamate (II), and then to carbamoyladenylate (III). The carbamoyl functional group is then mobilized to a cysteine on HypE's C-terminus (IV), where it is converted to thiocyanate (V).

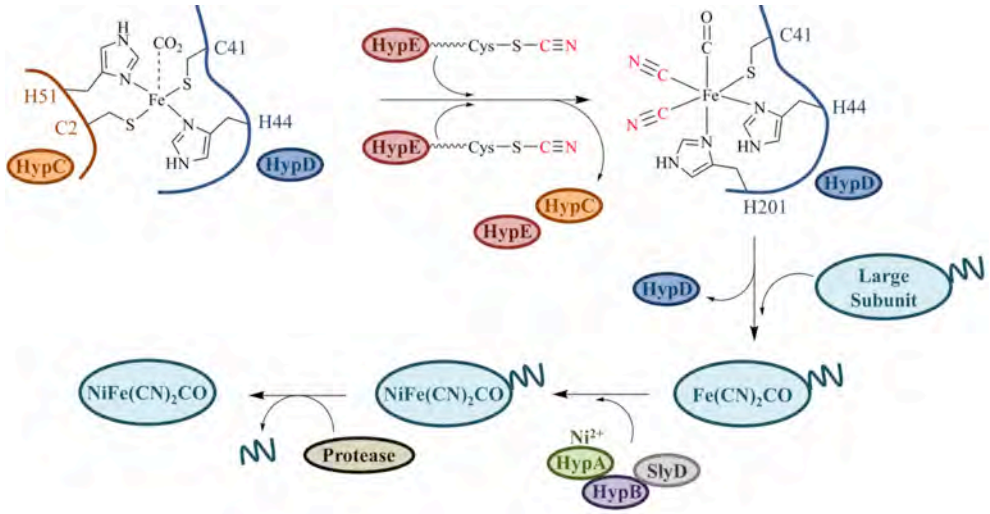

Figure 8. $Fe(CN)_2CO$ biosynthesis and large subunit processing in [NiFe]-hydrogenase maturation. Thiocyanate delivery from HypE to the HypC–HypD complex results in HypC dissociation. The $Fe(CN)_2CO$ unit bound to HypD (*E. coli* amino acid numbering) is then transferred to the large, precursor subunit of [NiFe]-hydrogenase. While the source of CO is unresolved, recent biochemical evidence has been presented showing the association of CO_2 with HypC (see main text), suggesting that HypC delivers Fe–CO_2 to HypD where it is reduced to CO. Accordingly, CO_2 is shown here to be bound to the HypC–HypD complex. Following insertion of Ni^{2+}, a short C-terminal peptide is proteolytically processed, affording the mature [NiFe]-hydrogenase enzyme.

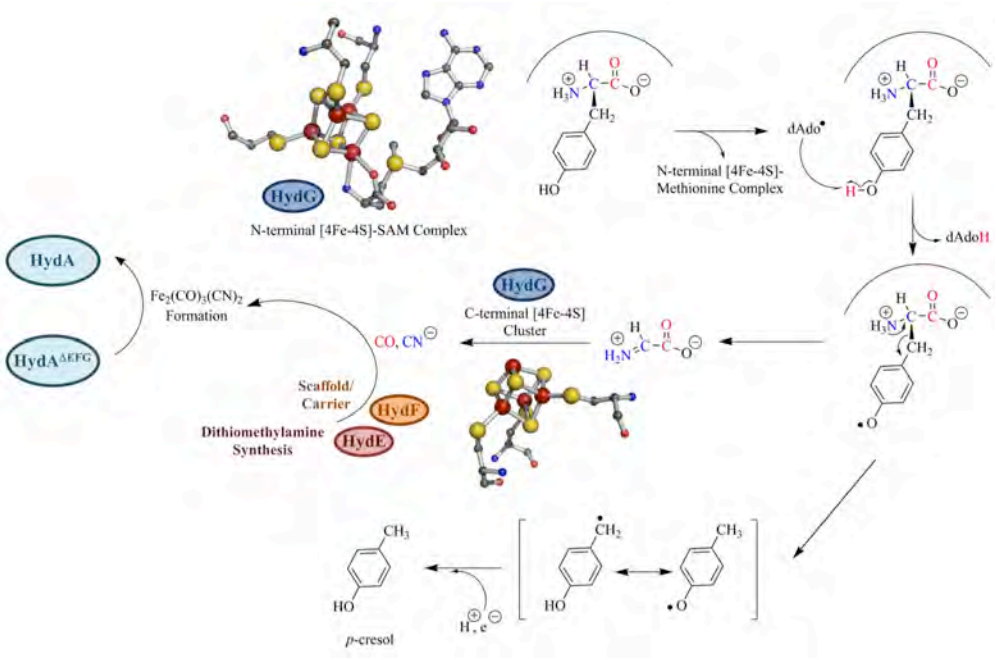

Figure 9. Maturation scheme detailing hypothetic 2Fe subcluster biosynthesis in [FeFe]-hydrogenase maturation. HydG reductively cleaves SAM into methionine and a 5'-deoxyadenosyl radical species; following H-atom abstraction from the *para* phenolic position, tyrosine undergoes heterolytic Cα–Cβ bond cleavage to generate a *p*-cresolate radical and dehydroglycine. CO and CN^- are subsequently formed from dehydroglycine by an unknown mechanism involving the site-differentiated, C-terminal [4Fe-4S] cluster of HydG. Stopped-flow FTIR studies have shown the existence of Fe–CO–CN species that form during HydG catalysis (see main text), leading to the hypothesis that the C-terminal cluster is cannibalized during biosynthesis. Maturation of the 2Fe subcluster is completed via dithiomethylamine synthesis by HydE. HydF acts as a scaffold or carrier protein during the assembly process and transfers the 2Fe subcluster to $HydA^{\Delta EFG}$ to achieve [FeFe]-hydrogenase activation.

Distribution, Abundance, and Diversity of Multimeric Bifurcating [FeFe]-Hydrogenases Along a Vertical Redox Gradient in Great Salt Lake, USA

Eric S. Boyd[1], Trinity L. Hamilton[2], Kevin Swanson[2], Alta Howells[2], Bonnie K. Baxter[3], Matthew C. Posewitz[4], and John W. Peters[2]

[1]*Department of Microbiology and Immunology, Montana State University, Bozeman, Montana 59717*

[2]*Department of Chemistry and Biochemistry, Montana State University, Bozeman, Montana 59717*

[3]*Department of Biology and the Great Salt Lake Institute, Westminster College, Salt Lake City, UT 84105*

[4]*Department of Civil and Environmental Engineering, Colorado School of Mines, Golden, CO 80401*

*To whom correspondence should be addressed. Email: eboyd@montana.edu.

Using FeFe-hydrogenase Endnote library.

Draft - In preperation

ABSTRACT (268 WORDS)

[FeFe] hydrogenases catalyze the reversible reduction of protons to yield H_2. Attempts to use these enzymes in scale up production of H_2 or other reduced bio-products have been limited by their sensitivity to oxygen. Here, we apply a PCR-directed approach to determine the distribution, abundance, and diversity of *hydA* gene fragments along co-varying salinity and O_2 gradients in a vertical water column environment of Great Salt Lake, Utah. The distribution of *hydA* was constrained to water column transects that had high salt and reduced, albeit measurable O_2 concentrations. The presence of [FeFe]-hydrogenase in these oxygen containing transects may be due to the lower solubility and bioavailability of O_2 in saline solutions. Recovered HydA protein fragments were predominantly bacterial and harbored insertions in regions of the protein that form gas channels that lead to the O_2-labile FeS cubane. HydA sequences recovered from GSL were enriched in hydrophilic amino acids when compared to HydA from less saline environments, suggesting adaptation to minimize salt-enhanced hydrophobic interactions during protein folding. A phylogenetic framework was created for use in predicting the accessory cluster composition and quaternary structure of recovered HydA protein sequences. HydA recovered from the GSL water column are predicted to harbor numerous N- and C-terminal accessory iron-sulfur cluster binding domains and form trimers; characteristics typical of bifurcating hydrogenase. This study indicates an important role for H_2-based bifurcating [FeFe]-hydrogenases in the functioning of the GSL ecosystem and provides new target enzymes and variants for use in identifying an O2 tolerant enzymes for use in biotechnological applications.

Draft - In preperation

INTRODUCTION

Hydrogen (H_2) is a diffusible electron carrier, has the highest energy content per unit mass of all naturally occurring fuels, and forms the basis of numerous interspecies interactions in natural microbial communities {McInerney, 2009 #212;Schink, 1997 #82}. [NiFe]- and [FeFe]-hydrogenase, which differ in the metal composition of their active site cluster, are principally responsible for H_2 cycling in natural environments. In general, [FeFe]-hydrogenases are found in anaerobic bacteria and are especially prevalent among the fermentative organisms (e.g., firmicutes) where they typically function in the regeneration of reduced electron carriers [NAD(P)H, ferredoxin (Fd)] coupled to the reduction of protons. They are also found in a number of lower eukaryotes including algae and protists but surprisingly they have yet to be found in cyanobacteria or in archaea {Meyer, 2007 #7}. In contrast, [NiFe]-hydrogenases, are frequently found in archaea, in addition to their common occurrence in a large number of bacteria {Vignais, 2007 #16;Vignais, 2001 #8}.

The majority of H_2 in natural environments is produced through fermentative processes {Conrad, 1996 #218}. While both classes of hydrogenase can function in the generation of H_2 during fermentation {Meyer, 2007 #7;Vignais, 2007 #16;Vignais, 2001 #8}, [FeFe]-hydrogenase are generally more efficient H_2 producing catalysts {Cammack, 1999 #213} and such have been subjected to extensive biochemical and structural characterization in an effort to optimize these enzymes for efficient bio-hydrogen production {Mulder, 2010 #214;Peters, 1998 #101;Posewitz, 2008 #12;Stapleton, 2010 #230;Stapleton, 2010 #231}. The best characterized [FeFe]-hydrogenases are monomeric, Fd-dependent enzymes {Meyer, 2007 #7;Vignais, 2001 #8}.

Draft - In preperation

Examples of these enzymes include those from eukaryotic algae such as *Chlamydomonas reinhardtii* {Mulder, 2010 #214;Meuser, 2012 #215;Stripp, 2009 #216} and clostridial species such as *Clostridium pasteurianum* {Peters, 1998 #101}. Whereas *C. reinhardtii* [FeFe]-hydrogenases comprise only the active site H-cluster, [FeFe]-hydrogenase from *C. pasteurianum* contains an additional three [4Fe-4S] cluster binding domains in the N terminus which may function to allow coupling with electron donors with differing redox potentials. Characterization of [FeFe]-hydrogenase diversity in genome sequences {Calusinska, 2010 #210;Meyer, 2007 #7} noted substantial variation in N- and C-terminal Fe-S cluster and accessory co-factor binding motifs (Fig. 3), suggesting potential interactions with a variety of redox partners. In addition, such analyses identified differences in [FeFe]-hydrogenase quaternary structure, including the identification of multimeric homologs that likely form dimers, trimers, or tetramers {Calusinska, 2010 #210;Meyer, 2007 #7}.

Biochemical characterization of multimeric [FeFe]-hydrogenase enzymes indicate that they are pyridine nucleotide (NAD(P)H- or NADH) linked H_2 producing enzymes {Malki, 1995 #219;Soboh, 2004 #220;Verhagen, 2001 #221;Malki, 1995 #219;Soboh, 2004 #220;Verhagen, 2001 #221}. The trimeric hydrogenase from *T. maritima* was shown to require both reduced Fd and NADH for efficient H_2 production {Schut, 2009 #222}. Conversely, the [FeFe]-hydrogenase from *Acetobacterium woodii* simultaneously reduces NAD^+ and ferredoxin (Fd) during H_2 oxidation. The key to the reversible oxidation of H_2 and simultaneous NAD^+ and Fd reduction is the coupling of their energetics; the exergonic reduction of NAD^+ by electrons derived from H_2 allows the endergonic reduction of Fd in a process now termed electron bifurcation {Herrmann, 2008 #223;Buckel, 2013 #224}. Thus, these enzymes function to create

Draft - In preperation

electrons with a very low redox potential by simultaneously creating an electron with a high redox potential {Buckel, 2013 #224;Wang, 2013 #225;Wang, 2013 #226;Schut, 2009 #222}. While the aforementioned examples indicate a directionality in the bifurcating process, [FeFe]-hydrogenases that bifurcate can in principle function *in vivo* in both the production and oxidation of H_2, as was recently shown for a bifurcating hydrogenase in *Moorella thermoacetica* {Wang, 2013 #226}. During growth on glucose, *M. thermoacetica* can intermittingly produce H_2 from Fd and NADH via the bifurcating hydrogenase. Likewise, this same hydrogenase can utilize produced H_2 and CO_2 to preform acetogenesis generating 3 mol of acetate per glucose. Although *M. thermoacetica* does not grow well autotrophically on H_2 and CO_2, it uses the bifurcating hydrogenase to produce reduced Fd to drive acetogenesis. The reversible production of such low potential metabolic electrons through the process of H_2 dependent electron bifurcation is of significant biotechnological interest since they could be modulated *in vivo* and directed toward the controlled production of highly reduced biofuel products.

Multimeric bifurcating [FeFe]-hydrogenase complexes now appear to be commonplace among anaerobic bacteria {Calusinska, 2010 #210;Meyer, 2007 #7}. However, like the monomeric forms of [FeFe]-hydrogenase, multimeric enzymes are oxygen sensitive which presents challenges in the application of such enzymes in large scale production efforts {Juszczak, 1991 #232}. Numerous biochemical and structural studies have been conducted to shed light on the basis of the oxygen sensitivity of [FeFe]-hydrogenase. One approach to address this problem is gene shuffling or randomized mutation, which generates a diverse recombinant hydrogenase library to screen for enhanced O_2 tolerance and/or stability {Nagy, 2007 #5;Stapleton, 2010 #230;Stapleton, 2010 #231;Bingham, 2012 #235}. Another approach is to

Draft - In Preparation

search natural diversity of these enzymes as they are distributed across geochemical gradients (e.g., O_2) through the use of PCR or metagenomic-directed approaches {Boyd, 2010 #191;Boyd, 2009 #108;Schmidt, 2010 #233;Chivian, 2008 #144;Warnecke, 2007 #147}. A previous application of a PCR-directed approach targeting a fragment of the gene encoding the large subunit (*HydA*) of [FeFe]-hydrogenase in a phototrophic mat community identified a number of substitutions and insertions in regions of the protein that coordinate the O_2 labile active site FeS cubane {Boyd, 2009 #108}. While the functional implications of these substitutions/insertions have yet to be followed up on biochemically, such findings provide impetus to continue searching natural systems for potential variants capable of tolerating higher O_2 concentrations.

Due to the limited supply of freshwater any large scale up production of biofuels is likely to employ salt water, creating the need to identify salt tolerant enzymes and organisms in addition to enzymes that also function in the presence of O_2 {Beer, 2009 #126}. Since both the solubility and the diffusion rate of O_2 are lower in (hyper)saline solutions {Lange, 1972 #237}, it is possible that salt tolerant [FeFe]-hydrogenase may maintain functionality in the presence of higher apparent concentrations of O_2 because cells are able to maintain a lower effective (bioavailable) intracellular concentration. Here, we apply a PCR-directed approach to determine the distribution and diversity of *hydA* gene fragments in a vertical water column environment of Great Salt Lake, Utah which exhibits strong and co-varying gradients in salt, oxygen, photosynthetically active radiation, pH, and temperature {Meuser, 2013 #209}. A phylogenetic framework was created for use in predicting the accessory cluster composition and quaternary structure of HydA protein sequences obtained along the vertical gradient. The results indicate an abundance of multimeric [FeFe]-hydrogenase that are putatively involved in electron bifurcating

Draft - In preperation

processes. Recovered HydA protein fragments revealed evidence of adaptation to elevated salt concentrations and harbored variations in regions of the protein that form gas channels leading to the O_2-labile FeS cubane of the active site. Similarly, novel substitutions were identified in residues that coordinate the O_2 labile active site. This study demonstrates that enzyme variants with desired properties can potentially be recovered by examining protein diversity in microbial assemblages that have evolved in the presence of a particular environmental stress.

METHODS

Site Description and Sample Collection. Samples were collected from the Division of Wildlife and Resources sample site number 3 (DWR3: Latitude 41.16746, Longitude -112.6696117) in June, 2007 (surface, 1M, 4M, 6M, 6.5M, and 8M depths and benthic sediments), by lowering a 2L Kemmerer collection bottle (Wildlife Supply, Yulee, FL, USA) to each depth sampled, with deionized water rinses between each sampling. Samples were transferred to sterile collection bottles leaving minimal headspace volume, stored on ice, and transported to the laboratory. Cells were then pelleted by centrifugation (4000 *g* for 15 min at 3°C) using a Sorvall centrifuge (Thermo Fisher, Waltham, MA, USA), the supernatant decanted, and biomass pellets resuspended in 1 mL of supernatant and stored at -80°C until used for DNA extraction.

Physical and chemical analysis. Chemical and physical measurements were compiled as a part of a previous study conducted on the DWR3 water column {Meuser, 2013 #209}.

Draft - In preperation

Briefly, quantum scalar irradiance of total available photosynthetic active radiation (PAR, 400-700 nm photons·m^{-2}·s^{-1}) was determined using a Li-Cor LI-193 underwater spherical quantum sensor and LI-250A light meter (Li-Cor Biosciences, Lincoln, Nebraska, USA). A Troll 9500 multi-sensor (In-Situ Inc., Fort Collins, CO, USA) was used to simultaneously acquire pH, temperature, salinity, and dissolved O_2 data at each DWR3 site sampling depth.

DNA Extraction, Amplification, Cloning, and Sequencing of *hydA*. Total DNA was extracted from ~ 200 mg aliquots of biomass using the PowerSoil™ DNA Isolation Kit (MoBio Inc., Carlsbad, CA, USA) following the manufacturer's instructions. DNA was quantified fluorometrically as previously described {Boyd, 2007 #107}. All DNA extracts were screened for the presence of 16S rRNA genes to ensure the presence of PCR-amplifiable DNA using 10 ng of DNA and primers bacterial 1070F (5'-ATGGCTGTCGTCAGCT-3') and universal 1492R (5'-GGTTACCTTGTTACGACTT-3') {Boyd, 2009 #142}. Approximately 500 bp fragments of *hydA* were PCR-amplified in triplicate from 10 ng of environmental genomic DNA as template and primer pair FeFe-272F and FeFe-427R using previously established reagent concentrations and reaction conditions {Boyd, 2009 #108}. Equal volumes of each replicate amplification were pooled and were purified using the Wizard PCR Preps DNA purification system (Promega, Madison, WI), quantified using the Low DNA Mass Ladder (Invitrogen, Carlsbad, CA), cloned using the pGem-T Easy Vector System (Promega), and sequenced using the M13F-M13R primer pair as previously described {Boyd, 2009 #142}. A total of 215 *hydA* gene sequences were sequenced in the present study and representatives of each phylotype (supplemental table 1) have been deposited in the GenBank, DDBJ, and EMBL databases under the accession numbers HM636647-HM636798.

Draft - In preperation

Primary Sequence Analysis. MEGA (ver. 4.0.1) {Tamura, 2007 #88} was used to translate and alisng *hydA* sequences specifying the Gonnet 250 protein weight matrix with a pairwise alignment gap opening penalty of 13 and gap extension penalty of 0.05. The aligned HydA sequences were screened for the presence of the L1 ([FLI]**TSC**[C/S]**P**[GAS]W[VIQH]) and L2 ([IVLF]M**PC**x[ASRD]**K**[KQ]xE) (conserved residues are in bold and underlined, and bracketed positions indicate "semiconserved" residues at that position) as outlined previously {Meyer, 2007 #7;Vignais, 2001 #8}. ClustalX {Larkin, 2007 #89} was also used to create a pairwise sequence identity matrix which was subsequently imported into DOTUR {Schloss, 2005 #36} to identify and group operational taxonomic units (OTUs) and to perform rarefaction analyses at a sequence identity threshold of 0.01. Indices describing the hydrophobicity of inferred protein sequences (aliphatic and grand average of hydropathicity [GRAVY] indices) were computed using the ProtParam tool available on the ExPASy proteomics server (http://au.expasy.org/tools/protparam.html) {Gasteiger, 2005 #35}. The aliphatic index is the relative volume occupied by aliphatic amino acid side chains (alanine, valine, isoleucine, and leucine) in a given protein or protein fragment and is calculated according to the formula X(Ala) + a * X(Val) + b * (X(Ile) + X(Leu)) where X(Ala), X(Val), X(Ile), and X(Leu) are mole percent (100 * mole fraction) of alanine, valine, isoleucine, and leucine and a and b are the relative volume coefficients for valine (a=2.9) and Leu/Ile (b=3.9) relative to alanine {Kyte, 1982 #37}, with higher indices indicative of a higher content of aliphatic side chains in the protein. The GRAVY index is the sum of the hydropathy values for each amino acid in a sequence divided by the number of residues {Kyte, 1982 #37}, with positive GRAVY indices indicative of hydrophobicity and negative GRAVY indices indicative of hydrophilicity. For

Draft - In preperation

218 comparison, aliphatic and GRAVY indices were computed for putative HydA previously
219 recovered from microbial mats inhabiting salterns from Guerrero Negro (GN), Mexico
220 (GenBank: FJ623894-FJ623958) {Boyd, 2009 #108} and from geothermal springs in
221 Yellowstone National Park (YNP), Wyoming (GenBank: GU362773-GU362867) {Boyd, 2010
222 #191} (Supplemental Table 2). Intervals of 0.04 GRAVY index units were empirically selected
223 for use in binning GRAVY indices for sequences recovered from the three geochemically-
224 distinct environments (GSL, YNP, GN). Indices were rounded downward to the nearest 0.04
225 unit interval prior to binning. *P*-values were obtained by using a two-tailed Student *t* test.
226
227 **Prediction of Environmental HydA Accessary Cluster Composition.** The sequences
228 used to develop the F- and C-cluster classification and tertiary structure scheme developed by
229 Meyer 2007 and further augmented by Calusinska et al., 2010 {Calusinska, 2010 #210} were
230 compiled and used to create a database for use in predicting the accessory cluster composition
231 and tertiary structure of putative HydA fragments recovered from the GSL water column (Supp.
232 Table 3). Additional sequences representing the closest BLASTp hits for each OTU were also
233 compiled and characterized for F- and C-cluster composition and tertiary structure scheme using
234 the criteria of Calusinska et al., 2010 {Calusinska, 2010 #210} and the Conserved Domain
235 Database as implemented with BLASTp {Marchler-Bauer, 2009 #211}. The classification of
236 these proteins, along with those reported by Calusinska et al., 2010, are reported in Supplemental
237 Table 3 and a schematic illustrating their F- and C-cluster structural variation is presented in Fig.
238 3.
239

Draft - In preperation

HydA protein sequences from GSL and from our database were aligned, trimmed to the length of the amplified protein fragment (positions 272 to 427 in HydA from *Clostridium pasteurianum*), and subjected to Maximum Likelihood phylogenetic reconstruction as described previously {Boyd, 2010 #191}. The C- and F-cluster composition and tertiary structure of environmental HydA was then predicted by phylogenetic clustering with HydA comprising our database. Sequences that formed lineages without a representative from our database were classified as "unknown" with respect to F- and C-cluster composition and tertiary structure.

***hydA* qPCR.** Quantitative PCR (qPCR) was used to estimate the number of *hydA* templates in GSL DNA extracts according to previously described methods {Boyd, 2011 #246}. Standard curves were generated from plasmid DNA containing *hydA* amplified from the GSL sample sites. Three plasmid clones were used in generating a standard curve that relates template copy number to threshold qPCR amplification signal. The threshold amplification signal as a function of copy number varied by less than 1 cycle for each of the three plasmid clones; thus, the standard curves generated using each plasmid clone were averaged for use in calculating the average template abundances and standard deviation in template abundances from replicate qPCRs. A standard curve was generated over 6 orders of magnitude ranging from 9.1×10^1 to 1.1×10^7 copies of template per assay ($R^2 = 0.995$).

qPCR assays were performed in a Rotor-Gene 300 quantitative real-time PCR machine (Qiagen, Valencia, CA) in 0.5 mL optically clear PCR tubes (Qiagen, Valencia, CA) using a SsoFast^{TM} EvaGreen Supermix qPCR Kit (Bio-Rad Laboratories, Hercules, CA). Assay reactions were amended to a final concentration of 0.4 mg ml^{-1} molecular-grade bovine serum

Draft - In preparation

albumin (Roche, Indianapolis, IN). qPCR cycling conditions were as follows: initial denaturation (95°C for 10 min) followed by 40 cycles of denaturation (95°C for 10s), annealing (56.5°C for 15s), and extension (72°C for 20 s). Specificity of the qPCR assays was verified by melt curve analysis. The reported template abundances are the average and standard deviation of qPCR assays performed in triplicate for each gene.

HydA Phylogenetic Diversity. The phylogenetic position of *hydA* homologs was assessed using PhyML-aBayes {Anisimova M., 2011 #204} with the nuclear prelamin A recognition factor-like protein-encoding gene (XM_414836), a distantly related homolog of *hydA* {Meyer, 2007 #7}, from *Gallus gallus* serving as the outgroup. The General Time Reversible (GTR) substitution model with gamma-shaped rate variation with a proportion of invariable sites was specified in the calculation, as recommended by Modeltest (ver. 3.) {Posada, 2006 #189}. The nuclear prelamin A recognition factor-like protein-encoding gene (XM_414836), a distantly related homolog of *hydA* {Meyer, 2007 #7}, from *Gallus gallus* served as the outgroup. The consensus phylogram was rate-smoothed using the multidimensional version of Rambaut's parameterization as implemented in PAUP (ver. 4.0) {Swofford, 2001 #94}. Rate-smoothing was performed according to the parameters identified using Modeltest. This included the identification of the substitution model, the gamma distribution of rate variation across sites, the proportion of invariant sites, nucleobase frequencies, and the rate matrix for each phylogram. Phylocom (ver. 4.0.1) {Webb, 2008 #114} was used to calculate Faith's index of phylogenetic diversity (PD) using the rate smoothed Bayesian chronogram. PD is the proportion of total branch length in the phylogeny associated with the taxa in a given sample or assemblage. A higher PD index for an assemblage is

Draft - In preperation

indicative of higher phylogenetic diversity (phylogenetic richness) relative to the total sequence pool.

RESULTS

Water column chemistry. Strong and often co-varying physical and chemical gradients were observed in the DWR3 vertical water column (Table 1). Salinity did not vary substantially over the interval from the surface to a depth of 6.0 meters but increased from 126 ppt at 6.0 meters to 203 and 247 ppt at depths of 6.5 and 8.0 meters, respectively. Likewise, water column temperature was nearly constant (23-24ºC) over the 0.0 to 6.0 meter vertical transect, but decreased abruptly at a depth of 6.5 and 8.0 meters (20 and 17ºC, respectively), indicating the presence of an inverted thermocline between depth intervals of 6.0 and 8.0 meters. pH varied from 5.95 to 8.05 over the eight meter depth, with the highest pH observed at a depth of 6.0 meters and the lowest pH observed at 8.0 meters. Photosynthetically active radiation (PAR) decreased systematically from 1800 µM at the surface to 175 µM at a depth of 4.0 meters and was below detection at a depth of 8.0 meters. Dissolved oxygen varied little over the 0.0 to 4.0 meter vertical transect, but decreased substantially from 5.13 mg L^{-1} to 2.3 mg L^{-1} over the 4.0 to 6.0 meter depth transect.

Abundance, composition, and diversity of *hydA* in GSL water column. *hydA* amplicons were not detected in surface samples (0.0 meters) or from samples collected from depths of 1.0 or 4.0 meters. In contrast, *hydA* genes were detected in samples collected from depth intervals of 6.0, 6.5, and 8.0 meters, as well as from benthic sediment samples collected at

Draft - In preperation

309 ~ 8.5 meters. The relative abundance of *hydA* templates, when normalized to total quantity of
310 extractable DNA, increased with increasing depth with the highest concentration of *hydA* genes
311 detected in associated with benthic sediment biomass (9.2±1.9 x 10^5 templates / ng DNA). The
312 distribution of *hydA* along the DWR3 water column is coincident with the position of the
313 thermocline and with decreasing levels of PAR and dissolved O_2 and increasing salinity. The
314 abundance of *hydA* templates was significantly and inversely correlated with temperature
315 (Pearson R = -0.96, P < 0.01) and dissolved oxygen (Pearson R = -0.85, P = 0.03) and was
316 positively correlated with salinity (Pearson R = 0.93, P < 0.01).
317
318 A total of 211 *hydA* sequences (47 to 58 clones per sample) that, when translated,
319 harbored signature motifs characteristic of HydA {Meyer, 2007 #7} were obtained in the current
320 study (Table 2). The average hydropathy of amino acids (GRAVY index) comprising the
321 inferred protein sequences was calculated and compared to sequences obtained with the same
322 primer sets from other environmental systems, including microbial mat communities inhabiting
323 salterns at Guerrero Negro (GN), Mexico {Boyd, 2009 #108} and hot springs in Yellowstone
324 National Park (YNP), USA {Boyd, 2010 #191}. The GRAVY index for HydA sequences
325 obtained from the GSL DWR3 water column spanned values ranging from 0.04 indicative of
326 average hydrophobic amino acid content to -0.56 which indicates a very low hydrophobic amino
327 acid content. There was no discernable pattern in the average GRAVY index for HydA
328 sequences obtained from the GSL with sampling depth (data not shown). However, the average
329 GRAVY index for sequences obtained from the GSL water column (14.9 to 24.7% salinity) was
330 -0.30 whereas average GRAVY indices obtained GN (8% salt) and YNP (0.5 to 3.1% salinity)

Draft - In preperation

were -0.26 and -0.15, respectively. This indicates that HydA assemblages from GSL on average comprise a greater number of hydrophobic amino acids than those from GN and YNP.

Faith's index of phylogenetic diversity (PD), a B-diversity metric that quantifies the proportion of total branch length in the phylogeny associated with sequences obtained from a given environment when compared to all environments when considered together, increased systematically with increasing depth (Table 2). *hydA* deduced amino acid sequences recovered from the four GSL environments were distantly related to HydA from cultivated organisms, with the average, minimum, and maximum observed sequence identities of 52%, 64%, and 76% (Supp. Table 1). The majority (99.6%) of the sequences obtained from the 4 GSL environments exhibited affiliation with bacteria, although a single sequence affiliated (62% identical) with a eukaryotic diatom *Thalassiosira pseudonana* was recovered from the benthic sediments. Despite significant variation in the taxonomic affiliation of HydA assemblages sampled at depth, binning the sequences at the class level of taxonomic resolution failed to uncover discernable patterns in the taxonomic composition of assemblages as a function of depth (Fig. 1B), consistent with previous studies indicating the tendency for *hydA* to be horizontally transferred {Schmidt, 2010 #233}. HydA affiliated with *Clostridia* were the most abundant regardless of the sampling depth.

Variation in H-Cluster Binding Motifs and Putative Gas Channels. A variety of substitutions were noted in the L1 motif, including a Cys to Ser substitution, relative to position 300 of the *Clostridium pasteurianum* (Cp1) HydA sequence (AAA23248). This residue is involved in coordinating the active site H-cluster {Peters, 1998 #101}. Interestingly, a number

Draft - In preperation

of substitutions were also observed in residues that line a putative gas channel that leads to the oxygen sensitive active site H cluster {Cohen, 2005 #234}. In particular, substitution of the much larger Phe for Lys and Ile (positions 283 and 287 of Cp1, respectively) were noted in several GSL sequences. Conversely, other proteins exhibited substitution of Lys for Phe (position 293 of Cp1). Intriguingly, a large insertion just upstream from the L1 motif was observed in a number of sequences recovered from GSL. These insertions occur in a region of HydA that forms the loop that caps one of the putative gas channels {Cohen, 2005 #234}. Similar insertions are common in phototrophic algae {Beer, 2009 #126}.

Inferred Structural Variation of GSL HydA. A database of HydA sequences (Supp. Table 3) was compiled from complete genome sequences present in GenBank based on previous characterizations of their N- and C-terminal cluster composition (Fig. 4) and quaternary structure {Calusinska, 2010 #210;Meyer, 2007 #7}. Additional sequences were obtained based on BLASTp searches and the primary sequence and quaternary structural characteristics were determined as described previously {Calusinska, 2010 #210}. These sequences and the modular composition of the N- and C-terminal domains (i.e., F- and C-clusters) and their quaternary structure was used to develop a Bayesian phylogenetic framework for predicting these features based on the *hydA* fragment obtained from GSL. Similar to previous phylogenetic analyses of the H-cluster domain {Calusinska, 2010 #210;Meyer, 2007 #7}, phylogenetic reconstruction of just the H-cluster fragment (positions 280 to 419 of HydA1 from Cp1) in sequences recovered from GenBank revealed clustering that corresponded to primary and quaternary structural characteristics (Fig. 5) indicating that the phylogenetic signal of the fragment was sufficient for predicting the characteristics of HydA from GSL at these levels of consideration. The majority

Draft - In preperation

(93.8% of total sequences) of HydA homologs recovered from GSL were nested within or formed clusters with reference sequences that have the M3 architecture and that form trimers (TRM3) (Supp. Table 1). Only a small fraction of sequences inferred to have a thermotogae monomeric configuration (5.3% of total sequences); there was no discernable pattern in the distribution of these sequences as a function of depth in the DWR3 water column (data not shown). In addition, 0.88% of the sequences did not cluster or nest phylogenetically with sequences comprising our database preventing prediction of the F- and C-cluster composition or quaternary structure. These sequences generally had low sequence identities.

DISCUSSION

A diversity of [FeFe]-hydrogenase were identified along the DWR3 vertical gradient in the GSL. While the phylogenetic framework developed here indicates that the majority of these sequences are trimeric and are possibly involved in H_2-based electron bifurcation, it is unclear if they are involved in the production or consumption of H_2. Examples of bifurcating [FeFe]-hydrogenase involved in oxidation and production of H_2 have been described. For example, an enzyme that functions to bifurcate electrons derived from the oxidation of H_2 coupled to the reduction of Fd and NAD^+ has been identified in *Acetobacterium woodii* {Schuchmann, 2012 #228} while other enzymes that function to couple the oxidation of Fd and NADH to the formation of H_2 have been identified in *Thermotoga maritima*, *Thermoanaerobacterium saccharolyticum,* and *Thermoanaerobacter tengcongensis* {Schut, 2009 #222;Soboh, 2004 #102;Shaw, 2009 #236}. Moreover, two recent studies reveal the presence of reversible

Draft - In preparation

399 bifurcating complexes. In the case of the acetogen *Moorella thermoacetica*, a reversible Fd- and
400 NAD-dependent trimeric [FeFe]-hydrogenase was identified {Wang, 2013 #226}.
401
402 The distribution of genes encoding putative bifurcating [FeFe]-hydrogenase was strongly
403 influenced by oxygen and salinity gradients. High salinity, such as that observed in along the
404 DWR3 vertical gradient, is generally unfavorable to proteins due to lower water activity,
405 increases in the strength of hydrophobic interactions during protein folding, and a reduction in
406 electrostatic interactions in proteins residing in the cytoplasm {Lanyi, 1974 #24;Dennis, 1997
407 #25}. HydA recovered from the hypersaline GSL water column were enriched in hydrophilic
408 amino acids as indicated by significantly lower GRAVY indices when compared to HydA
409 sequences obtained from lower salinity mats inhabiting Guerrero Negro salterns (~ 8.0% salt)
410 and Yellowstone National Park hot springs (~0.5-3.1% salt). This finding is consistent with the
411 results of previous investigations of the proteomes of a variety of halophilic and non-halophilic
412 organisms which indicate lower hydrophobicity indices than for non-halophilic counterparts.
413 Lower hydrophobicity in proteins is a feature that is hypothesized to reduce the effects of salt-
414 driven non-specific inter or intramolecular interactions in hydrophobic side-chains, which lead to
415 protein mis-folding and/or aggregation {Reistad, 1970 #38;Lanyi, 1974 #24;Spahr, 1962
416 #40;Visentin, 1972 #41;Hutcheon, 2005 #43;Joo, 2005 #44}. Similar results were also obtained
417 from a comparative genomic and proteomic analysis of 6 halophilic and 24 non-halophilic
418 isolates, spanning both the bacterial and archaeal domains, which also indicated a lower
419 hydrophobicity for halophilic proteins {Paul, 2008 #42}. Thus, the lower hydrophobicity of
420 HydA in the GSL HydA suggests that these proteins are uniquely adapted to the high salt
421 conditions present in their natural environment.

Draft - In preperation

HydA was identified in transects of the DWR3 water column where salt levels were high (15-24%) but where dissolved O_2 was depleted relative to surface waters. The hypoxic (dO_2 range 0.98 – 2.32 mg/L) of the DWR3 transects where hydA was detected implies either anaerobic microniches that allow anaerobes to exist in otherwise sub-oxic conditions, a lower effective exposure of the organism or its oxygen sensitive enzymes to O_2, or enhanced tolerance to O_2. The solubility and bioavailability of O_2 is lower in hypersaline solutions {Lange, 1972 #237} which may allow anaerobic organisms to inhabit otherwise hypoxic conditions Intriguingly, many of the hydrogenases described in this study exhibit novel substitutions in the L1 sequence motifs, which are involved in the coordination of the oxygen-labile [4Fe-4S] subcluster of the H cluster of HydA {Nicolet, 2000 #99;Nicolet, 1999 #100;Peters, 1998 #101}. Substitutions in this region may have implications for the redox properties of this [4Fe-4S] cluster and thus may be important in conferring stability in the presence of O_2 {Posewitz, 2008 #12}.

Most organisms that harbor a bifurcating [FeFe]-hydrogenase harbor additional non-bifurcating enzymes {Calusinska, 2010 #210;Meyer, 2007 #7}. It is therefore a surprise that the majority of sequences recovered in the present examination of HydA diversity in GSL were predicted to be of the bifurcating type. It is possible that the primers used in the present study are biased toward homologs that form trimers and that are thus potentially involved in bifurcation (e.g., TRM3) {Calusinska, 2010 #210;Meyer, 2007 #7}. Indeed, a prior comparison of the primers used in this study with other primer designs found that each is biased toward a different spectrum of HydA diversity {Schmidt, 2010 #233}. Application of untargeted shotgun

Draft - In preperation

445 metagenomic sequencing approaches, which are currently ongoing, will provide a mechanism to
446 *1*) evaluate the potential bias associated with the recovery of predominantly bifurcating enzymes
447 in the present study and *2*) to evaluate the predictive capacity of the phylogenetic approaches
448 used here to assign secondary and quaternary structure to the recovered protein sequences.
449
450 The detection of abundant putative trimeric bifurcating [FeFe]-hydrogenase along the
451 GSL DWR3 vertical gradient coupled with the numerous studies that continue to expand the
452 functional capabilities of these enzymes {Schuchmann, 2012 #228;Schut, 2009 #222;Wang,
453 2013 #225;Wang, 2013 #226} may have a significant application in biofuel production. One
454 limitation for the production of highly reduced bioproducts is that a large proportion of the
455 metabolic electron flow is directed towards reduction of pyridine nucleotides (i.e., to NAD(P)H).
456 Thermodynamically the reduced pyridine nucleotides are not sufficient in energy for the
457 production of a number of desirable, highly reduced biofuel products. [FeFe]-hydrogenase
458 catalyzed electron bifurcation potentially overcomes this thermodynamic challenge by
459 combining electrons from the reduced pyridine nucleotides with other lower potential electrons
460 from reduced Fd {Buckel, 2013 #224;Wang, 2013 #225;Wang, 2013 #226;Schut, 2009 #222}.
461 This increases the reducing potential of electrons from reduced pyridine nucleotides such that a
462 larger flux is directed toward the production of desired biofuels (i.e., reduced products). That
463 other electron donors (e.g., CO, formate) {Wang, 2013 #225} can potentially feed into these
464 complexes expands the potential use of these enzymes in the directing the flux of metabolic
465 electrons toward desired biofuels. Effort aimed at isolating representatives of the dominant, yet
466 uncharacterized organisms harboring the unique [FeFe]-hydrogenase enzymes identified herein
467 should continue to expand our understanding of the diversity of biochemical reactions catalyzed

Draft - In preperation

by this unique class of enzyme and which may prove useful in overcoming key bioengineering barriers.

ACKNOWLEDGEMENTS. This research is part of the United States Air Force Office of Scientific Research under Grant FA9550-11-1-0211 and FA9550-11-1-0218 to MCP and JWP.

Draft - In preperation

491 **REFERENCES**

492

Draft - In preperation

Table 1. Geographical, physical, and chemical data for the water column depths sampled[a].

Depth (m)	Latitude	Longitude	Salinity (ppt)	Dissolved O_2 (mg/L)	PAR (μM)	Temp (C)	pH
0.0	41.1674600	-112.6696117	149	5.46	2079	24.17	7.21
1.0	41.1674600	-112.6696117	151	5.38	1219	24.16	7.46
4.0	41.1674717	-112.6696117	143	5.13	175	23.77	7.83
6.0	41.1674717	-112.6696417	151	2.32	75	23.37	8.07
6.5	41.1674833	-112.6696200	203	1.68	44	*20.20*[b]	*7.10*[b]
8.0	41.1674817	-112.6696083	247	0.98	0	16.59	5.95

[a]Previously reported in Meuser et al., 2013

[b]Data points were not measured, but were interpolated based on observed trends.

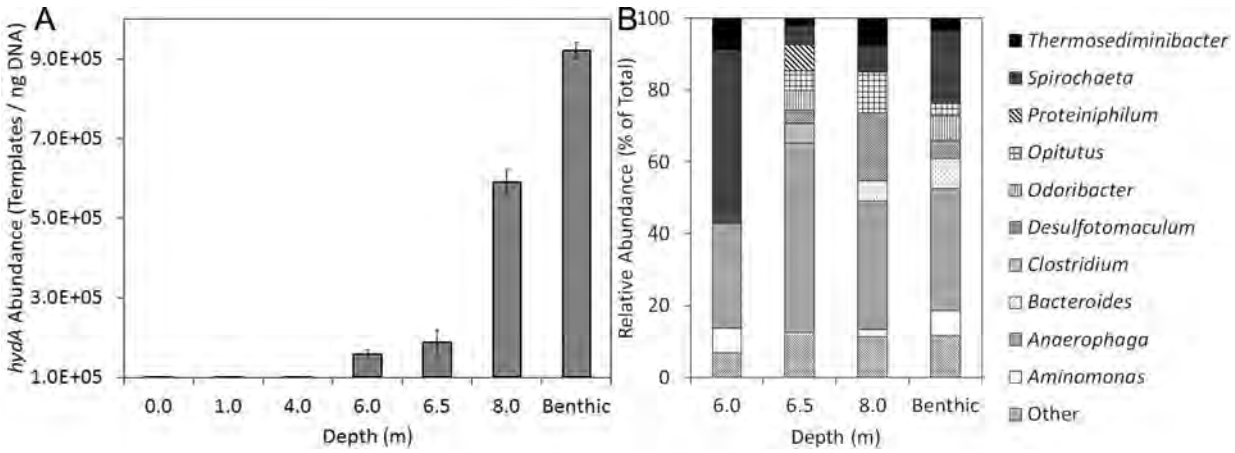

Figure 1. Abundance of *hydA* templates as a function of depth at DWR3 (A). Taxonomic composition of HydA protein sequences as determined by BLASTp analysis (B). Further details of the taxonomic composition of HydA are located in Supp. Table 1.

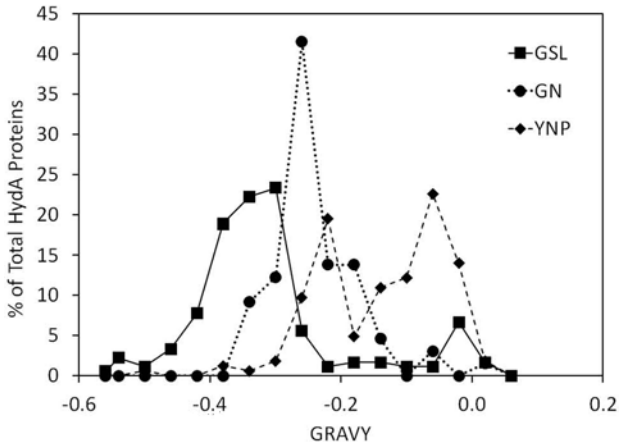

Figure 2. Hydropathy values associated with HydA from GSL, Guererro Negro (GN), and Yellowstone National Park (YNP), as assessed using the GRAVY index. GRAVY indices for sequences from each environment were binned at 0.04 increments (rounded up).

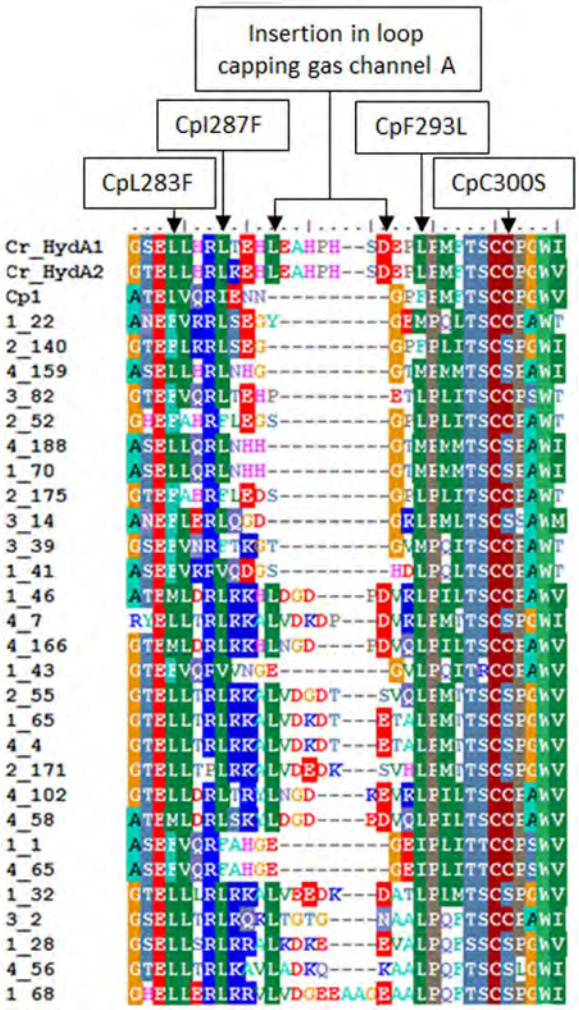

Figure 3. Unique substitutions in the L1 motif and insertions upstream from the L1 motif observed in recovered GSL HydA protein fragments. HydA1 and HydA2 from *Chlaymdomonas reinhardtii* (Cr_HydA1 and Cr_HydA2, respectively) and HydA1 from *Clostridium pasteurianum* (Cp1) are indicated. Substitutions and insertions are outlined above in reference to the Cp1 sequence.

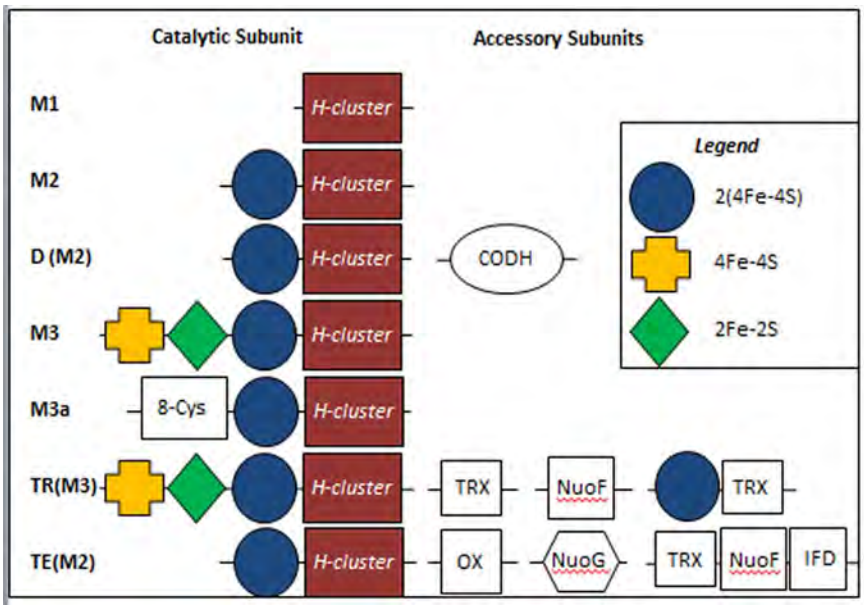

Figure 4. Accessary cluster domains associated with diverse HydA. The composition of N- and C- terminal modules (F- and C-clusters, respectively) as identified in Meyer et al., 2007 and as modified by Calusinska et al., 2010 are presented.

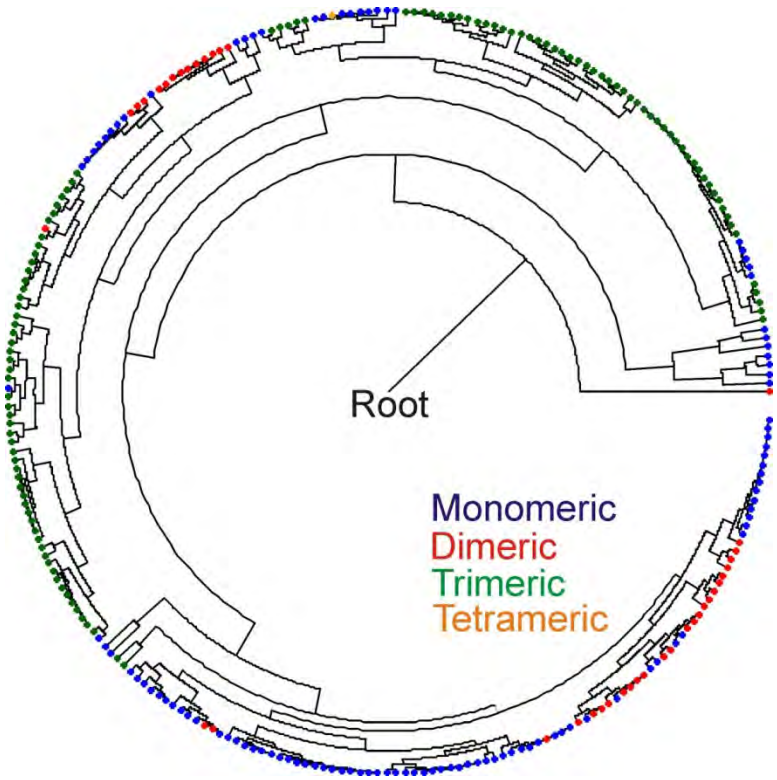

Figure 5. Bayesian phylogenetic reconstruction of 263 HydA protein sequences compiled from Calusinska et al., 2010 and from GenBank (Supp. Table 3). The phylogeny was generated using only the region of HydA corresponding to the fragment obtained from the GSL water column [positions 280 to 419 of HydA1 from *Clostridium pasteurianum* (AAA23248)]. The primary quaternary structure of the homologs (monomeric, dimeric, trimeric, tetrameric) as outlined in Meyer, 2007 and more recently in Calusinska et al., 2010 are overlaid on the phylogeny. Architectures correspond with those presented in Fig. 3.

Draft genome and targeted transcriptional analysis of *Clostridium pasteurianum* (strain W5) provides insights into possible determinants of H_2 oxidation and reduction

Jesse B. Therien,[1] Trinity L. Hamilton,[1] Zhenfeng Liu,[2] Seth M. Noone[3], Paul W. King[3], Donald A. Bryant,[2] John W. Peters[1#]

Department of Chemistry and Biochemistry, Montana State University, Bozeman, Montana 59717[1]; Department of Biochemistry and Molecular Biology, The Pennsylvania State University, University Park, Pennsylvania 16802[2]; National Renewable Energy Laboratory, Biosciences Center, Golden, CO 80401[3]

Draft in preparation

Abstract

Clostridium pasteurianum (strain W5) has been the model organism for the study of nitrogen fixation and hydrogen metabolism for over a century. The first generation of biochemical characterization of complex iron-sulfur cluster containing [FeFe]-hydrogenases and Mo-nitrogenase were carried out on enzymes purified from *C. pasteurianum.* It was demonstrated that two [FeFe]-hydrogenases are expressed differentially under nitrogen-fixing and non nitrogen-fixing conditions. It was proposed that the first characterized [FeFe]-hydrogenase (CpI) had a primary role in central metabolism in recycling reduced electron carriers that accumulated during fermentation under non nitrogen-fixing conditions via proton reduction, while the second characterized hydrogenase, CpII, was proposed to have a role in capturing reducing equivalents lost as hydrogen during nitrogen reduction. In support of this, previous in vitro biochemical characterization of CpI and CpII indicate CpI has elevated proton reduction activity in comparison to CpII and CpII has elevated hydrogen oxidation in comparison to CpI. We have sequenced the genome of *C. pasteurianum* (strain W5) to gain further insight into the role of hydrogenases in metabolism. The genome sequence provides evidence of four hydrogenases including a previously unidentified third [FeFe]-hydrogenase and a [NiFe]-hydrogenase. Under nitrogen-fixing conditions we have shown that the transcription of an [FeFe]- and the [NiFe]-hydrogenase are increased in concert with down regulation of the canonical [FeFe]-hydrogenase involved in central metabolism. Comparison of the primary sequences of CpI and CpII and their close homologues provides the basis for identifying key potential determinants of modulating hydrogen production and hydrogen oxidation activities.

Draft in preparation

Introduction

Clostridium pasteurianum (strain W5) is a gram-positive, spore-forming, obligately anaerobic bacteria found in soil and was the first free-living nitrogen-fixing organism to be isolated (1). For over 100 years, it has been a model for studying the biochemistry of nitrogen fixation and hydrogen metabolism. The first generation of biochemical characterization of complex iron-sulfur clusters from an [FeFe]-hydrogenase and Mo-nitrogenase were carried out from enzymes purified from *C. pasteurianum*. Following the discovery of hydrogenase in *C. pasteurianum* (2) the first preparations of a soluble hydrogenase were obtained from this organism (3, 4). Subsequently, the presence of a second [FeFe]-hydrogenase (CpII) was revealed (5) and its physical and catalytic properties were studied along with the first (CpI) (6). Decades later the first structure of an [FeFe]-hydrogenase (CpI) was determined from *C. pasteurianum* (7).

The *Clostridia* are a diverse group of anaerobes that produce many fermentative metabolites. In general, clostridia gain their energy from the conversion of a hexose to butyrate, acetate, CO_2 and H_2. Fermentation typically consists of the conversion of glucose to pyruvate through the glycolytic pathway. Reduced NADH produced during glycolysis can subsequently reduce ferredoxin via NADH:ferredoxin oxidoreductase which then can reduce protons to H_2 via hydrogenase. At this point, pyruvate can be drained away through the action of lactate dehydrogenase, but otherwise is converted to acetyl-CoA via pyruvate:ferredoxin oxidoreductase with the concomitant production of CO_2. During this step, reduced ferredoxin can again be used to supply hydrogenase with ability to reduce protons to H_2. Acetyl-CoA is then converted to either acetate or one of many alcohols.

Draft in preparation

In order to help Clostridia maintain the proper redox state during fermentation, hydrogenases reversibly couple electrons (i.e. excess reducing equivalents) with protons to form hydrogen.

$$2H^+ + 2e^- \leftrightarrows H_2$$

Many hydrogenases preferentially catalyze this reaction in one direction (8). Therefore, it may benefit an organism to possess a hydrogenase tuned for hydrogen production and another tuned for hydrogen oxidation, such that either hydrogenase could be used dependent upon specific metabolic needs. In fact, a large number of Clostridial species have been shown to have multiple hydrogenases (8, 9), including C. pasteurianum, from which the 60.5kDa CpI and 53 kDa CpII were first isolated. After its initial characterization (3), CpI was observed to produce H_2 in vitro using methyl viologen as an electron carrier (4), while CpII was first thought to be a unidirectional H_2-oxidizing hydrogenase (5). It was later shown that CpI and CpII are bidirectional and catalyze both the production and uptake of H_2 (10). A comparison of the rates of H_2 evolution and oxidation revealed that CpI produces H_2 550 times faster than CpII (5,500 vs. 10 μmol of H_2/min*mg respectively) while it oxidizes H_2 about 30% slower than CpII (24,000 vs. 34,000 μmol of H_2/min*mg respectively) (11). With the ability to purify CpI and CpII, it was shown colorimetrically that CpI contains 20.1 ± 0.7 moles of iron per mole of protein while CpII contains 13.8 ± 0.4 (12). In both CpI and CpII, fourteen of these iron atoms were attributed to a six-iron hydrogenase cluster (H-cluster (13)), thought to be where catalysis takes place, and two [4Fe4S] accessory "ferredoxin" clusters (F-clusters (13)) suspected of facilitating electron transfer to and from the H-cluster (12, 14). Using Resonance Raman spectroscopy, an additional [2Fe2S] cluster was detected in CpI, but not CpII (15). Thus, in total, CpI was shown to contain a six-iron H-cluster three [4Fe4S] clusters and a [2Fe2S] cluster, while CpII was lacking one [4Fe4S] and the [2Fe2S] F-cluster in comparison to CpI.

Draft in preparation

Hydrogen-producing hydrogenases in anaerobes, as mentioned, are used as a way to dispose of reducing equivalents during fermentation (16). This explains the role of CpI, but does not explain the biological function of CpII, which we hypothesize functions metabolically as an uptake hydrogenase. Hydrogen uptake hydrogenases are typically coupled to energy yielding/conserving reactions, for example, nitrogen fixation. Here, for every mole of dinitrogen reduced, eight protons, eight electrons, and 16 ATP are used to produce two moles of ammonia and one mole of dihydrogen (17); the reaction is shown below.

$$N_2 + 8H^+ + 8e^- + 16MgATP \rightarrow 2NH_3 + H_2 + 16MgADP + 16Pi$$

The high ATP/electron demand of nitrogen fixation can stress an organism energetically; therefore the presence of an uptake hydrogenase is of value in order to recycle electrons. Fittingly, *C. pasteurianum* is a nitrogen fixer and would benefit from an uptake hydrogenase during nitrogen fixation. In some nitrogen fixing organisms such as *Azotobacter vinelandii* (18), *Rhodopseudomonas palustris* (19), and others (20, 21), uptake hydrogenases have been shown to be co-transcribed with the nitrogen fixing machinery. However without the gene sequence of CpII, similar transcriptional studies are not possible. Thus, we decided to sequence the genome of C. *pasteurianum*. The draft genome would not only allow us to perform the transcriptional analysis necessary to determine whether CpII indeed is upregulated during nitrogen fixation and thereby recycling H_2 to conserve energy, but also allow us to identify the gene context of both CpI and CpII. Furthermore, the gene context of the previously sequenced nitrogenase (*nif*) gene cluster (22) could provide insight into the relationship between nitrogenase and the hydrogenases.

MATERIALS AND METHODS

Draft in preparation

Growth conditions. Freeze-dried *C. pasteurianum* W5 (ATCC® 6013™) was obtained from ATCC and rehydrated with Difco™ Reinforced Clostridial Medium following the ATCC protocol. Sealed 25 ml glass serum vials (Weaton) containing 10 ml of Difco™ Reinforced Clostridial Medium under a headspace of 10% H_2-10% CO_2-80% N_2 were then inoculated with the rehydrated culture and incubated at 37°C following ATCC propagation procedures for this organism. Agar plates of the above medium were used to store *C. pasteurianum* W5 for further use; initially grown at 37°C for 24-48 hours before being stored at room temperature in an anaerobic chamber.

For genome sequencing, cultures were inoculated from a single colony from a plate of Difco™ Reinforced Clostridial Medium that was inoculated into a sealed 25ml serum vials containing 10ml of the same media, under a headspace of 10% H_2-10% CO_2-80% N_2 were then incubated overnight at 37°C. 1 ml of culture was then spun down at 14,000 x g at room temperature before extracting DNA.

For qRT-PCR, cultures were begun in a similar manner as above, after which 1-5 ml of overnight culture were used to inoculate 50 ml of both DM-11 (23) (N+; containing NH_4Cl and $(NH_4)_3SO_4$) and DM-11-N (N-; fixed nitrogen free) media to an OD_{650} = ~0.020 and were then sparged with 10% H_2-10% CO_2-80% N_2 for 10 minutes and incubated overnight. This was repeated once more after which point a C_2H_2 reduction assay (24) was performed to ensure N_2 fixation was taking place in the N- culture. Then, in sealed 123 mL serum vials, 1 mL (N+) was added to 50 mL of N+ media, and 6 mL of (N-) were added to 50 mL of N- media, in order to make a starting OD_{650} = ~0.020 for each culture. The vials were once again sparged with the gas

Draft in preparation

mix and incubated overnight at 37°C. The following day, another C_2H_2 reduction assay was performed to ensure the N- culture was fixing N_2. 500 µl samples were mixed with 1 ml of QIAGEN RNAprotect Bacterial Reagent® following the included procedure, and either used immediately for RNA extraction or frozen at -20 °C until later RNA extraction.

Genome sequencing. Total genomic DNA of *C. pasteurianum* W5 was extracted using a Promega Wizard® Plus SV minipreps DNA purification system and its concentration determined by a NanoDrop 1000 Spectrophotometer to be 220 ng/µl ($Abs_{260/280}$ = 2.04). Genomic DNA was then submitted to the Genomics Core Facility at The Pennsylvania State University for SOLiD sequencing (25). With the help of the Genomics Core Facility, contigs were assembled onto six scaffolds, leaving thirty standalone contigs that did not initially fit onto the scaffolds.

Gaps were closed by PCR using primers designed approximately 200 bases from the end of each contig. GoTaq® 2x Master Mix reagent by Promega was used for the PCR on a Techne Touchgene Gradient Thermal Cycler. Amplicons were then purified either directly using QIAquick PCR Purification Kit or from agarose gels using the Qiaex II Gel Extraction Kit, both from QIAGEN. Purified PCR products were then sequenced by Davis Sequencing in Davis, CA. Sequence data was then assembled using BioEdit.

Putative Gene annotation analysis was completed using the RAST (Rapid Annotation using Subsystem Technology) prokaryotic genome annotation server (26). The protein sequence of the H-cluster domain of CpI was used to BLAST the draft genome in RAST and all matches with an

Draft in preparation

expect value (E-value) below 1.0 were aligned using ClustalW to determine whether they contained previously published signature motifs L1, L2, and L3 found in [FeFe]-hydrogenases.

Preparation of total RNA. RNA of *C. pasteurianum* W5 was extracted using QIAGEN RNeasy® Mini Kit followed by a DNase treatment step using RQ1 RNase-Free DNase by Promega and a re-purification using the QIAGEN RNeasy® Mini Kit. RNA concentration was then determined using Qubit® RNA Assay Kit and was then frozen at -20 °C until further analysis.

Quantitative RT-PCR (qRT-PCR). Primers were designed for the 4 hydrogenases (CpI, CpII, CpIII and the large subunit of [NiFe]), 3 nitrogenase α-subunits (*nifD, vnfD*, and *anfD*) and the 16S rRNA small subunit using the Integrated DNA Technologies SciTools qPCR online primer designing software. qRT-PCR was performed on a Rotor-Gene-Q real-time PCR detection system from Qiagen using the *Power* SYBR® green RNA-to-C_T™ *1-Step* Kit from Applied Biosystems according to the included protocol. Reactions were done in triplicate with control reaction mixtures containing no reverse transcriptase.

RESULTS/DISCUSSION

Genome. Initial sequencing resulted in 145 contigs ranging from 511 to 251,858 bases yielding an estimated genome size of 4,206,741 bp. The average contig length was 29,012 bases and the average number of reads per contig was 1,618. As with most other *Clostridial* species (27) (28), the GC content was very low at 30%.

Draft in preparation

204 After closing 90% (131 of 145) of the gaps, annotation analysis predicted 4347 protein coding
205 sequences (CDSs), which accounted for 83% of the genome coverage. The Tandem Repeats Da-
206 tabase v2.30 (23) indicated the presence of 216 tandem repeats; the highest copy number was
207 17.5 for the 2 base repeat of TA and the longest repeat was 408 bases with 2 copies. There were
208 69 RNA genes.
209
210 According to RAST, the closest neighbors with a completed genome were shown to be numerous
211 (twelve) strains of *Clostridium botulinum*, *Clostridium novyi* NT, and *Clostridium sporogenes*
212 ATCC 15579. *C. botulinum* strains are quite numerous and represent the largest species of clos-
213 tridia with complete genomes; according to NCBI, 13 complete genomes and 11 partial genomes
214 currently exist.

Hydrogenases. The genome confirms the presence of three [FeFe]-hydrogenases, CpI, CpII, and what we designate CpIII, in addition to one [NiFe]-hydrogenase and all necessary hydrogenase maturation genes. All 4 hydrogenases are distributed throughout the largest contig (2,726,463 bp) (Fig. 1). While many [FeFe]-hydrogenase-containing genomes possess multiple copies of structural genes, as exemplified by *C. pasteurianum* and other clostridia (9) (8), most often there is only one copy of the maturase genes *hydE*, *hydF*, and *hydG* (7). Both HydE and HydG belong to the radical S-adenosylmethionine superfamily of proteins while HydF is a GTPase (31). The genes encoding the maturases can be found together as a cluster (hydEFG), as two sets (hydEF, hydG or hydE, hydFG), or individually (7) as was observed in *C. pasteurianum*. Figure 1 shows the delocalization of the maturase genes on the genome.

Draft in preparation

The encoded protein sequence of CpII (458 residues) is slightly shorter than that of CpI (574 residues), while CpIII is shorter still (450 residues). As seen in figure 2, [FeFe]-hydrogenases contain the strictly conserved [FeFe]-hydrogenase H-cluster signature motifs; ^{299}**C**C**C**Px, ^{254}P**C**xxK, and ^{495}ExMx**C**xxG**C**xxG (numbered according to CpI) (8, 29). These motifs encompass the H-cluster binding cysteines, denoted in figure 2 with an H. previous phylogenetic clustering of Clostridial [FeFe]-hydrogenases H-cluster domains has shown a variety of distinct clusters, designated A1-A5, A7, A8, and B1-B3 (16). Group A2, where CpI is found, is comprised of soluble, hydrogen-producing enzymes. Enzymes of group A4, into which CpII clusters, contain a long C-terminal domain that ligates two small rubredoxins and one rubrerythrin center (9). Members of group B2 such as CpIII have an average size of 450 aa and an additional characteristic cysteine residue in the P1 motif (TS**C**CCPxW) of the H-cluster (8). Interestingly, the ferredoxin-binding motif closest to the N-terminus of clostridial B2 members is $Cx_2Cx_2Cx_3C$; this is similar to that of the *nif*-associated ferredoxin in *Rhizobium meliloti* which is $Cx_2Cx_8Cx_3C$ (8).

The [NiFe]-hydrogenase gene cluster contains the required accessory genes (*HypABCEFD* and *HoxN),* downstream of the structural genes, *HyaAB*, which encode the large and small subunits, respectively. The protein sequence of the large subunit contains previously described (29) L1 and L2 signatures characteristic of membrane-bound H_2 uptake hydrogenases. The L1 and L2 motifs encompass the highly conserved cysteine pairs (CxxC) near each terminus that ligate the NiFe center. Unlike [FeFe]-hydrogenases, maturases for the [NiFe]-hydrogenase are often found in a single gene cluster with the structural genes, as is the case for the *C. pasteurianum* genome. This gene cluster is not in close proximity to any other hydrogenase or nitrogenase genes. The

Draft in preparation

large subunit (*HyaB*) clusters phylogenetically with other *Clostridia* in group 1 (8) (data not shown) which are membrane-associated uptake hydrogenases (29).

Transcriptional analysis. Transcriptional experiments were repeated a minimum of three times using RNA from separate growths. Magnitudes of transcript abundance for the genes of interest varied in magnitude, especially for *nifD* which varied over an order of magnitude in one instance (data not shown). Despite the variation in magnitude, results consistently displayed a similar trend. Transcripts of the three [FeFe]-hydrogenase genes of *C. pasteurianum* all changed under N_2-fixing conditions. In complementary experiments performed by our collaborators at NREL (National Renewable Energy Laboratory, Golden, CO), transcripts for the hydrogenases and the nitrogenase in *Clostridium acetobutylicum* were monitored under nitrogen fixing conditions yielding similar increases in *nifD* and the [NiFe]-hydrogenase. The reduction of dinitrogen to ammonia and the reduction of protons to dihydrogen both depend on reducing equivalents. However, the assimilation of nitrogen is much more important and the electron requirement of nitrogenase (16 electrons) far exceeds that of hydrogenase (2 electrons). Therefore, it would be in the cell's interest shut down any competing metabolism.

Under N_2-fixing conditions transcripts of CpII were observed to increase an average of 7.4 fold (Fig. 3). Other experiments have demonstrated that N_2 fixing cultures of *C. pasteurianum* oxidized twice as much H_2 as cultures growing on media containing NH_3, that the ratio of CpII/CpI expressed in cultures fixing N_2 was 50% higher than in cultures not fixing N_2 (5), and that CpII had low H_2 producing rates (compared to CpI) and high H_2 oxidizing rates *in vitro* (11). Together, these observations suggest that the increase in transcription of CpII likely leads to an increase in CpII enzyme, which in turn increases the rate of H_2 oxidation. Oxidation of H_2 then produces

Draft in preparation

reducing equivalents, which would be in demand during N_2-fixation. In contrast to CpII, the transcription of CpI and CpIII from cells grown in media devoid of fixed nitrogen contained fewer transcripts (averaging -2.9 and -2.0 fold respectively) when compared to cells grown in nitrogen replete media, indicating that neither CpI nor CpIII function as uptake hydrogenases.

When compared to cultures grown in media containing NH_3, qRT-PCR indicated an average of an 8.7 fold increase in the number of transcripts for the large subunit of the [NiFe]-hydrogenase in cultures grown in the absence of fixed nitrogen. In *C. acetobutylicum*, results were nearly identical (figure 3). The increase in transcription of [NiFe]-hydrogenase is similar to what was found in two unrelated nitrogen fixers, *A. vinelandii* (18) and *R. palustris* (19). Both studies suggested the [NiFe]-hydrogenases likely function to recycle H_2 during N_2-fixation.

Hydrogenases in Clostridial metabolism

Our transcriptional analysis suggests that CpII and/or the [NiFe]-hydrogenase acts to recycle H_2 produced as a byproduct of nitrogen fixation. Unlike CpII, our qRTPCR results for CpIII transcription provide little insight into its metabolic function. Figure 5 illustrates our proposed metabolic scheme for CpI, CpII and the [NiFe]-hydrogenase during fermentation and nitrogen fixation respectively.

A search through the genomes of over 40 fully sequenced Clostridial species using the NCBI BLAST tool showed that all but two species (*C. kluyveri* and *C. butyricum*) that possess nitrogenase also contain a [NiFe]-hydrogenase (figure 4). The two exceptions each have three or more [FeFe]-hydrogenases, suggesting that one or more of them may serve as an uptake hydrogenase, thereby supplanting the need for a [NiFe]-hydrogenase during nitrogen fixation.

Draft in preparation

Structural basis for hydrogen production / hydrogen oxidation activities

Given that CpI and CpII have such dramatic differences between their abilities to produce and oxidize hydrogen, we hypothesize that there must be some structural features responsible for this difference. Homology models of CpII (Fig. 2a) and CpIII (not shown) generated using Swiss-Model (30), as well as sequence alignments and iron incorporation numbers, indicate the absence of accessory domains seen in CpI. Starting at the N-terminus of CpI, there are conserved cysteine residues for each cluster sequentially binding clusters FS2, FS4C, FS4B and FS4A. The N-terminus lacks residues responsible for binding accessory clusters FS2 and FS4C (Fig. 2). However, conserved regions binding the remaining [4Fe4S] and [2Fe] clusters of the H-cluster and two [4Fe4S] accessory clusters have been identified. In CpIII, the N-terminal arrangement of cysteines is unique. Sequence alignment (Fig. 2) reveals that the FS4A binding motif is conserved, while the FS4B motif lacks two of the four cysteine residues typically seen ligating this cluster.

Hydrogenases are well known to have differing FeS cluster binding motifs (31), however, comparison among these proteins does not illuminate a trend in hydrogen oxidation to production ratios. It is currently unclear to what extent additional clusters play in the role of kinetic and catalytic bias, though these clusters may be partially responsible for determining catalytic bias to an extent that is not yet clear. Most likely, a suite of structural features are responsible for tuning the directionality of a given hydrogenase. The particular amino acids involved in gas channel lining, proton transfer, electron transfer, and H-cluster ligand environment may all play a role. Interestingly, in the case of [NiFe] hydrogenases, Leǵer et al report that mutations in the gas channel that partially block the channel push the catalytic bias towards oxidation, while mutating an electron-transferring FeS cluster coordinating histidine residue to a glycine resulted in biasing

Draft in preparation

the enzyme to favor hydrogen production (32). The work demonstrates that changes far away from the active site of the hydrogenase may impact the kinetics of hydrogenase, often in unpredictable ways.

Knörzer *et al* showed that the most frequent substitution for M353 in 409 CpI homologues was T353, as in CpII, and used site directed substitution to change this residue from M353 to L353 in *C. pasteurianum*. A significant decrease in H_2 production (15% of WT) and a small decrease in H_2 oxidation (74% of WT) was observed and was attributed to lowered turnover rate. This indicates that the residue at position 353 is capable of influencing the enzymatic preference for hydrogen oxidation/production, with the leucine causing the enzyme to favor oxidation to a greater degree relative to the methionine. EPR suggested slight differences in the elctronic structure and it was thought this might impede the the transition between different redox states. Cyclic voltametry of the mutated enzyme showed slightly lowered K_m, but similar catalytic bias for both the forward and reverse reactions. The authors therefore concluded that differences in assay conditions led to the observed difference in hydrogen oxidation/production compared to WT.

Winkler and cowworkers stated that it was unclear whether hydrogenases with a threonine corresponding to CpI position 353 were active, but suggested that the enzymes "might exhibit interesting features" (33). We hypothesized that, similar to Knörzer's leucine, the biologically-relevant threonine may play a role in tuning the catalytic bias of the enzyme. Having made the mutation, hydrogen production and uptake assays simply showed a decrease in activity compared to the WT, and did not show a significant change in the ratio of oxidation/production (data not shown).

Draft in preparation

CONCLUSIONS

Our initial analysis of the *C. pasteurianum* W5 genome has identified a [NiFe]-hydrogenase and confirmed the presence of a third [FeFe]-hydrogenase. It is quite common for Clostridia to possess numerous [FeFe]-hydrogenases and the majority of sequenced species have a [NiFe]-hydrogenase. Fewer of the sequenced Clostridia have a nitrogenase. Out of the 40 Clostridial species we examined, nearly all nitrogenase-containing clostridia also had a [NiFe]-hydrogenase. Furthermore, the observed increase in transcription of [NiFe]-hydrogenase under N_2-fixing conditions in both *C. pasteurianum* and *C. acetobutylicum* suggests the [NiFe]-hydrogenase is involved in recycling/uptake of H_2 produced as a byproduct during the nitrogenase-catalyzed reduction of atmospheric N_2 to NH_4^+. Biochemical and transcriptional data for CpII similarly suggests that CpII is involved in H_2 uptake during nitrogen fixing conditions. So far, the use of CpIII by C. *pastuerianum* is unclear, and additional characterization of this enzyme may clarify its function. Based on the observed characteristics of CpI and CpII, as well as other evidence in the literature, we believe that it may be possible to tune the catalytic directionality of [FeFe] hydrogenases by introducing novel mutations to CpI.

Draft in preparation

ACKNOWLEDGEMENTS. This research is part of the United States Air Force Office of Scientific Research under Grant FA9550-11-1-0218 to JWP.

Draft in preparation

REFERENCES

1. **Winogradsky S.** 1895. Recherches sure l'assimilation de l'azote libre de l'atmosphere par les microbes. Archives des science biologique **3:**297-352.
2. **Valentine RC, Mortenson LE, Carnahan JE.** 1963. The Hydrogenase System of Clostridium pasteurianum. Journal of Biological Chemistry **238:**1141-1144.
3. **Nakos G, Mortenson L.** 1971. Purification and properties of hydrogenase, an iron sulfur protein, from Clostridium pasteurianum W5. Biochimica et Biophysica Acta (BBA) - Enzymology **227:**576-583.
4. **Chen J-S, Mortenson LE.** 1974. Purification and properties of hydrogenase from Clostridium pasteurianum W5. Biochimica et Biophysica Acta (BBA) - Protein Structure **371:**283-298.
5. **Chen J-S, Blanchard DK.** 1978. Isolation and properties of a unidirectional H2-oxidizing hydrogenase from the strictly anaerobic N2-fixing bacterium Clostridium pasteurianum W5. Biochemical and Biophysical Research Communications **84:**1144-1150.
6. **Adams MW, Mortenson LE.** 1984. The physical and catalytic properties of hydrogenase II of Clostridium pasteurianum. A comparison with hydrogenase I. The Journal of biological chemistry **259:**7045-7055.
7. **Meyer J.** 2007. [FeFe] hydrogenases and their evolution: a genomic perspective. Cell. Mol. Life Sci. **64:**1063-1084.
8. **Calusinska M, Happe T, Joris B, Wilmotte A.** 2010. The surprising diversity of clostridial hydrogenases: a comparative genomic perspective. Microbiology (Reading, England) **156:**1575-1588.
9. **Calusinska M, Joris B, Wilmotte A.** 2011. Genetic diversity and amplification of different clostridial [FeFe] hydrogenases by group-specific degenerate primers. Letters in applied microbiology **53:**473-480.
10. **Adams MWW, Mortenson LE.** 1984. The purification of hydrogenase II (uptake hydrogenase) from the anaerobic N2-fixing bacterium Clostridium pasteurianum. Biochimica et Biophysica Acta (BBA) - Bioenergetics **766:**51-61.
11. **Adams MW.** 1990. The structure and mechanism of iron-hydrogenases. Biochimica et biophysica acta **1020:**115-145.
12. **Adams MW, Eccleston E, Howard JB.** 1989. Iron-sulfur clusters of hydrogenase I and hydrogenase II of Clostridium pasteurianum. Proceedings of the National Academy of Sciences **86:**4932-4936.
13. **Adams MW.** 1987. The mechanisms of H2 activation and CO binding by hydrogenase I and hydrogenase II of Clostridium pasteurianum. Journal of Biological Chemistry **262:**15054-15061.
14. **Rusnak FM, Adams MW, Mortenson LE, Munck E.** 1987. Mossbauer study of Clostridium pasteurianum hydrogenase II. Evidence for a novel three-iron cluster. The Journal of biological chemistry **262:**38-41.
15. **Macor KA, Czernuszewicz RS, Adams MW, Spiro TG.** 1987. An investigation of hydrogenase I and hydrogenase II from Clostridium pasteurianum by resonance Raman spectroscopy. Evidence for a [2Fe-2S] cluster in hydrogenase I. The Journal of biological chemistry **262:**9945-9947.
16. **Meuser JE, Ananyev G, Wittig LE, Kosourov S, Ghirardi ML, Seibert M, Dismukes GC, Posewitz MC.** 2009. Phenotypic diversity of hydrogen production in chlorophycean algae reflects distinct anaerobic metabolisms. Journal of Biotechnology **142:**21-30.
17. **Fay P.** 1992. Oxygen relations of nitrogen fixation in cyanobacteria. Microbiological Reviews **56:**340-373.
18. **Hamilton TL, Ludwig M, Dixon R, Boyd ES, Dos Santos PC, Setubal JC, Bryant DA, Dean DR, Peters JW.** 2011. Transcriptional profiling of nitrogen fixation in Azotobacter vinelandii. Journal of bacteriology **193:**4477-4486.

Draft in preparation

19. **Oda Y, Samanta SK, Rey FE, Wu L, Liu X, Yan T, Zhou J, Harwood CS.** 2005. Functional genomic analysis of three nitrogenase isozymes in the photosynthetic bacterium Rhodopseudomonas palustris. Journal of bacteriology **187:**7784-7794.
20. **Brito B, Martinez M, Fernandez D, Rey L, Cabrera E, Palacios JM, Imperial J, Ruiz-Argueso T.** 1997. Hydrogenase genes from Rhizobium leguminosarum bv. viciae are controlled by the nitrogen fixation regulatory protein nifA. Proceedings of the National Academy of Sciences of the United States of America **94:**6019-6024.
21. **Lindberg P, Hansel A, Lindblad P.** 2000. hupS and hupL constitute a transcription unit in the cyanobacterium Nostoc sp. PCC 73102. Archives of microbiology **174:**129-133.
22. **Chen JS, Johnson JL.** 1993. Molecular biology of nitrogen fixation in the clostridia. Biotechnology (Reading, Mass.) **25:**371-392.
23. **Gelfand Y, Rodriguez A, Benson G.** 2007. TRDB—The Tandem Repeats Database. Nucleic Acids Research **35:**D80-D87.
24. **Hardy RWF, Holsten RD, Jackson EK, Burns RC.** 1968. The Acetylene-Ethylene Assay for N2 Fixation: Laboratory and Field Evaluation. Plant Physiology **43:**1185-1207.
25. **Mardis ER.** 2008. Next-Generation DNA Sequencing Methods. Annual Review of Genomics and Human Genetics **9:**387-402.
26. **Overbeek R, Olson R, Pusch GD, Olsen GJ, Davis JJ, Disz T, Edwards RA, Gerdes S, Parrello B, Shukla M, Vonstein V, Wattam AR, Xia F, Stevens R.** 2014. The SEED and the Rapid Annotation of microbial genomes using Subsystems Technology (RAST). Nucleic Acids Research **42:**D206-D214.
27. **Sakaguchi Y, Hayashi T, Kurokawa K, Nakayama K, Oshima K, Fujinaga Y, Ohnishi M, Ohtsubo E, Hattori M, Oguma K.** 2005. The genome sequence of Clostridium botulinum type C neurotoxin-converting phage and the molecular mechanisms of unstable lysogeny. Proceedings of the National Academy of Sciences of the United States of America **102:**17472-17477.
28. **Yutin N, Galperin MY.** 2013. A genomic update on clostridial phylogeny: Gram-negative spore formers and other misplaced clostridia. Environmental Microbiology **15:**2631-2641.
29. **Vignais PM, Billoud B.** 2007. Occurrence, classification, and biological function of hydrogenases: an overview. Chemical reviews **107:**4206-4272.
30. **Arnold K, Bordoli L, Kopp J, Schwede T.** 2006. The SWISS-MODEL workspace: a web-based environment for protein structure homology modelling. Bioinformatics (Oxford, England) **22:**195-201.
31. **Mulder DW, Shepard EM, Meuser JE, Joshi N, King PW, Posewitz MC, Broderick JB, Peters JW.** 2011. Insights into FeFe -Hydrogenase Structure, Mechanism, and Maturation. Structure **19:**1038-1052.
32. **Abou Hamdan A, Dementin S, Liebgott P-P, Gutierrez-Sanz O, Richaud P, De Lacey AL, Rousset M, Bertrand P, Cournac L, Léger C.** 2012. Understanding and Tuning the Catalytic Bias of Hydrogenase. Journal of the American Chemical Society **134:**8368-8371.
33. **Winkler M, Esselborn J, Happe T.** 2013. Molecular basis of FeFe -hydrogenase function An insight into the complex interplay between protein and catalytic cofactor. Biochim. Biophys. Acta-Bioenerg. **1827:**974-985.

Draft in Preparation

Figure Legends.

Figure 1. Draft genome of *Clostridium pasteurianum* and location of hydrogenase and nitrogenase genes and gene clusters. CpI, CpII, and CpIII indicate the [FeFe]-hydrogenases. *nif* cluster refers to the Mo-dependent nitrogenase while the *vnf* and *anf* clusters refer to the V-dependent and Fe-only nitrogenases respectively.

Figure 2. Protein sequence alignment of the [FeFe]-hydrogenases of *C. pasteurianum* and *C. acetobutylicum*. FeS cluster ligating residues indicated with A, B, C, or 2 to denote the cluster they ligate; H – the H-cluster, A – proximal cluster (FS4A), B – FS4B, C – FS4C, and 2 – FS2. Key residues within a 5 angstrom radius of the H-cluster are denoted with a star. These residues are conserved among representatives of phylogentically clustering members of groups containing CpI/CaI, CpII and CpIII/CaIII.

Figure 2a. Residues that may play an important role in "tuning" the H-cluster of CpI and CpII.

Figure 3. Fold change of hydrogenase transcript abundance in *C. pasteurianum* and *C. acetobutylicum* under N_2-fixing conditions as determined by qRT-PCR.

Figure 4. Presence of nitrogenase and hydrogenase genes in sequenced clostridial species. [FeFe]-hydrogenases 100% (Red), [NiFe]-hydrogenase 55% (Blue), Mo-nitrogenase 37% and 11% (large and small purple respectively), and alternative nitrogenases 3% and 3% (green).

Draft in preparation

Figure 5. Proposed metabolic function of CpI, CpII and the [NiFe]-hydrogenase in *C. pasteurianum*.

Draft in preparation

Figures.

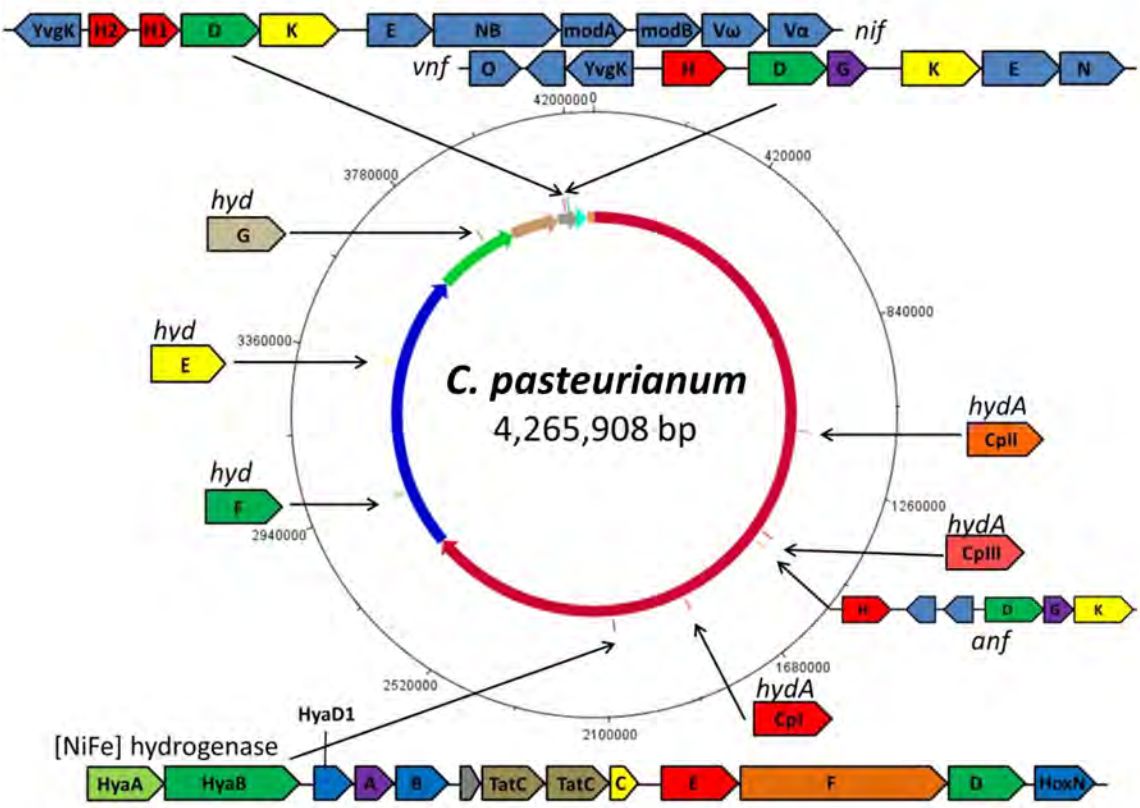

Figure 1.

Draft in p

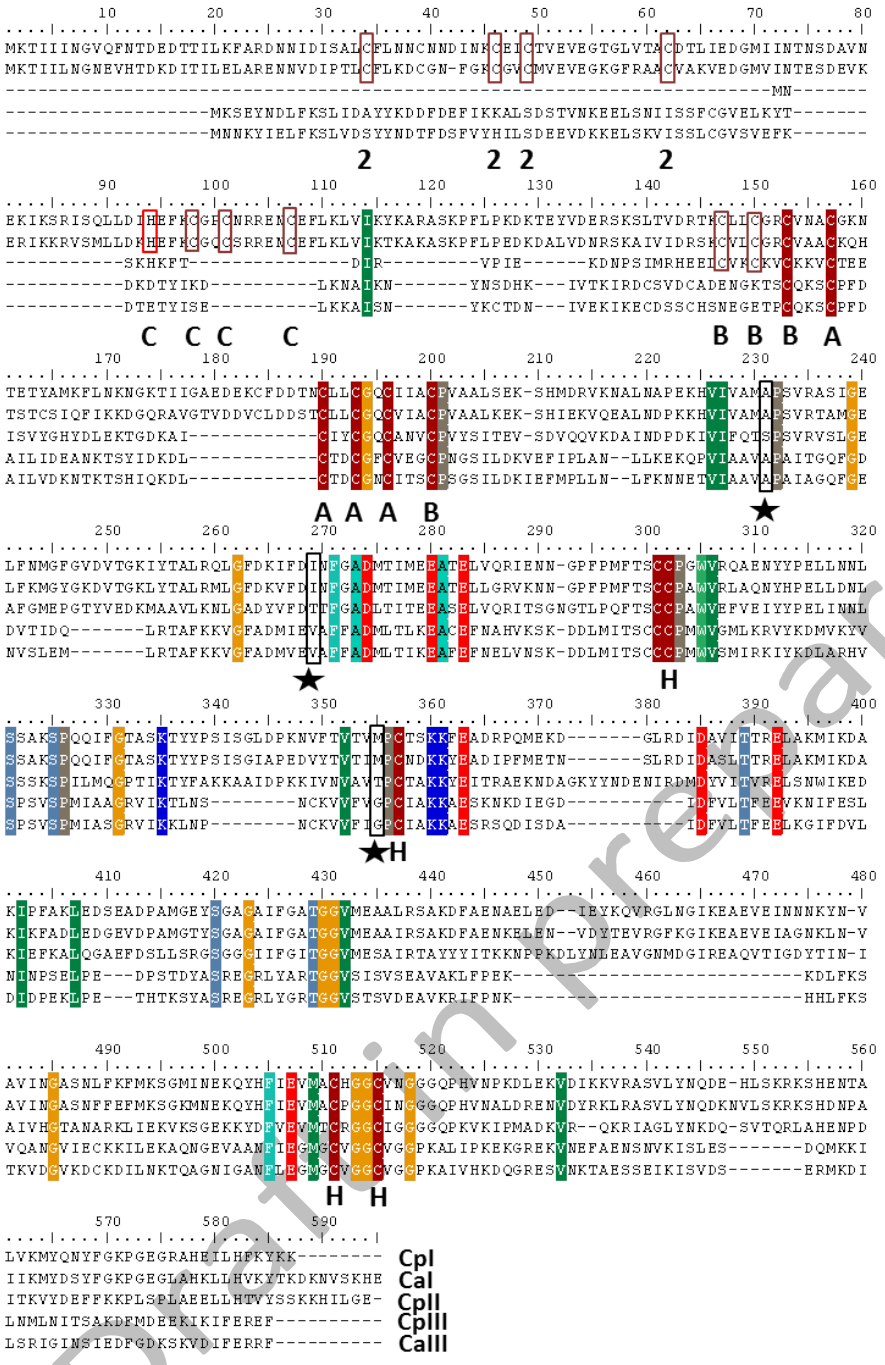

Figure 2a.

Draft in preparation

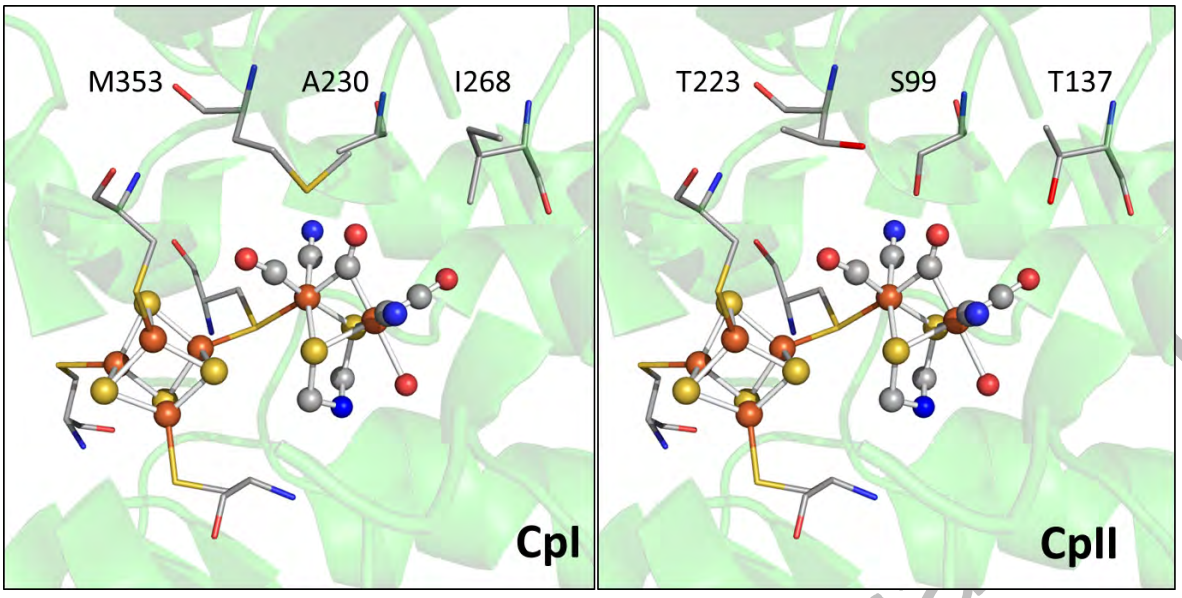

Figure 2b

Draft in prepara

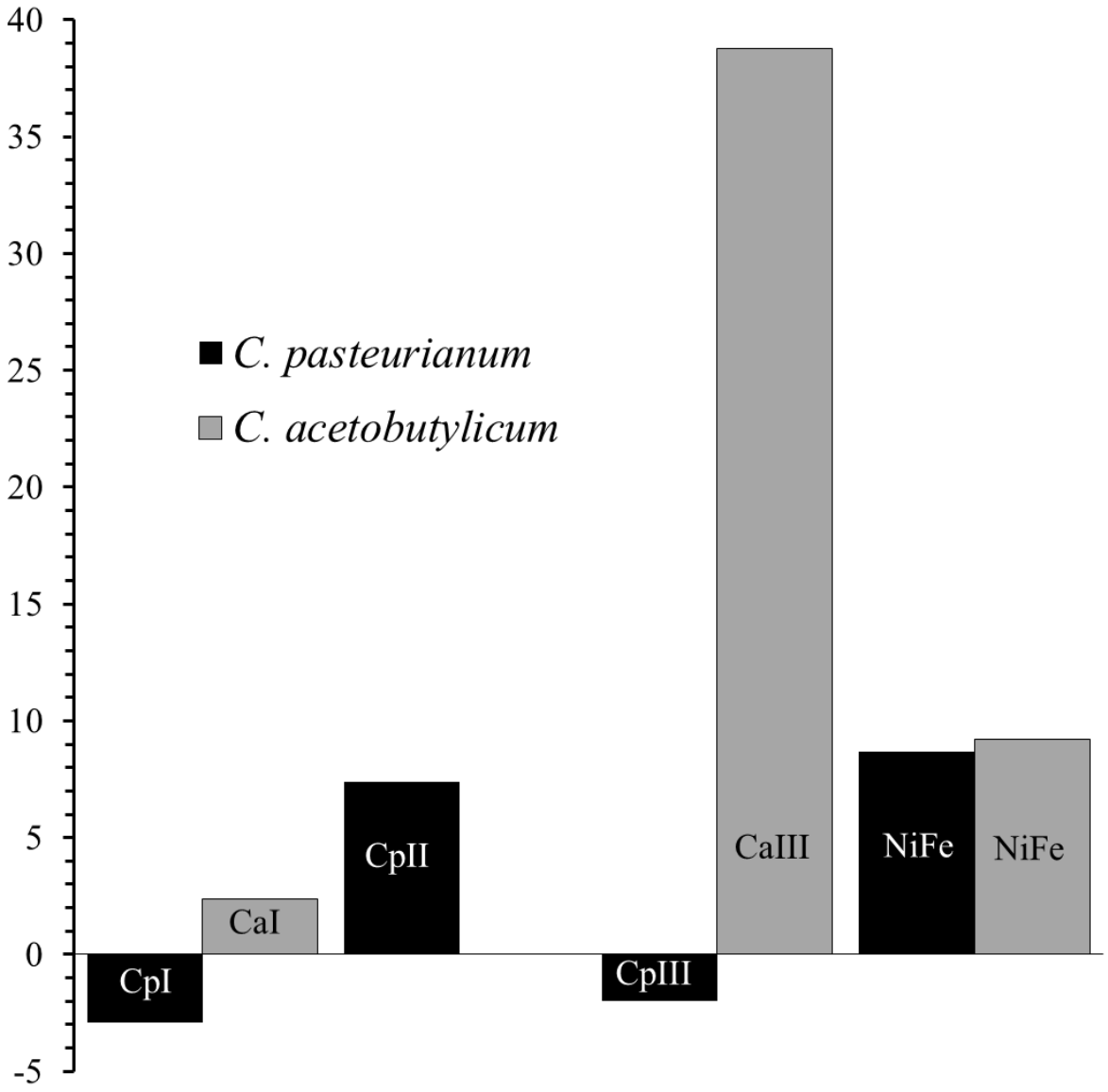

Figure 3.

Figure 4.

Draft

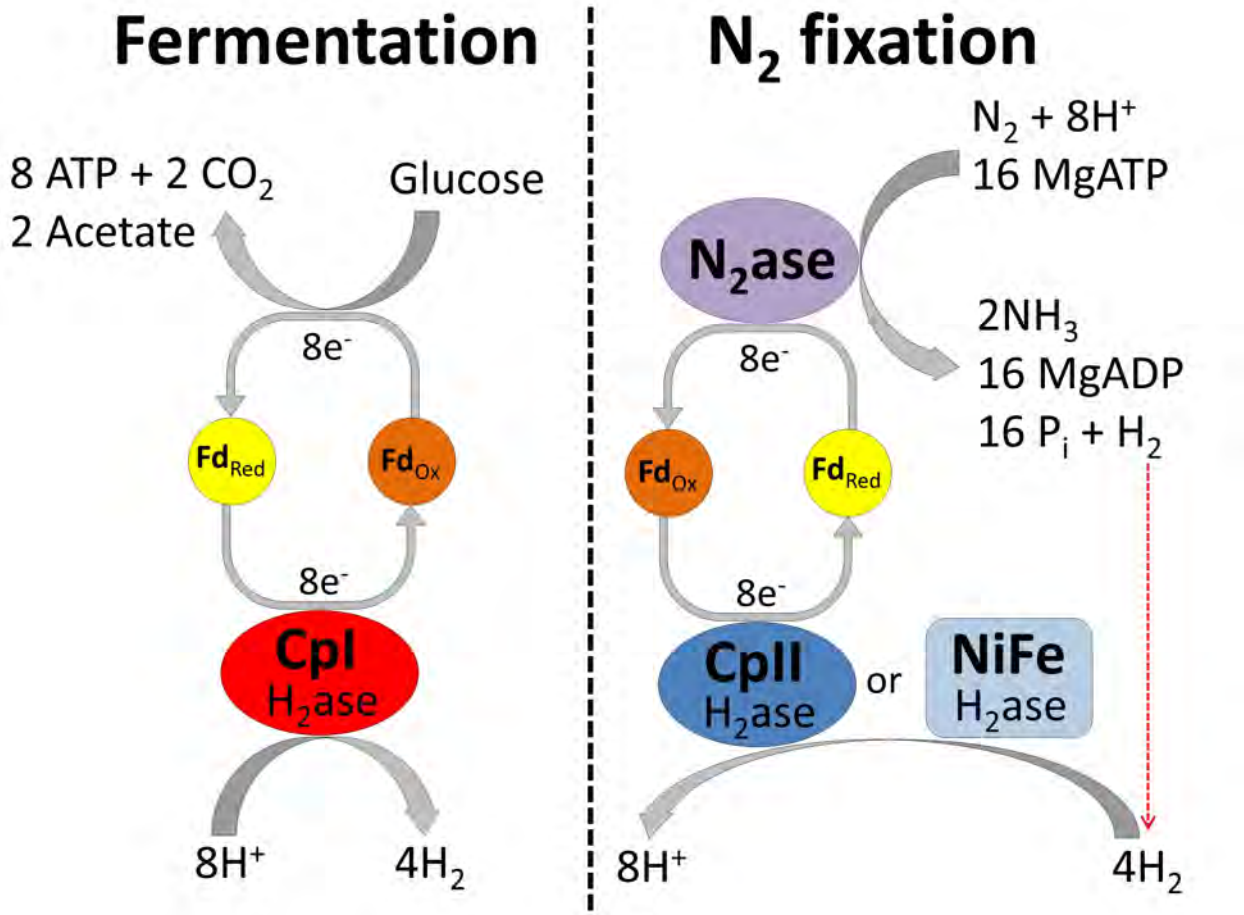

Figure 5.

Draft in P